CANADIAN THESES ON MICROFICHE

I.S.B.N.

THESES CANADIENNES SUR MICROFICHE

National Library of Canada
Collections Development Branch

Canadian Theses on
Microfiche Service

Ottawa, Canada
K1A 0N4

Bibliothèque nationale du Canada
Direction du développement des collections

Service des thèses canadiennes
sur microfiche

NOTICE

The quality of this microfiche is heavily dependent upon the quality of the original thesis submitted for microfilming. Every effort has been made to ensure the highest quality of reproduction possible.

If pages are missing, contact the university which granted the degree.

Some pages may have indistinct print especially if the original pages were typed with a poor typewriter ribbon or if the university sent us a poor photocopy.

Previously copyrighted materials (journal articles, published tests, etc.) are not filmed.

Reproduction in full or in part of this film is governed by the Canadian Copyright Act, R.S.C. 1970, c. C-30. Please read the authorization forms which accompany this thesis.

THIS DISSERTATION
HAS BEEN MICROFILMED
EXACTLY AS RECEIVED

AVIS

La qualité de cette microfiche dépend grandement de la qualité de la thèse soumise au microfilmage. Nous avons tout fait pour assurer une qualité supérieure de reproduction.

S'il manque des pages, veuillez communiquer avec l'université qui a conféré le grade.

La qualité d'impression de certaines pages peut laisser à désirer, surtout si les pages originales ont été dactylographiées à l'aide d'un ruban usé ou si l'université nous a fait parvenir une photocopie de mauvaise qualité.

Les documents qui font déjà l'objet d'un droit d'auteur (articles de revue, examens publiés, etc.) ne sont pas microfilmés.

La reproduction, même partielle, de ce microfilm est soumise à la Loi canadienne sur le droit d'auteur, SRC 1970, c. C-30. Veuillez prendre connaissance des formules d'autorisation qui accompagnent cette thèse.

LA THÈSE A ÉTÉ
MICROFILMÉE TELLE QUE
NOUS L'AVONS REÇUE

NL-339 (r. 82/08)

Canada

NUCLEAR MAGNETIC RESONANCE AND ELECTRON PARAMAGNETIC RESONANCE STUDIES OF MEMBRANE PROBES

by

Michael Gerard Taylor

A thesis presented to the School of Graduate Studies
and Research of the University of Ottawa
in partial fulfillment of the requirements
for the degree of Doctor of Philosophy

Ottawa, Ontario
August 1981

TO MY FAMILY

From the books of Bokonon:

We do, doodley do, doodley do, doodley do,
What we must, muddily must, muddily must, muddily must;
Muddily do, muddily do, muddily do, muddily do,
Until we bust, bodily bust, bodily bust, bodily bust.

- Kurt Vonnegut, Jr.
in "Cat's Cradle"

ABSTRACT

The study presented here deals with the properties of magnetic resonance probes used in the study of the structure and dynamics of phospholipid membranes. Emphasis is placed on the utility of the various probes as reporters of membrane properties.

The reliability of the widely used nitroxide spin probes is examined. Since these probes are not natural membrane components, it cannot be assumed that the spin probe data accurately reflect the true state of the membrane. The reliability of the spin probes is tested by comparison of data derived from EPR spectroscopy of nitroxide spin probes and ^{2}H NMR spectroscopy of deuterium-labelled analogs. The deuterium nucleus is a non-perturbing reporter of the state of the membrane, so that the ^{2}H NMR results serve as a calibration reference for the spin probe EPR results. Several discrepancies are noted between for the spectral behaviour of each type of probe. For labelled fatty acid probes, the most severe discrepancies are noted for spin probes bearing nitroxide labels at positions 5-9 of the fatty acid chain. For these label positions, the spin probe data does not show even qualitative agreement with the reference ^{2}H NMR data. For nitroxide labels at positions 12-16 of the fatty acid, the spin probes display qualitatively reliable behaviour, although poor quantitative agreement with the ^{2}H NMR results is found as in the

case of the nitroxides labelled at positions 5-9. In contrast, good qualitative and quantitative agreement is found in the comparison of nitroxide- and deuterium-labelled steroids.

Further studies examine the feasibility of employing nitroxide spin probes in the study of the bulk phase behaviour of phospholipids which exhibit mesomorphic phase transitions. In this work, the spin probe behaviour is compared with that of the non-perturbing ^{31}P and ^{2}H NMR probes. It is shown that problems associated with the time scale resolutions of the different magnetic resonance probes rule out the use of nitroxide spin probes in such studies.

The anomalous behaviour of the nitroxide probes is investigated in greater detail using ^{2}H NMR of specifically deuterium-labelled nitroxides. ^{2}H NMR provides a closer examination of the properties of the spin probes. These data, combined with the results of the comparison studies suggest that the details of the geometry of the nitroxide spin probes intercalated in phospholipid membranes seriously contribute to the anomalous behaviour noted for the nitroxides. Although it is not possible to determine conclusively all the sources of anomalies due to the multiplicity of factors governing magnetic resonance spectra, some suggestions are made for the choice of spin probes to obtain reliable information in membrane studies.

^{2}H NMR is also used to probe the behaviour of cholesterol in membranes. The amplitude and symmetry of the anisotropic motion of cholesterol is examined with the measurement of residual quadrupole splittings for several deuterium label sites on the sterol. These studies yield the orientation of cholesterol in the membrane and provide information on the motional behaviour of different regions of the molecule. The dynamic aspects of the motion of the probe are investigated using measurements of the ^{2}H nuclear spin relaxation times.

ACKNOWLEDGEMENTS

It is a pleasure to thank the many individuals who provided assistance in the course of my studies. In particular I wish to thank Drs. A.P. Tulloch and T. Akiyama for their generous gifts of compounds; Dr. Harold Jarrell, without whose advice concerning synthetic organic procedures, even lower yields would have been obtained; Dr. R. Andrew Byrd, whose home-built ^{2}H NMR probe, software modifications and advice concerning operation of the spectrometer aided in the NMR studies; Dr. Keith Butler for his assistance in the EPR studies and Mrs. Lise Bramall whose encyclopedic knowledge of the IBM/TSS system and inexhaustible supply of patience aided greatly in the writing of computer programs. I would also like to express my gratitude to all the members of the Molecular Biophysics group. The congenial atmosphere, diversity of interests and excellent technical support in the group provided a unique learning experience. Comic relief was graciously supplied by my fellow graduate students. I am grateful to the National Research Council for allowing me to use facilities through the Guest Worker program and to the Natural Sciences and Engineering Research Council for financial support. The manuscript was expertly typed by Mrs. Yvonne Rowe.

Finally, I wish to express my gratitude to my supervisor, Dr. Ian C.P. Smith for providing advice, support, and most importantly, a challenge during our association.

TABLE OF CONTENTS

ABBREVIATIONS

CSA	Chemical Shift (Shielding) Anisotropy
CSL	Doxyl Derivative of Cholestan-3-one
Doxyl	Trivial Name for the N-oxyl-4',4'-Dimethyloxazolidinyl Derivatives of Ketones
EPR	Electron Paramagnetic Resonance
FID	Free Induction Decay
FT	Fourier Transform
Lyso PC	Lysolecithin, 1-acyl-sn-glycero-3-phosphocholine
NMR	Nuclear Magnetic Resonance
PC	Phosphatidylcholine,1,2-diacyl-sn-glycero-3-phosphocholine
PC-n-SASL-d_2	PC Derived by Acylation of Lyso PC with n-SASL-d_2
PE	Phosphatidylethanolamine,1,2-diacyl-sn-glycero-3-phosphoethanolamine
PE-d_4	PE Derived by Transphophatidylation of egg PC with Ethanolamine-1,2,2,2-d_4
ppm	Parts per Million
n-SASL	Stearic Acid Spin Label, the Doxyl Derivative of n-oxostearic Acid
n-SASL-d_2	Spin Label Derived from Condensation of n-oxostearic Acid and 2-amino-2-methyl-1-propanol-1,1-d_2
5-SASL-d_6	Doxyl Derivative of 5-oxostearic Acid-2,2,4,4,6,6-d_6
S_{mol}	Order Parameter Referenced to the Axis of Motional Averaging of a Molecule
S_Z	Order Parameter Referenced to the Z-axis of a Label

FIGURE CAPTIONS

Figure 1. A. Schematic representation of the molecular structure of the phospholipids. B. Structure of the lamellar bilayer phase adopted by lipids dispersed in water. The lamellae are separated by aqueous layers. C. Structure of the H_I hexagonal phase. The cylinders form hexagonally packed assemblies.

Figure 2. Variation of the EPR spectra observed for different orientations of a nitroxide. The angle θ is between the magnetic field and the axis of motional averaging of the probe.

Figure 3. Variation of the ^2H NMR spectra observed for different orientations of a deuterium-labelled fragment. The angle θ is between the field and the axis of motional averaging.

Figure 4. Variation of the ^{31}P spectra observed for different orientations of a phosphate group. The angle θ is between the field and the axis of motional averaging.

Figure 5. Angular distribution function for spherical symmetry. The axes of motional averaging are oriented with equal probability over the sphere. All axes falling on the indicated circle are at angle θ to the field. The lower portion illustrates the powder spectra observed in EPR, ^{31}P- and ^2H-NMR.

Figure 6. Order parameter description of anisotropic motion. The rectangle represents a molecule in the membrane with a magnetic resonance reporter group.

Figure 7. Structures of nitroxide spin probes employed.

Figure 8. Structure of the 12-SASL spin probe, illustrating the components of the static hyperfine coupling tensor.

Figure 9. Representative EPR spectra for fatty acid spin probes in oriented lipid samples. Solid line spectra taken with the field parallel to the phospholipid long axes. Broken line spectra taken with the field perpendicular to the long axes.

Figure 10. Representative spin probe EPR spectra for liposome samples.

Figure 11. Variation of molecular order parameters derived from EPR and ^2H NMR measurements with increasing cholesterol concentration in egg PC bilayers. The label position for each probe is indicated on the Figure.

Figure 12. Order parameter label position profiles for ^2H NMR and EPR of labelled stearic acid probes for zero (circles) and 30 mole % cholesterol (squares).

Figure 13. Ratio of the spin probe and ^2H NMR order parameters at zero (circles) and 30 mole % cholesterol (squares).

Figure 14. Cholesterol response profiles for ^2H NMR and EPR probes. Δ is 1000 x the slope of the S vs. cholesterol concentration line in Figure 11. For the EPR profile, the solid line is for oriented films and the broken line is for liposomes.

Figure 15. Ratio of the Δ parameter for EPR and ^2H probes. The solid line is for ratios calculated for oriented film EPR experiments and the broken line is derived from liposome samples.

Figure 16. Schematic representation of the interaction between cholesterol and a nitroxide-labelled fatty acid. The rectangle represents cholesterol and the ellipse on the fatty acid chain represents the area occupied by the nitroxide group.

Figure 17. Structure of the cholestane spin label (CSL) showing the components of the hyperfine coupling tensor.

Figure 18. A. EPR spectrum of CSL in an oriented film. B. ^2H NMR spectrum of cholesterol-3α-d_1 in bilayers. Both spectra are for 40 mole % cholesterol in egg PC. The measurements of the spectral parameters for calculations of order parameters are shown.

Figure 19. Temperature dependence of the order parameters derived from CSL (triangles) and cholesterol-3α-d_1 (squares) for 30 mole % cholesterol.

Figure 20. Variation of order parameters with cholesterol concentration for CSL (triangles) and cholesterol-3α-d_1 (squares). Sample temperatures: CSL, 25°C; cholesterol-3α-d_1, 30°C.

Figure 21. Angular dependence of the hyperfine splittings for CSL (squares), 5-SASL (triangles) and 14-SASL (crosses). The angle θ was measured between the direction of the static magnetic field and the normal to the flat cell surface.

Figure 22. Temperature variation of EPR spectra in equimolar cholesterol-Egg PE for A. 5-SASL and B. 12-SASL.

Figure 23. End view of single cylinder representing hexagonal phase lipids. The long axes of the probes radiate from the

centre of the circle. The angle θ is between field direction and the probe's director.

Figure 24. Simulated EPR spectra for CSL in a single cylinder. The angle α is between the field and the cylinder long axis. Spectral simulation parameters are given in Appendix I.

Figure 25. Simulated EPR spectra for CSL in an ensemble of cylinders oriented on a flat surface. The long axes of the cylinder are randomly distributed in the plane of the surface. The angle ϕ is between the field and the normal to the flat surface.

Figure 26. Experimental EPR spectra for CSL in equimolar cholesterol-Egg PE at 35°C oriented in a flat cell. The measured angle is between the field and the normal to the flat cell surface.

Figure 27. Temperature variation of the EPR spectra of CSL in equimolar cholesterol-Egg PE taken with the field parallel (solid line) and perpendicular (broken line) to the normal to the flat cell surface.

Figure 28. Simulated EPR spectra for CSL for two types of lipid organization in oriented systems. A. Planar distribution of cylinders. B. Summation of spectra for oriented bilayers (10 mole %) plus random dispersions (90 mole %). In A and B, the field is parallel (solid line) and perpendicular (broken line) to the normal to the flat cell surface.

Figure 29. Temperature-dependence of the ^{31}P and ^{2}H spectra of an equimolar mixture of cholesterol and PE derived from egg PC via transphosphatidylation with deuterated ethanolamine. ^{31}P spectra; 125 KHz sweep width, 0.17 s. recycle time, 1500-5000 transients: ^{2}H spectra; 250 KHz sweep width, 0.1 s. recycle time, 6000 transients. The sample contained 150 mg total lipids in 0.5 ml buffer.

Figure 30. ^{2}H NMR spectra of 5-SASL-2,2,4,4,6,6,-d_6 in egg PC membranes with the indicated cholesterol concentrations at 30°C. Spectra were recorded with a recycle time of 0.1 s. acquiring 72,000 scans.

Figure 31. Variation of observed quadrupole splittings with cholesterol concentration for the 2-10 positions of stearic acid (squares), the 2 position of 5-SASL-d_6 (triangles), and the 4, 6 positions of 5-SASL-d_6 (diamonds).

Figure 32. ^2H NMR spectra of the phospholipid spin probes deuterated at the methylene carbon of the oxozalidine ring for position 5 (a), and 12 (B). The probes were incorporated at 5 mole % in egg PC bilayers at 25°C. Spectra were accumulated using a recycle time of 0.1 seconds with a total accumulation time of 8-10 hours.

Figure 33. ^2H NMR spectra of the hydroxylamine derivatives of the phospholipid spin probes deuterated at the methylene carbon of the oxozalidine ring for position 5 (A), and 12 (B). Sample conditions as in Figure 32.

Figure 34. High resolution ^2H NMR spectrum, (46.1 MHz), of cholesterol-2,2,4,4,6,-d_5 in CCl_4 at 25°C and a concentration of approximately 50 mg/ml. Continuous broad-band ^1H decoupling was applied. 1,500 transients were collected with a recycle time of 4 seconds.

Figure 35. ^2H NMR spectrum, (46.1 MHz), of cholesterol-2,2,4,4,6-d_5 in egg phosphatidylcholine liposomes at 50 mole % concentration and 25°C. 150,000 transients were collected with a recycle time of 0.1 seconds.

Figure 36. ^2H NMR spectra, (46.1 MHz) of cholesterols, stereospecifically labelled as indicated at position 7 in egg phosphatidylcholine liposomes at 50 mole % concentration and 25°C. 50,000 transients were collected with a recycle time of 0.1 seconds.

Figure 37. Stereo plot of the A-D ring system of cholesterol. The small filled circles are the deuteron label positions used in this study. The straight line which passes through the oxygen atom represents the calculated orientation of the rotation axis.

Figure 38. Temperature dependence for observed quadrupole splittings for cholesterol-3α-d_1 (squares) and cholesterol-7,7-d_2 (triangles) in bilayers consisting of 30 mole % cholesterol in egg PC.

Figure 39. Variation of quadrupole splittings with cholesterol concentration for cholesterol-3α-d_1 and cholesterol-7,7-d_2 in egg PC bilayers at 30°C.

Figure 40. Variation with temperature (triangles) and cholesterol concentration (squares) of the derived molecular order parameters for cholesterol in egg PC.

TABLES

CHAPTER I

INTRODUCTION

I.1 Phospholipid Membranes

The phospholipids are a large class of naturally occurring molecules. They are widely studied due to their role in the formation of cell membranes (1). Figure 1A shows the general formula of a phospholipid. The general features of the phospholipids are: 1) a glycerol "backbone", 2) fatty acids ester linked to the 1 and 2 positions of glycerol, and 3) a phosphate ester at position 3 of glycerol. In natural phospholipids, a variety of fatty acids is found with differing chain lengths and degrees of unsaturation. In addition, the phosphate is usually esterified by a second alcohol to give different sub-classes of phospholipids. Thus, the general features of a phospholipid are a long, apolar hydrocarbon "tail" and a strongly polar "head group." This combination of polar and apolar regions in the molecule causes special solubility properties for the phospholipids. The polar head groups are readily hydrated but the apolar tails have low aqueous solubilities. When dispersed in water, the phospholipids may adopt a variety of structures which compensate for this solubility difference (2).

Figure 1B shows one of the phases available to hydrated phospholipids. In this lamellar bilayer phase, the polar

A.

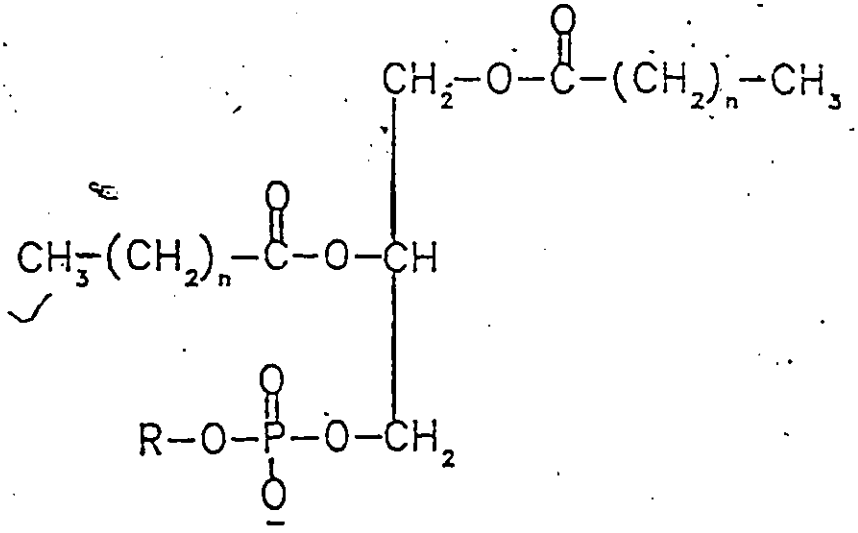

$R=CH_2CH_2\overset{+}{N}(CH_3)_3$

PHOSPHATIDYLCHOLINE (PC)

$R=CH_2CH_2\overset{+}{N}H_3$

PHOSPHATIDYLETHANOLAMINE (PE)

B. LAMELLAR BILAYER

C. HEXAGONAL

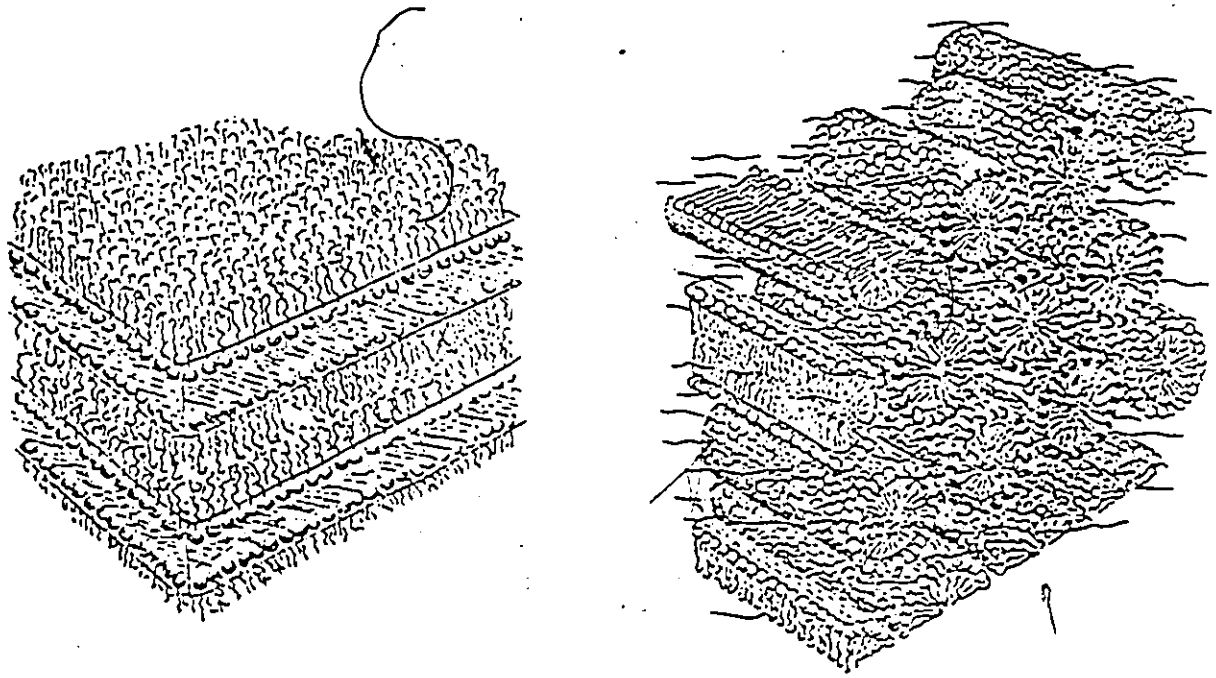

Figure 1. A. Schematic representation of the molecular structure of the phospholipids. B. Structure of the lamellar bilayer phase. The lamellae are separated by aqueous layers. C. Structure of the H_I hexagonal phase. Adapted from F.B. Rosevar, J. Soc. Cosmetic Chem., 19,581-94,(1968).

head groups are exposed to water while the apolar hydrocarbon tails have been removed from the aqueous medium. This phase is spontaneously formed by a large number of the sub-classes of phospholipids. Such a structure is very well suited to form a membrane between two aqueous compartments in a cell or organelle. Species present in the aqueous regions on either side of the membrane may not readily diffuse through the region of low dielectric constant in the hydrocarbon region.

A second phase available to the phospholipids is illustrated in in Figure 1C. In this phase, the lipids pack in long cylindrical rods with the polar head groups and associated water along the surface of the cylinder and the tails oriented perpendicular to the cylinder long axis. These cylindrical assemblies tend to associate with hexagonal packing into larger structures. This phase, with the head groups at the surface of the cylinder, is referred to as the H_I hexagonal phase.

The phase adopted by a particular phospholipid is determined by its concentration in water and the temperature. In the work presented here, two phospholipids were employed. The first, phosphatidylcholine derived from egg yolk (Egg PC), forms the lamellar bilayer phase. The second, phosphatidylethanolamine derived from egg yolk (Egg PE), exists in the lamellar bilayer phase at low temperature and undergoes a

transition to the H_{II} hexagonal phase as the temperature is increased. The H_{II} phase is similar to H_I, except that the polar head groups are located along cylindrical water channels in the interior of the lipid-water assemblies.

These liquid crystalline systems have been studied by a wide variety of physical techniques (3). Interest has been centred on their bulk phase behaviour, structure and conformation at the molecular level, and the dynamics of the lipid molecules. In the next section, the application of magnetic resonance techniques to the study of membrane systems will be discussed.

I.2 Magnetic Resonance in Membranes

The membrane phases described above are anisotropic structures. The amplitude of motion of a molecule in the membrane phase is restricted to a limited range about its equilibrium position. Such a molecule can best be studied by employing an experimental technique which is capable of exhibiting an anisotropic response in one of its properties. There are several such properties available for the magnetic resonance techniques. In the following discussion, the general features of these properties will be treated followed by specific examples for each of the magnetic resonance techniques employed in this work.

I.2.1 Tensor Representation and Motional Averaging

The properties discussed below may all be represented in the form of second rank tensors (4). An arbitrary property, P, may be described by the 3x3 matrix:

$$\begin{bmatrix} P_{xx} & P_{xy} & P_{xz} \\ P_{yx} & P_{yy} & P_{yz} \\ P_{zx} & P_{zy} & P_{zz} \end{bmatrix}$$

In order to use this representation, it is necessary to specify an axis system for the molecule, as shown below for a fragment, F, in the molecule.

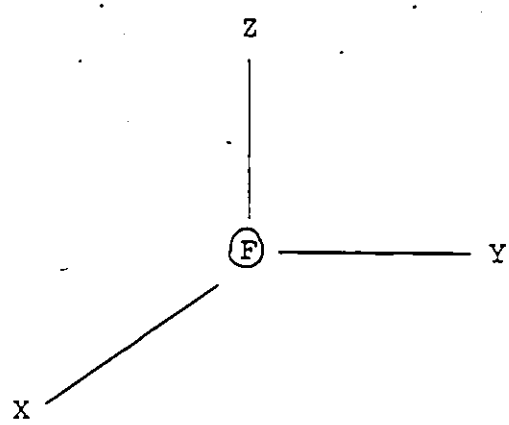

In this axis system, a measurement of P along the X axis will result in an observed value of P_{xx} and similarily for the other two axes. For a measurement along a arbitrary orientation, the observed value of the property is given by:

$$P = P_{xx}\text{Cos}^2\theta_x + P_{yy}\text{Cos}^2\theta_y + P_{zz}\text{Cos}^2\theta_z \qquad (1)$$

where the angles, θ, are between the direction along which the measurement is made and the axis indicated by the subscript. This treatment is appropriate for a static single crystal system.

Molecules in the membrane have a dynamic rather than static, nature and the presence of motion has a strong effect on the strengths of the observed anisotropic interactions (5, 6, 7). In a non-viscous liquid, rapid molecular tumbling allows the molecule, (and the reference axis system attached to a fragment), to rotate through all possible angles. This isotropic tumbling completely averages the anisotropic portion of the property P so that a measurement yields only the isotropic value of P. In the membrane, molecular motion is restricted in amplitude so that the magnetic resonance properties are not fully averaged. Motional averaging in a membrane is likely to be complicated, since membrane components have several degrees of rotational freedom. In general, the components of the motionally averaged tensor will reflect contributions from each of the three principal components of the static tensor. For an elongated, rod-like molecule such as a phospholipid, rotation about the long axis is expected to be much more facile than rotations perpendicular to the long axis. If the long axis rotation is of three-fold, or higher, symmetry, the static tensor is averaged to the axially-symmetric form (4):

$$\begin{bmatrix} P_{\perp} & 0 & 0 \\ 0 & P_{\perp} & 0 \\ 0 & 0 & P_{\parallel} \end{bmatrix}$$

where $P_{\parallel}$ is the averaged component along the rotation axis and $P_{\perp}$ is the component in the plane perpendicular to the rotation axis. As a simple example, if the molecule can rotate about only the Z axis, the components of the averaged tensor would be $P_{\parallel} = P_{zz}$ and $P_{\perp} = 1/2(P_{xx} + P_{yy})$. If this example were modified by allowing additional, restricted motion perpendicular to the long axis, the component $P_{\parallel}$ would then assume contributions from the static X and Y components as $P_{\perp}$ would take on a contribution from the Z component. As the amplitude of this restricted motion increases, the values of $P_{\parallel}$ and $P_{\perp}$ tend to converge and finally become equal at the isotropic tumbling limit where each of the static components makes equal contribution to the averaged tensor. Thus, the difference between $P_{\parallel}$ and $P_{\perp}$ can indicate the amplitude of restricted motion in the membrane.

An observation of the property P in a motionally averaged system has the same characteristics as one made in the static system. Thus, measurement parallel to the axis of motional averaging, (which is also referred to as the director), yields the value $P_{\parallel}$ and similarily measurement perpendicular to this axis yields $P_{\perp}$. For such an axially symmetric tensor, the

following simplification can be used. The tensor, P, can be replaced by an isotropic scalar part P_{ISO} which is observed for isotropic tumbling (and may be equal to zero), and an anisotropic scalar part P_{ANISO} which is equal to $2/3(P_{\parallel} - P_{\perp})$. In this case, the observed value of P for an arbitrary orientation is given by (7):

$$P = P_{ISO} + P_{ANISO} \times \frac{3\cos^2\theta - 1}{2} \qquad (2)$$

where θ is the angle between the measurement axis and the axis of motional averaging of the molecule. There are three noteworthy values of the angle θ. At $\theta = 0^\circ$, the anisotropic contribution to P is P_{ANISO}. At $\theta = 90^\circ$ the contribution is $-0.5\ P_{ANISO}$. When θ is equal to one half the tetrahedral angle ($\sim 54.7^\circ$), the so-called "magic angle", the function $(3\cos^2\theta - 1)/2$ is equal to zero and the anisotropic part of P disappears. Thus, for this orientation, the value of P is equal to its isotropic value, P_{ISO}.

With this general introduction, the particular properties of the technique employed in this work can be discussed. Each type of spectroscopy will be discussed in terms of the spectra expected for an oriented, axially symmetric phase. Such a system can be achieved by orienting multilayers of the lamellar bilayer phase (Figure 1B) on a planar surface. In this phase, the axis of motional averaging, Z' in this discussion, is

along the long axis of the phospholipid.

I.2.2 Electron Paramagnetic Resonance (EPR)

Much of the work presented here deals with the EPR spectroscopy of nitroxide free radical spin probes. For these probes, the anisotropic hyperfine coupling between the free electron and the nitrogen atom of the nitroxide system is exploited in membrane studies (8). The coupling of the electron with the spin=1 ^{14}N nucleus splits the EPR resonance into a 1:1:1 triplet. This coupling is inherently anisotropic due to the anisotropic circulation of the electron about the ^{14}N nucleus, particularly in the ^{14}N p orbital. The angular dependence of the hyperfine splitting, A, in an axially symmetric environment is shown in Figure 2. The hyperfine splitting is measured as one-half the separation of the outermost lines in the spectrum which is recorded in first derivative mode in order to enhance sensitivity. The hyperfine interaction has a non-zero isotropic part which is observed for a probe oriented at the magic angle with respect to the field or freely tumbling in solution.

I.2.3 Deuterium Nuclear Magnetic Resonance (^2H NMR)

The anisotropic interaction used in the ^2H NMR experiment is the coupling between the quadrupole moment of the nucleus and the anisotropic electric field gradient surrounding the

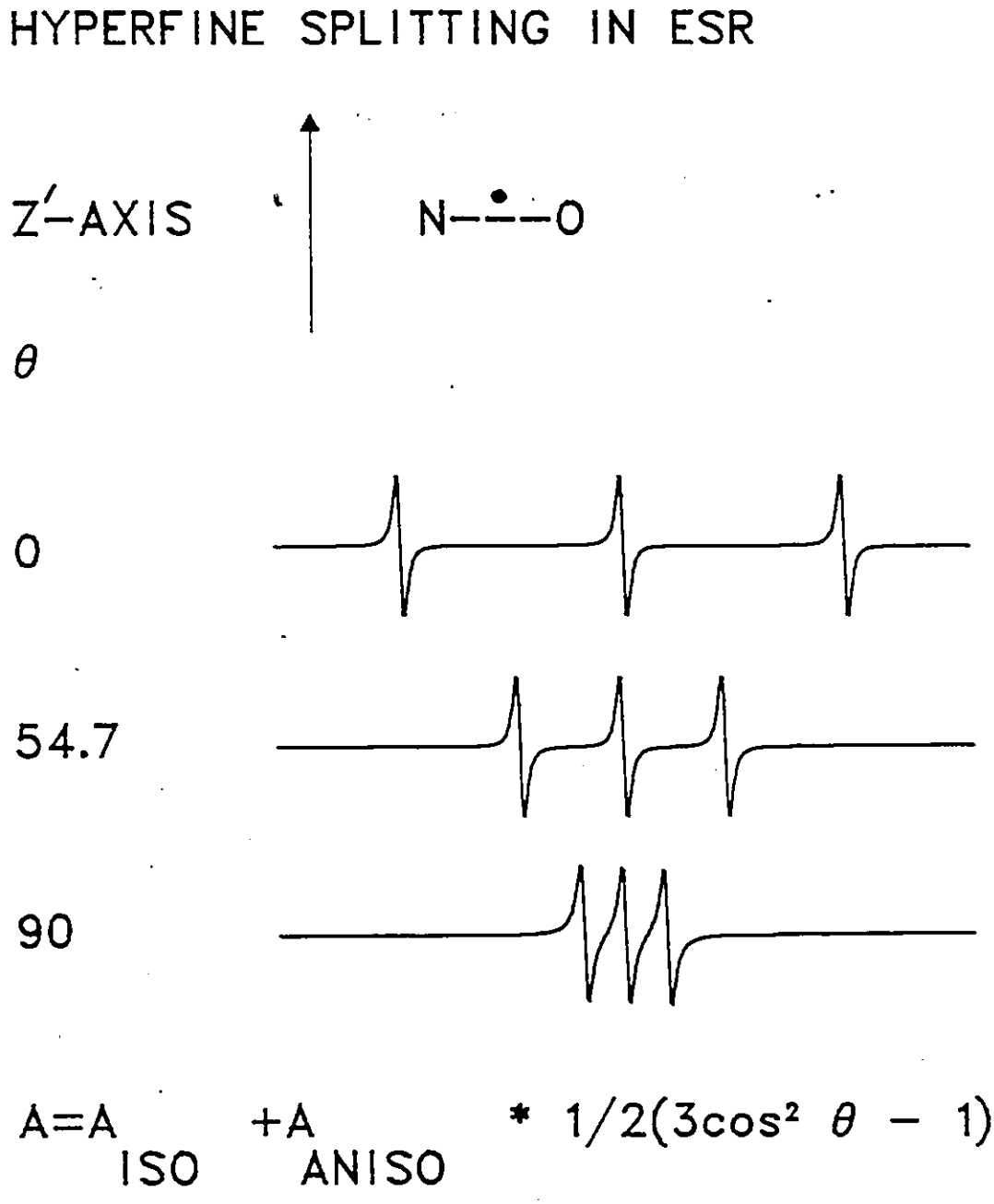

Figure 2. Variation of the EPR spectra observed for different orientations of a nitroxide. The angle θ is between the magnetic field and the axis of motional averaging of the probe.

deuterium nucleus (6, 9). This interaction splits the deuterium resonance into a 1:1 doublet. The magnitude of the splitting depends on the orientation of the electric field gradient with respect to the magnetic field in the fashion illustrated in Figure 3. The isotropic part of the interaction is zero, so that a single line is observed for a molecule at the magic angle or in free solution

I.2.4 Phosphorus-31 Nuclear Magnetic Resonance (^{31}P NMR)

The chemical shift anisotropy, (CSA), of the ^{31}P nucleus of a phospholipid can be used to study the motional state of a membrane phospholipid. The chemical shift of a ^{31}P nucleus is influenced by the distribution of electrons about the nucleus In a phosphate group, the electron distribution about the ^{31}P nucleus is spatially anisotropic, resulting in an orientation-dependent chemical shift (7). Figure 4 illustrates the orientation dependence of the shift for an axially symmetric environment. As for the other techniques described above, the isotropic value is observed at the magic angle. Since chemical shifts are relative values, the isotropic shift value is often used as a reference and is thus assigned a chemical shift of zero.

I.2.5 Spectra in Non-oriented Samples

The discussion above is appropriate for the description of samples which are oriented with a known direction for the

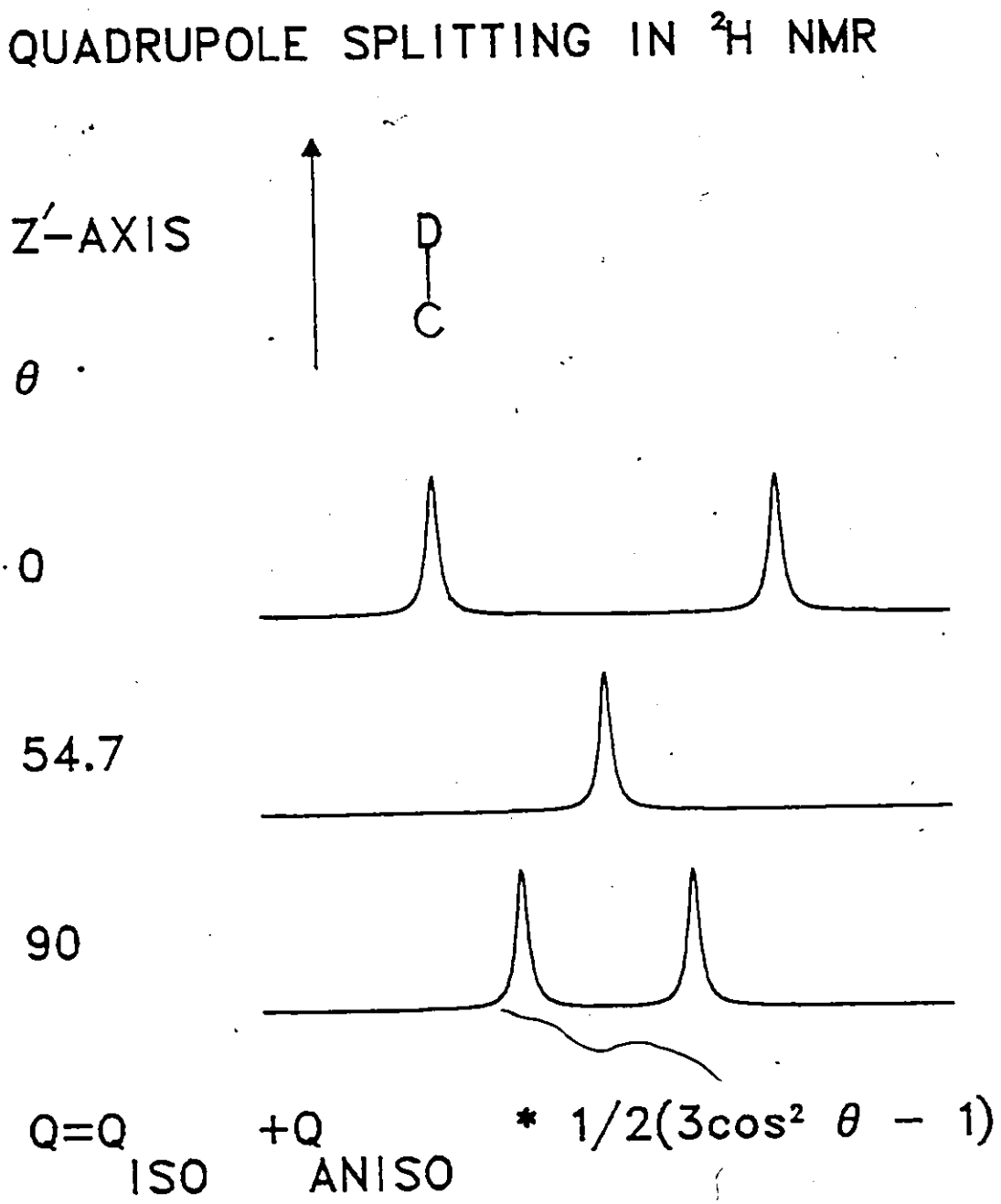

Figure 3. Variation of the ^{2}H NMR spectra observed for different orientations of a deuterium-labelled fragment. The angle θ is between the field and the axis of motional averaging.

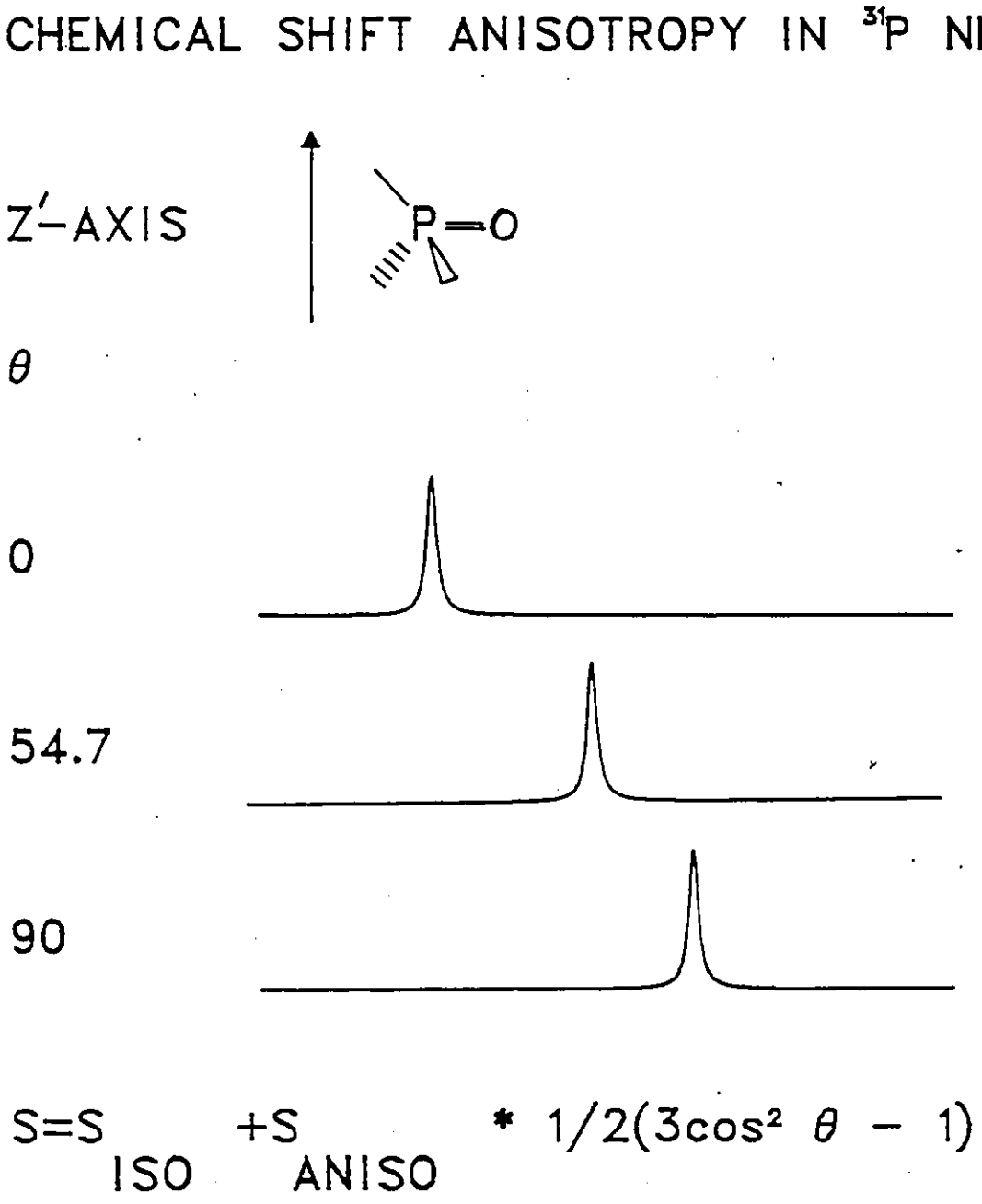

Figure 4. Variation of the ^{31}P spectra observed for different orientations of a phosphate group. The angle θ is between the field and the axis of motional averaging.

axis of motional averaging. It is not always possible to prepare membrane samples in which the phospholipids share a common orientation. In such cases, random dispersons of phospholipids, usually referred to as liposomes, may be used. In such a sample, the Z' axes of the phospholipids are oriented with equal probability over the surface of a sphere. In the magnetic resonance experiment, these axes are oriented with all possible angles, θ, with respect to the magnetic field. Spectra observed for these systems consist of a superposition of the sub-spectra expected for each value of θ. The various sub-spectra do not make equal contributions in intensity to the total lineshape. In Figure 5 the distribution of the Z' axes in a spherical sample is illustrated. For the indicated value of θ, all molecules with Z' axes oriented along the circumference of the circle indicated will contribute to the summed "powder" lineshape the value of the measured interaction for that value of θ. It is clear that as the value of θ is increased, the number of molecules oriented at θ will increase. Thus, there is a probability distribution $p(\theta)$ for finding a molecule oriented with Z' axis at θ which is given by: $p(\theta)=(1/2\pi)\sin\theta$ for a system with spherical symmetry (4). At the bottom of Figure 5, examples of the powder lineshapes for the three methods employed here are illustrated. In each case, comparison with the appropriate illustration for the oriented system (Figures 2, 3, 4) indicates that the greatest intensity in the

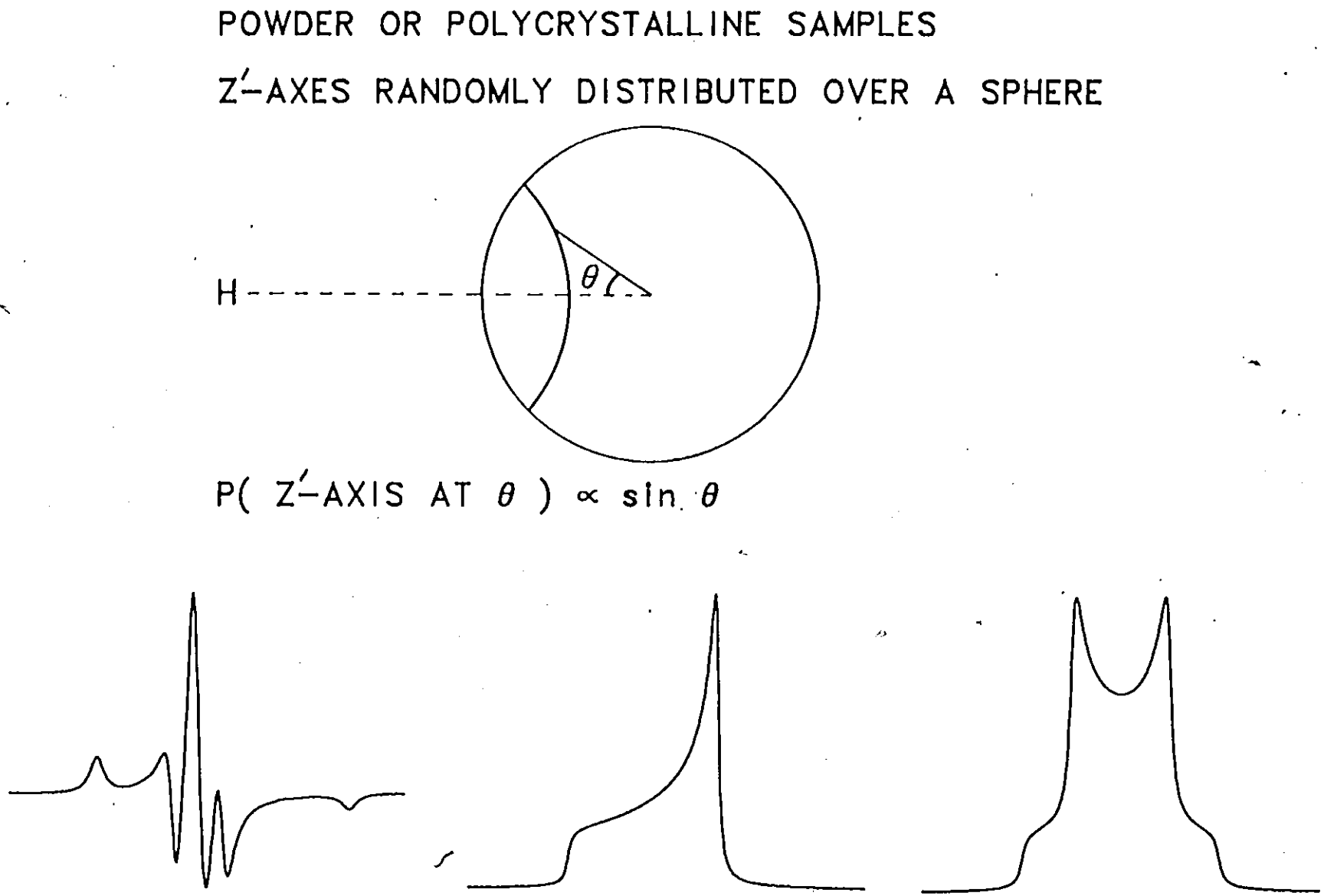

Figure 5. Angular distribution function for spherical symmetry. The axes of motional averaging are oriented with equal probability over the sphere. All axes falling on the indicated circle are at angle 0 to the field. The lower portion illustrates the powder spectra observed in EPR, ^{31}P- and ^{2}H-NMR.

powder spectrum is associated with molecules oriented with Z' close to 90°. Thus, the components $P_{\parallel}$, $P_{\perp}$ or the associated $P_{ANISO} = 2/3(P_{\parallel}-P_{\perp})$ can be measured from either a set of spectra for an oriented system at a variety of angles or a powder spectrum for a random dispersion sample.

I.2.6 Order Parameters

It was pointed out above that the restricted motion of a molecule in a membrane phase partially averages the anisotropic magnetic resonance properties. The extent to which a static anisotropy is averaged is indicative of the nature of the motion present in the membrane. For the EPR and ^2H NMR experiments discussed here, the degree of motional averaging can readily be expressed in quantitative form using the order parameter. The order parameter S_i for a reference axis, i, is defined as (6):

$$S_i = \frac{1}{2} < 3 \, Cos^2 \, \gamma_i - 1 > \qquad (3)$$

where γ_i is the angle between the axis of motional averaging and the instantaneous orientation of the i reference axis. The angular brackets indicate that a time average is taken over the fluctuations of the reference axis. The angle γ_i can be expressed in terms of two angles, α and β as shown in Figure 6. The angle β measures the fluctuations of the molecule about its equilibrium position. The angle α measures the angle between the reference axis and the director axis.

MOTIONAL AVERAGING AND ORDER PARAMETERS

THE ANGLE α IS FIXED BY THE GEOMETRY OF THE LABEL ON THE MOLECULE

THE ANGLE β FLUCTUATES IN TIME AS THE MOLECULE UNDERGOES ANISOTROPIC REORIENTATION ABOUT THE DIRECTOR AXIS

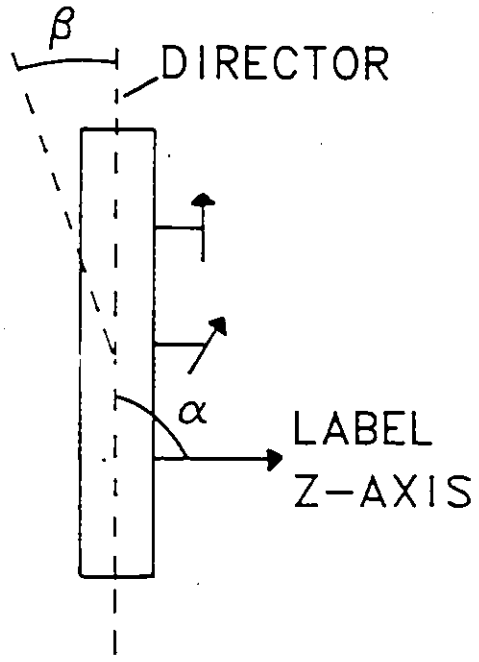

$$S_z = 1/2\ (3\cos^2\alpha - 1) \times 1/2\ \langle 3\cos^2\beta - 1 \rangle$$

$$S_{MOL} = \frac{S_z}{1/2\ (3\cos^2\alpha - 1)}$$

Figure 6. Order parameter description of anisotropic motion. The rectangle represents a molecule in the membrane with a magnetic resonance reporter group.

The angle α is fixed by the geometry of the reporter group with respect to the molecule. For the case shown in Figure 6, the order parameter for the Z axis is given by:

$$S_Z = \frac{1}{2}(3\ \mathrm{Cos}^2\alpha - 1) \cdot \frac{1}{2} < 3\ \mathrm{Cos}^2\beta - 1 > \qquad (4)$$

Thus, the order parameter depends on both the random fluctuations of the molecule (β term) and the particular orientation of the label under observation (α term). Since the angle, α, is fixed, its effect on the order parameter can be removed to allow calculation of an order parameter for the molecule. This molecular order parameter, S_{mol}, is given by (6):

$$S_{mol} = \frac{S_i}{\frac{1}{2}(3\ \mathrm{Cos}^2\alpha_i - 1)} \qquad (5)$$

where α_i is the angle between the reference axis and the motional averaging axis. S_{mol} represents only the fluctuation of the molecule and is independent of the geometry of the reporter group used. The magnitude of S_{mol} varies from 1 for the perfectly ordered system and decreases as the amplitude of fluctuations increases. For a system undergoing isotropic reorientation, S_{mol} is equal to 0. The calculation of order parameters is described in detail in the Results Sections.

CHAPTER II

SCOPE OF THE STUDIES

Magnetic resonance techniques have been widely applied to the study of model and biological membrane systems. Excellent reviews are available for the applications of nitroxide spin probe EPR (8, 10), ^{2}H NMR (6, 9, 11) and ^{31}P NMR (7, 12) in membranes.

Two main subjects are dealt with in this work. Firstly, the reliability of the nitroxide spin probes as reporters of membrane properties was examined. The validity of the interpretation of the EPR spectra of the spin probes in terms of the properties of membranes is questionable since the probes are not natural membrane constituents. The possible problems associated with the use of spin probes were investigated through comparison of the data derived from EPR spin probe studies and parallel studies employing the non-perturbing NMR probes. Order parameter trends for variation of label position, cholesterol concentration and temperature were compared for nitroxide- and deuterium-labelled fatty acids and steroids intercalated in egg phosphatidylcholine membranes. The EPR spectral behaviour of the spin probes in a phospholipid system which undergoes a lamellar to hexagonal phase transition was compared with the behaviour of ^{2}H and ^{31}P NMR probes. Finally, the spin probes were examined in greater detail using ^{2}H NMR

of specifically deuterium-labelled nitroxides.

Secondly, the properties of cholesterol in egg phosphatidylcholine were examined using ^2H NMR of a series of specifically deuterium-labelled probes. The orientation of cholesterol in the membrane was determined through analysis of the residual quadrupole splittings of probes with different label positions. Knowledge of the orientation of the probe allowed an analysis of the amplitude of motion of cholesterol in terms of molecular order parameters for variation of temperature or cholesterol concentration. Differences in motional properties for different regions of the cholesterol molecule were examined using various labelling sites. Finally, dynamic aspects of the motion of the sterol were probed through the measurement of nuclear spin relaxation times.

CHAPTER III

MATERIALS AND METHODS

III.1 Syntheses

III.1.1 Phosphatidylcholine

The method of Singleton et al. (13) was slightly modified. The yolks of 30 extra large eggs (~600 g) were homogenized in 1 ℓ acetone. The suspension was then filtered through Whatman No. 1 paper with suction. The solids were then treated as above three more times. The resulting precipitate from the fourth acetone treatment was homogenized in 1 ℓ 95% ethanol. The filtrate was stored and the precipitate re-homogenized with 500 ml 95% ethanol. The combined ethanol filtrates were evaporated to dryness at 30°C and then placed under high vacuum. The resulting yellow syrup was dissolved in 200 ml ether. The ether solution was vigorously stirred under N_2 and 800 ml acetone was added. The suspension was then stirred in the refrigerator for 10 minutes. The precipitate was allowed to settle and the solvent was decanted. The precipitate was treated with ether and acetone as above twice more. After the final treatment, the solids were dried under vacuum and then dissolved in 100 ml $CHCl_3$.

Column chromatography was carried out on 500 g alumina (Woelm Activity I). The column was packed in $CHCl_3$ and allowed to settle. After washing the column with $CHCl_3$, the

lipids were loaded onto the column in $CHCl_3$. Elution was started with $CHCl_3$ at a flow rate of 10 ml/min. A rapidly moving yellow band was first eluted completely. The solvent was then changed to: $CHCl_3/CH_3OH$ (9/1). Fractions, (250 ml), were collected under N_2 and were tested by thin layer chromatography on silica gel plates in the solvent system: $CHCl_3/CH_3OH/H_2O$ (65/25/4). The first fractions contained neutral lipids (R_f ~.9). Subsequent fractions contained phosphatidylcholine at high concentration. Elution was continued until the appearance of sphingomeylin or lyso-phosphatidylcholine. Fractions containing phosphatidylcholine were combined and evaporated to dryness. The product was dissolved in re-distilled hexane and 1500 ml re-distilled acetone was added under N_2 with vigorous stirring. The suspension was then stirred in the refrigerator for 15 minutes. The precipitate was then rapidly filtered with suction and transferred while still moist to a beaker where it was flushed with N_2. The product was dissolved in 50 ml $CHCl_3/CH_3OH$ (1/1, re-distilled) and centrifuged 10 min at 5000 x g to remove alumina particles. The supernatant was stored tightly stopperd under N_2 at -20°C. The final product was colourless and chromatographically homogeneous. Yields varied to a maximum of ~14 g. The distribution of fatty acids, as determined by gas-liquid chromatography, coresponded to reported distributions.

III.1.2 Lysolecithin From Egg PC

Egg PC (11 g) was dissolved in 1 ℓ diethyl ether containing 25 ml methanol. Lyophilized Crotaleus adamanteus venom (50 mg, Sigma) was dissolved in 10 ml buffer (14) (0.22 M NaCl, 0.02 M $CaCl_2$, 1 mM EDTA, pH 7.5). The ether solution was vigorously stirred and the buffered enzyme solution was added. Addition of enzyme was repeated after 5 and 10 minutes of reaction (15). Precipitate appeared after addition of the second aliquot. Stirring was continued for 20 minutes after all the enzyme had been added. Solvents were then removed under reduced pressure. The residue was taken up in 250 ml methanol and centrifuged 10 min at 500 rpm. The methanol supernatant was evaporated and solids were dissolved in chloroform (~25 ml). The lysolecithin was purified by column chromatography on 400 g silicic acid (Biosil, 100-200 mesh). The column was prepared in chloroform and lipids were washed onto the column in chloroform. Elution was carried out using methanol in chloroform in the following proportions and volumes:

% methanol in chloroform	Volume ℓ
0	1
25	1
37.5	1
50	1
75	2

The lysolecithin began to elute after the 75% methanol and elution was continued with this solvent until lysolecithin was removed. Elution of the lysolecithin from the column was monitored via thin layer chromatography. Fractions containing lysolecithin were pooled and evaporated to dryness. The solid was dissolved in absolute ethanol and precipitated with diethyl ether. The precipitate was filtered and dried under vacuum to yield 3.2 g lysolecithin. Lysolecithin from another source appeared to contain alcohol which interferes in the acylation of lysolecithin. To avoid this problem, the lysolecithin was lyophilised twice from 100 ml water. This procedure has a secondary advantage, in that the freeze-dried material is very finely divided and can thus be readily dispersed in the organic solvents used in subsequent acylations.

III.1.3 Methyl-5-Oxostearate

The procedure for 5-oxopalmitate (16) was adopted. Magnesium turnings (4.8 g) were covered with 100 ml anhydrous diethyl ether. An ether solution (100 ml) of 1-bromotridecane (50 g) was added slowly to the magnesium. After addition of approximately 25 ml of the bromide, a crystal of iodine was added. After initiation of the reaction, the remaining bromide was added at a rate which maintained a gentle reflux (~20 min.). After the addition was complete, the solution was refluxed a further 20 minutes so that little unreacted magnesium remained.

The ether solution was then cooled in an ice bath and anhydrous $CdCl_2$ (18 g) was added in a single portion with vigorous stirring. The ice bath was removed and the solution was stirred for 30 minutes. Ether was almost completely removed by distillation under water aspirator vacuum. Dry benzene (300 ml) was added and the suspension was broken up with vigorous stirring. A solution of methyl-4-(chloroformyl)-butyrate (33 g) in benzene (70 ml) was added over 10 minutes. The solution was stirred rapidly and heated to reflux. After 10 minutes, a gel-like precipitate formed so that the solution could not be stirred efficiently. In order to avoid charring, heating was removed and the suspension was stirred for an additional 40 minutes. The mixture was then cooled in an ice bath and 100 ml water was added over 10 minutes. The mixture was transferred to a separatory funnel and 200 ml 0.1 N H_2SO_4 was added. The aqueous layer was removed and the benzene layer was washed with 500 ml H_2O. The benzene solution was separated and dried over anhydrous Na_2SO_4. After filtering, the solution was evaporated to dryness and pumped under high vacuum overnight. The solids were recrystallised twice from hexane to yield 30 g methyl-5-oxostearate.

III.1.4 Methyl-12-Oxostearate

Crude 12-hydroxy stearic acid (Eastman) was converted to its methyl ester. The crude methyl-12-hydroxystearic acid (3 g) was dissolved in 50 ml acetone. Oxidizing agent,

(1 g $Na_2Cr_2O_7.2H_2O$) in 10 ml 35% H_2SO_4) was added to the acetone solution dropwise over 5 minutes (17). The mixture was stirred and maintained at 10°C in a water bath during the addition. A dark oil separated during the reaction. Water (50 ml) was added and the solution was brought to room temperature. The mixture was then extracted with ether (100 ml, 50 ml, 25 ml). The combined ether extracts were dried over Na_2SO_4 and evaporated to dryness to yield 2 g methyl-12-oxostearate. Purity was improved by crystallization from hexane as indicated by thin layer chromatography on silica gel plates with solvent system: hexane/ether (7/3). Purity of the oxo-stearates was also monitored by ^{13}C-NMR.

III.1.5 Spin Labelled Stearic Acids (X-SASL)

For the preparation of non-deuterium-labelled spin probes, the method of Waggoner et al. (18) was employed. For the deuterated species, the oxazolidine step was modified to avoid the use of acid catalyst and the use of a large excess of 2-amino-2-methyl-1-propanol. The modified method is illustrated by the preparation of 5-SASL-2,2,4,4,6,6-d_6.

In order to avoid deuterium exchange, the labile protons of 2-amino-2-methyl-1-propanol were removed by treatment with a 60-fold excess of D_2O followed by removal of the water under reduced pressure. This step was omitted for synthesis of non-labelled spin probes or syntheses using labelled amino

alcohol. The amino alcohol (1.3 g) and the methyl-oxostearate were dissolved in 25 ml dry benzene. To this solution was added I_2 (~10 mg) (19) and the solution was refluxed under N_2, with disappearance of the I_2 colour, in a flask fitted with a Dean Stark trap for removal of water. The side arm of the trap was charged with molecular sieve 3A (Linde) and filled with dry benzene. The progress of the reaction was monitored by thin layer chromatography of the reaction mixture on silica gel plates in the solvent system: hexane/ether (7/3). In this system, the methyl oxostearate has R_f~0.6 and the oxazolidine has R_f~0.2 The reflux was terminated after 1 week.

The solution was extracted twice with saturated $NaHCO_3$ (50 ml) and H_2O (50 ml). The benzene phase was dried with Na_2SO_4 and evaporated to dryness. The lightly coloured syrup was then dissolved in ether (100 ml) and stirred in an ice bath. A solution of m-chloroperbenzoic acid (1.7 g in 50 ml ether) was added dropwise over 30 minutes. A yellow colour developed in the stirred solution during the addition. After the addition, the solution was stirred at room temperature for 2 days. The ether solution was then extracted with saturated NaCl (100 ml). The ether phase was dried over Na_2SO_4 and reduced in volume to 50 ml. The solution was cooled to -20°C to precipitate excess oxo-ester and was centrifuged 10 minutes at 5000 x g. The supernatant was then evaporated to dryness.

Preliminary purification was carried out by column chromatography on 100 g silica gel (60-200 mesh) eluting with 10% ethyl acetate in hexane. The yellow nitroxide band was collected and solvent was evaporated to yield 700 mg slightly contaminated product. Final purification was carried out by preparative thin layer chormatography on five 20 cm X 20 cm silica gel plates (0.5 mm thickness). The plates were developed twice in hexane/ether (7/3). The yellow nitroxide band was scraped off the plate and silica gel was stirred in 100 ml methanol for 1 hour. The suspension was filtered to remove the silica gel particles and the filtrate was evaporated to dryness to yield ~500 mg methyl-5-SASL-d_6.

The methyl ester was hydrolysed by refluxing in 90% aqueous methanol containing a slight excess of NaOH for three hours. The solution was acidified (0.1 N HCl) and extracted by addition of $CHCl_3$ and H_2O to the methanolic solution to give a mixture with solvents in the proportions: $CHCl_3/CH_3OH/H_2O$) (2/2/1.8) which yields two phases. The $CHCl_3$ phase was dried with Na_2SO_4 and evaporated to dryness to yield 420 mg 5-SASL-d_6.

III.1.6 2-amino-2-methyl-1-propanol-1, 1-d_2

The labile protons of 2-amino-2-methyl-1-propanol (45 g, .5 mole) were exchanged by addition of 30 ml D_2O followed by removal of water under reduced pressure. This procedure was repeated twice more. Approximately 25 g of Raney nickel

suspended in water (W.R. Grace) was washed three times with 20 ml D_2O to remove H_2O. The Raney nickel/D_2O suspension was added to the amino alcohol solution and the mixture was refluxed under N_2. The exchange was monitored by ^1H NMR. After 1.5 hours reflux, 50 ml water was distilled off and replaced by fresh D_2O. After a further 45 minute reflux, the suspension was cooled and filtered to remove the catalyst which was subsequently decomposed with 6N HCl. The filtrate was distilled to remove D_2O and the amino alcohol was collected at boiling point 164-166°C, yield 13 g. ^1H NMR indicated greater than 90% exchange at the 1 position.

III.1.7 Methyl-5-oxostearate-2,2,4,4,6,6-d_6

Methyl-5-oxostearate was hydrolyzed by refluxing in 90% aqueous methanol with a slight excess of NaOH. The salt was acidified and extracted to yield 5-oxostearic acid. The acid (10 g) was suspended in 200 ml H_2O at 90°C and was neutralized by addition of 0.1 N NaOH; water was removed by lyophilization. The sodium salt (10 g) was suspended in 100 ml D_2O containing 1 g NaOD and was transferred to a stainless steel autoclave. The suspension was heated at 200°C during 60 hours (20). After cooling, the gel-like soap was removed from the autoclave, using H_2O to remove final traces. The suspension was brought to pH 3 using 1 N HCl and immediately extracted with $CHCl_3$. The chloroform solution was dried with Na_2SO_4 and evaporated to

dryness. The acid was dissolved in a mixture of 25 ml CH_3OD, 40 ml C_6H_6 and 1 ml 7N DCl in D_2O and was refluxed under N_2 for 4 hours. The solution was evaporated and dried under vacuum and the solids were crystallized twice from hexane to yield 6.2 g methyl-5-oxostearate-2,2,4,4, 6,6-d_6. The ^1H NMR spectrum showed greater than 90% deuterium incorporation at the indicated positions.

III.1.8 Spin Labelled Phospholipids

Doxyl-labelled fatty acid (0.5 mmole) in 1 ml dry benzene was added to a solution of 1, 1-carbonyldiimidazole (1 mmole) in 2 ml dry benzene (22). The mixture was protected from atmospheric moisture and allowed to react for 1 hour. Egg lysolecithin (0.5 mmole) was dispersed with brief sonication in 5 ml dry benzene to give a viscous, cloudy suspension. Under a direct flow of dry N_2, the solution of fatty acid imidazolide was added to a suspension of NaH (0.5 mmole) in 1 ml dry benzene. To this mixture was added the suspension of lysolecithin. The solution bubbled vigorously on addition of the lysolecithin. After 20 minutes, the mixture was transferred to a separatory funnel containing $CHCl_3$ (100 ml), CH_3OH (100 ml) and 0.1 N HCl (90 ml). The $CHCl_3$ layer was separated, dried over Na_2SO_4, filtered and evaporated to dryness. The resulting syrup was dissolved in a minimal volume of $CHCl_3$ and applied to five silica gel plates (20 cm

X 20 cm, 0.5 mm thickness). The plates were developed in $CHCl_3/CH_3OH/H_2O$ (65/25/4). The yellow band of the spin-labelled lecithin was scraped off the plates and the silica gel was stirred in 100 ml CH_3OH. The suspension was filtered and evaporated to dryness yielding 153 mg (~.18 mmole, 36% yield).

III.1.9 Hydroxylamine Derivatives of Spin-Labelled Phospholipids

The method described by Rozantsev and Golubev (21) was used. Adams catalyst (platinum oxide, 10 mg) was suspended in 10 ml CH_3OH in a hydrogenation flask. A solution of spin-labelled phospholipid (15 mg in 1 ml CH_3OH) was then added. The flask was then thoroughly flushed with H_2 gas and the system was then sealed under a slight pressure of H_2. As the solution was stirred, the catalyst was rapidly reduced, turning from brown to black. The reduction of the nitroxide to its hydroxylamine derivative then commenced as indicated by loss of the yellow colour in the solution. After complete loss of colour, the solution was stirred for a further hour under slight H_2 pressure. The mixture was then flushed with Ar and tightly stoppered. Catalyst particles were removed by filtering the suspension through tissue paper in a Pasteur pipette. The filtrate was added directly to a $CHCl_3$ solution of egg phosphotidylcholine (250 mg) and the combined lipids were evaporated under N_2 and placed under high vacuum over night.

III.1.10 Deuterated Ethanolamine

The labile $-NH_2$ and -OH protons of ethanolamine were exchanged for deuterons by adding D_2O (20 ml) to 30 g of ethanolamine and distilling off the water at reduced pressure. This procedure was repeated two more times. Approximately 25 g of Raney nickel catalyst suspended in water (W.R. Grace) was treated with D_2O (20 ml) three times followed each time by decantation of the water. The resulting Raney nickel/D_2O suspension was added to the deuterium-exchanged ethanolamine along with 50 ml D_2O. The suspension was heated and 25 ml of water was distilled off. Fresh D_2O (25 ml) was added and distilled off. ^1H NMR of an aliquot of the suspension indicated that the exchange was incomplete. A further 25 ml of D_2O was added to the suspension and it was refluxed for 1 hour. The proton NMR spectrum indicated incomplete exchange. Fresh D_2O-washed Raney nickel (~50 g) was added with 100 ml D_2O and the suspension was refluxed for 1 hour. The suspension was filtered to remove the catalyst which was subsequently decomposed with 3N HCl. Water (100 ml) was distilled from the filtrate and the distillation was continued under vacuum (water aspirator). An ethanolamine fraction was collected at 55-60°C to yield 18.8 g. Labile deuterons were removed by repeated addition and evaporation of methanol. The ethanolamine was then treated with H_2O and distilled under water

aspirator vacuum to yield 12.5 g deuterated ethanolamine. ^1H NMR indicated >90% exchange at the hydroxymethylene carbon. ^2H NMR indicated that the extent of deuteration at the amino-methylene carbon was approximately 50%.

III.1.11 Phosphatidyl Ethanolamine -d_4

Deuterated ethanolamine (7 g) was added to 25 ml H_2O and titrated to pH 5.6 with glacial acetic acid (23). After addition of 0.74 g $CaCl_2 \cdot 2H_2O$, the solution was diluted to 50 ml. Crude phospholipase D prepared from Savoy cabbage (180 mg, Calbiochem) was then added. Egg phosphatidylcholine (2 g) was dissolved in 50 ml diethyl ether and added to the above aqueous solution. The mixture was vigorously stirred in a 37° water bath. Phospholipase D (180 mg in 2.5 ml H_2O) was added after 30 and 60 minutes of reaction. After 2 hours of reaction, 100 ml of 0.1 M Na_2EDTA solution was added to stop the reaction. Ether was evaporated under reduced pressure. The aqueous suspension was mixed with 215 ml of chloroform/methanol (5:8, V/V) and stirred for 15 minutes. The mixture was filtered and stirred with 50 ml of water and 150 ml of chloroform. The chloroform layer was separated and evaporated to dryness.

Purification was carried out by chromatography on carboxymethyl-celluose (23). The column was prepared using 400 g of Whatman CM-52. The material was washed several times with methanol to remove fines. The slurry was added to a 5 cm

diameter column. Methanol was removed by washing the column with 2 ℓ of chloroform. The sample was dissolved in 25 ml chloroform and applied to the column. The material was eluted using chloroform-methanol in the following proportions and volumes:

% methanol in chloroform	Volume ℓ
0	3
5	1
7.5	0.5
9	2
10	3
11	2
12	2

Fractions were collected in 1 ℓ flasks with a strong current of N_2 bubbled into the eluate. Elution of lipids was monitored via thin layer chromatography on silica gel plates developed in chloroform/methanol/water (65/25/4, V/V/V). Samples were stored under N_2 at -20°C. The phosphatidylethanolamine began to elute with 9% methanol. Fractions containing phosphatidylethanolamine were pooled and evaporated to yield ~800 mg. This material was dissolved in hexane and precipitated with cold distilled acetone. The precipitate was dissolved in $CHCl_3$ and stored under N_2 at -20°C.

III.1.12 Cholesterol-2,2,4,4,6-d_5

The method of Gruenke and Craig (24) was followed. Methanol-OD (20 ml, Merck, Sharp and Dohme) was added to

160 mg NaH to give a solution of sodium methoxide in methanol-OD. To this solution was added Δ^4-cholesten-3-one prepared according to Fieser (25). The solution was refluxed overnight under dry N_2. The solvent was evaporated with a stream of N_2 and replaced by fresh methanol-OD and refluxed for 8 hours. Evaporation and replacement of solvent was repeated followed by overnight reflux. After cooling, 5 ml D_2O was added and the solution was dried over Na_2SO_4, filtered and evaporated to dryness. Crystallization from hexane yielded 6.4 g Δ^4-cholesten-3-one-2, 2, 4, 6, 6-d_5. ^{13}C NMR showed loss of signals at the chemical shifts corresponding to these carbons. This compound was added to 6 ml isopropenyl acetate with 1 drop concentrated H_2SO_4. The mixture was heated at 100°C for 1 hour under N_2. Anhydrous sodium acetate (0.5 g) was added to the yellow solution and the mixture was extracted with $CHCl_3$. The $CHCl_3$ was evaporated and crystallization from methanol/chloroform yielded 2.5 g yellowish crystals of the enolacetate. The enolacetate was dissolved in 30 ml tetrahydrofuran and added dropwise to a solution of 2.5 g $NaBH_4$ in 20 ml methanol-OD containing 2 ml D_2O. After addition, the solution was refluxed 1 hour. After cooling, 30 ml concentrated HCl was added and the solution was poured into 100 H_2O. The aqueous mixture was extracted with CH_2Cl_2 (3 x 90 ml). The combined CH_2Cl_2 layers were evaporated yielding yellowish crystals. The solids were recrystallised several times, but remained

quite coloured. The solids were taken up in 25 ml $CHCl_3$ and treated with ~1 g activated charcoal. The solution was filtered to remove the charcoal and evaporated to dryness. Crystallization from absolute ethanol yielded 120 mg of material melting at 141°C. The mother liquor was evaporated giving 320 mg of lightly coloured crystals. This fraction was purified via the dibromide method as described by Fieser (25). This fraction was crystallized from methanol to yield 110 mg of cholesterol-2, 2, 4, 4, 6-d_5 with melting point 120-130°C. The final purification was carried out by column chromatography.

Alumina, (10 g, Woelm Activity I), was packed in a 1 cm diameter column in hexane. Cholesterol was loaded onto the column in hexane. The product was eluted with a stepped gradient of ethyl acetate in hexane at a flow rate of 5 ml/min., collecting 5 ml fractions. The following solvent sequence was used:

% ethyl acetate in hexane	Volume ml
0	100
5	100
10	200
20	100
30	300

The eluates were tested by thin layer chromatography on silica gel plates in the solvent system hexane/ether/acetic acid:80/20/1, using cholesterol and epi-cholesterol as standards. The fractions containing cholesterol were pooled

and evaporated to dryness. Recrystallization from methanol yielded 55 mg cholesterol-d_5, mp 144-145°

III.2 Sample Preparation

III.2.1 Spin Probe Studies

Samples of oriented lipid films were prepared as described by Smith and Butler (ref. 8, chap. 11). Lipids were dissolved in $CHCl_3$ to give an egg PC concentration of 4 mg/ml. The spin probes were used at a concentration of 1 mole % relative to the egg PC and cholesterol at variable mole ratios with respect to the total lipid content. The $CHCl_3$ lipid solution (0.15 ml) was placed in a stoppered rectangular quartz cell with dimensions 10 cm x 1 cm x .02 cm. N_2 gas was bubbled through the solution to evaporate the $CHCl_3$ and deposit the lipids on the inner walls of the cell. The cells were then placed under high vacuum overnight to remove residual solvent. The lipids were hydrated by filling the cell with distilled water and were allowed to equilibrate for at least 30 minutes. Excess water was drained from the cell before obtaining the EPR spectrum.

Liposome samples were prepared by evaporating the $CHCl_3$ solution, described above, under N_2 followed by high vacuum overnight. The lipids were hydrated with 1 ml distilled water. The suspension was dispersed by vigorous agitation

on a Vortex mixer and were allowed to equilibrate for at least 30 minutes.

III.2.2 NMR Studies

Lipid mixtures were prepared in $CHCl_3$ and were then evaporated nearly to dryness under N_2. The samples were then placed under high vacuum. The "bumping" which occurred as the residual solvent was rapidly evaporated caused the lipids to splatter over the walls of the sample container in small particles. This procedure was followed since large amounts (up to 500 mg) of lipid were employed and evaporation of such a sample to dryness under N_2 produces a syrup which may trap residual solvent. Removal of residual solvent from the syrup is likely to be difficult since solvent diffusion of the solvent out of the sample is slow due to its low surface area to volume ratio.

After standing overnight under high vacuum, the lipids were hydrated with water. The amount of water added was adjusted such that the weight of water used was twice the weight of total lipids in the sample. Deuterium-depleted water was used to reduce the intensity of the water peak in the ^2H NMR spectra. The lipids were tightly sealed under N_2 and were then dispersed by vigorous agitation using a Vortex mixer. In order to improve sample homogeneity, the lipid dispersions were taken through several freeze-thaw cycles.

The samples were frozen at -20°C and then allowed to warm to room temperature. The warmed samples were again vigorously agitated and then were taken through another freeze-thaw cycle. Generally, three such cycles were performed so that the samples appeared macroscopically homogeneous and would readily flow from the sample container. The hydration behaviour of the phosphotidylethanolamine samples was slightly different in that the lipids formed a particulate precipitate as noted previously (12).

III.3 Spectroscopic Methods

III.3.1 Spin Probe Studies

EPR spectra were obtained using a Varian E-9 spectrometer at a nominal frequency of 9.3 GHz and field strength of 3,200 Gauss (0.32 Tesla). Most spectra were obtained using a magnetic field sweep of 100 Gauss over 4 minutes with field modulation of 1 Gauss. The scan time and recorder time constant were adjusted to maintain a good signal to noise ratio with minimal distortion of the spectral lineshape. Temperature was regulated by flowing thermostatted N_2 gas past the sample. For liposome samples, the Varian temperature regulation insert was employed. A home-built unit (K.W. Butler, unpublished) was employed for oriented film cells. In both cases, temperature was monitored using a digital thermometer (Newport, Ca.) with the thermocouple placed directly above the sample portion of the cell. Microwave power was attenuated to avoid excessive

heating of the samples. For studies of the orientation dependence of the spectra of film samples, a home-built goniometer was used for measurement of angles between the static magnetic field and the film cell.

III.3.2 NMR Studies

A Bruker CXP-300 spectrometer was employed using a superconducting magnet at 70,000 Gauss (7.0 Tesla). The spectrometer is equipped with an Aspect-2000 computer, with 80 K words of memory, for control of spectrometer functions and data processing. Spectra were stored on a Diablo high density disk. Temperature was regulated by flowing thermostatted N_2 gas or air past the sample contained in a vacuum-jacketted glass dewar. Temperature was monitored via a thermocouple located ~2 cm from the sample.

The ^{31}P spectra were obtained at 121.5 MHz using quadrature detection. The Cyclops phase sequence, which rotates the transmitter phase through 90° steps, was employed to reduce distortions caused by imbalance in the amplitudes and phases of the quadrature receiver channels. A 10 mm double tuned solenoid coil was used allowing ^{31}P observation and broad band ^{1}H decoupling on the single coil. A low pass filter was employed between the receiver pre-amplifier and the probe to shield the receiver from the 300 MHz ^{1}H decoupling signal. No field/frequency lock system was used since the superconducting magnet showed negligible field drift during the course of a

typical experiment.

^2H spectra were obtained at 46.1 MHz. A home-built (R.A. Byrd, unpublished) 10 mm solenoid coil probe was used. The resonant frequency and impedance of the coil were adjusted such that the probe acted as a 50 ohm load at the excitation frequency. Under this condition, the 90° pulse width of the probe was approximately 4.5 microseconds. Radio frequency excitation was provided at the Larmor resonant frequency (the centre of the symmetric quadrupole pattern) and the phase relationship between the transmitter pulse and the quadrature receiver channels was adjusted so that the detected signal was present in only one of the quadrature channels. A software modification (R.A. Byrd, unpublished) allowed replacement of the noise present in the second quadrature channel by zeroes. This operation results in "folding" of the transformed spectrum about the zero frequency with a concomitant increase of $(2)^{1/2}$ in signal to noise with respect to the normal quadrature spectrum.

Spectra were acquired using the quadrupole echo sequence (26). The pulse sequence used was:

$$90^\circ_x - \tau_1 - 90^\circ_y - \tau_2 - \text{acquire}$$

The phases of the first and second 90° pulses differ by 90°, and the phase of the first pulse was varied by 180° on alternate scans; echo signals were alternately added and subtracted in

memory. Generally, the value of the first delay, τ_1, was set at 50 microseconds and the second delay was set at 40 microseconds. In this fashion, acquisition of the echo signal begins before the maximum point of the echo signal. The Fourier transform of the signal was subsequently performed starting at the echo maximum. The use of the quadrupole echo sequence is necessary in order to obtain undistorted line-shapes in the transformed spectra (26). Values of the ^2H spin-lattice relaxation time, T_1, were measured by the inversion recovery sequence (27) modified for use with the quadrupole echo. The pulse sequence employed was:

$$180^\circ - \tau_R - \text{(quadrupole echo)} - \text{acquire}$$

where τ_R is a variable delay to allow relaxation. The values of τ_R were chosen to provide several (4-5) points on each side of the zero crossing point of the magnetization recovery curve. The values of T_1 were calculated graphically using the relationship.

$$(M_\infty - M_\tau) = M_\infty e^{-\tau/T_1} \qquad (6)$$

where M_∞ and M_τ are the magnitudes of the Z magnetization at times greater than $5T_1$ and τ, respectively. Peak heights of the transformed spectra were used and the value of T_1 was taken as the negative reciprocal of the slope of the straight line found by plotting $\ln(M_\infty - M_t)$ against τ.

Values of T_{2e}, the quadrupole echo decay time constant, were determined using the quadrupole echo sequence described above with variable values for τ_1 (28). Peak heights of the spectra were analyzed using the relationship:

$$I_t = I_0 e^{-t_1/T_{2e}} \tag{7}$$

where I_t is the intensity of the spectrum observed for the delay between 90° pulses equal to t/2. The values of T_{2e} were determined from the negative reciprocal of the slope of the straight line found by plotting $\ln(I_t)$ as a function of t. The values of T_{2e} were used in simulations of the ^2H spectra to calculate the component Lorentzian linewidth:

$$\Delta\nu_{\frac{1}{2}} = \frac{1}{\pi T_{2e}} \tag{8}$$

where $\Delta\nu_{1/2}$ is the width at half-height of a component of the powder pattern.

III.4 Computations and Spectral Simulations

Computations were performed on an IBM 370/TSS system. The listings for several of the Fortran programs written are given in the Appendix section. Figures and simulated spectra were plotted using the DISSPLA plotting software package with a Hewlett-Packard 7221A digital plotter.

CHAPTER IV

EXPERIMENTAL RESULTS AND DISCUSSION

IV.1 Reliability of Fatty Acid Spin Probes

IV.1.1 Introduction

The nitroxide spin probes have been widely used in the study of phospholipid membranes (8, 10). The structures of some of the probes used in this work are illustrated in Figure 7. As discussed in the Introduction, the anisotropy of the hyperfine coupling to ^{14}N is used to monitor the motion of the probe in the membrane. Figure 8 shows the components of the static hyperfine coupling tensor for a fatty acid probe in the molecular axis system. The largest splitting, A_{zz} (~32 G), is parallel to the p orbital of the ^{14}N nucleus and is along the long axis of the fatty acid. The A_{xx} and A_{yy} components, perpendicular to the long axis, are smaller and approximately equal. In a dynamic, axially symmetric membrane environment, these components are partially averaged to $A_{\parallel}$ and $A_{\perp}$. The order parameter, S_z, for the Z reference axis is readily calculated from an EPR spectrum by (8):

$$S_z = \frac{A_{\parallel}-A_{\perp}}{A_{zz}+\frac{1}{2}(A_{xx}+A_{yy})} \qquad (9)$$

Assuming that the long axis of the fatty acid is the axis of motional averaging for the probe, the order parameter for

NITROXIDE SPIN PROBES

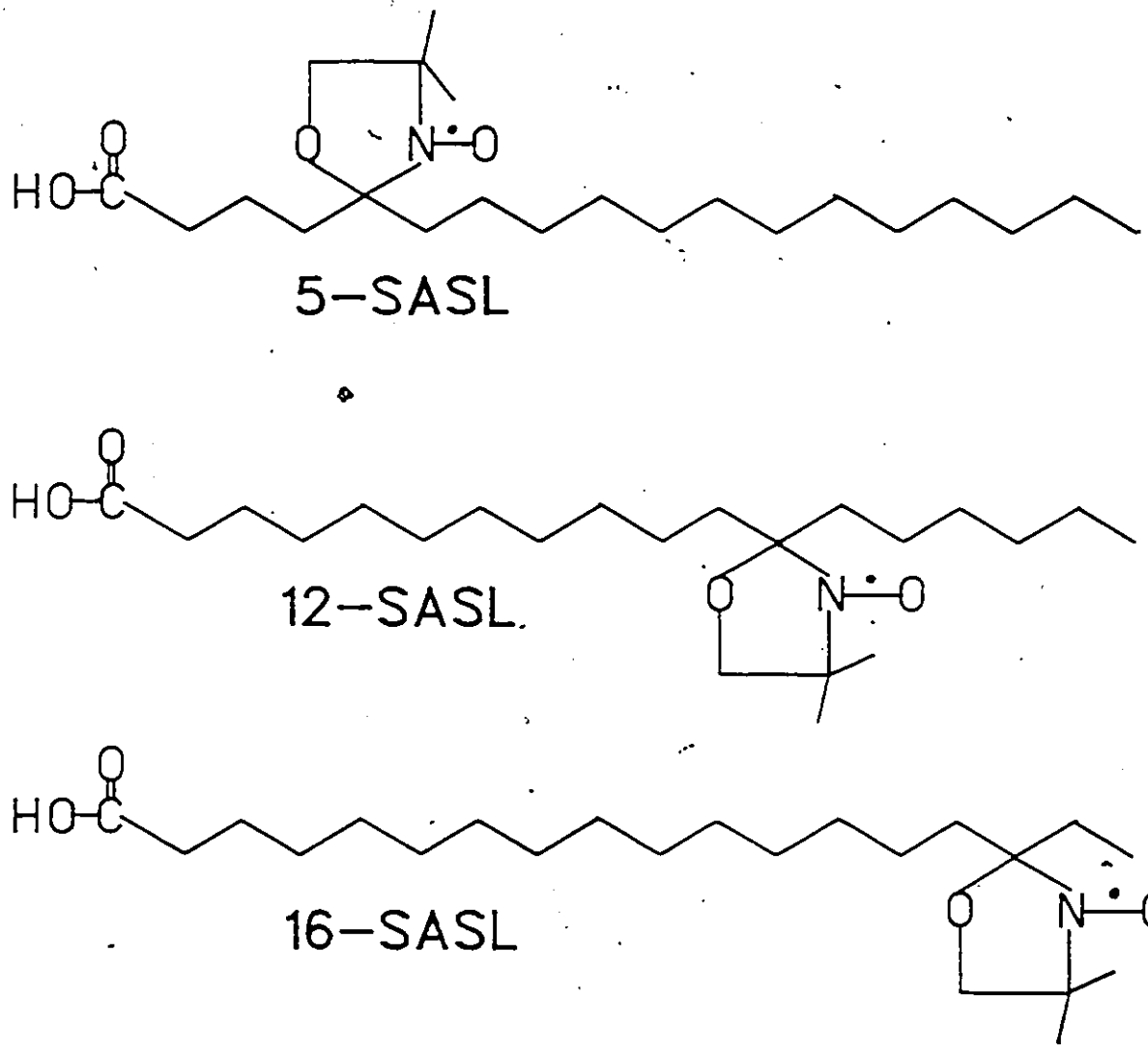

Figure 7. Structures of nitroxide spin probes employed.

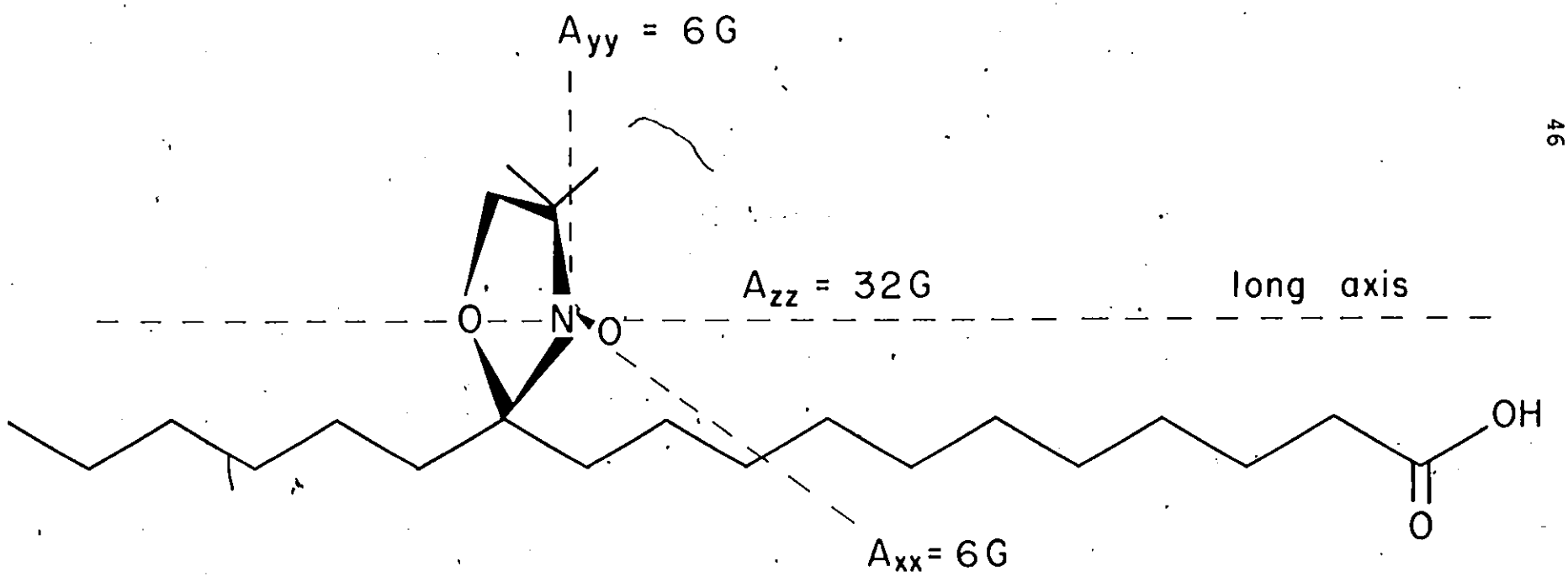

Figure 8. Structure of the 12-SASL spin probe, illustrating the components of the static hyperfine coupling tensor.

the Z axis is equal to the molecular order parameter, S_{mol}.

Quantitative information concerning motion in membranes can easily be obtained using nitroxide spin probes. For example, an EPR spectrum with excellent signal-to-noise ratio can be obtained in less than five minutes for a sample with a very dilute (~1 mole percent) concentration of spin probe in a phospholipid membrane. There are problems, however, associated with the interpretation of the spin probe data. Since the spin probe is not a natural membrane component, one cannot be certain that the spin probe results reflect only the true state of the membrane and are not affected by perturbations of the membrane structure caused by the insertion of the probe. Nitroxide-induced perturbations may result from two main sources.

Firstly, the nitroxide group is quite bulky. Thus, at the labelled position of a fatty acid probe, the diameter of the molecule is about twice that of an unlabelled fatty acid. One may expect that the insertion of such a probe would result in a disturbance of the chain packing in the hydrocarbon region of a membrane. A second potential source of perturbation is the high polarity (29) of the nitroxide group. The nitroxide must insert into the low dielectric constant, hydrocarbon region of the membrane. The presence of a highly polar group may cause a local disturbance in the chain packing.

The interpretation of spin probe data in terms of the true state of the membrane could be performed with more confidence if the extent of the nitroxide perturbations were understood. The assessment of the problem is somewhat difficult due to the manner in which a spin probe reports on its environment. The spin probe's behaviour is most strongly affected by the environment immediately surrounding the label. Thus, a local perturbation by the nitroxide is sufficient to cause a response by the probe which is not representative of the general state of the membrane. Because of this, the nitroxide perturbation cannot be probed by a technique which measures bulk or average properties of the membrane. Rather, it is necessary to use techniques which respond in a similar microscopic fashion.

The first examination was performed by a direct comparison of the responses of nitroxide-labelled and deuterium-labelled fatty acid probes. In principle, both types of probes should exhibit the same response to alterations in the membrane. The deuterium label is non-perturbing, however, so that the deuterated probes may serve as a calibration reference for the nitroxide spin probes. In this first series of experiments, the response of each type of probe to changes in label position and membrane cholesterol concentration was compared.

IV.1.2 Results and Discussion

The spin probe experiments were carried out using oriented film samples and random dispersion liposome samples. Figure 9 shows representative EPR spectra obtained for egg PC bilayers deposited on a planar quartz surface. The solid line spectra for each position were taken with the flat cell mounted such that the static magnetic field was parallel to the long axes of the membrane lipids, that is, at a right angle to the planar surface. The dashed line spectra are those obtained with the flat cell surface along the field direction. These orientations are depicted schematically in the lower portion of the figure. Figure 10 illustrates typical spectra for the probes in liposome samples for different label positions. For both types of spectra, the method for measuring the hyperfine splitting components, $A_{\parallel}$ and $A_{\perp}$ is shown. Using these values, the spin probe S_{mol} can be calculated as described above. For most of the comparisons presented below, oriented film samples were used rather than liposomes due to the problem in separating the effects of amplitude and rate of motion on the EPR spectra for liposomes (30).

Figure 11 shows the variation of S_{mol} as functions of label position and cholesterol content measured by EPR probes and the corresponding ^2H NMR probes. The ^2H NMR data were taken from previously published work (31). For the spin probe data, each

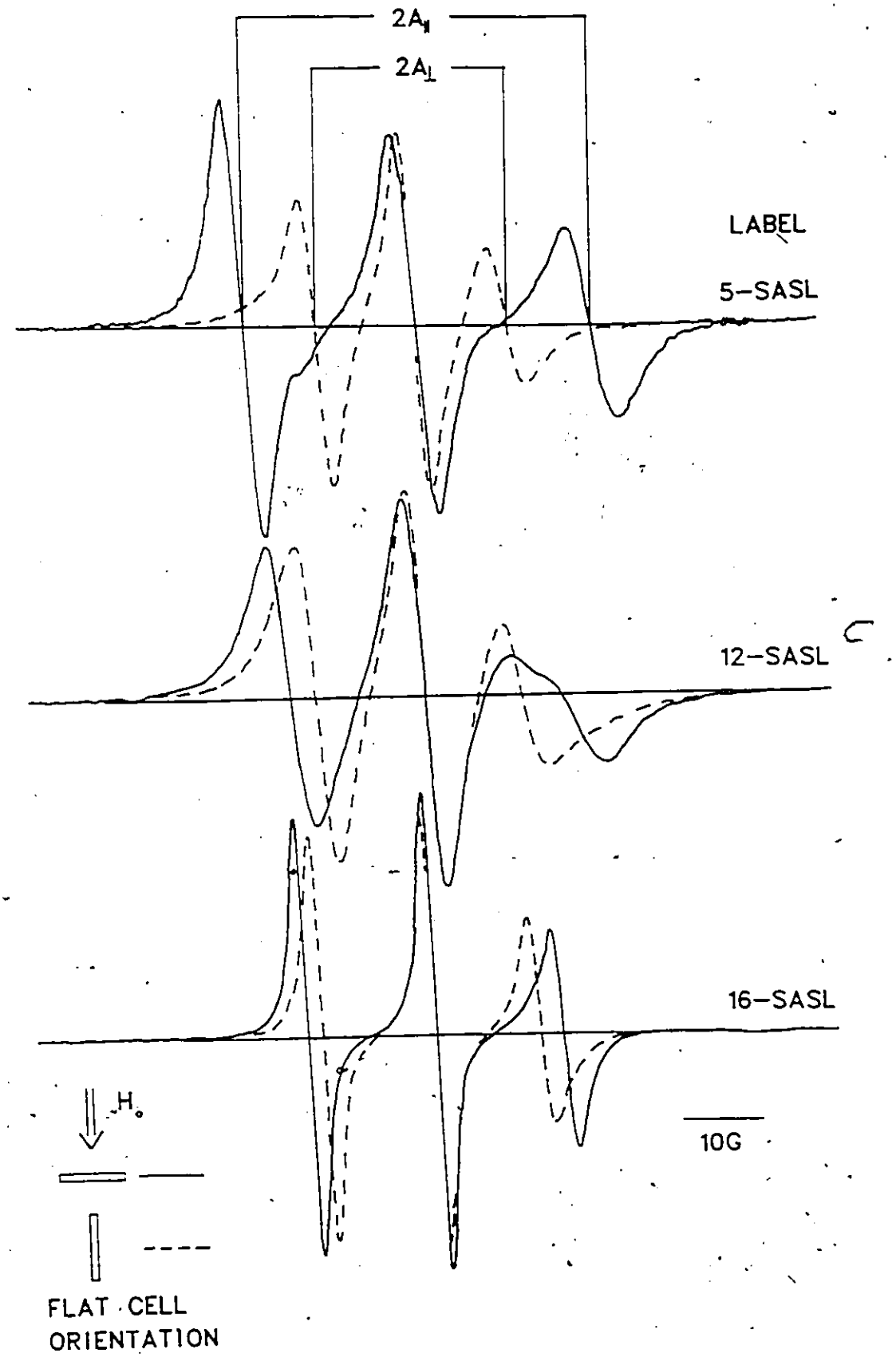

Figure 9. Representative EPR spectra for fatty acid spin probes in oriented lipid samples. Solid line spectra taken with the field parallel to the phospholipid long axes. Broken line spectra taken with the field perpendicular to the long axes.

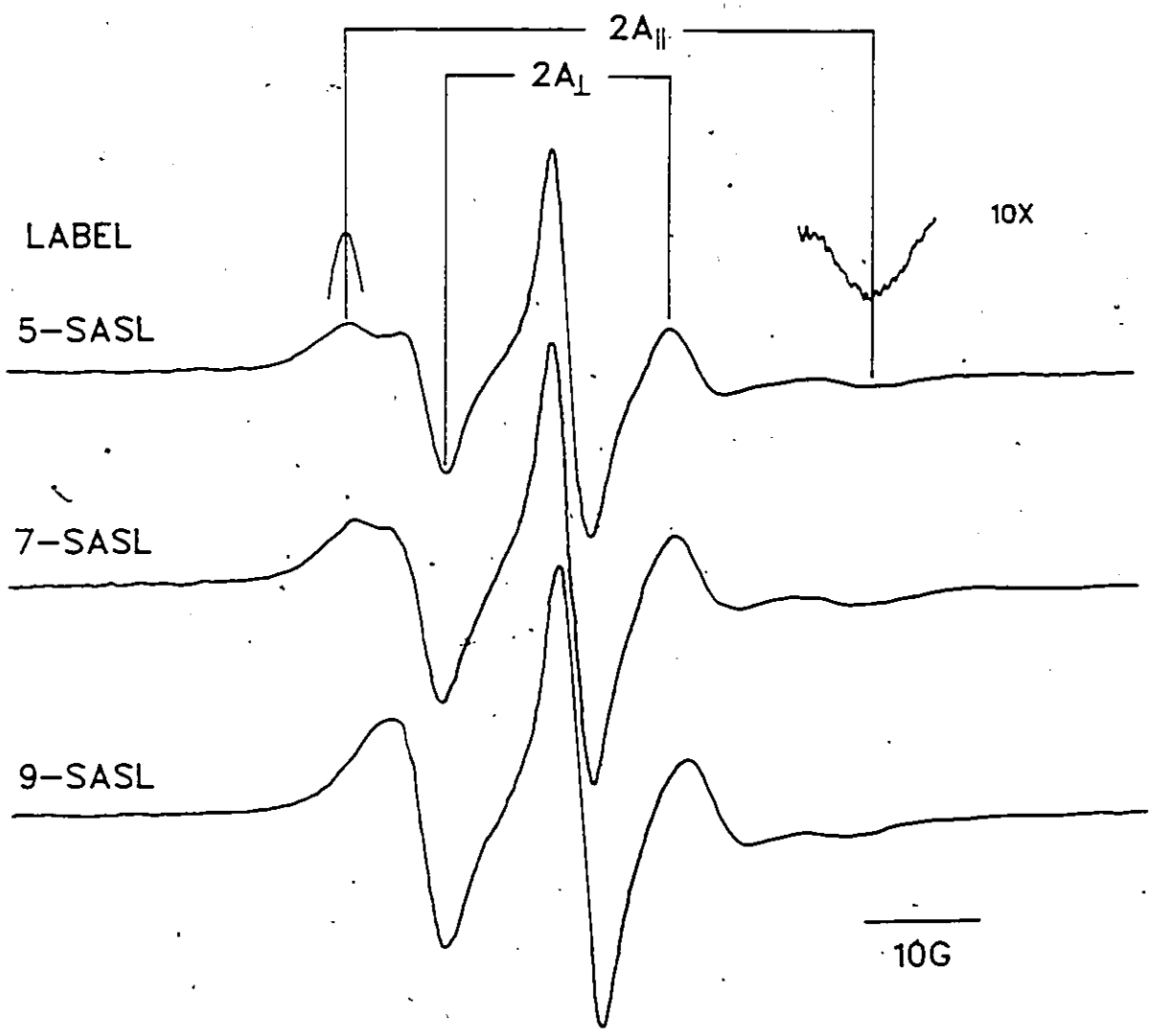

Figure 10. Representative spin probe EPR spectra for liposome samples.

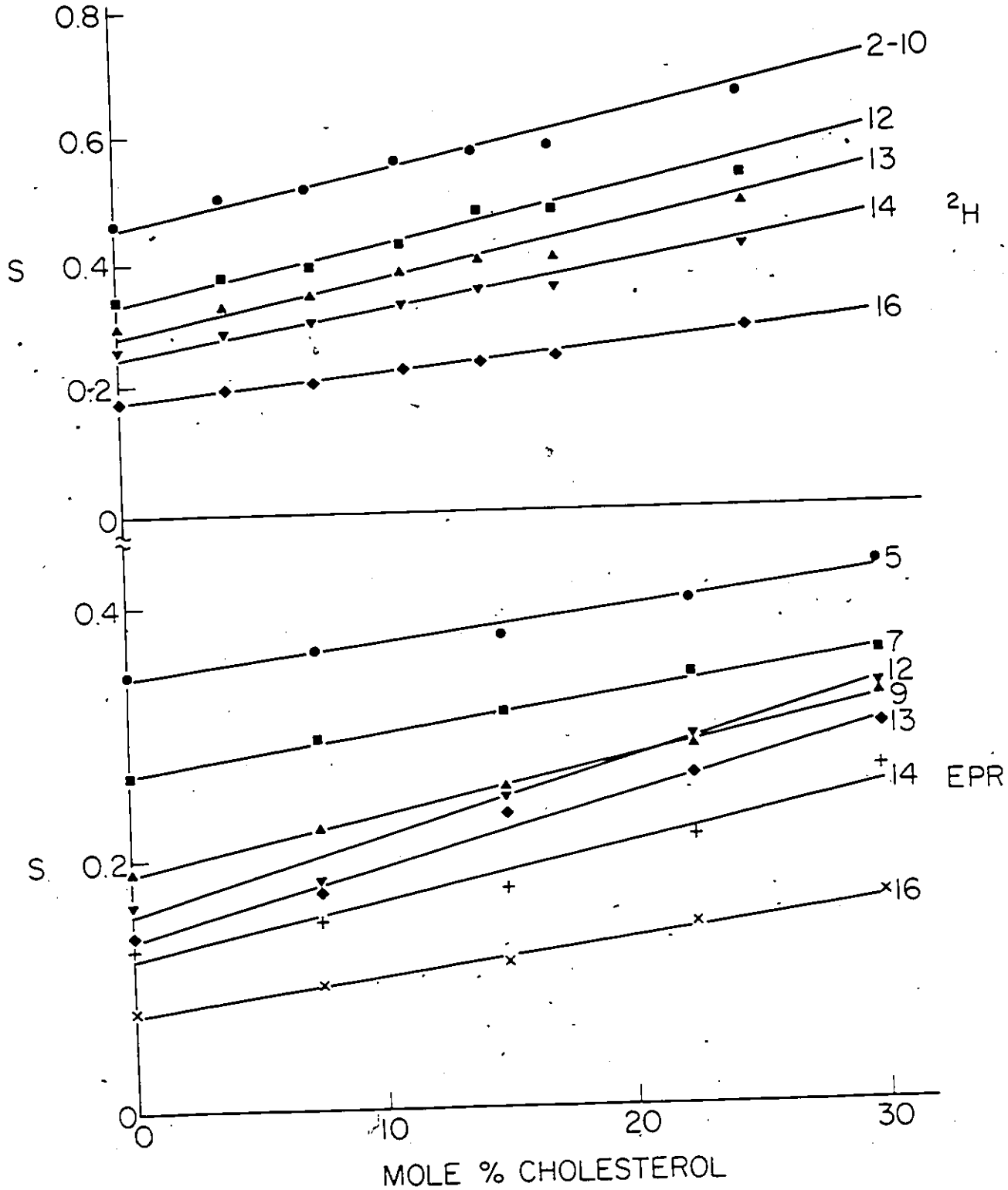

Figure 11. Variation of molecular order parameters derived from EPR and ^{2}H NMR measurements with increasing cholesterol concentration in egg PC bilayers. The label position for each probe is indicated on the Figure.

point represents the average of 2-5 films. The range of S values at each point is 0.03 S units for the worst case and the average range for the entire set of points is 0.01 units. The straight lines were fitted by linear regression with correlation coefficients ≥ 0.98 for all lines. For the subsequent data analysis, values of S for 0 and 30 mole percent cholesterol were taken from the straight lines.

Order Parameter-Label Position Profiles

The ^2H NMR and spin probe profiles are depicted in Figure 12, which shows the order parameters at zero (circles) and 30 mole percent (squares) cholesterol. The deuterium profile shows the characteristic order parameter "plateau" (6, 31) for the upper portion of the bilayer followed by a decrease in S as the terminal methyl group is approached. In contrast, the spin probe order parameters decrease continuously as the label approaches the terminal methyl group of the probe as noted previously (32, 33). In addition, the spin probe order parameters are smaller than the corresponding values of S determined in the ^2H NMR experiment.

The difference in the shapes of the spin probe and ^2H NMR profiles has been attributed to a tilt of the phospholipid chains (32). If the lifetime of the tilt is short on the ^2H NMR time scale but long on the spin probe time scale, the deuterium quadrupole splittings would reflect an additional

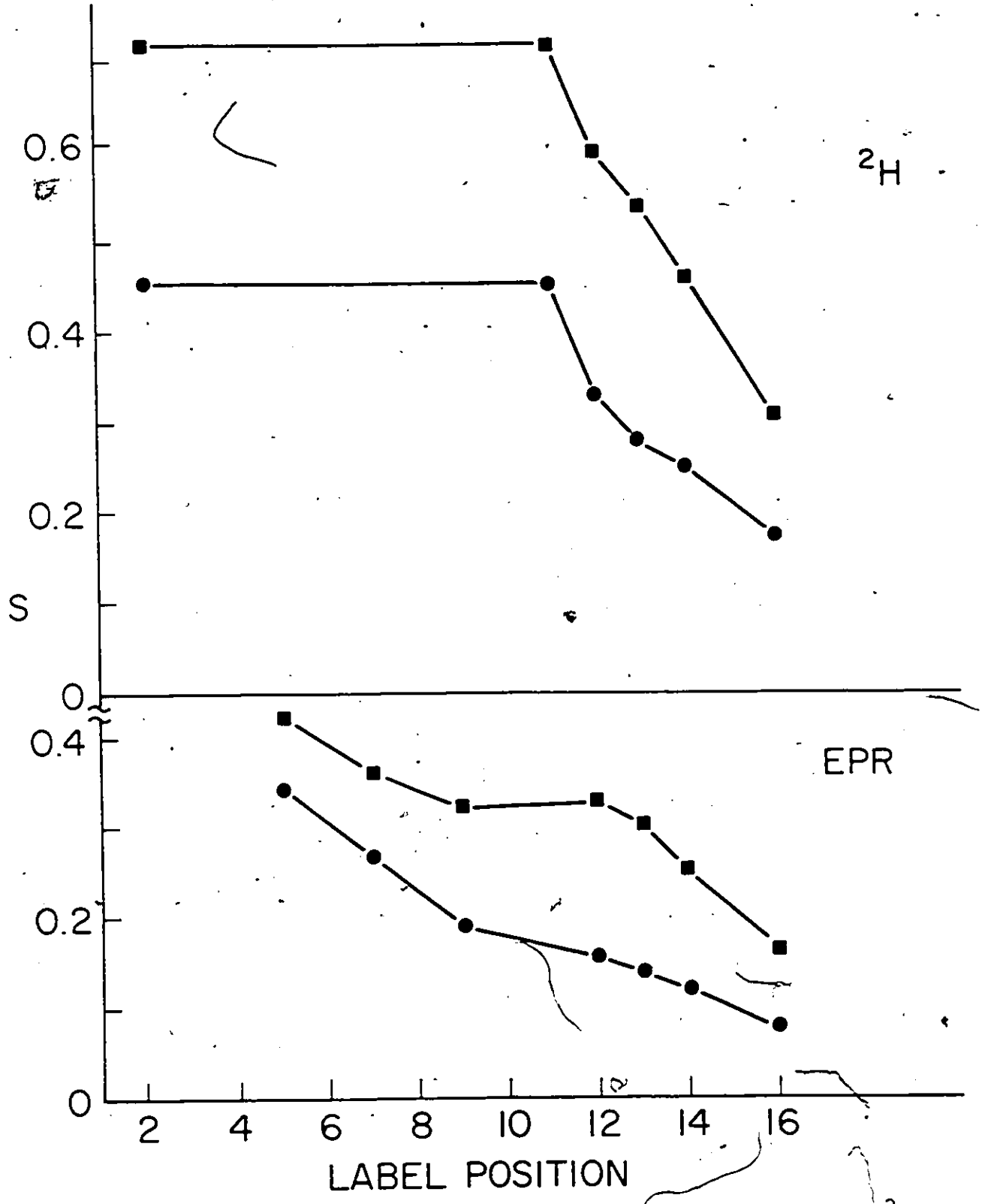

Figure 12. Order parameter-label position profiles for ^{2}H NMR and EPR of labelled stearic acid probes for zero (circles) and 30 mole % cholesterol (squares).

averaging not observed for the spin probes. If only the upper portion of the bilayer is tilted, this additional averaging may be responsible for the appearance of an order parameter plateau observed by ^2H NMR but not by the spin probes. In this case, however, the ^2H NMR order parameters are expected to be smaller than the corresponding spin probe order parameters (6), in contrast to the present and earlier (34) data.

The differences in the techniques can be seen more clearly in Figure 13 which illustrates the ratios of the observed spin probe and ^2H order parameters for each position at 0 (circles) and 30 mole percent (squares) cholesterol. The continuous decrease for positions 5-9 reflects the absence of an order parameter plateau for the spin probes. For positions 12-16 the ratio is approximately constant both with and without cholesterol.

A similar comparison of the two methods employing a different type of liquid crystalline system has been previously published (34). The observed behaviour of the two types of probes was similar in that a continuous dependence of the spin probe order parameter on position was found whereas a plateau of S values was observed in the ^2H NMR experiment. The difference in behaviour was attributed to the larger radius of the spin probes. Disruption of the packing of the alkyl chains by the bulky doxyl group may create a defect volume at the label site allowing a higher proportion of gauche rotamers

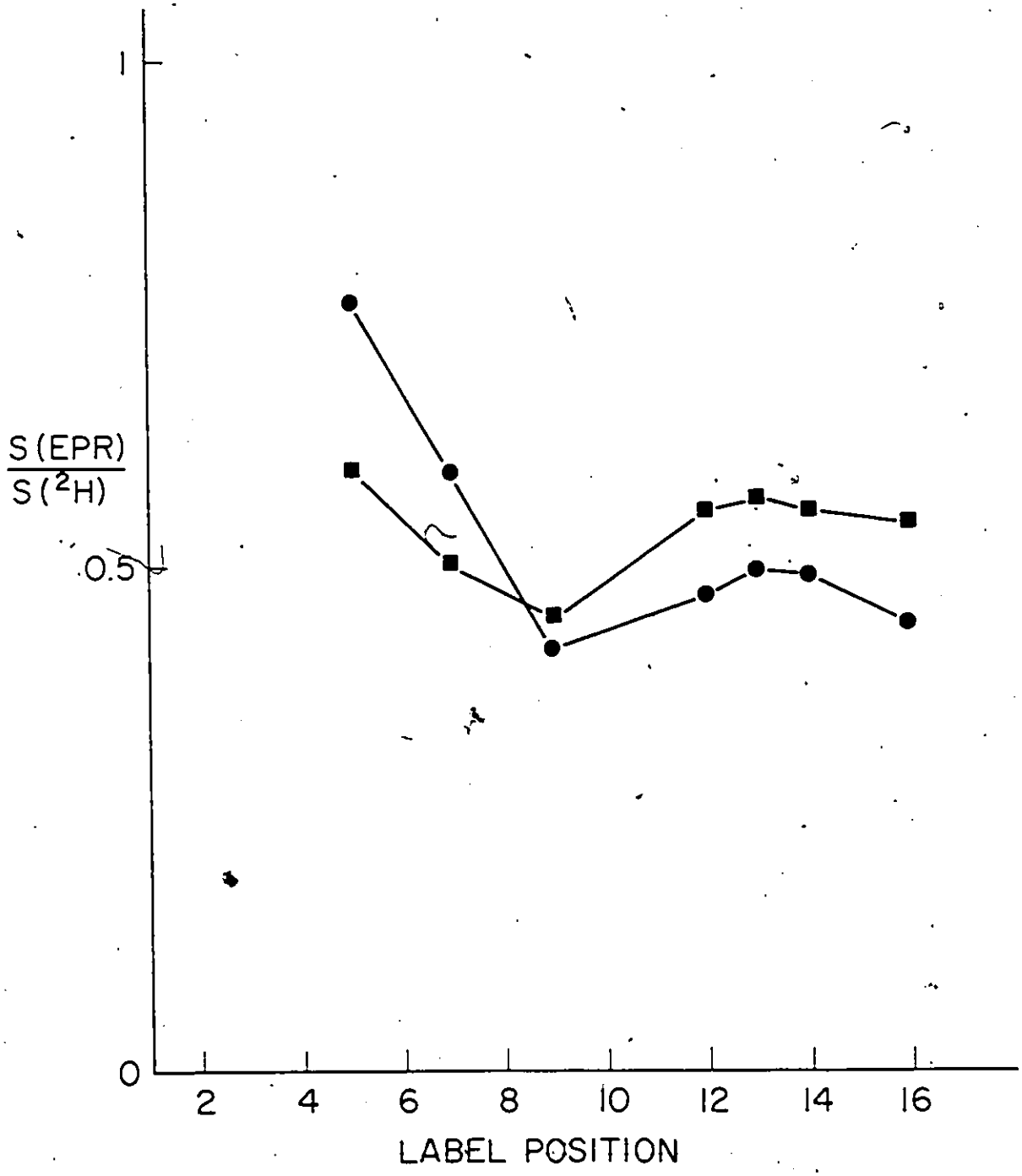

Figure 13. Ratio of the spin probe and ^2H NMR order parameters at zero (circles) and 30 mole % cholesterol (squares).

and hence a smaller order parameter. As was noted (34), the spin probe order parameter-position profiles have been accounted for by models which consider only trans-gauche isomerizations and neglect interactions between chains (34 and references cited therein). In addition, Belle and Bothorel (35) were able to reproduce a spin probe profile using a model which treated both intra- and intermolecular interactions. However, it was necessary to assume an unusually large inter-chain distance. With smaller inter-chain distances, the profiles were similar to the ^2H NMR results. The agreement of the spin probe data with models which neglect interactions between chains suggests that the spin probes are somewhat isolated from their surrounding lipid matrix. From this point of view, spin probes are not expected to yield an accurate picture of the absolute magnitude of order in membranes. In the next section this problem is discussed in terms of changes in order determined by spin probes.

Profiles of the Effect of Cholesterol on Order Parameters

Nitroxide-induced perturbations which result in inaccurate values of order parameters do not necessarily rule out the use of spin probes in biological studies. Often it is only necessary to have a reliable monitor of the changes in membrane properties with changes in added agents. This section compares the effect of added cholesterol on the order parameters observed

by the two techniques. The response to cholesterol is measured as the slope of the dependence of the order parameter on cholesterol content for each label position.

The results for both methods are depicted in Figure 14. The delta (Δ) parameter is 1000 x the slope of the order parameter vs. cholesterol content line (Figure 11) for each label position and provides a measure of the response of the bilayer to added cholesterol. For the EPR profile, the solid line is derived from oriented film experiments and the broken line from liposome samples (vide infra).

Two differences between the techniques are readily apparent. Firstly, the spin probes show a much weaker response that the corresponding deuterium probes. Secondly, the shapes of the two profiles are distinctly different. In Figure 15, the ratio of the slopes observed for both techniques at each label position is plotted. A qualitatively similar response is seen for both methods with labels in positions 12-16. For positions 5-9 there is a much larger discrepancy since the spin probe response decreases continuously toward the carboxyl group whereas the ^2H data show a constant response in this region.

The weaker response of the spin probes may be due to the same perturbation which results in the smaller values of the spin probe order parameters. As stated above, the spin probe data appear to be consistent with models in which interactions

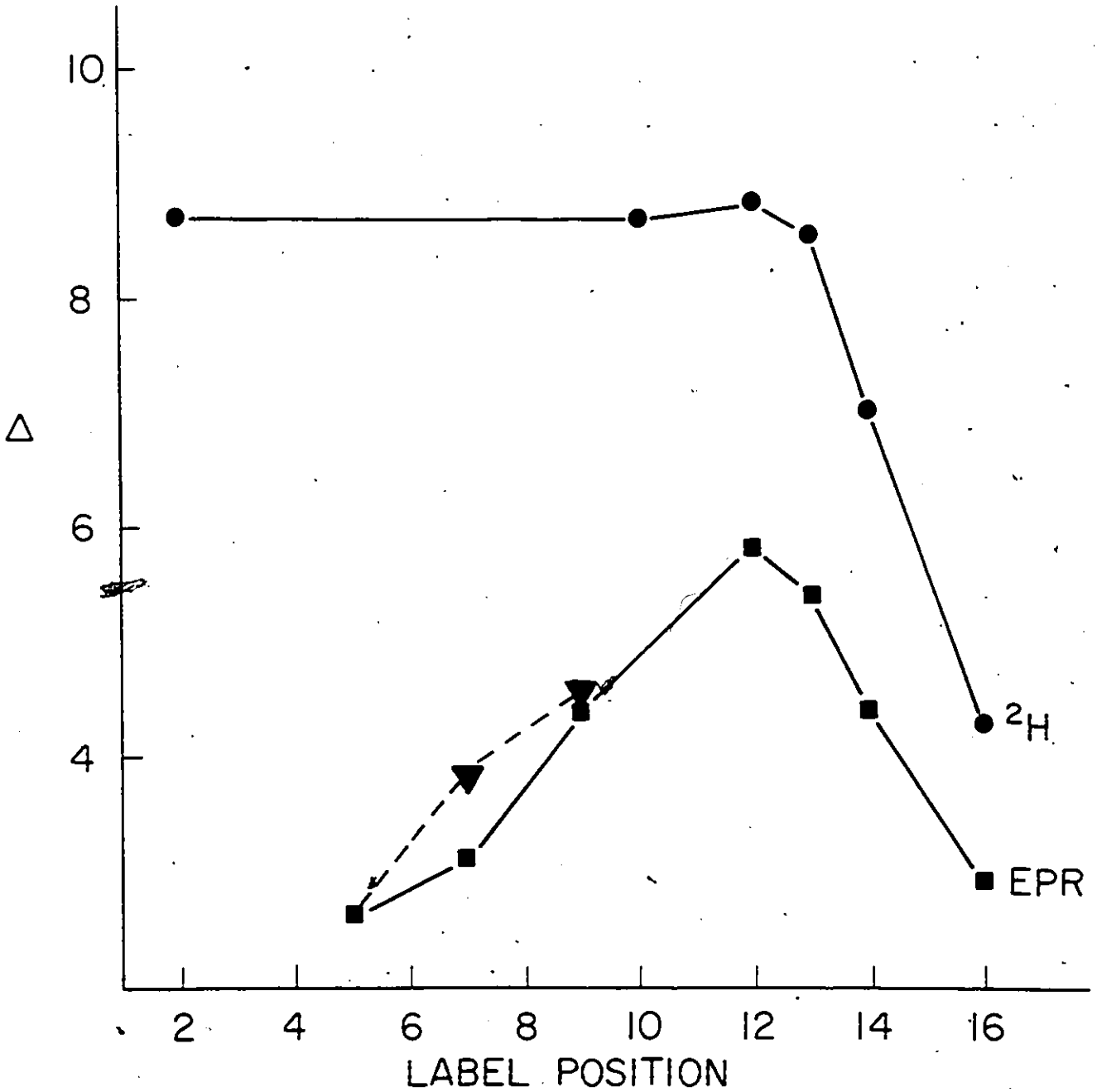

Figure 14. Cholesterol response profiles for ^{2}H NMR and EPR probes. Δ is 1000 x the slope of the S vs. cholesterol concentration line in Figure 11. For the EPR profile, the solid line is for oriented films and the broken line is for liposomes.

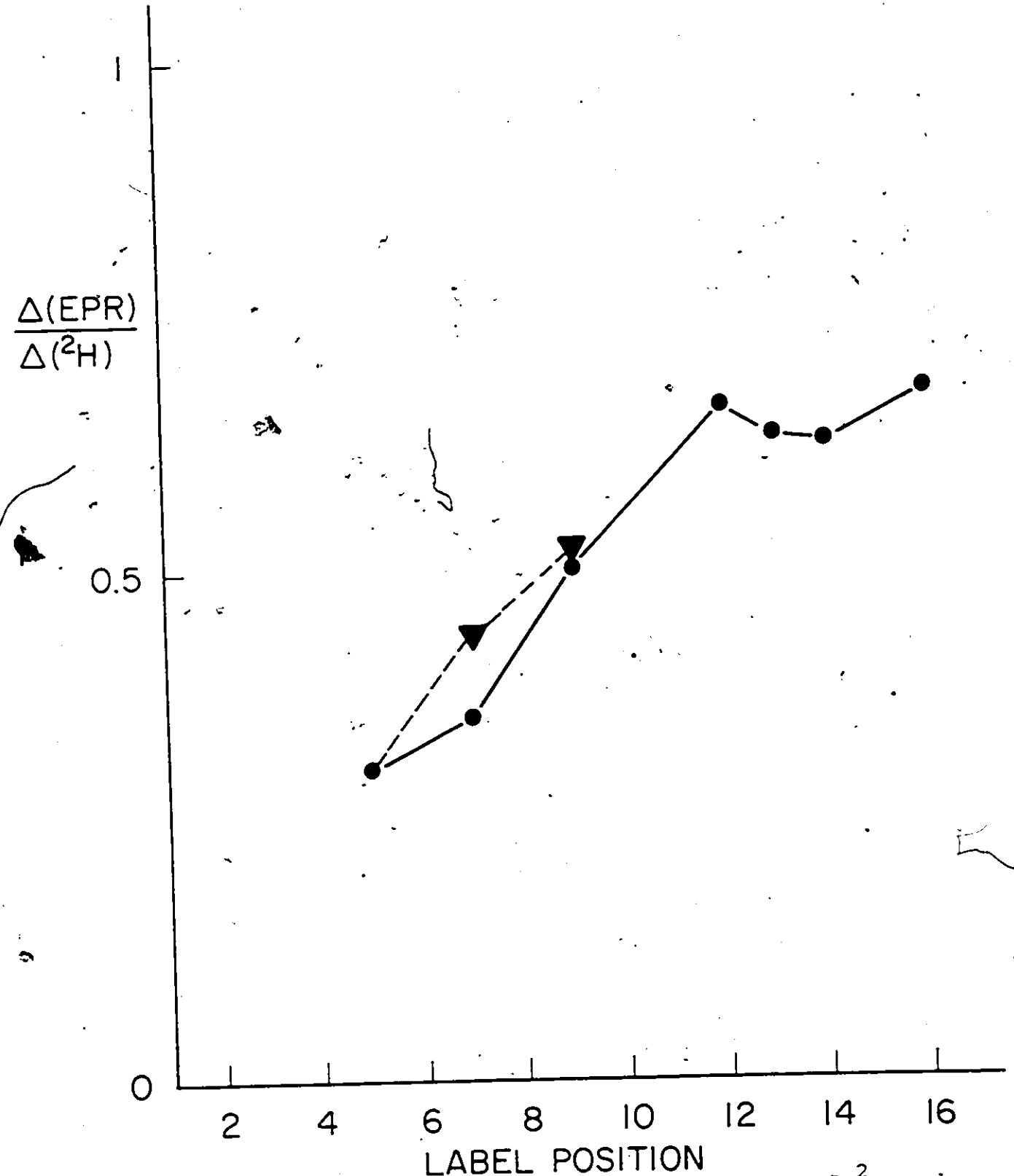

Figure 15. Ratio of the Δ parameter for EPR and ^{2}H probes. The solid line is for ratios calculated for oriented film EPR experiments and the broken line is derived from liposome samples.

between chains are not important. If the spin probes are not well "coupled" to the lipid matrix, they may be expected to be somewhat insensitive to changes in the surrounding lipid.

The difference in the shapes of the response profiles is more difficult to interpret. The approximately constant response for the first 12 carbons seen by deuterium NMR can be understood on the basis of the structure of cholesterol (31). This upper portion of the bilayer interacts with the steroid nucleus of cholesterol. Since this portion of the molecule is rigid, it exerts a constant effect on the surrounding lipids. For the remaining chain positions, the effect of cholesterol diminishes toward the terminal methyl group. This portion of the bilayer interacts with the more flexible alkyl side-chain of cholesterol so a lesser effect is expected.

For the upper portion of the bilayer, the spin probe data indicates a decreasing response as the carboxyl terminal is approached. This may result from a disturbance of chain packing which lowers the cholesterol concentration in the lipid pool surrounding the spin probe. If cholesterol does not readily enter this pool, an erroneously small response will be seen since the spin probes reflect most strongly their immediate environment.

This effect is shown schematically in Figure 16. For the upper portion of the bilayer, the packing disturbance would be most severe in terms of excluding cholesterol since this region corresponds to the rigid steroid framework of cholesterol. One might expect that this perturbation would be worst for spin probes with labels near the lipid-water interface since this is the anchoring site for cholesterol. For positions 12-16, the spin probes and deuterium probes exhibit a similar profile. Chain packing disturbances would not have as severe an effect on local cholesterol concentrations in this region since the flexible side chain would more readily adapt to the perturbation.

Thus far, the comparisons between ^2H and spin probe order parameters have been made using data derived from oriented films for spin probes and liposomes for ^2H NMR. In order to exclude the possibility that the discrepancies noted resulted from structural differences in the two systems or imperfections in the oriented films, parallel studies were performed using spin probes in liposomes. Only spin probes labeled at positions 5, 7 and 9 were used since these probes yield spectra with well resolved hyperfine splittings.

In the liposome system, the values of the measured order parameters are much higher than those found for the corresponding oriented films. For the 5-doxyl stearate probe, the liposome order parameter was equivalent to the ^2H NMR order parameter.

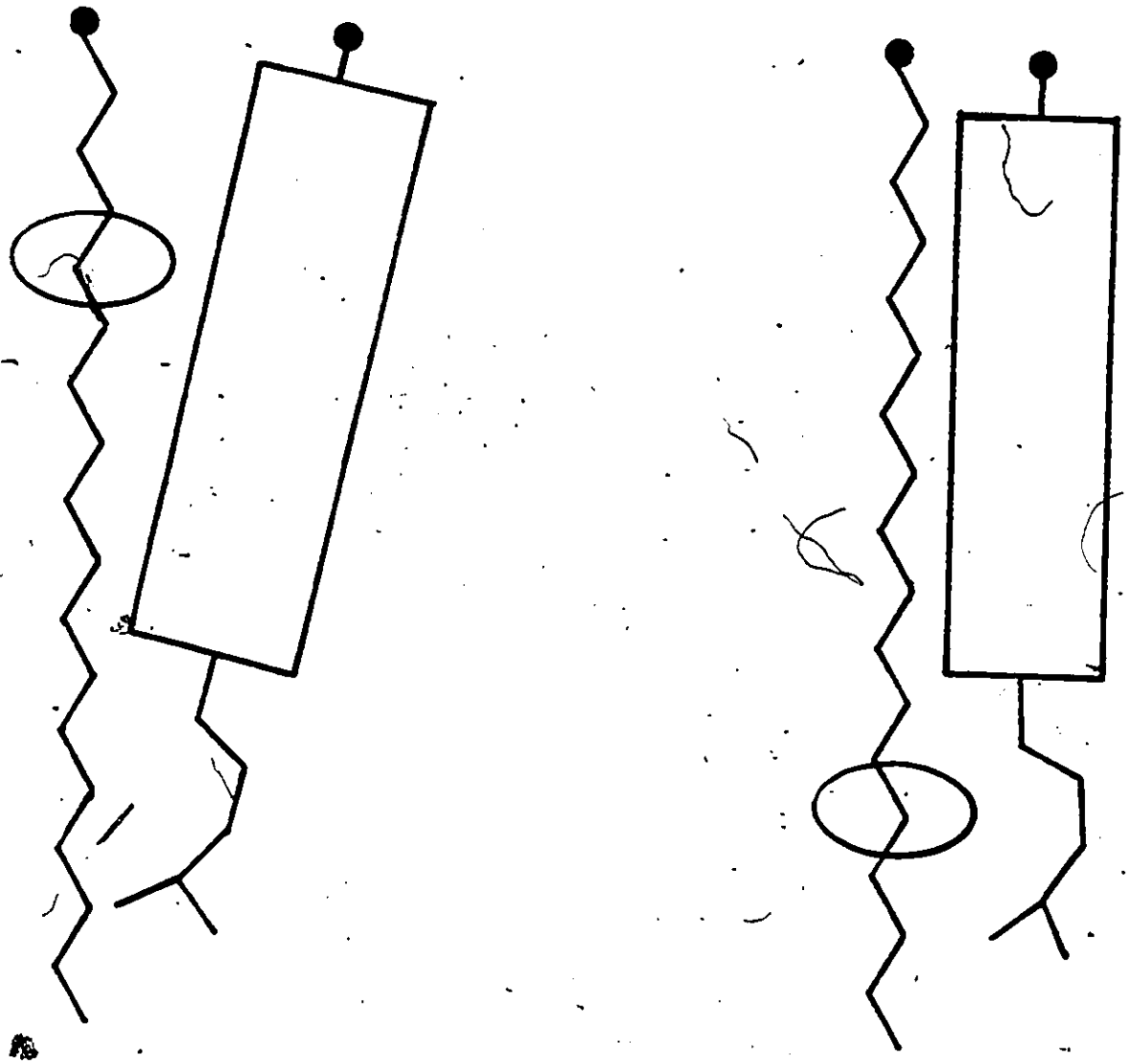

Figure 16. Schematic representation of the interaction between cholesterol and a nitroxide-labelled fatty acid. The rectangle represents cholesterol and the ellipse on the fatty acid chain represents the area occupied by the nitroxide group.

However, the order parameter decreases for positions 7 and 9 as in the oriented film experiments.

The difference in the EPR order parameters observed in the liposomes and oriented systems may result from a net tilt of the phospholipid chains (32, 36, 15) or the effects of slow motion (30, 37). In order to resolve the contributions from these effects, it is necessary to perform simulations of the spectra of oriented and liposome systems which is not generally possible for biological systems.

Significantly, the slopes measured in the cholesterol response experiments are equivalent (within ~10%) for spin probes in both the liposome and oriented film experiment as shown in Figures 14 and 15.

The quantitative agreement between liposomes and oriented films for the response profiles and the qualitative agreement for the position profiles indicates that the discrepancies between spin probes and ^2H NMR are not due to differences in the structures of liposomes and planar films.

IV.1.3 Conclusions

Using ^2H NMR as a reference, some insight can be gained into the nature of the perturbation introduced by the nitroxide label. The view that the spin probes are partially isolated from the bilayer matrix is supported both by the profile of order parameter as a function of label position and by the weak

response of the spin probes to added cholesterol.

The magnitude of the discrepancy between the spin probe and deuterium depends strongly on the position of the labels. For positions 12-16, both techniques give qualitatively similar results for the effects of position and cholesterol content on the observed order parameters. Presumably, this reflects the greater ease with which this region of lower inherent order can adapt to a steric perturbation. However, measurements of order parameters are difficult for these probes, especially in liposomes or biological membranes due to the lower degree of ordering at these positions.

The 5-doxyl stearate probe gives spectra characteristic of a high degree of anisotropy and the magnitude of the order parameter is the most similar to that of the corresponding deuterium probe examined. It shows the greatest discrepancy, however, for the ordering effect of cholesterol. Thus, it may be the least attractive spin probe for studies examining the effects of external agents.

IV.2 Comparison of Nitroxide- and Deuterium-Labelled Steroids

IV.2.1 Introduction

The experiments described in the previous section pointed out several discrepancies between the fatty acid spin probes and their deuterium-labelled analogs. These discrepancies indicate that some caution is required in the interpretation of spin probe data, in particular for probes labelled in the

upper part of the acyl chain. The investigation of this problem was extended by examining the behaviour of another widely used (ref. 8, chap. 11) spin probe, 3-doxyl cholestane (CSL). The structure of this probe with the components of its static hyperfine coupling tensor is shown in Figure 17. In this probe, the nitroxide label is fixed on the rigid steroid framework. Thus, the EPR spectral response of the probe should reflect the overall motion of the entire molecule. This feature is important since the probe orients with the nitroxide close to the phospholipid/water interface (38) so that the rigid steroid ring system is located in the upper region of the phospholipid acyl chains.

The behaviour of the CSL probe was compared with that of a deuterium-labelled analog, cholesterol-3α-d_1. The structure of these two probes are quite similar except at the site of the magnetic resonance label. Thus, the ^2H NMR behaviour of cholesterol-3α-d_1 is used as a reference standard for the nitroxide spin probe.

The behaviour of each probe was examined in egg PC bilayers, measuring the effects of variation of temperature and cholesterol concentration on the order parameters derived from their spectra. In addition, the angular dependence of the EPR spectra of CSL, 5-SASL and 14-SASL in oriented film samples was examined. S_{mol} for cholesterol-3α-d_1 can be calculated from (6):

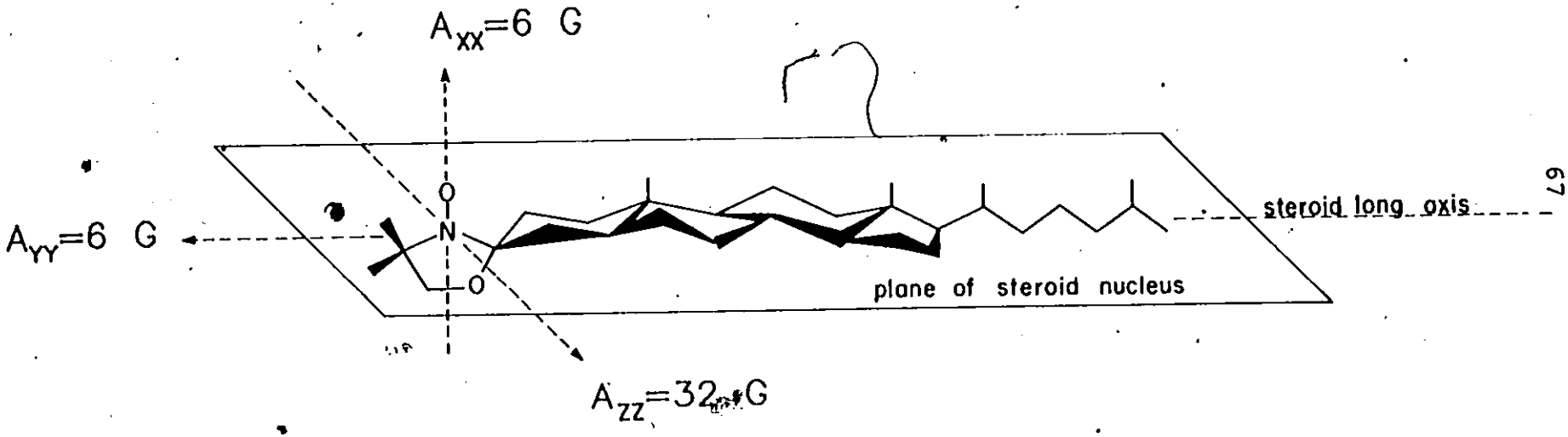

Figure 17. Structure of the cholestane spin label (CSL) showing the components of the hyperfine coupling tensor.

$$\Delta\nu = \frac{3}{4}\frac{e^2qQ}{h}\frac{(3\cos 2\alpha - 1)}{2}S_{mol} \qquad (10)$$

where $\Delta\nu$ is the quadrupole splitting measured from the separation of the intense peaks of the ^2H powder spectrum as shown in Figure 18B, e^2qQ/h is the static quadrupole coupling constant for the C-^{2}H bond (~170 KHz) and α is the angle between the C-^{2}H bond and the rotation axis of the molecule. In a separate study (see Section IV.5) this angle was determined to be 79±2°.

IV.2.2 Results and Discussion

Figure 18 shows a representative EPR spectrum, (A), of CSL and a ^2H NMR spectrum, (B), of the cholesterol-3α-d_1 in 40 mole % cholesterol/egg PC bilayers. As for the fatty acid spin probes, the CSL spectra were obtained using oriented film samples. The order parameter, S_z is calculated with equation 9. Unlike the fatty acid probes, the nitroxide axis is not located along the axis of motional averaging so that S_{mol} is not equivalent to S_z. The molecular order parameter for CSL, assuming that the Z axis is perpendicular to the averaging axis (39, 40), is given by equation 5 with α equal to 90°. Thus,

$$S_{mol} = \frac{S_z}{-0.5} \qquad (11)$$

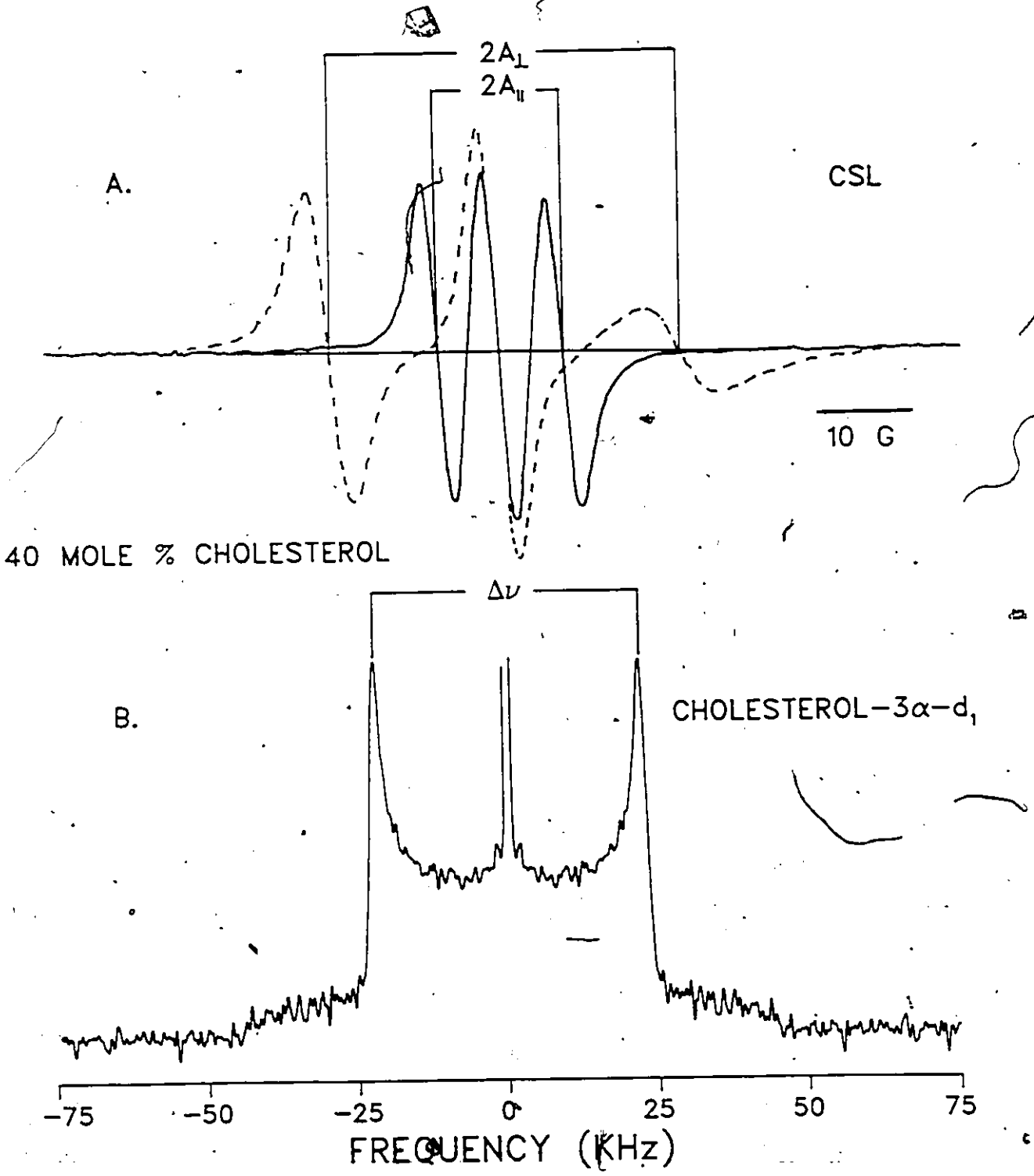

Figure 18. A. EPR spectrum of CSL in an oriented film. B. ^2H NMR spectrum of cholesterol-3α-d_1 in bilayers. Both spectra are for 40 mole % cholesterol in egg PC. The measurements of the spectral parameters for calculations of order parameters are shown.

The first comparison between the two steroid probes is made on the basis of response to temperature variation. Figure 19 illustrates the temperature dependence of the order parameters derived from CSL (triangles) and cholesterol-3α-d_1 (squares) for bilayers formed from 30 mole % cholesterol in egg PC. Below 20°C, broadening of the resonances for CSL precludes accurate measurement of its order parameter. Each probe shows a rather weak linear response to temperature variation which is more pronounced for the CSL probe. It is interesting to note that the order parameters for CSL are greater than those for the deuterated cholesterol. This is in sharp contrast to the previous comparison of nitroxide- and deuterium-labelled fatty acids where the discrepancies in order parameter were much greater, and the order parameters for the nitroxide-labelled fatty acids were always less than those of their deuterium-labelled analogs. The difference in magnitudes of the order parameters will be discussed in more detail below. In general, it can be seen that the qualitative and quantitative features of the responses of both probes are quite similar.

A second comparison can be made on the basis of the response of each probe to variation of cholesterol concentration in the membrane. Figure 20 shows the dependence of order parameters on cholesterol concentration for CSL (triangles) and cholesterol-3α-d_1 (squares). The CSL probe shows a stronger,

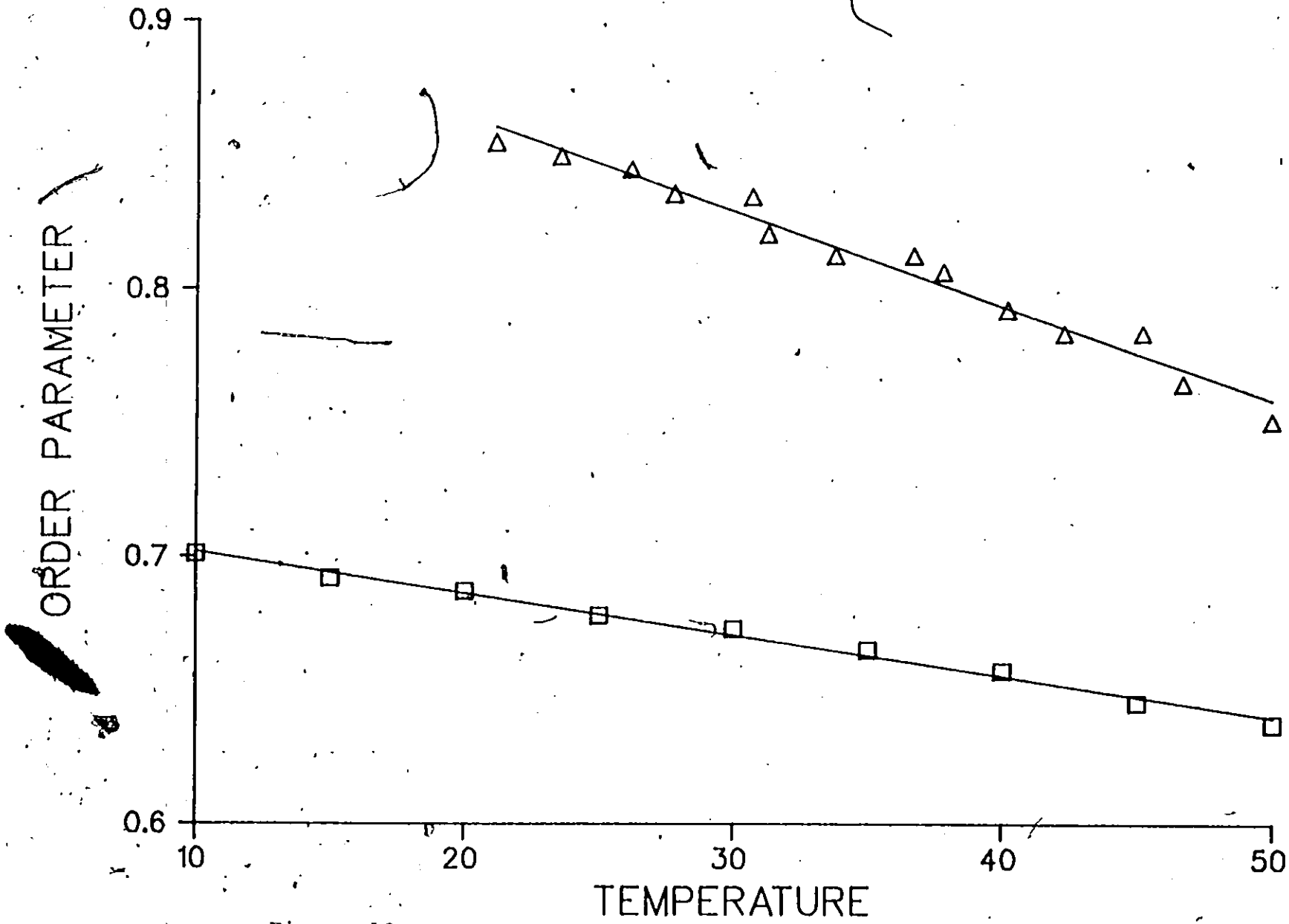

Figure 19. Temperature dependence of the order parameters derived from CSL (triangles) and cholesterol-3α-d_1 (squares) for 30 mole % cholesterol.

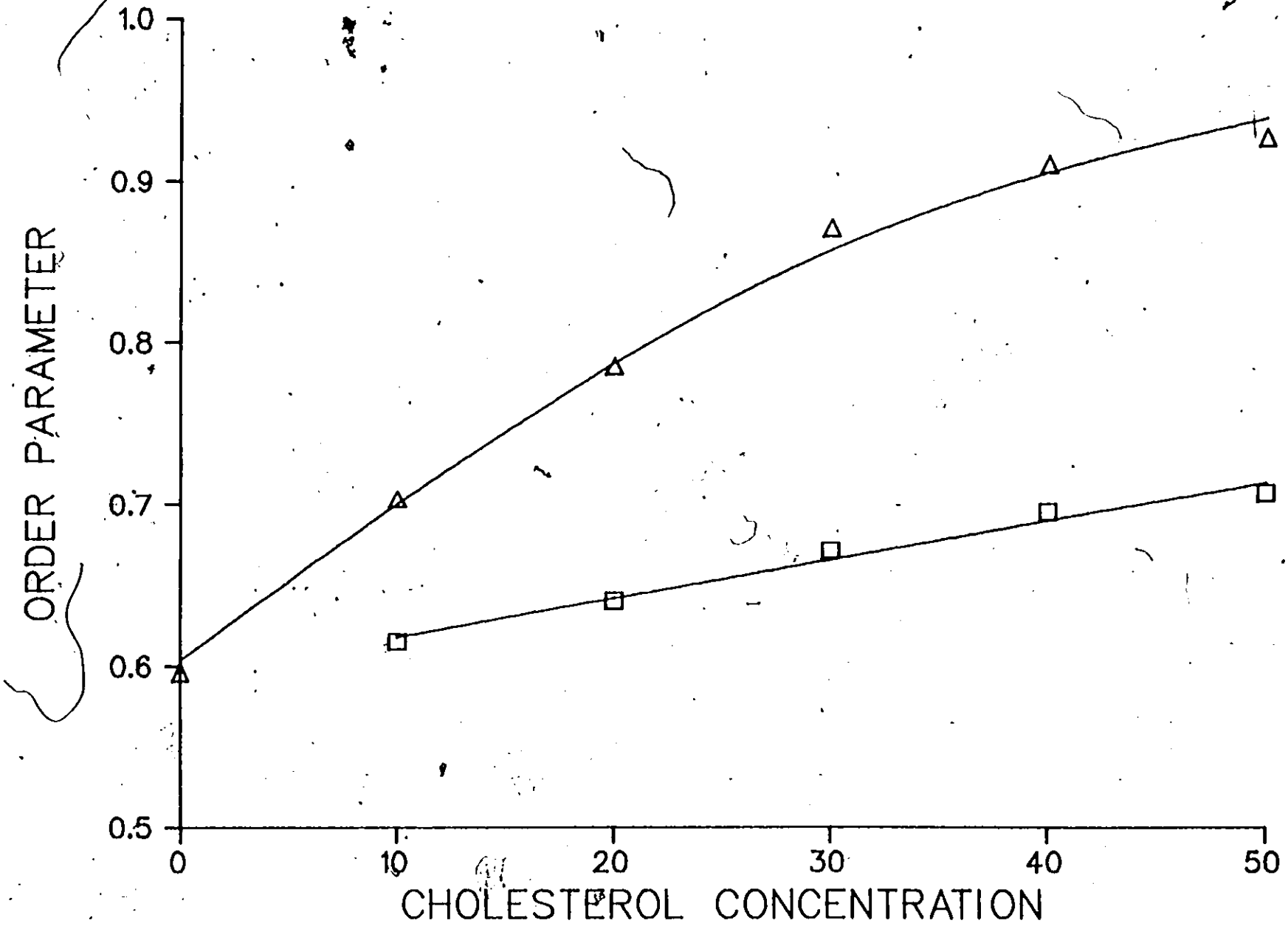

Figure 20. Variation of order parameters with cholesterol concentration for CSL (triangles) and cholesterol-3α-d_1 (squares). Sample temperatures: CSL, 25 °C; cholesterol-3α-d_1, 30 °C.

and non-linear, response to cholesterol addition than the deuterated cholesterol, particularly at lower cholesterol concentrations. The two probes exhibit essentially parallel responses at higher cholesterol concentrations. The results for CSL show reasonable agreement with a previous study of CSL in egg PC (41).

The present data indicate that the behaviour of the two probes is quite similar. The greatest discrepancy observed between the probes is in the magnitudes of the calculated molecular order parameters. In comparing the values of the order parameters for the two types of probes, it must be kept in mind that their magnitudes are sensitive to the assumed values for the static hyperfine or quadrupole couplings and the orientation of the axis about which the probe undergoes anisotropic motion. It has been shown (39, 40) that to a good approximation, the motion of the CSL probe is axially symmetric about the nitroxide y axis, as was assumed here. The rotation axis of cholesterol, as shown in Section IV.5 is located at ~79° to the C-^{2}H bond at position 3 of cholesterol. It should be noted, however, that small deviations from this assumed geometry would result in an increase in the calculated values of molecular order parameters.

The larger order parameters observed for CSL may also be due to inherent differences in the properties of the two probes. It can be seen in Figures 19 and 20 that the correspondence

between the magnitudes of the order parameters for the two probes is best in situations of low inherent order (high temperature or low cholesterol concentration) and diverges as the membrane is rigidified. This may be due to a changing balance in the factors which influence the motions of the probes in the membrane. Each probe is amphiphilic with a polar region which anchors the probe at the aqueous interface and a large, rigid steroid framework embedded in the phospholipid acyl chain region. The behaviour of both probes is influenced by interactions between the lipid acyl chains and the apolar region of the steroid and by the strength of polar interactions in the interface region. In an environment of low order (high temperature or low cholesterol concentration) the acyl chains undergo large amplitude motions and the apolar interactions may dominate the motion of the steroid probes. In this case, similar behaviour can be expected for both types of probes. As the membrane is rigidified, polar interactions at the anchoring site of the probes may influence the motional behaviour of the probes more strongly. In this case, higher order parameters for the CSL probe may be expected due to the high polarity of the nitroxide group (29) relative to the hydroxyl function of cholesterol.

In any case, it would be unreasonable to expect exact agreement for the order parameters of the two probes. The observation of large order parameters for the CSL probe

indicates that this particular nitroxide does not seriously disrupt the organization of the membrane. In assessing the reliability of CSL as a membrane probe, it is more important to consider the order parameter trends observed with changes in the membrane rather than their absolute magnitudes. Satisfactory agreement is found between the responses of CSL and cholesterol-3α-d_1 for temperature and cholesterol concentration variation, which indicates that CSL can yield reliable information regarding changes in the membrane organization.

The reasonable agreement found for CSL and cholesterol-3α-d_1 can be contrasted with the results of the previous comparison of spin-labelled and deuterium-labelled fatty acids. For that system, particularly poor agreement was noted in order parameter trends for label positions in the upper (carbon atoms 2-10 of stearic acid) portion of the acyl chains. It is interesting to note the difference between the behaviour of CSL and these particular doxyl fatty acids. Similar behaviour could be expected for a steroid and the upper region of the acyl chains since the rigid framework of the steroid lies in this region. Such similarities are, in fact, observed by deuterium NMR of deuterated cholesterol and acyl chains deuterated in this region. Essentially equal quadrupole splittings were observed for cholesterol-3α-d_1 and the 5-position of palmitic acid in an equimolar mixture of cholesterol

and dipalmitoyl PC (42). The same observation can be made by comparing the order parameters for cholesterol-3α-d_1 (this study) and the 2-10 positions of stearic acid (31) in egg PC-cholesterol (30 mole %).

The different responses of steroid and acyl chain spin probes may be due to special conformational features of fatty acid spin probes labelled in the upper chain. Previous EPR spin probe studies have provided evidence for tilting of the phospholipid chains (32, 36, 43). In the models derived from these studies, the acyl chains are tilted away from the normal to the bilayer plane with a greater tilt angle for the upper portion of the chain. The rotational behaviour of the spectra of spin probes in oriented films of egg PC-cholesterol (30 mole %) was examined to determine if such a tilted structure exists in this lipid system. Figure 21 illustrates the variation in the observed hyperfine splittings for CSL, 5-SASL, and 14-SASL with the angle, theta, between the field and the normal to the flat cell surface. The hyperfine splittings were measured as one half the separation between the zero crossing points of the low and high field resonances. For all orientations, the spectra for CSL and 14-SASL consisted of 3 well-resolved symmetric lines. In contrast, the 5-SASL probe gave such a spectra only for angles near 0° or 90°. Such a position-dependent behaviour has been noted for phospholipids spin-labelled at positions 5 and 16 (32, Figures 9A

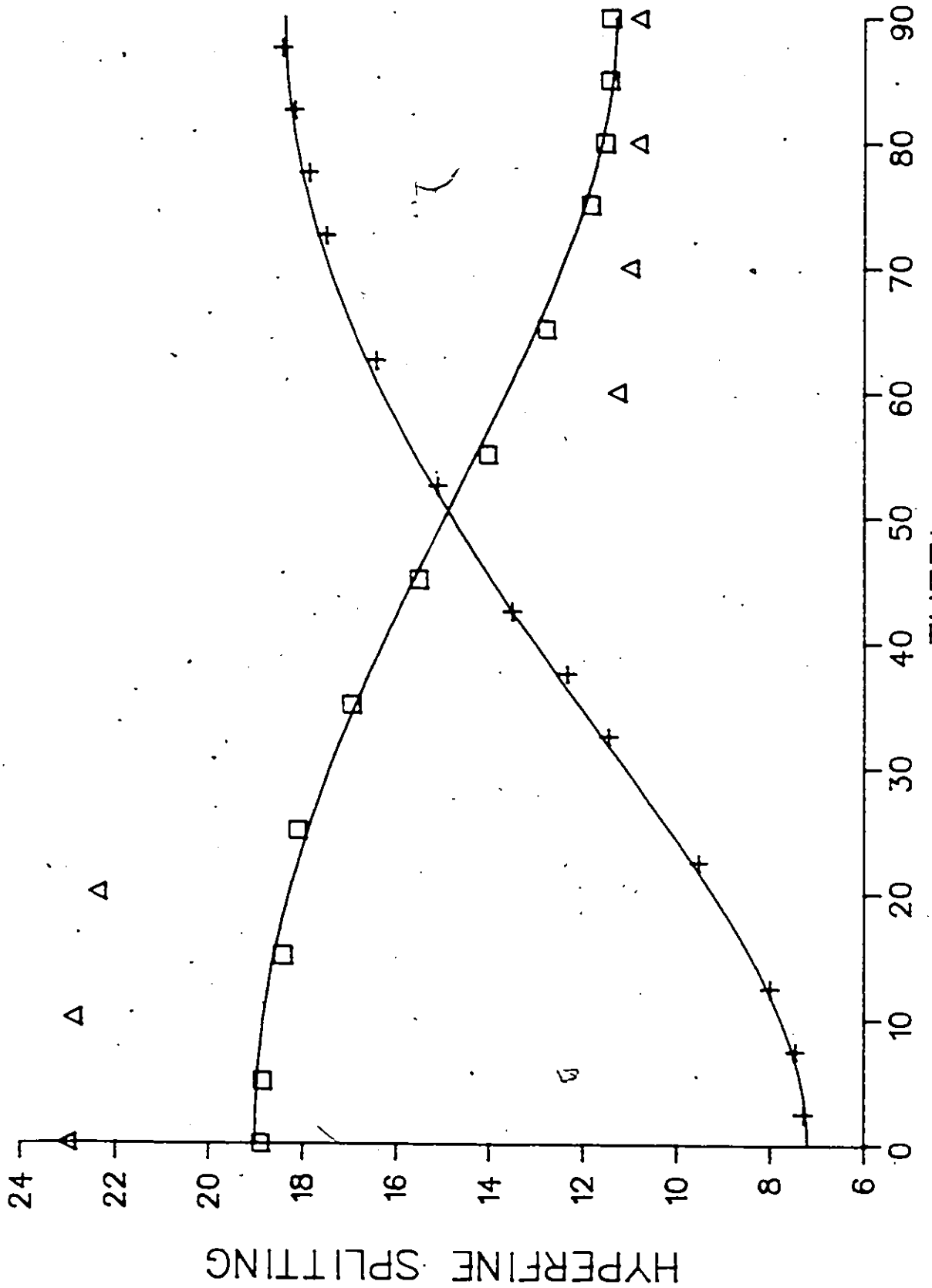

Figure 21. Angular dependence of the hyperfine splittings for CSL (squares), 5-SASL (triangles) and 14-SASL (crosses). The angle θ was measured between the direction of the static magnetic field and the normal to the flat cell surface.

and 9B) and was attributed to a position-dependent tilt of the fatty acyl chains. The solid lines of Figure 21 represent the equation:

$$A(\theta) = (A_{\parallel}^2 \cos^2\theta + A_{\perp}^2 \sin^2\theta)^{1/2} \qquad (12)$$

where $A(\theta)$ is the observed hyperfine splitting at angle θ and $A_{\parallel}$ and $A_{\perp}$ are the splittings observed for the field parallel and perpendicular to the axis of motional averaging, respectively. This relationship should be obeyed if the phospholipid chains are oriented along the normal to the bilayer plane rather than tilted away from it. In addition, if the acyl chains orient perpendicular to the bilayer plane, the splitting observed at the "magic angle" ($\theta \approx 54.7^{\circ}$) should be equal to the isotropic splitting. Good agreement with theory is observed for the CSL and 14-SASL probes, indicating that these probes orient perpendicular to the membrane plane. The angular dependence of the spectra for 5-SASL indicates that this probe is not oriented in such a fashion. It might be possible to simulate the rotational behaviour of the 5-SASL spectra using models with tilted acyl chains, but it is difficult to explain the presence of a tilt of the fatty acid chains in this region in view of the result for CSL. As stated above, the steroid probe should display behaviour similar to that of the upper portion of the acyl chains and, in particular, it could be expected to orient in a tilted fashion if the

phospholipids were tilted. It is important to note that CSL and the doxyl fatty acids are sensitive to motions with similar time scales, so that both types of probe should sense a tilt if it is present. This is not necessarily the case with deuterium NMR where a tilt may not be observable due to the lower time resolution of deuterium NMR (32). The discrepancy between CSL and the doxyl fatty acids may be due to difficulties associated with the insertion of the doxyl group into the upper region of the bilayer. The results of deuterium NMR studies of a number of phospholipids (15, 44, 45, 46) indicate that this region of the bilayer shows a high and essentially constant degree of order. A tilting of the nitroxide moiety of the 5-SASL probe may represent a conformational adaptation by the probe to allow insertion of the bulky nitroxide group into this efficiently packed region. Such a perturbation diminishes the utility of this probe in biological studies since it is difficult to distinguish between effects due to inherent membrane properties and those resulting from difficulties in the incorporation of the probe.

IV.2.3 Conclusions

Based on these and the previous comparative studies of nitroxide spin probes and deuterated probes, it would appear that the most reliable spin probe experiments for membranes can be performed using the cholestane spin probe or doxyl

fatty acids labelled in the lower portion of the acyl chains. The behaviour of these probes is at least qualitatively similar to that of the corresponding deuterium probes in terms of their response to variation of cholesterol concentration, temperature or label position. The CSL probe is suitable for studies of bulk effects in membrane systems due to its large, rigid structure which penetrates deeply into the bilayer (ref. 8, chap. 11). For studies requiring information on effects in a particular region of the bilayer, doxyl fatty acids labelled in the lower portion of the chain appear to yield data which are at least qualitatively reliable. Clearly, however, either type of study is best performed with a non-perturbing technique such as deuterium NMR.

The use of either type of nitroxide spin probe discussed above is somewhat limited by the nature of the EPR spectra observed for these probes in membranes. In order to calculate order parameters for these probes it is necessary to determine the parallel and perpendicular components of the hyperfine splitting. For CSL and some of the doxyl fatty acids, the difference between these components is too small to allow accurate determination of the order parameter for random dispersion (liposome) samples. In egg PC, for example, it is not possible to extract the splittings for random dispersion samples for label positions beyond carbon 12 of the stearic acid chain (Section IV.1). Thus, reliable spin probe studies

for these probes are restricted to oriented lipid film systems. This limits the usefulness of these probes, since many systems, in particular natural membranes, are difficult to orient. In addition, the interpretation of spectra for oriented systems can be complicated if the lipids adopt non-bilayer phases (Section IV.3).

IV.3 Comparison of Spin Probe EPR, ^{31}P- and ^{2}H-NMR in the Study of Hexagonal Phase Lipids

IV.3.1 Introduction

In spite of the problems in the quantitative interpretation of spin probe data, it is still possible to use these probes for qualitative studies of membranes. For example, if drastic alterations of the state of a membrane take place, the spin probes may reveal this event through large, characteristic changes in their EPR spectra. A possible candidate for this type of study is the lipid phase transition noted for some phospholipids. As discussed in Section I.1, some phospholipids undergo transitions between the lamellar bilayer phase and the hexagonal phase (2).

This type of phase transition has been well studied by ^{31}P NMR (12) and less extensively by ^{2}H NMR (47, 48). The phase transition produces characteristic changes in the NMR spectra of the phospholipids. The observed spectral behaviour is due to the nature of the motional averaging of the relevant anisotropic properties for each nucleus. In the bilayer phase,

the motion of the phospholipids is axially symmetric about the axis perpendicular to the planar membrane surface. This motion results in averaged tensors, P, with components $P_{\parallel}^{B}$ and $P_{\perp}^{B}$ where the B superscript refers to the bilayer phase. In the hexagonal phase, these components are further averaged by rapid diffusion of the phospholipids about the long axes of the cylindrical assemblies which make up the hexagonal phase. This additional rotation results in a large, characteristic change in the tensor, P. The bilayer components $P_{\parallel}^{B}$ and $P_{\perp}^{B}$ are averaged to produce a new axially symmetric tensor with components $P_{\parallel}^{H}$ and $P_{\perp}^{H}$ where the superscript H refers to the hexagonal phase. The values of $P_{\parallel}^{H}$ and $P_{\perp}^{H}$ are given by (7):

$$P_{\parallel}^{H} = \frac{1}{2}(P_{\parallel}^{B} + P_{\perp}^{B}) \qquad (13)$$

$$P_{\perp}^{H} = P_{\parallel}^{B}$$

For each tensor, the anisotropic part, P_{ANISO} can be calculated as discussed in Section I.2.1. If the anisotropic parts of the tensors for the two phases are compared, it is seen that:

$$P_{ANISO}^{H} = -\frac{1}{2} P_{ANISO}^{B} \qquad (14)$$

This effect has been noted in the ^{31}P and ^{2}H NMR spectra of phospholipids and other liquid crystals (47, 48). In addition, this property was observed in the EPR spectra of spin probes

in a soap-like system (49). If such an alteration were observed for spin probes in phospholipid membranes, the EPR method could be used in a qualitative fashion to examine these transitions in membranes. The high sensitivity of EPR relative to NMR would make spin probe studies an attractive alternative to ^{31}P or ^{2}H NMR.

The feasibility of such a diagnostic use of spin probes was examined in the system: egg phospholidylethanolamine (Egg PE)/cholesterol where a temperature-induced bilayer to hexagonal phase transition is known to occur (50). For purposes of comparison, the ^{31}P and ^{2}H NMR behaviour of a specifically deuterated PE was also examined.

IV.3.2 Results and Discussion

I. Spin Labels

A. Dispersions

Figure 22 shows the EPR spectra obtained for 5-SASL and 12-SASL in equimolar mixtures of cholesterol and egg PE at a series of temperatures. ^{31}P NMR experiments (data not shown) indicate that this lipid mixture undergoes a hexagonal to bilayer phase transition in the temperature range 30-35°C in agreement with previous work (50). This transition has very little effect on the EPR spectra as seen in Figure 22.

A continuous decrease in anisotropy is observed as the temperature is increased, which is more pronounced for the

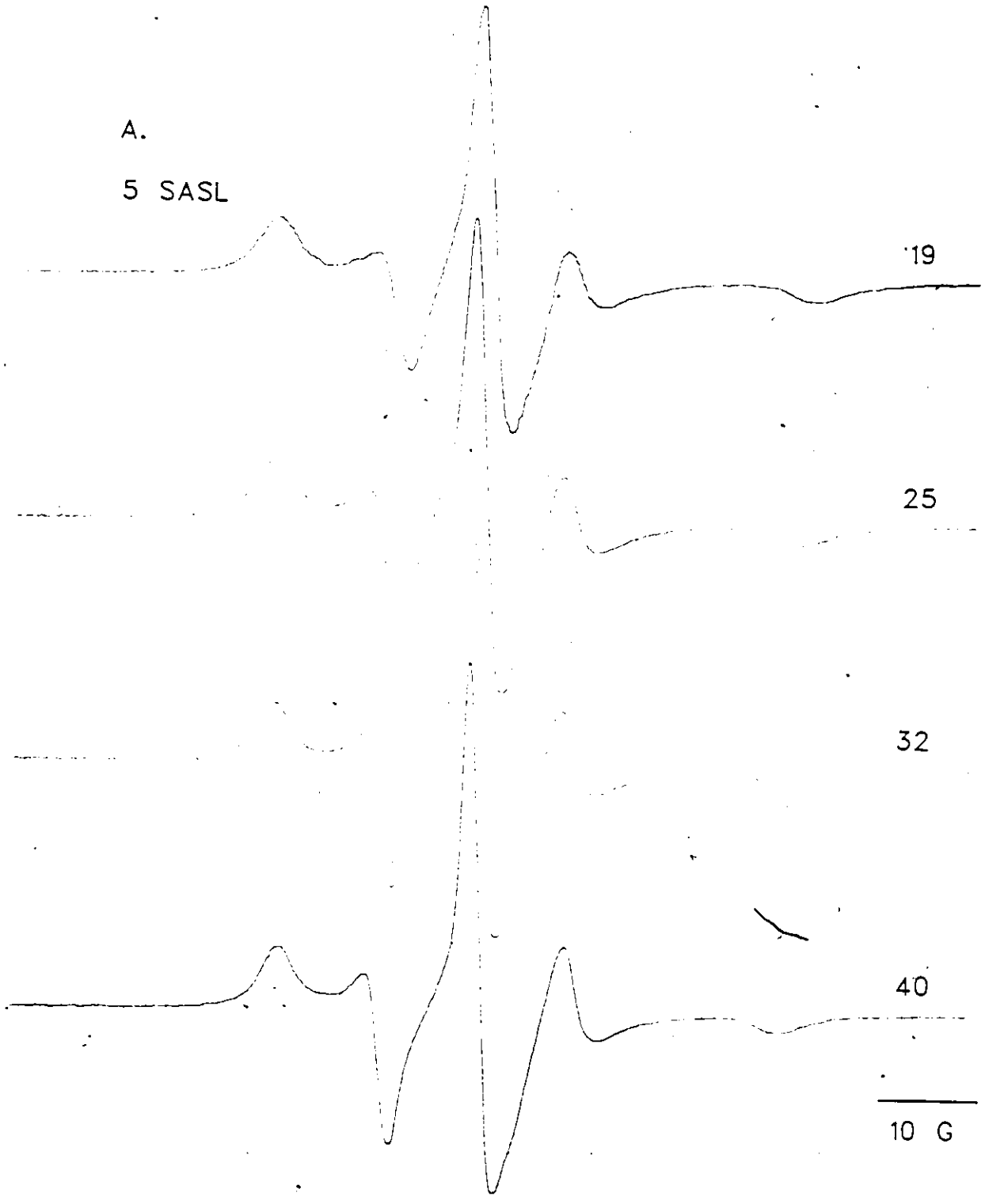

Figure 22. Temperature variation of EPR spectra in equimolar cholesterol-Egg PE for A. 5-SASL and B. 12-SASL.

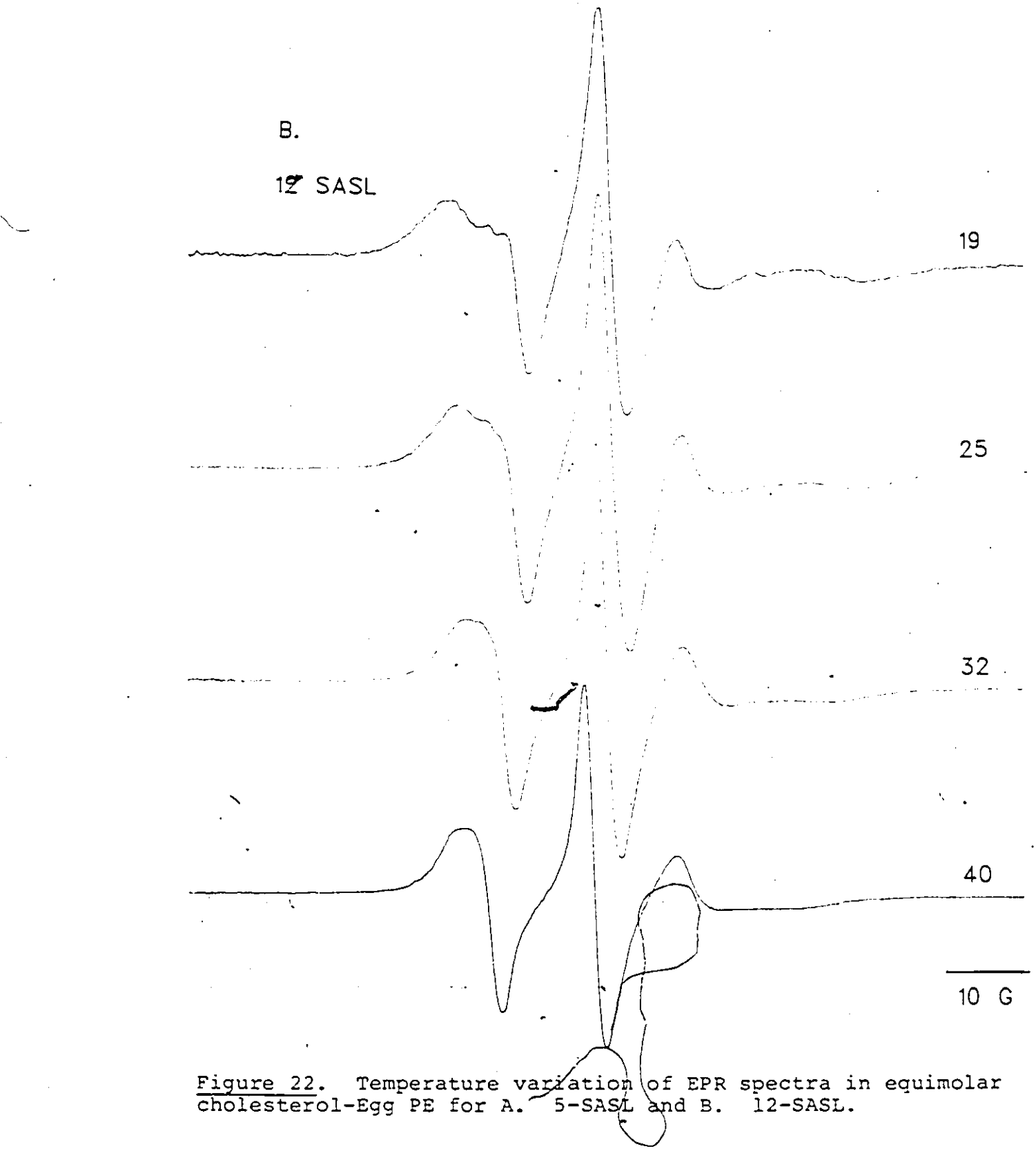

Figure 22. Temperature variation of EPR spectra in equimolar cholesterol-Egg PE for A. 5-SASL and B. 12-SASL.

12-SASL probe. The stronger response at the 12 position could arise in several ways. One might expect an increasingly strong response as the label position is moved toward the terminal methyl group for a transition from the bilayer to the H_{II} hexagonal phase. In the H_{II} phase, the lipids pack in cylinders with the headgroups at the core and the acyl chains directed toward the outer surface (2). In such a structure, the gradient of order proceeding toward the terminal methyl may be larger than in the bilayer phase. The larger response of the 12-SASL probe may, however, be due to a perturbation of the lipid system by the nitroxide probe. As discussed in Section IV.1, the 12-SASL probe exhibits an anomalously large response to the addition of cholesterol in egg PC bilayers. In that system, the spin probe method detects a maximal increase in order with addition of cholesterol at approximately the 12-position, whereas ^{2}H NMR (31) indicates an approximately constant response for the first 10-12 positions. Because of this, it is not possible to assign unambiguously the cause of the differential response noted in the hexagonal phase.

The spectra of Figure 22 do indicate clearly that the spin probes do not exhibit any large additional motional averaging on entering the hexagonal phase. In spin probe spectra, averaging about the cylinder axis could produce two large and characteristic effects analogous to those observed in ^{31}P NMR. The first effect is a two-fold reduction in the

spectral anisotropy. The second feature is the reversal in the sense of the anisotropy. As a practical example, consider a fatty acid spin probe in a well ordered bilayer characterized by an axially-symmetric hyperfine splitting tensor with components $A_{\parallel} = 32G$ and $A_{\perp} = 6G$, where $\parallel$ and $\perp$ refer to the symmetry axis of the tensor. If such a probe is now subject to rapid diffusion about a cylinder axis perpendicular to the probe long axis, the hyperfine tensor is averaged to yield components $A_{\parallel} = 6G$ and $A_{\perp} = 19G$. The most characteristic feature of the transformation is not the absolute reduction in the hyperfine anisotropy, which could arise from many types of averaging, but rather the change in the sense of the anisotropy. The latter feature has a strong effect on the overall shape of the spectrum. For a random dispersion of probes, the spectral intensity in the powder pattern is weighted according to $\sin\theta$, where θ is the angle between the field and the symmetry axis of the A and g tensors. Thus, for a bilayer type spectrum, there is greater intensity in the region of the inner hyperfine splittings since the perpendicular component of the A tensor is smaller. In the hexagonal type spectrum, the outer extrema are more intense because the sense of the tensor has been reversed and the perpendicular component is now larger. Such effects in the overall shape of spin probe spectra have been noted for a liquid crystal which can exist in both phases (49).

The spectra in Figure 22 show no discontinuities due to the transition from bilayer to hexagonal phase. For each probe the spectral anisotropy decreases smoothly with temperature and the distribution of intensity maintains the same sense. The lack of the expected spectral response to the phase transition can be attributed to a slow rate of diffusion about the cylinder axis. If such motion is slow relative to the degree of anisotropy of the spectrum, no averaging effect is observed and the spin probes continue to exhibit bilayer type spectra. An analogous effect is observed in the spin probe spectra of sonicated vesicles. The spectra of spin probes in such preparations are quite similar to those from large multilamellar dispersions (41). Thus, although the vesicles have a small radius and high curvature, the lateral diffusion rate is not large enough to produce an averaging of the spectra.

This effect of diffusion rate in the hexagonal phase will most likely occur for all phospholipids so that the type of experiment described above will not be useful in a diagnostic fashion. The oriented film system was also examined since larger effects on the spin probe spectra could be expected in an oriented system.

B. Oriented Samples

In a spin probe study of hexagonal phase lipids, Boggs and Hsia (51, 52) obtained results similar to those described

above for dispersion samples. In addition, based on spectra obtained from oriented samples of Ca^{2+}-cardiolipin, they proposed that the lipid cylinders could be macroscopically oriented on a flat surface (52). In this type of organization, the long axes of the cylinders are oriented parallel to the flat surface and their directions are distributed randomly in the plane of the surface. Such an organization has been observed by ^2H NMR in a soap-water system (47). The orientation dependence of the EPR spectra of CSL, which yields well-resolved, strongly angular dependent spectra for the bilayer phase was examined, to determine whether this type of experiment can be used to study the hexagonal phase. Since one can expect rather complicated lineshapes in this system, EPR spectral simulations were performed for oriented cylinders, in the absence of rapid lateral diffusion. Before presenting the experimental results, some of the qualitative features expected for the EPR spectra of spin probes in oriented cylinders, are presented below.

Single Cylinder

In this model, the long axes of the probe are oriented in a circular fashion at right angles to the cylinder axis. If the cylinder is oriented with its axis along the field, all the probes are perpendicular to the field. In this case a 3 line spectrum is expected with g value and hyperfine splitting characteristic of the perpendicular component of

each tensor. If the cylinder axis is perpendicular to the field, the probes take up all angles with respect to the field. The spectrum is thus an envelope of those for all g and hyperfine values. This is similar to the spectrum obtained from a liposome sample except that the intensities are distributed differently in the two cases. For the liposome (or a random distribution of cylinders) there is a sin θ weighting, where θ is the angle between the field and the probe long axis (4). The distribution function for θ in the cylinder can be determined as shown below. Figure 23 shows an end view of a cylinder with probes located in the plane. The relative number of probes at angle θ from the field is calculated as the ratio of the surface area swept out in moving from θ to $\theta + d\theta$ to the total surface area. The total surface for a cylinder of length t and radius r is $2\pi rt$. The area element between θ and $\theta + d\theta$ is $rtd\theta$. The distribution function for θ is then:

$$dP = \frac{rtd\theta}{2\pi rt} = \frac{1\ d\theta}{2\pi} \qquad (15)$$

Thus, for this geometry the probes are evenly distributed with respect to θ, and the spectrum of a cylindrical sample perpendicular to the field will exhibit greater intensity in the spectral regions corresponding to probes at small angles with

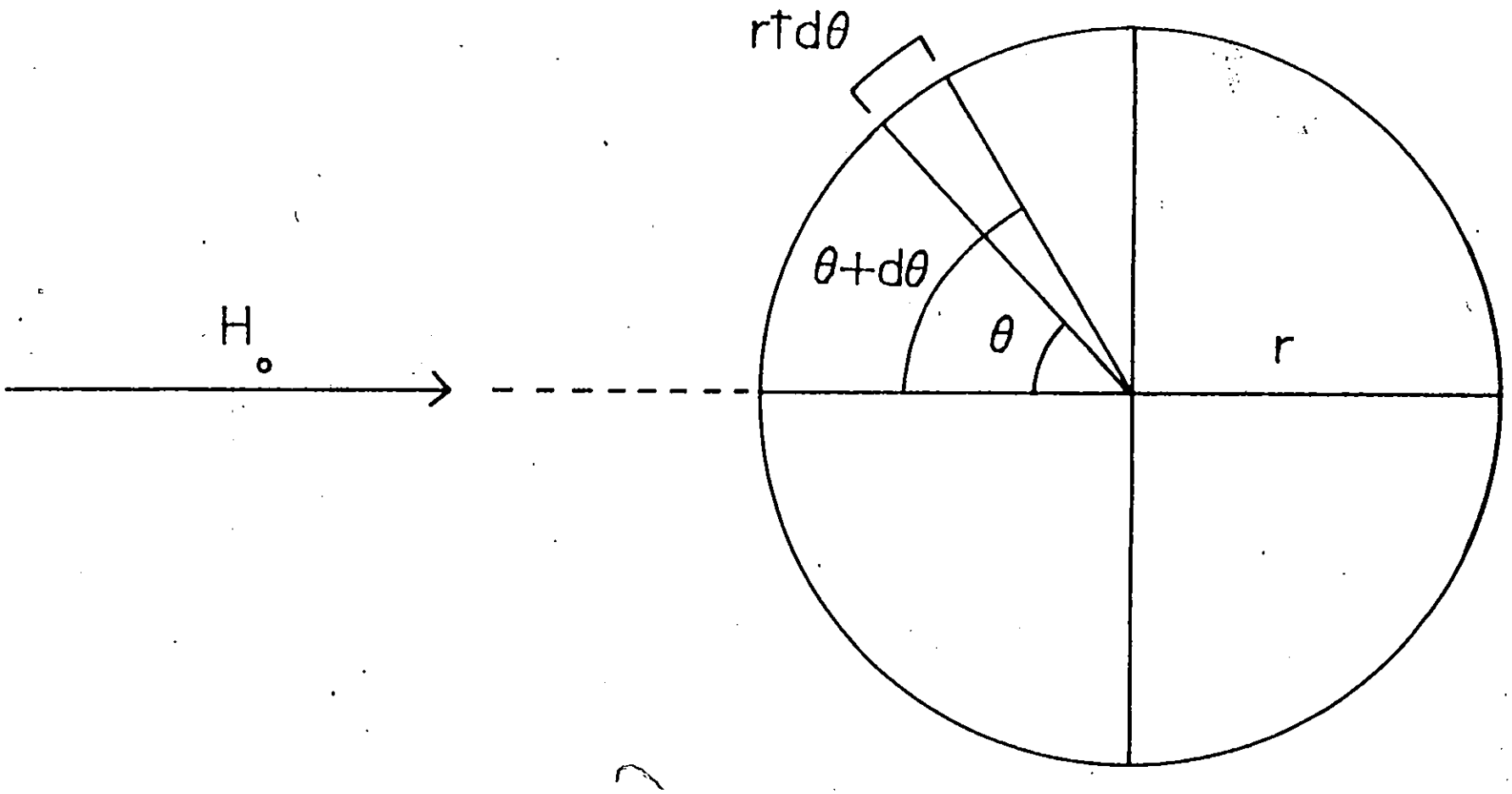

Figure 23. End view of single cylinder representing hexagonal phase lipids. The long axes of the probes radiate from the centre of the circle. The angle θ is between field direction and the probe's director.

respect to the field than will the spectrum of a completely random dispersion. This feature has been illustrated for fatty acid and steroid spin labels (ref. 8, chap. 10).

For a cylinder oriented at an intermediate angle, α (where α is the angle between the field and the long axis of the cylinder), the spectrum consists of a superposition of spectra for probes oriented between 90° and $90^\circ-\alpha$. Figure 24 shows a series of simulated spectra for the CSL probe oriented in a cylinder illustrating the change in spectrum expected for rotation of the cylinder. The 0° and 90° spectra show reasonable agreement with experimental spectra for CSL in a cylindrical sample (ref. 8, chap. 10).

Planar Distribution of Cylinders

The treatment above can be readily extended to deal with the case of an ensemble of cylinders oriented on a flat surface. Since the spectrum arising from a cylinder oriented at any angle can be calculated as above, it is only necessary to determine the distribution of cylinder orientations in order to calculate the spectrum. The qualitative features of the spectra for the cases where the flat surface is perpendicular or parallel to the field can be determined by inspection.

In the perpendicular orientation of the flat surface with respect to the field, all cylinder axes are at right angles to the field. This is equivalent to the case of a single cylinder at 90° and gives rise to a spectrum as shown in Figure 24.

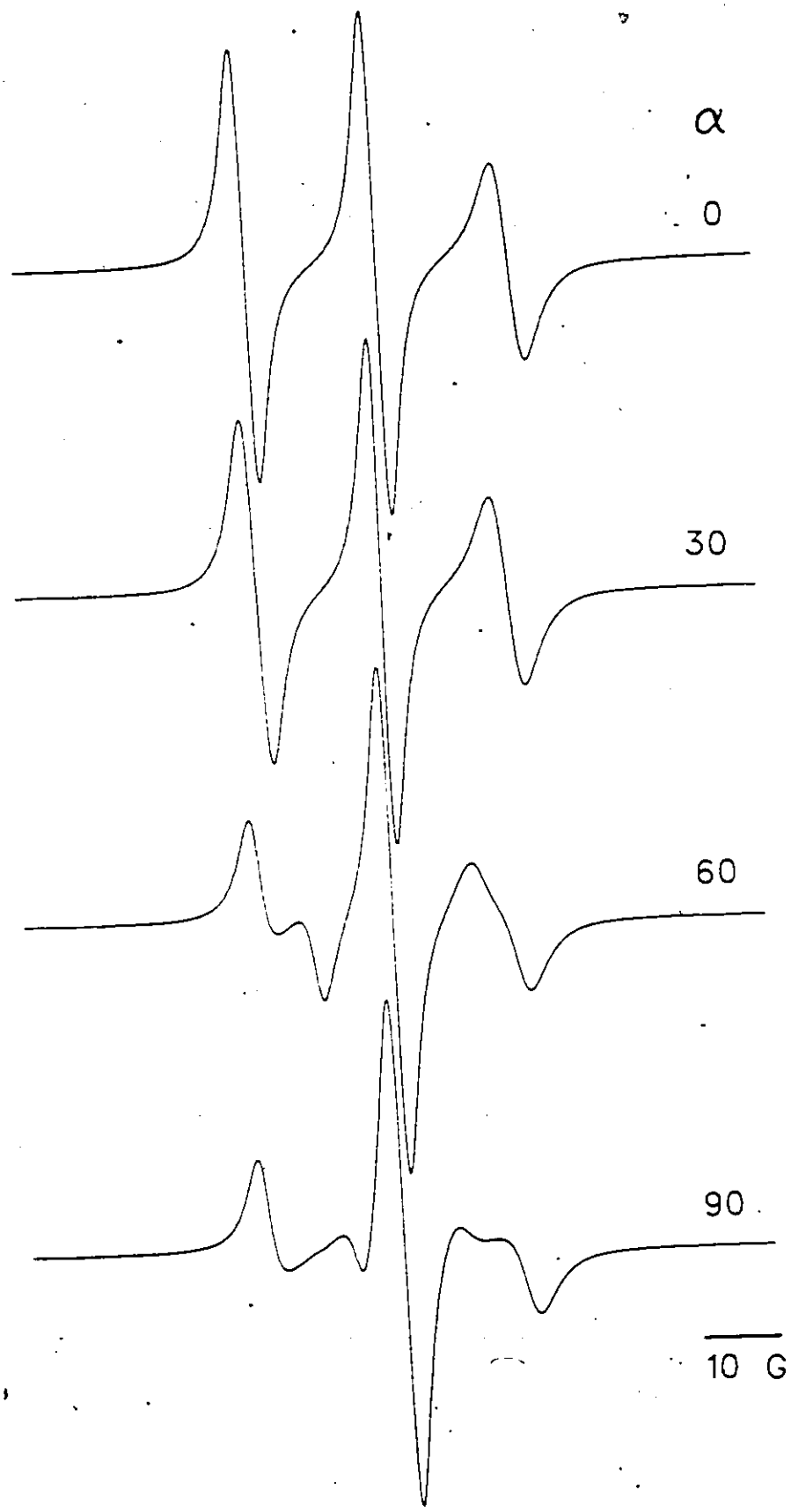

Figure 24. Simulated EPR spectra for CSL in a single cylinder. The angle α is between the field and the cylinder long axis. Spectral simulation parameters are given in Appendix I.

With the field parallel to the flat surface, the cylinder axes take up all angles with respect to the field. In this case, both polar angles describing the orientation of individual probes relative to the field are fully allowed. Thus, the spectrum obtained from this orientation is the same as that of a randomly-dispersed sample.

For both of these orientations powder type spectra are obtained which differ only in the weighting of intensities in the different regions of the spectrum. Thus, the variation in the spectra with rotation of the surface is much less dramatic than in the case of a single cylinder. A series of simulated spectra illustrating the rotation behaviour is shown in Figure 25, where ϕ is the angle between the field and the normal to the flat surface as in Figure 1. The details of the calculations are given in Appendix I.

Experimental Results

The angular-dependence of the EPR spectra for CSL in an oriented equimolar mixture of cholesterol and PE was studied. At the temperature of the experiment, ^{31}P NMR spectra of dispersions indicate that the lipid has entered the hexagonal phase (data not shown and ref. 50). Figure 26 shows the spectra obtained as the angle between the field and the normal to the surface of the flat cell is varied. Comparison with Figure 25 indicates that, qualitatively, the features expected for a planar distribution of cylinders are observed in this system. Since the

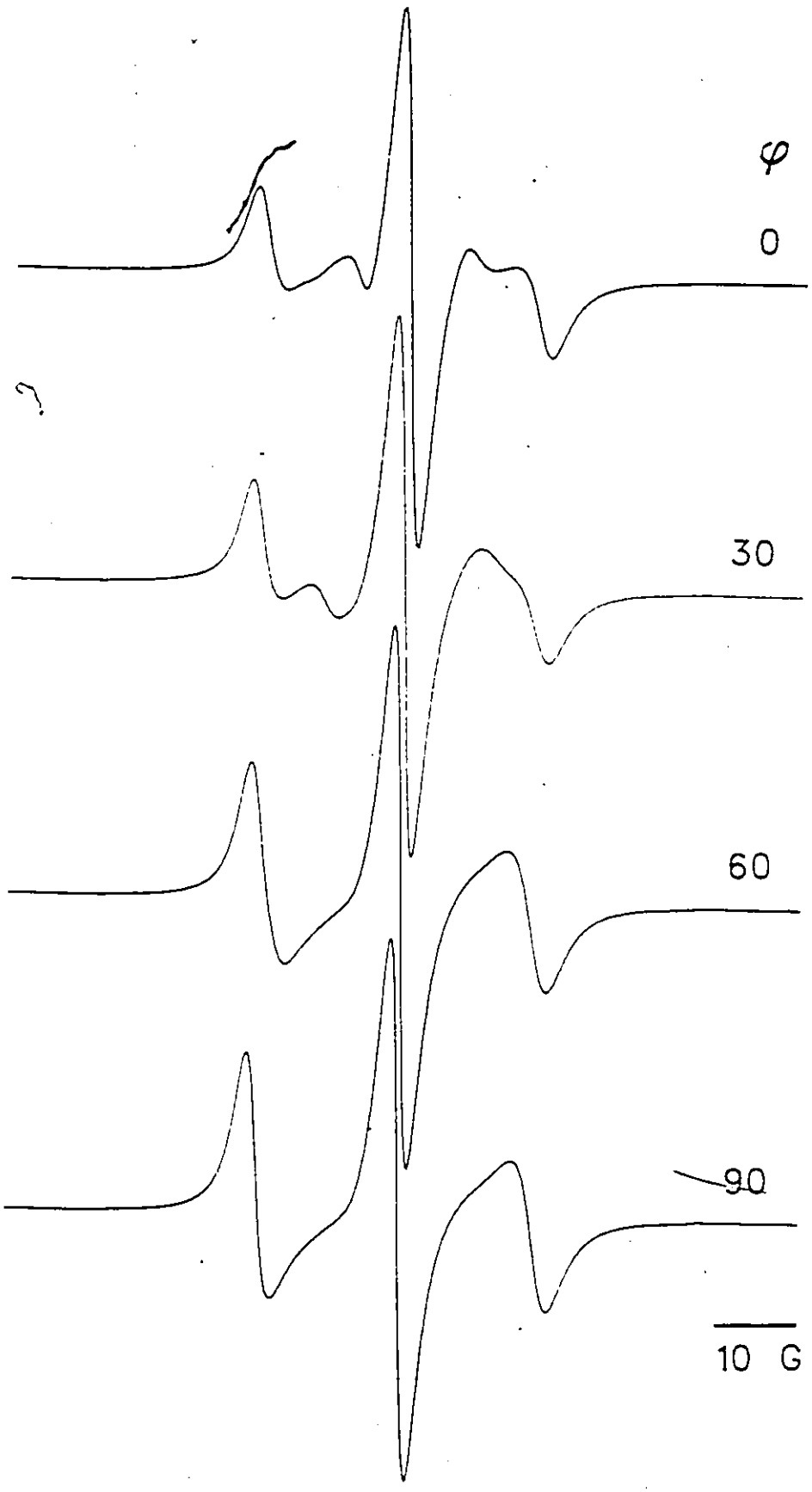

Figure 25. Simulated EPR spectra for CSL in an ensemble of cylinders oriented on a flat surface. The long axes of the cylinder are randomly distributed in the plane of the surface. The angle ϕ is between the field and the normal to the flat surface.

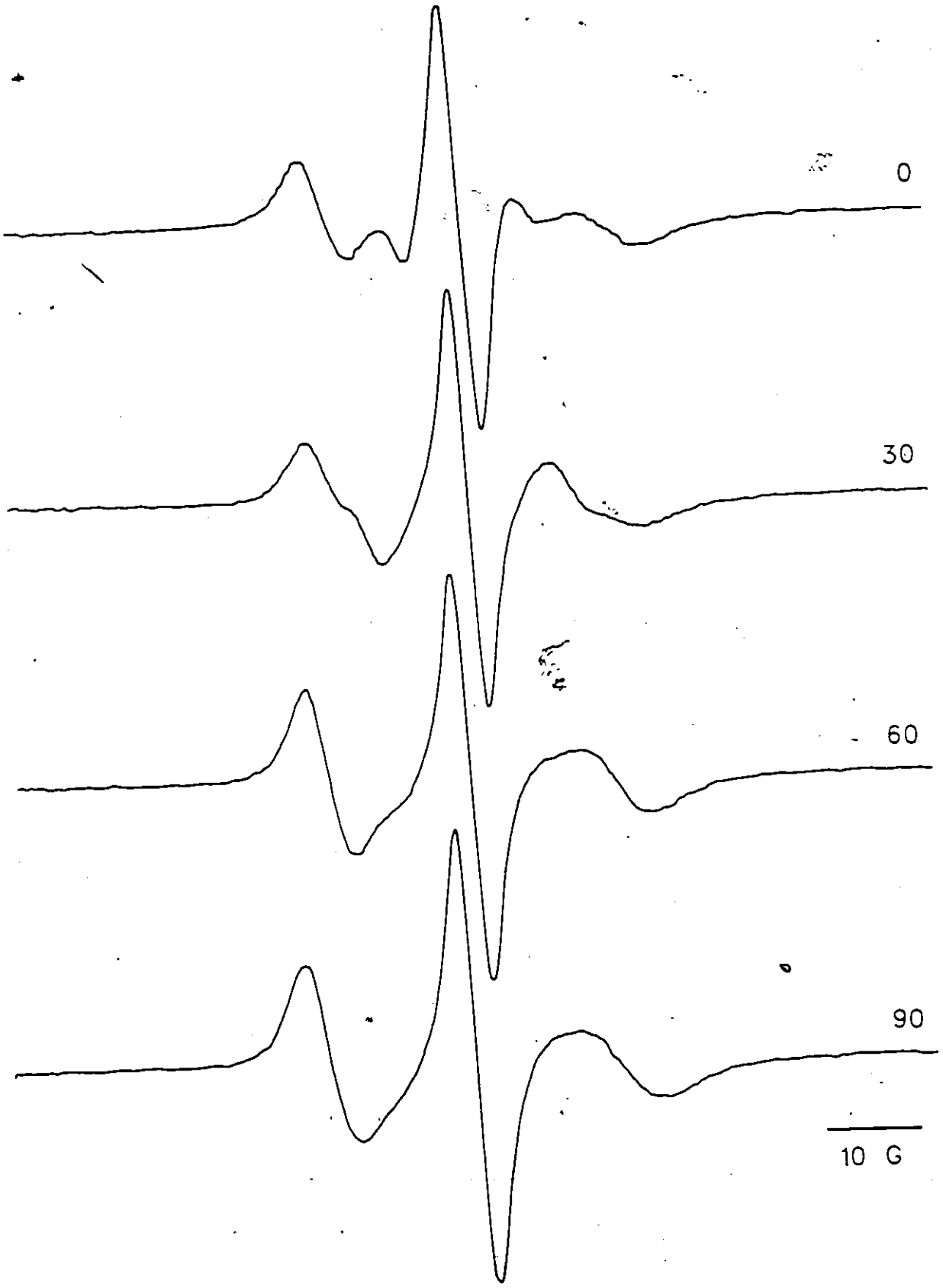

Figure 26. Experimental EPR spectra for CSL in equimolar cholesterol-Egg PE at 35°C oriented in a flat cell. The measured angle is between the field and the normal to the flat cell surface.

simulations were performed in order to predict qualitative features of the spectra, no attempt was made to improve the match between simulated and experimental spectra. It might be possible to obtain even better correspondence by adjustment of the spectral parameters, particularly by accounting for the effects of orientation-dependent linewidths and allowing a static misalignment of the cylinder axes out of the plane of the cell surface. However, an examination of the temperature dependence of the spectra indicates that other effects may be responsible for the lineshapes observed (vide infra).

In Figure 27, the spectra obtained with the field parallel (solid line), and perpendicular (broken line), to the normal to the flat surface are shown for a series of temperatures. The spectra at the lowest temperature are typical for CSL in a highly-ordered and well-oriented set of stacked bilayers. As the temperature is increased, this large anisotropy gradually decreases. At the highest temperature examined, there is very little difference observed in the spectra for the two orientations. Cooling the sample to the starting temperature results in a complete reversion to well-oriented bilayers. This temperature behaviour suggests that it is necessary to consider an alternative model for the macroscopic organization of the lipids at temperatures above that of the bilayer to hexagonal transition.

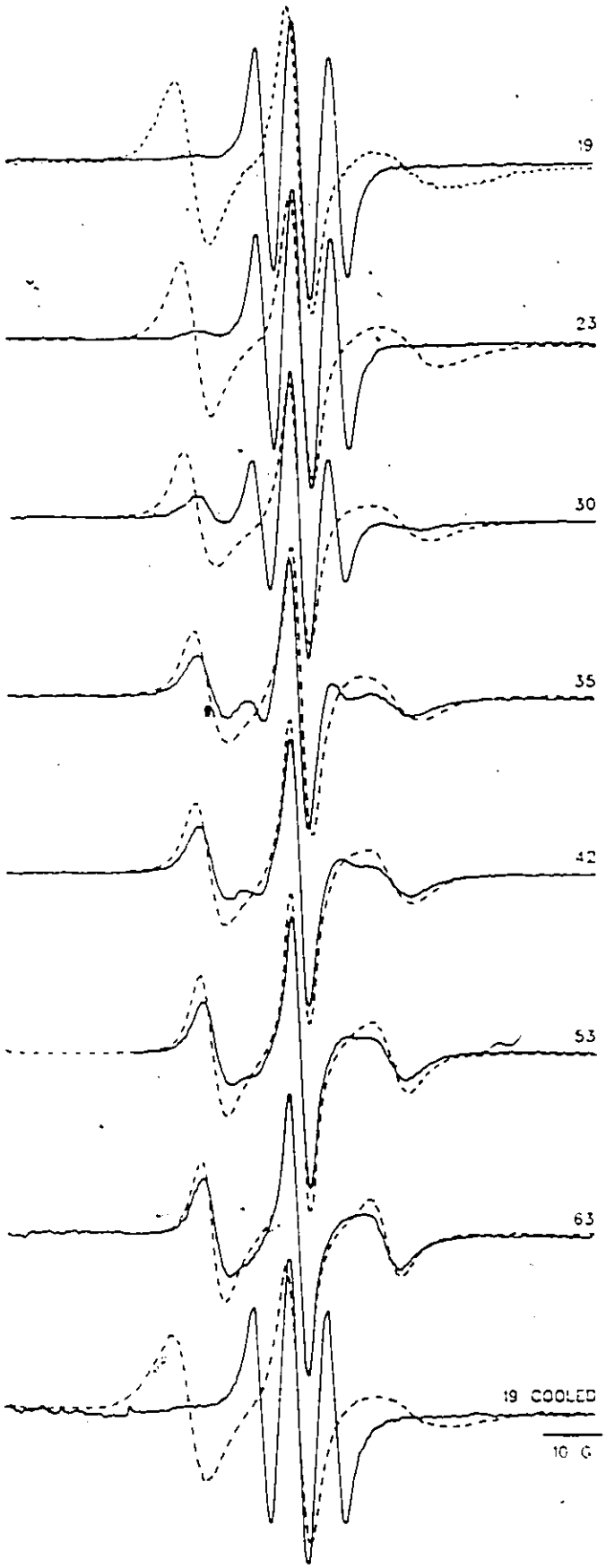

Figure 27. Temperature variation of the EPR spectra of CSL in equimolar cholesterol-Egg PE taken with the field parallel (solid line) and perpendicular (broken line) to the normal to the flat cell surface.

As the temperature is increased, a fraction of the lipids may remain aligned in a bilayer fashion on the flat surface. This fraction decreases with increasing temperatures, but the complete realignment on cooling suggests that some oriented bilayers persist and act as a "seed" for the formation of stacked bilayers on cooling. It is difficult to determine the orientation of the hexagonal phase lipids relative to the flat surface. As discussed above, the spectra from a planar distribution of cylinders differ from those of a random dispersion only in the relative weighting of intensities. The situation described above, where a fraction of the lipid remains in oriented bilayers is difficult to analyze, since the non-bilayer lipids may be randomly dispersed. The spectrum from such an ensemble, with the field perpendicular to the surface, will appear as a random powder spectrum with increased intensity in the region corresponding to probes oriented parallel to the field. This is, however, qualitatively very similar to the type of spectrum expected for a planar set of cylinders.

Simulations of the EPR spectra expected for these two types of organization were performed to determine how readily one can distinguish between them. For this set of simulations, a lower order parameter for the CSL probe was assumed. Figure 28 shows the spectra expected for the field aligned perpendicular (solid line) and parallel (broken line) to the flat

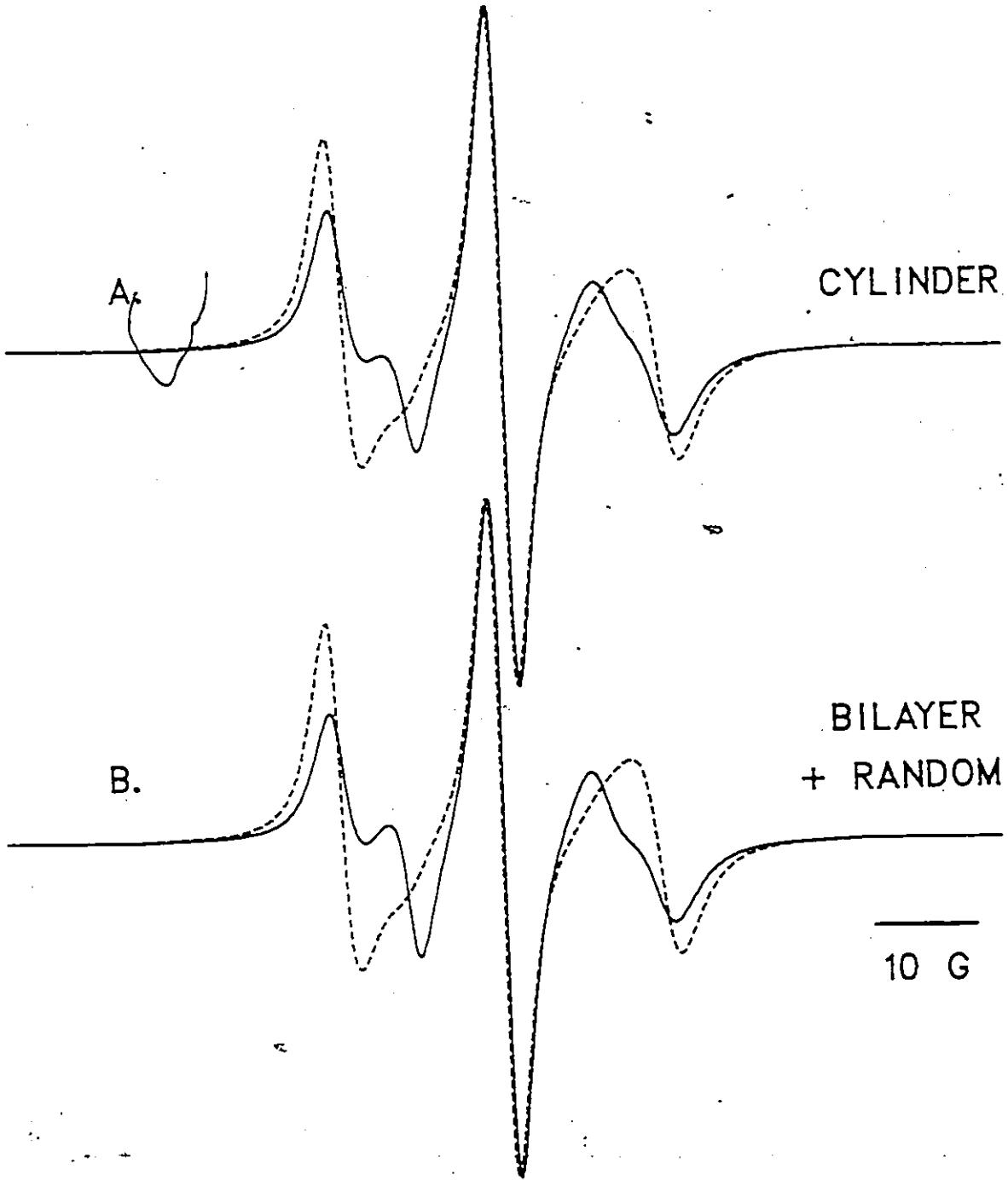

Figure 28. Simulated EPR spectra for CSL for two types of lipid organization in oriented systems. A. Planar distribution of cylinders. B. Summation of spectra for oriented bilayers (10 mole %) plus random dispersions (90 mole %). In A and B, the field is parallel (solid line) and perpendicular (broken line) to the normal to the flat cell surface.

surface. The spectra in Figure 28A are those of a planar distribution of cylinders. Those in 28B are the result of adding the spectra for stacked bilayers to a random dispersion of lipids to yield 10 mole percent bilayers. It is clear that these two cases could be distinguished only with the most careful simulations and a complete study of the rotation behaviour. It becomes increasingly difficult to distinguish the two cases as the spectral anisotropy decreases, due to possible low inherent order in the lipids or static misalignment on the flat surface.

In view of the similarity of these two types of spectra, caution must be exercised in the interpretation of spin label spectra in oriented systems where the phase behaviour of the lipids is unknown. Lineshapes of the type described above may result from the formation of oriented cylinders or simply from a partial orientation of bilayer phase lipids. Similar difficulties with spectral interpretation have been pointed out by Schreier-Muccillo et al. (53).

^{2}H and ^{31}P NMR

Deuterium NMR should prove more useful than spin label EPR as an alternative to ^{31}P NMR in the investigation of non-bilayer phases. ^{2}H NMR has been shown to be sensitive to the formation of the hexagonal phase in soaps and phospholipids (47, 48). The phase behaviour of a specifically-deuterated PE, derived from egg PC, was examined by ^{2}H- and ^{31}P-NMR. Figure 29 shows the spectra obtained for an equimolar mixture

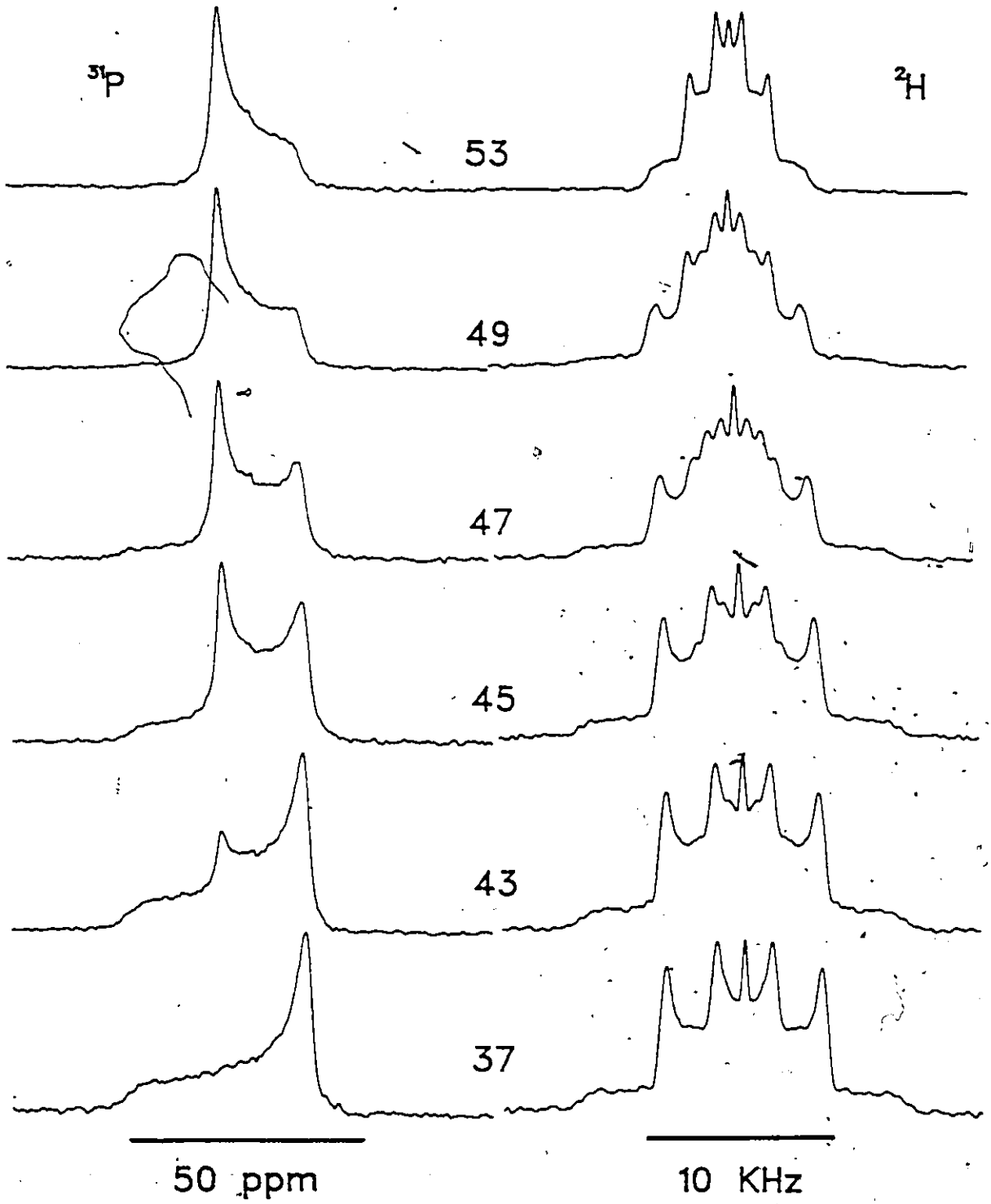

Figure 29. Temperature-dependence of the ^{31}P and ^{2}H spectra of an equimolar mixture of cholesterol and PE derived from egg PC via transphosphatidylation with deuterated ethanolamine. ^{31}P spectra; 125 KHz sweep width, 0.17 s. recycle time, 1500-5000 transients: ^{2}H spectra; 250 KHz sweep width, 0.1 s. recycle time, 6000 transients. The sample contained 150 mg total lipids in 0.5 ml buffer.

of cholesterol and deuterated PE for the two nuclei as a function of temperature.

The ^{31}P spectra are similar to those observed for other lipids which undergo temperature-dependent bilayer to hexagonal phase transitions. In the low temperature phase, the ^{31}P powder pattern exhibits a chemical shift anisotropy of approximately -39 ppm. As the temperature is increased, a second powder pattern gradually appears, increasing in intensity at the expense of the low temperature pattern. At the highest temperature, the spectrum again consists of a single powder pattern with an anisotropy of approximately 19 ppm. This reversal in sign and decrease in the magnitude of the ^{31}P powder pattern is expected for such a phase transition (7, 12). Note that the phase transition occurs at a higher temperature than with egg PE, due to the different acyl chain composition of egg PC from which this PE was synthesized.

Similar behaviour is noted in the ^{2}H spectra over the same temperature range. At low temperature, two splittings of 8.2 KHz and 2.9 KHz are observed. These resonances can be assigned to the α and β positions of the ethanolamine group, respectively (54). As the temperature is increased, a second set of splittings at 4.1 KHz and 1.4 KHz gradually appear. These splittings can be assigned to the α and β positions of

ethanolamine in lipids which have entered the hexagonal phase. At the highest temperature, only the latter set of splittings is observed. These spectral changes are analogous to those observed in the ^{31}P experiment, except that one cannot determine the sign of the quadrupole coupling since the powder pattern is symmetric about the central frequency.

In both the ^{2}H and ^{31}P experiments, the factor by which the spectral anisotropies were reduced was very close to 2. This indicates that the dynamic configuration of the entire headgroup must be similar in both phases. If the phase change were accompanied by a reorganization of the headgroup, this factor would be different from two. This observation can be contrasted with the behaviour of the acyl chains in dielaidoyl PE where an approximately three-fold reduction in the quadrupole splitting of the 9, 10 position was noted, indicating an increase in the amplitude of motion of the acyl chains (48).

The results presented above show that ^{2}H NMR can readily be used as a probe of non-bilayer formation. A method for quantitating the amounts of each phase in the mixed phase temperature region has been described (55).

IV.3.3 Conclusions

The experiments described demonstrate that spin label EPR will not provide a very useful alternative to ^{31}P NMR in the study of phospholipids which form non-bilayer phases.

As long as lateral diffusion about the cylinder axis is slow relative to the g and A tensor anisotropies, the spectra of randomly-dispersed cylinders and liposomes are indistinguishable. The oriented system can, in principle, be used as a monitor of hexagonal phase formation. The interpretation may become ambiguous, however, in cases of low inherent order or poor macroscopic alignment. In such cases, rigorous spectral simulations would be required to extract useful information. In addition, there is a strong possibility of confusing an oriented set of cylinders with a mixture of oriented bilayers and liposomes. All of the factors outlined above mitigate against the use of spin labels in a diagnostic sense.

Deuterium NMR can be used as an alternative to, or in conjunction with, ^{31}P NMR in the study of such phases. Unlike the ESR experiment, a large change is observed in the spectra of randomly dispersed lipids. The major advantages of ^{2}H NMR lie in the possibility of specifically-labelling different components in a lipid mixture or different sites in a single molecule, and the study of lipids containing no phosphorus in order to obtain a more detailed description of the organization of lipids in different phases.

IV.4 Deuterium NMR of Specifically Deuterated Nitroxide Spin Probes

IV.4.1 Introduction

In the previous three sections, problems associated with the use of nitroxide spin probes have been investigated through

comparison of the behaviour of the spin probes and non-perturbing NMR probes. The most serious discrepancies were noted for fatty acid nitroxide probes. In general, the order parameters for these probes were less than those observed for the corresponding deuterium-labelled probes and the nitroxide probes showed weaker responses to addition of cholesterol than did the deuterated probes. The most severe discrepancies were noted for nitroxide label positions in the upper region of the acyl chain. Spin probes with labels in the lower portion (carbons 12-16) of the chain showed behaviour which was at least qualitatively similar to that of the corresponding deuterium probes.

In contrast, good qualitative and quantitative agreement was found in the comparison of nitroxide- and deuterium-labelled steroids. This observation indicates that the discrepancies discussed above do not result from a general feature of the spin probe experiment, for example, the differences in the time scales of the EPR and NMR experiments. The angular dependence of the EPR spectra of spin probes in oriented film systems provided further evidence of problems with fatty acid spin probes labelled in the upper region of the chain.

The anomalous behaviour of the fatty acid spin probes was investigated in more detail using specifically deuterium-labelled fatty acid nitroxides. With these doubly labelled compounds, ^{2}H NMR can be used to obtain more specific information

on the motion of the spin probes. The spin probes employed were deuterium-labelled on the fatty acid chain and in the ring system of the nitroxide group. The probes were incorporated in egg PC bilayers as fatty acids or as the phosphatidylcholines derived from acylation of lyso-PC with a fatty acid spin probe. In addition, the diamagnetic N-hydroxy derivatives of the nitroxides were employed to avoid problems associated with obtaining NMR spectra in a paramagnetic system.

In the discussion, the data for the deuterated spin probes are combined with the results of the previous sections in an attempt to provide a unified explanation of the anomalous behaviour noted for the spin probes.

IV.4.2 Results and Discussion

The first studies dealt with a fatty acid probe bearing a nitroxide label at position 5 and deuterium labels at positions 2, 4 and 6 (5-SASL-d_6). The samples studied consisted of 25 mg spin probe in 250 mg egg PC with variable amounts of cholesterol. The ^2H NMR spectra for the probe are shown in Figure 30. Three sets of quadrupole splittings are observed for the probe. On the basis of a previous study (56) of a related deuterated spin probe, the smaller splittings can be assigned to the deuterons adjacent to the nitroxide and the larger splitting to the deuterons at position 2. These results may be compared with data for deuterated stearic acid intercalated

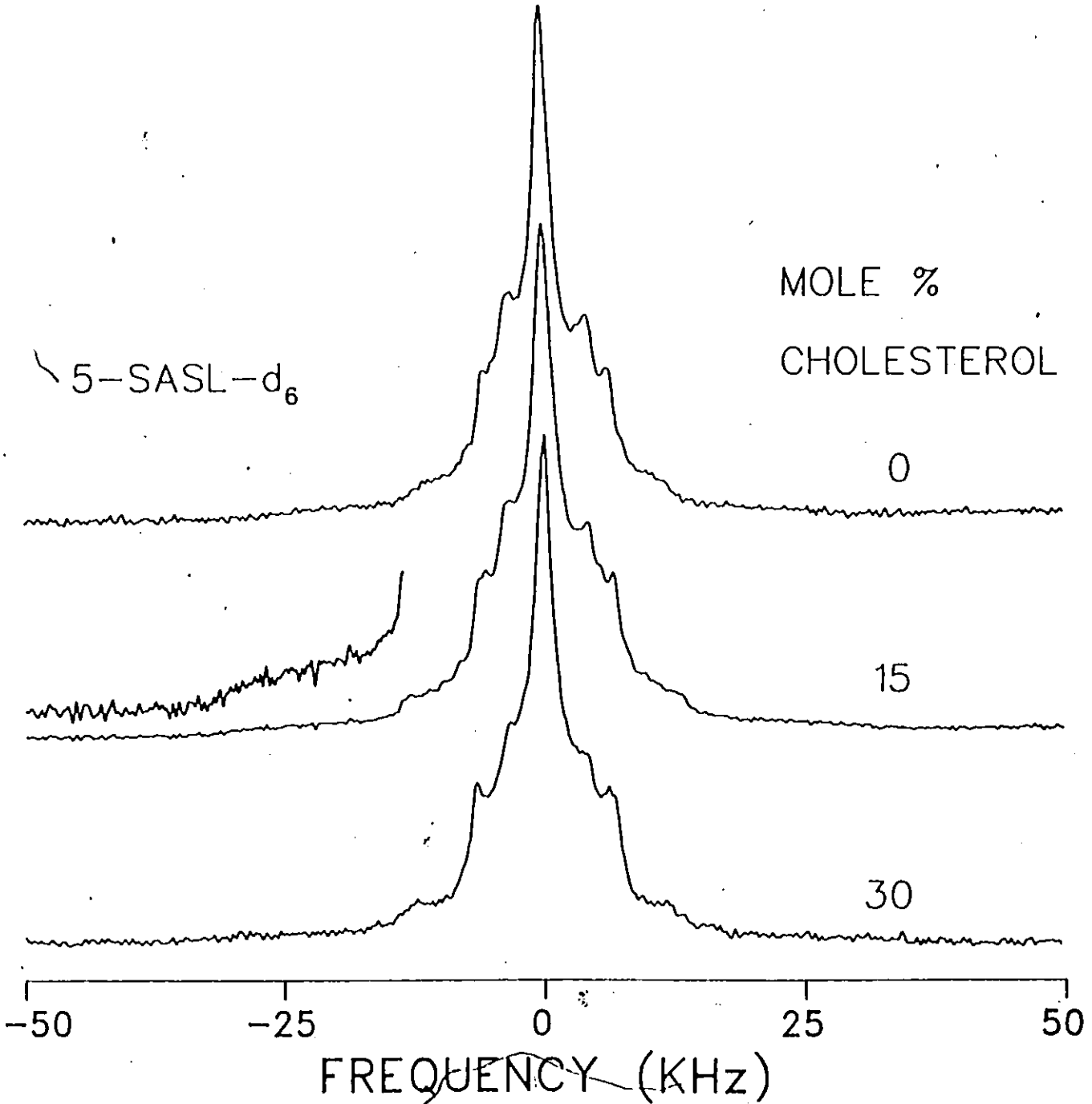

Figure 30. ^2H NMR spectra of 5-SASL-2,2,4,4,6,6,-d_6 in egg PC membranes with the indicated cholesterol concentrations at 30°C. Spectra were recorded with a recycle time of 0.1 s. acquiring 72,000 scans.

in egg PC bilayers (31). In Figure 31, the quadrupole splittings observed for different cholesterol concentrations are plotted for the 2-10 positions of stearic acid (squares); the 2 position of 5-SASL-d_6 (triangles); and the 4, 6 positions of 5-SASL-d_6 (diamonds). For the stearic acid probe, a sharp increase is noted in the quadrupole splittings as the cholesterol concentration is increased, reflecting the increase in order produced by addition of cholesterol.

Rather anomalous behaviour is noted for the 5-SASL-d_6 probe. Firstly, the quadrupole splittings for the probe are much smaller than those of the non-spin labelled fatty acid, particularly for the positions adjacent to the nitroxide. Secondly, an unusual response to the addition of cholesterol is noted. For the 2 position, the quadrupole splitting increases slightly on cholesterol addition whereas the splittings for the deuterons adjacent to the nitroxide show a much weaker response with both a slight increase and decrease in the magnitudes of the resolved splittings. These data can be compared with the behaviour of the stearic acid probe.

For the 2 position of 5-SASL-d_6, the quadrupole splitting is distinctly smaller than that of the normal stearic acid probe. This is likely due to an increase in motional freedom at this position due to the presence of the bulky nitroxide group at position 5. At the site of the nitroxide label, the cross sectional area of the probe is much greater than that of a normal fatty acid. Because of this, the acyl chains of the

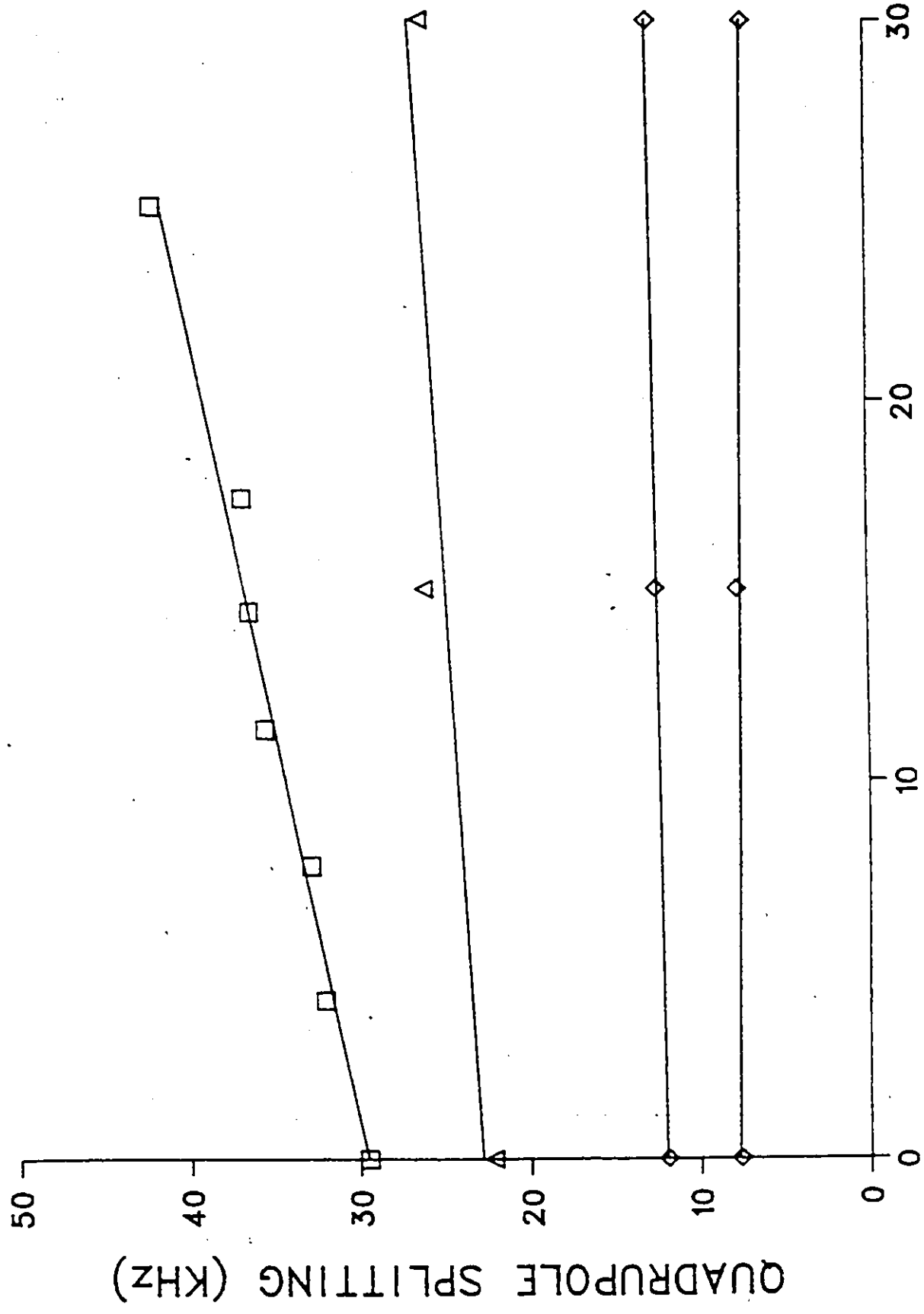

Figure 31. Variation of observed quadrupole splittings with cholesterol concentration for the 2-10 positions of stearic acid (squares), the 2 position of 5-SASL-d6 (triangles), and the 4, 6 positions of 5-SASL-d_6 (diamonds).

surrounding phospholipid matrix may not pack as efficiently near the label site. As a result, the methylene groups of the spin probe near the label site would have a greater volume available in which to move. An increase in the amplitude of motion for the methylene group at position 2 would result in smaller quadrupole splittings, relative to the normal fatty acid, as noted here.

The weak response of the quadrupole splittings for position 2 observed for addition of cholesterol may also be associated with packing difficulties for the bulky spin probe. As discussed in Section IV.1, the concentration of cholesterol in the local region surrounding the spin probe may not be as great as in the bulk of the membrane. This would lead to an apparently weaker effect of cholesterol on the probe.

The behaviour of the deuterons adjacent to the nitroxide is much more complex. The magnitudes of the observed splittings are much smaller than those of the normal fatty acid and also those of the 2 position of the probe. Also, the splittings diverge as cholesterol is added with differences between the splittings of 4.6 KHz and 6.0 KHz at 0 and 30 mole % cholesterol, respectively. The origin of the reduced magnitude of the splittings might be assigned to the same effect postulated for the 2 position of the probe. The response to cholesterol addition, however, indicates that such a simple explanation is not sufficient to describe the behaviour of the probe close to the nitroxide label site.

The factors which regulate the motional averaging of magnetic resonance parameters must be considered individually. As discussed in the Introduction, the degree of averaging of the hyperfine or quadrupole coupling tensors is affected by both the amplitude and geometry of the motion of a probe in an anisotropic medium. The present data for the effect of cholesterol indicate that it is necessary to consider the effects of probe geometry more closely. It is known from other experimental techniques (57) that cholesterol decreases the amplitude of motion in fluid bilayer systems such as egg PC. This increase in molecular order is expected to result in an increase in the anisotropy of the tensor properties of magnetic resonance probes as was noted above in Sections IV.1 and IV.2. The anomalous behaviour for the 4, 6 deuterons of 5-SASL-d_6 suggests that geometric factors strongly influence the spectroscopic properties of the spin probes. This possibility was investigated in greater detail using spin probes bearing deuterons on the methylene carbon of the nitroxide oxazolidine ring system. The ^2H NMR behaviour of such probes should be most informative in comparison with the EPR behaviour of the spin probes since, in both cases, the magnetic resonance label is attached to the ring system of the nitroxide. Care was taken in these experiments to minimize extraneous perturbations resulting from the use of high concentrations of fatty acid spin probes in the membrane. Thus, the probes used were the

phosphatidylcholine probes derived from the acylation of lyso-PC with a deuterated fatty acid spin probe. The probe concentration was reduced to 5 mole % which more closely approximates the concentration employed in EPR studies (typically 1-2%). In addition, ^2H NMR spectra were obtained using the diamagnetic hydroxylamine derivatives of the nitroxides to eliminate paramagnetic effects on the ^2H NMR spectra. These derivatives, produced by catalytic hydrogenation of the nitroxides, differ from the nitroxides only by replacement of the N-O bond by an N-OH group. This alteration is expected to have minimal effect on the structure of the oxazolidine ring system.

Figure 32 illustrates the ^2H NMR spectra for the phosphatidylcholine spin probes bearing ring-labelled deuterated nitroxide groups at positions 5, (A), and 12, (B) in egg PC bilayers at 5 mole % concentration. In each spectrum, two sets of quadrupole patterns are observed. For the 5 position, a component with splitting ~4 KHz is found as well as a second, broad component with splitting ~25 KHz.

The poor signal to noise ratio for the spectrum results partially from the low probe concentration and partially from paramagnetic broadening due to the nitroxide group. The effect of the paramagnetic nitroxide is more severe for these samples than for the previous samples due to the low concentration of the spin probe in the present case. At high

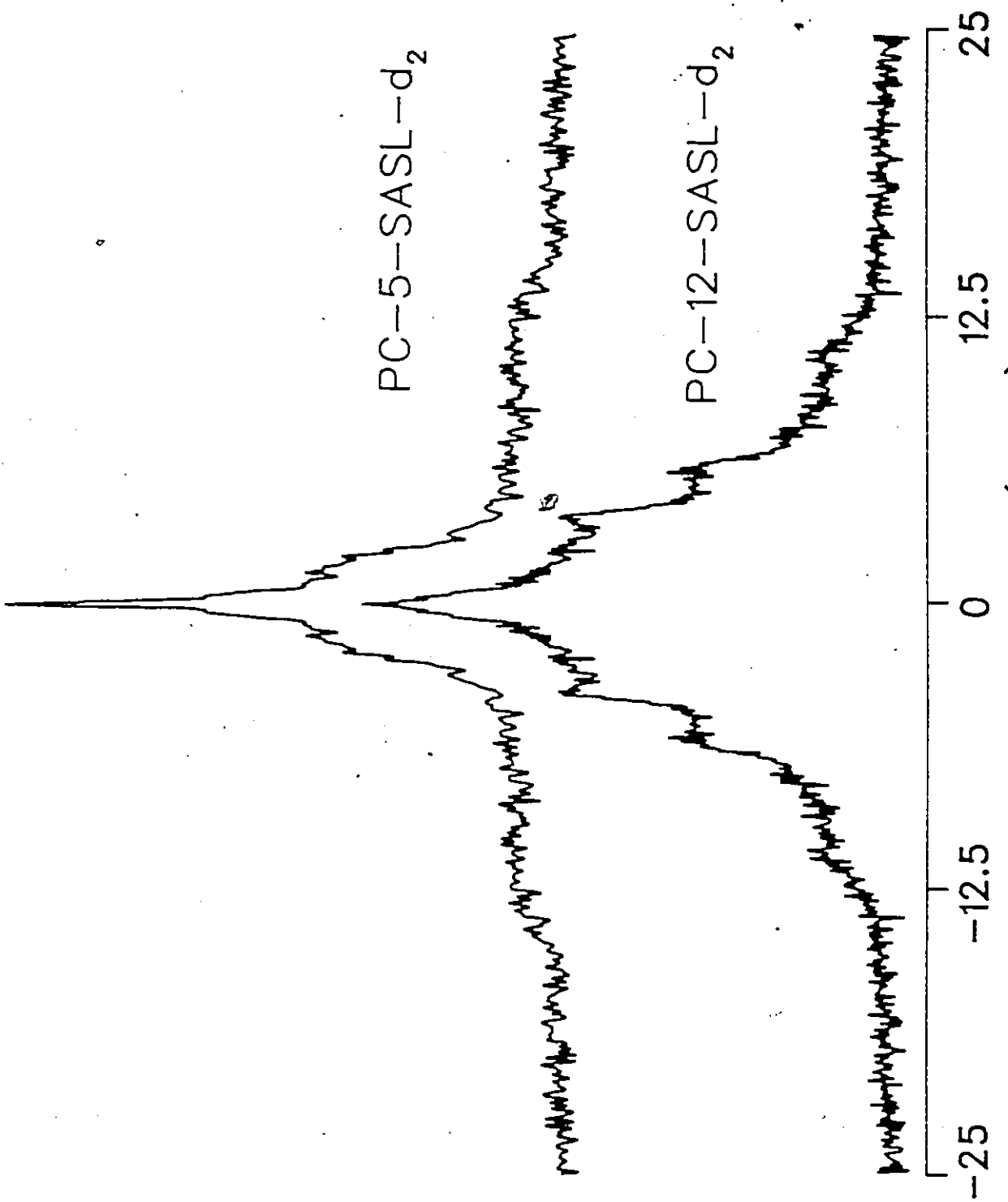

Figure 32. ^{2}H NMR spectra of the phospholipid spin probes deuterated at the methylene carbon of the oxozalidine ring for position 5 (a), and 12 (B). The probes were incorporated at 5 mole % in egg PC bilayers at 25°C. Spectra were accumulated using a recycle time of 0.1 seconds with a total accumulation time of 8-10 hours.

concentration, the broadening is reduced since spin exchange between paramagnetic probes tends to uncouple the effect of the free electron on the NMR spectra (58). Since spin exchange requires collisions between nitroxides, it is less efficient at low probe concentrations resulting in the large degree of broadening observed.

For the 12 position, two components with splittings of approximately 8 and 12 KHz are readily observed.

In order to verify that the two component spectra observed for these probes did not arise as a result of the paramagnetic nature of the nitroxides, these experiments were repeated employing the diamagnetic hydroxylamine analogs. The ^{2}H NMR spectra are shown in Figure 33 for the 5, (A), and 12, (B), positions. For the 5 position, 3 components are observed. The first component with splitting ~4 KHz is assigned to the presence of residual nitroxide in the sample. The hydroxylamine derivatives are rather unstable (21), and during the course of the experiment, may regenerate the parent nitroxide leading to the 4 KHz splitting observed in the spectrum of the original nitroxide as seen in Figure 32A. The other components, with splittings ~6 and ~19 KHz are assigned to the deuterons of the hydroxylamine analog. For the 12 position, a splitting is clearly observed at ~12 KHz as well as a broad, unresolved central component.

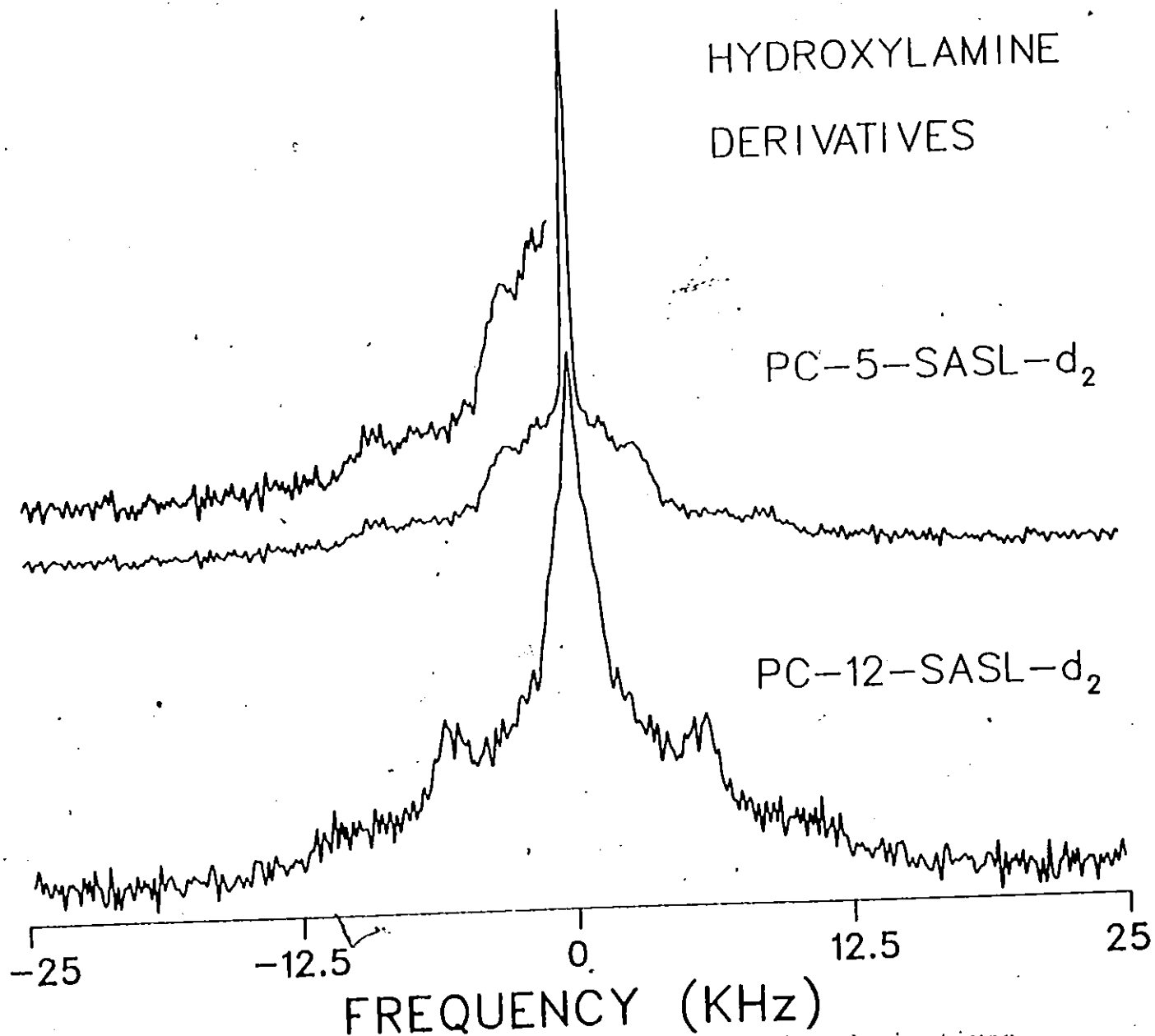

Figure 33. ^{2}H NMR spectra of the hydroxylamine derivatives of the phospholipid spin probes deuterated at the methylene carbon of the oxozolidine ring for position 5 (A), and 12 (B). Sample conditions as in Figure 32.

The differences in the magnitudes of the splittings observed for the nitroxides and their hydroxylamine derivatives may be due to an alteration of the conformation of the five-membered oxazolidine ring system. In addition, severe line broadening in the paramagnetic systems may distort the ^{2}H NMR lineshapes. In either case, the important point is that the deuterons of the ring system give rise to inequivalent quadrupole splittings in both the paramagnetic and diamagnetic systems.

The observation of inequivalent deuterons on the oxazodiline ring system provides direct evidence for an unexpected geometry for the nitroxide group. In the analysis of the EPR spectra of fatty acid spin probes, it is generally assumed that the oxazolidine ring is oriented rigidly perpendicular to the axis of motional averaging of the probe. If this were the case, both methylene deuterons of the ring system would be oriented at the same angle to the averaging axis. For this geometry, equal quadrupole splittings are expected in the ^{2}H NMR spectra in contrast to the experimental observations. The indication of a deviation from the assumed geometry has serious consequences for the interpretation of the spin probe EPR spectra.

As discussed above, the extent of motional averaging of a tensor property, such as the hyperfine splitting of a nitroxide, depends simultaneously on the amplitude of anisotropic motion of the probe and the geometry of the probe

relative to the motional averaging axis. For the nitroxide spin probes, the effects of probe motion and geometry on the EPR spectra cannot be separated using only the measurement of the residual hyperfine splittings. In order to allow interpretation of the EPR spectra in terms of the amplitude of motion of the probes, i.e., in terms of order parameters, it is necessary to assume a particular geometry for the nitroxide group. With the standard assumed geometry discussed above, the EPR-active N-O function of the nitroxide is oriented with the principal component of the hyperfine coupling tensor along the axis of motional averaging. This geometry leads to the maximum possible anisotropy for the hyperfine splittings for a probe located in a fluid anisotropic medium. Any deviation from the assumed geometry will lead to a reduction in the observed hyperfine anisotropy. Thus, for a constant amplitude of anisotropic motion, the observed hyperfine anisotropy of a spin probe may be reduced simply by alteration of its geometry. This clearly complicates the interpretation of the EPR spectra since an observed reduction in the hyperfine anisotropy may be due to geometric factors or an increase in the amplitude of probe motion or even a combination of these.

A further complication arises from the interpretation of the EPR spectra in terms of molecular order parameters for the probes. The EPR spectra yield directly only the order parameter for the Z-axis of the N-O fragment of the nitroxide.

In order to convert this order parameter to the molecular order parameter, it is again necessary to assume a geometry for the N-O function. Thus,the reliability of the derived order parameters depends directly on the validity of the assumptions concerning the probe geometry. Geometric problems with the interpretation of spin probe data in terms of molecular order parameters have been discussed (59).

An analogous situation is found in the interpretation of the ^{2}H NMR spectra of phospholipids bearing deuterated oleic acid (cis-9,10-octadecenoic acid) acyl chains (60, 61). In the region of the cis double bond, the observed quadrupole splittings are much smaller than those of positions far removed from the double bond, or those of the same label positions on fully saturated acyl chains. In that case, it was possible to demonstrate that the small magnitude of the splittings in the double bond region was due to the geometry about the cis double bond rather than an increase in the amplitude of motion of the acyl chain (60). It was possible to separate the effects of geometry and amplitude in that study using the known geometry of the deuterons on the rigid double bond and additional evidence from infrared dichroism (62). In the present study using deuterated spin probes, this separation cannot be performed since the angular relationships between the various deuterons are unknown and the probes have an unknown degree of internal freedom of motion. Such a study is described, however, in the

following section for deuterated cholesterol.

The results of the previous comparisons of nitroxide- and deuterium-labelled probes (Section IV.1 and IV.2) can be rationalized in terms of the geometry at the nitroxide label site. As discussed above, any deviation from the standard, assumed geometry for the nitroxide group would result in a reduction of the hyperfine anisotropy and erroneously small derived molecular order parameters. In the comparison of the fatty acid probes, (Section IV.1), it was noted that the EPR order parameters were less than those derived from the corresponding deuterated analogs which is consistent with the effect expected for alteration of the nitroxide geometry.

It is possible to speculate on the physical origin of this perturbation based on the evidence discussed above. The probe geometry may be altered as an adaptation by the probe to allow its insertion into the ordered matrix of the membrane. In the assumed geometry, the cross-sectional area of the probe is twice that of an unlabelled chain. It is clear that such a probe would not easily pack into the ordered structure of the membrane. The cross-sectional area of the probe could be reduced by twisting the acyl chain in the region of the nitroxide group such that the oxazolidine ring system would no longer be perpendicular to the long axis of the probe. This possibility is supported by the effects observed with addition of cholesterol. As cholesterol is added, the acyl chains

of the membrane tend to pack more efficiently which should increase the stress on the nitroxide group. Evidence for this effect is seen in the ^2H NMR behaviour of the deuterons adjacent to the nitroxide group of 5-SASL-d_6. For these positions, the quadrupole splittings diverged as the cholesterol concentration was increased. This effect would not be noted if the probe maintained a constant geometry as the cholesterol concentration was increased.

Secondly, the response to addition of cholesterol noted in the EPR behaviour of the spin probes was much smaller than that observed for the ^2H NMR behaviour of the deuterated stearic acid probes. This weak response could represent a balance between the effects of cholesterol on the amplitude of motion of the probes and their geometry. The addition of cholesterol should increase the hyperfine anisotropy for the probes by decreasing the amplitude of their motion. The expected effect would be attenuated, however, since the increased degree of order of the phospholipid matrix would induce a greater deviation from the assumed orientation of the oxazolidine ring resulting in reduction of the hyperfine anisotropy.

Further evidence for the importance of chain packing for the orientation of the nitroxides is obtained from the label position-dependence of the spectral behaviour of the probes. As noted above, the upper region of the membrane is characterized

by a high and essentially constant degree of order. Because of this, packing induced effects on the nitroxide orientation should be more pronounced for this region than for the less ordered lower region of the membrane. This suggestion is supported by the orientation dependence of the EPR spectra of the 5-SASL and 14-SASL probes in oriented lipid film samples. As discussed in Section IV.2, the 14-SASL probe displays the behaviour expected for the assumed probe geometry whereas the 5-SASL probe shows a marked deviation from the expected behaviour. The results of the ^{2}H NMR study of the phosphatidylcholine spin probes deuterated on the oxazolidine ring may also be interpreted in terms of a position-dependent orientational effect. As was stated above, the methylene deuterons would exhibit equal quadrupole splittings if the oxazolidine ring system were oriented perpendicular to the motional averaging axis. As seen in Figure 32 the inequivalence of the splittings for these deuterons is greater for the 5-position probe which is expected if the higher efficiency of chain packing in this region induces a larger alteration in the nitroxide geometry.

As a final observation, it is interesting to note the effects of paramagnetism on the ^{2}H NMR spectra of the deuterium labelled nitroxides. As stated above, line broadening may occur in the ^{2}H spectra, particularly at low nitroxide concentration. In addition, it is possible to observe effects on the chemical shift behaviour of the ^{2}H resonances. This contact shift

results from the strong, local magnetic field produced by the unpaired electron. The net magnetic field experienced by a ^2H nucleus on the spin probe is the sum of the fields due to the unpaired electron and the static field of the spectrometer. Thus, the resonance frequency of the nucleus is shifted, relative to a diamagnetic species, due to the added field of the electron. The effect of the unpaired electron is transmitted through the contact hyperfine interaction, so that the magnitude and sign of the contact shift is dependent upon the nature of the hyperfine coupling constant between the ^2H nucleus and the unpaired electron (58). The relationship between the contact shift and the hyperfine coupling constant is given by (58):

$$\delta = \frac{\hbar\gamma_e^2 a}{4\gamma_n kT}$$

where $\hbar$ is Planck's constant, k is Boltzmann's constant, T is the temperature, γ_e and γ_n are the gyromagnetic ratios for the electron and nucleus, respectively, and a is the hyperfine coupling constant between the electron and the nucleus. The dependence of the contact shift on the hyperfine coupling constant has been used in many studies to determine the sign of the coupling constant which may not be directly determined from the EPR spectrum of free radicals.

Close examination of the ^2H NMR spectra for 5-SASL-d_6, (Figure 30), reveals that the quadrupole patterns for the

deuterons adjacent to the nitroxide label site are not symmetric about the zero frequency but rather are shifted to higher frequency. In the case of the nitroxide probes with deuterons at the methylene carbon of the oxazolidine ring, (Figure 32), no contact shift is evident. These observations are consistent with ^{1}H NMR studies of related oxazolidine nitroxides where shifts to higher frequency were noted for protons at corresponding positions (58). The signs and magnitudes of the shifts noted here indicate a much larger, negative hyperfine coupling constant for the deuterons on the acyl chain than for those of the methylene carbon of the oxazolidine ring. Quantitative values of the shifts and derived hyperfine coupling constants would best be obtained through high resolution ^{2}H NMR of the nitroxides and their diamagnetic hydroxylamine derivatives.

IV.4.3 Conclusions

The ^{2}H NMR data for the deuterated spin probes presented in this section give evidence for unexpected geometrical properties for the nitroxide spin probes. These geometric effects are important for the interpretation of the EPR spectra of spin probes due to their influence on the spectral pro-

perties of probes inserted in anisotropic media. It is seen that several of the findings discussed in previous sections may be explained in terms of alteration of the nitroxide geometry. This discussion is necessarily speculative, since the influence of geometry on the observed spectra cannot be separated from the influence of the degree of motional freedom of a probe. The inability to separate these factors presents a serious problem in the interpretation of the EPR spectra of spin probes in membranes. Generally, the spin probe spectra are interpreted only in terms of order parameters based on an assumed geometry. The data presented here, for the dependence on label position and cholesterol concentration, indicate that ignoring the geometric effects may result in serious misinterpretation of the spin probe data.

IV.5 Determination of the Axis of Motional Averaging of Cholesterol

IV.5.1 Introduction

As discussed in the Introduction, the motional averaging of the anisotropic magnetic resonance parameters in a membrane phase depends on both the overall fluctuations of the molecule and the geometry of the director with respect to the molecular frame. If the orientation of the director is unknown, it is not possible to separate the effects of fluctuation amplitude

and geometry on the observed spectra. It is possible to determine the director orientation in a rigid molecule through the use of labels with different orientations on the same molecule. Thus, with the known label geometries and the observed anisotropic interactions from the spectrum, the angular relationship between the director and the molecular frame can be deduced.

This section discusses the calculation of the orientation of the director of cholesterol in equimolar egg PC/cholesterol bilayers. This study was carried out using ^2H NMR of the deuterated cholesterol probes: cholesterol-2,2,4,4,5-d_5 (cholesterol-d_5, Section III.1.12) and cholesterol-7,7-d_2 (a generous gift of Dr. T. Akayami). Since all the deuterium labels are bonded to the inflexible steroid ring system, analysis of the quadrupole splittings for each label position can yield the director orientation. Knowledge of the orientation allows calculation of S_{mol} for cholesterol from the observed ^2H quadrupole splittings. In addition, the quadrupole splittings expected for any label position may be calculated. This latter feature allows design of a probe molecule with favourable spectral properties.

In conjunction with the determination of the director orientation, relaxation measurements were made using the

cholesterol-d_5 probe. The relaxation times are sensitive to the rate of the anisotropic motion of the probe. The observation of different relaxation times for the different label positions can be correlated with their orientations with respect to the director.

IV.5.2 Results and Discussion

The high resolution spectrum of cholesterol-d_5 is shown in Figure 34. The spectrum agrees well with that of Sawan et al. (63) except for the appearance of a minor peak in the present spectrum at 3.4 ppm. The relative intensity of this peak did not change during the stages of purification of the compound. Its chemical shift agrees with that expected for the 3α position of cholesterol, indicating that a small amount of deuterium was unexpectedly incorporated at this position in the course of the synthesis.

The spectrum of cholesterol-d_5 incorporated in egg phosphatidylcholine bilayers is shown in Figure 35. The features of spectrum, labelled A-E in the figure, can be assigned in the following manner.

In the region of the largest quadrupole splittings, there is an intense peak, B and a less intense shoulder at A. The intense feature is assigned to the axial deuterons at C_2 and C_4 and the weaker shoulder to C_3. These three deuterons have approximately parallel carbon-deuterium bonds, and thus should give rise to similar splittings. The magnitude of the splitting

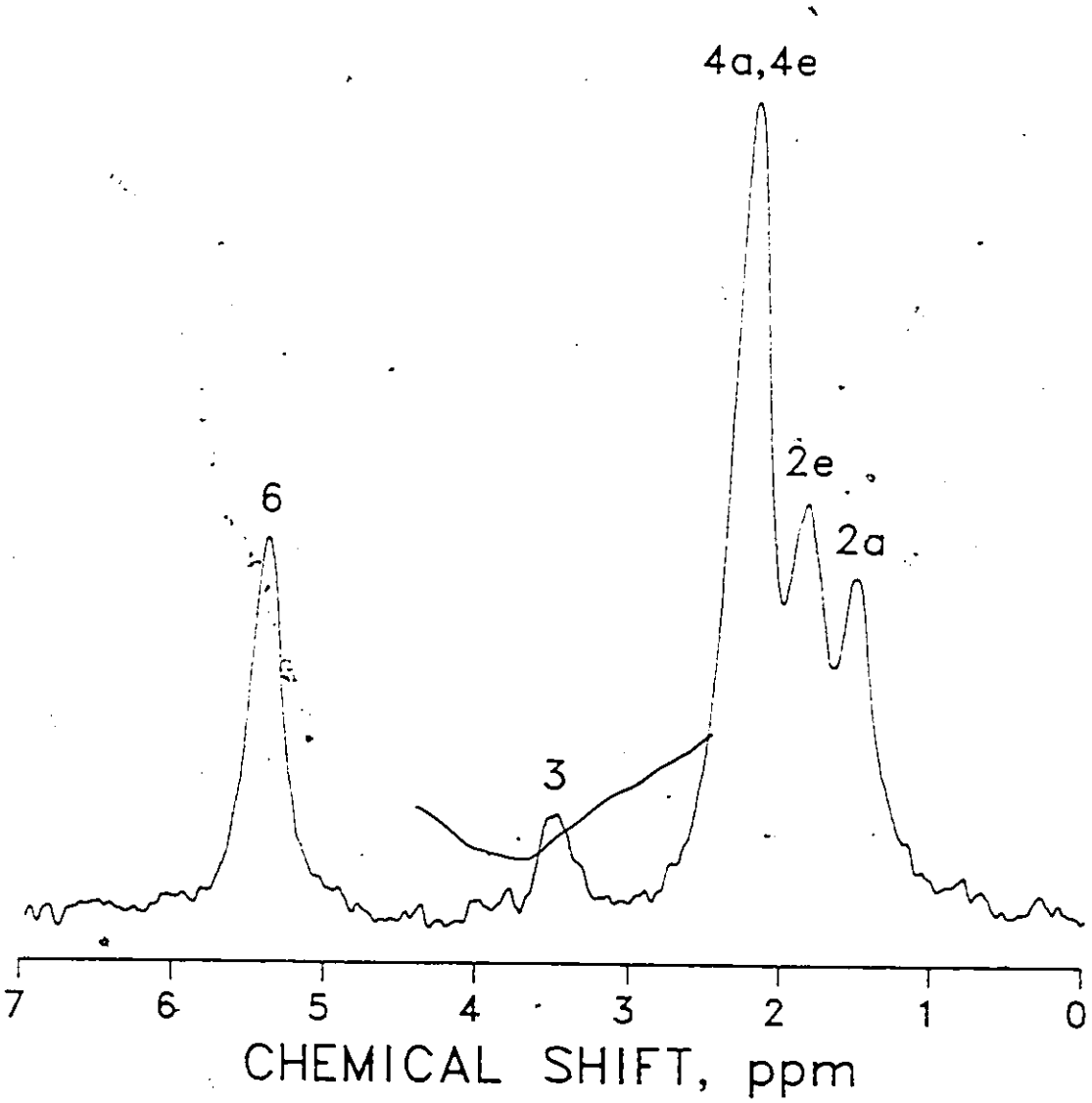

Figure 34. High resolution ^{2}H NMR spectrum, (46.1 MHz), of cholesterol-2,2,4,4,6,-d_5 in CCl_4 at 25 C and a concentration of approximately 50 mg/ml. Continuous broad-band ^{1}H decoupling was applied. 1,500 transients were collected with a recycle time of 4 seconds.

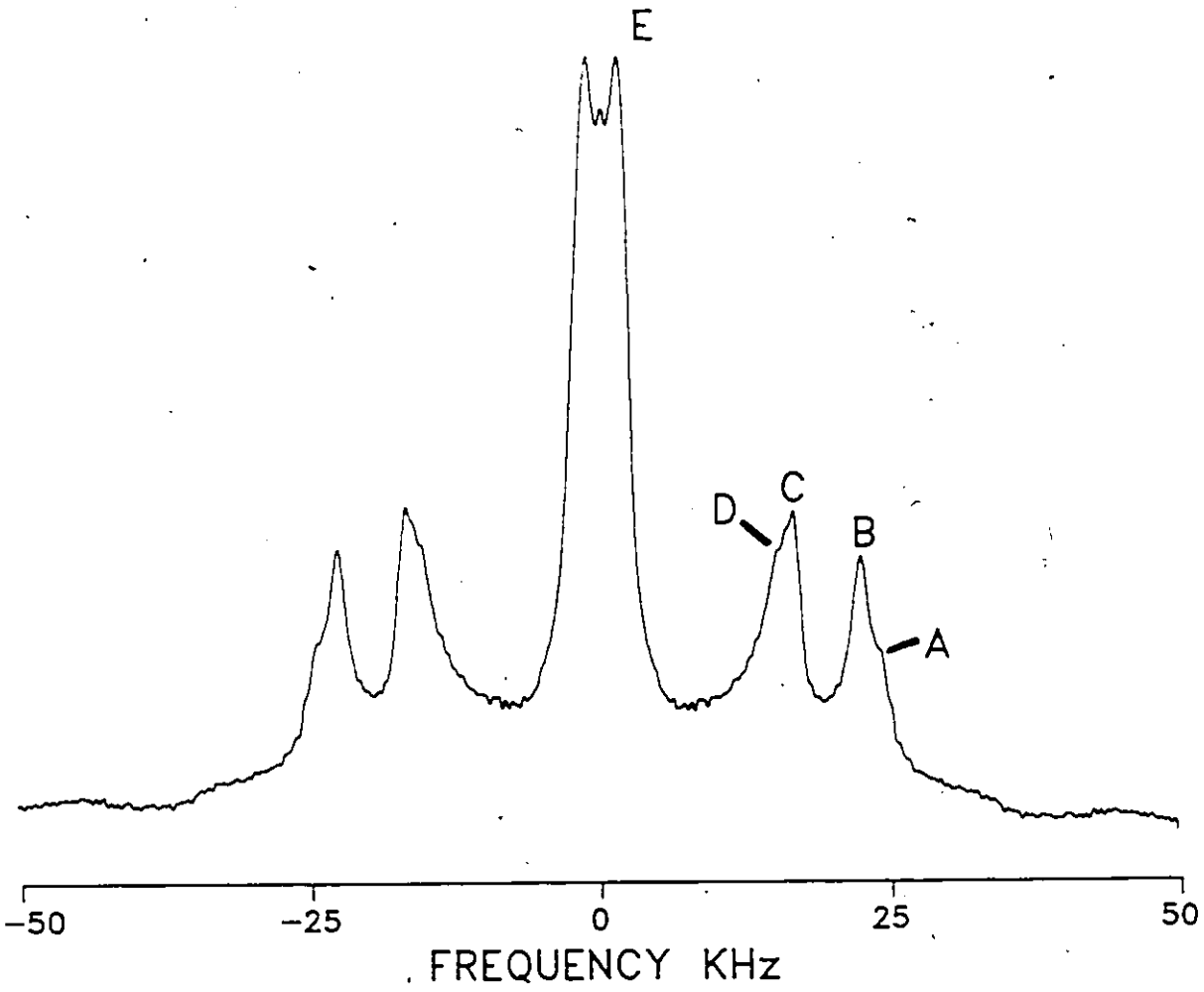

Figure 35. ^{2}H NMR spectrum, (46.1 MHz), of cholesterol-2,2,4,4,6-d_5 in egg phosphatidylcholine liposomes at 50 mole % concentration and 25°C. 150,000 transients were collected with a recycle time of 0.1 seconds.

for the deuteron at C_3 agrees with previous studies (15, 42, Section IV.2). In the region of about 30 KHz splitting, there are two barely resolved peaks, C and D. These splittings are assigned to the equatorial deuterons at C_2 and C_4. The narrowest splitting, E, is assigned to the deuteron at C_6.

Spectra of cholesterol, stereospecifically labelled at position 7, are shown in Figure 36. Essentially equal quadrupole splittings are observed for both α and β deuterons at this position. The quadrupole splittings observed for the various positions are listed in Table 1.

The variation in quadrupole splittings can be related to the angles between the individual C-^{2}H bonds and the axis about which the molecule undergoes rotation. For deuterons attached to a rigid structure, the quadrupole splitting for the i'th deuteron is given by :

$$\Delta\nu_i = \frac{3}{4}\frac{e^2qQ}{h}\left(\frac{3\cos^2\alpha_i - 1}{2}\right) < \frac{3\cos^2\beta - 1}{2} > \qquad (16)$$

where e^2qQ/h is the static quadrupole coupling constant (~170 KHz), α_i is the angle between the i'th C-^{2}H bond and the rotation axis and the term in angular brackets describes the anisotropic motion of the rotation axis. This last term, S_{mol}, is of interest since it defines the anisotropic motion of the entire molecule. Since S_{mol} is not known, this equation cannot be used to calculate directly the various values of the angles between the rotation axis and the C-^{2}H bonds. One can

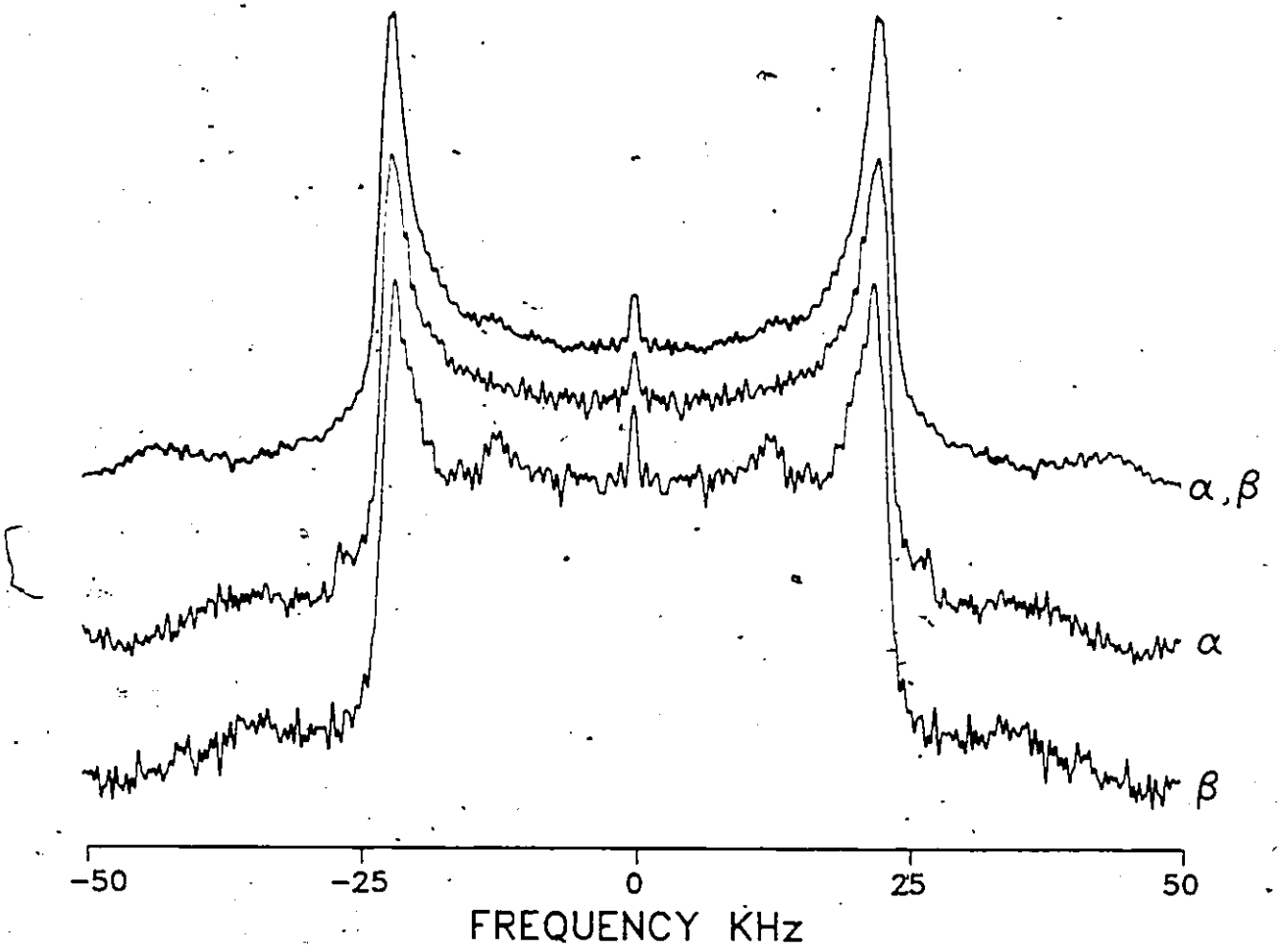

Figure 36. ^{2}H NMR spectra, (46.1 MHz) of cholesterols, stereospecifically labelled as indicated at position 7 in egg phosphatidylcholine liposomes at 50 mole % concentration and 25°C. 50,000 transients were collected with a recycle time of 0.1 seconds.

Table 1

POSITIONAL DEPENDENCE OF QUADRUPOLE SPLITTINGS[a] AND SPIN-LATTICE RELAXATION TIMES (T_1)[b]

Label Position	Quadrupole Splitting KHz	T_1 msec.
C_6	3.6	3.5
C_2, C_4 equatorial	31.1, 33.8	4.3
C_2, C_4 axial	45.4	5.3
C_7-α	44.9	-
C_7-β	43.9	-
C_3	49.5	-

a) Equimolar cholesterol/egg phosphatidylcholine dispersed in deuterium-depleted water at a ratio of 1:2 (weight:volume) at 25°C.

b) Average of two determinations using the inversion recovery quadrupole echo sequence.

however calculate relative values of the splittings since S_{mol} is constant for the rigid steroid nucleus. Thus, ratios, R_k can be expressed as:

$$R_k = \frac{\Delta\nu_i}{\Delta\nu_j} = \frac{(3\cos^2\alpha_i - 1)}{(3\cos^2\alpha_j - 1)} \qquad (17)$$

assuming equal quadrupole coupling constants for the various deuterons. At least three quadrupole splittings are required to determine the orientation of the rotation axis. Equation 17 could be solved analytically using the various splitting ratios and the atomic coordinates of the molecule to determine orientations of the C-^{2}H bonds.

A numerical solution was used, however, since this more readily yields an estimate of the error in the determination of the orientation of the axis. Details of the method used are given in Appendix II.

Before discussing the results of the numerical solution, a reasonable estimate of the orientation of the axis can be made by examination of the spectra of the deuterated sterols. Consideration of the geometry of cholesterol indicates that the rotation axis should run through the long axis of the rod-like molecule. The magnitude of the splittings for the C_3 and the axial C_2, C_4 deuterons indicates that the axis is oriented at close to 90° with respect to these bonds. The similarity of the splittings for the equatorial C_2 and C_4 deuterons suggests that the rotation axis makes approximately

equal angles with these bonds. This means that the axis must lie approximately in the plane defined by C_3, the hydroxyl oxygen and the C_3 deuteron, or the Y-Z plane in the axis system used here. Finally, the small splitting for the C_6 deuteron indicates that this bond must be oriented at close to the "magic angle", 54.7°, from the rotation axis.

There are two possible causes for the similarity of the splittings for the deuterons at C_7. Firstly, since the signs of the observed splittings are unknown, it is possible that the two positions have splittings of equal magnitude but opposite sign. This could occur if the angles between the C-^{2}H bonds and the rotation axis both lie in the region between 35.3° and 90° where the value of the function $(3\cos^2\alpha-1)/2$ varies between +0.5 and -0.5. The second possibility is that both C-^{2}H bonds are oriented at approximately equal angles to the rotation axis. Widely different splittings are observed for the axial and equatorial deuterons at C_2 and C_4 but this situation is not necessarily expected at C_7 since the double bond causes a large departure from chair geometry for the B ring of cholesterol.

The orientation of the axis is defined more precisely in terms of the polar angles θ and ϕ which locate this axis with respect to the origin of the coordinate system. In the nomenclature used here, θ refers to the angle with respect to the Z axis, (C_3-^{2}H bond), and ϕ is the angle with respect to

the X axis as shown in Figure 54. In view of the simple treatment discussed above, the orientation should lie near the (θ,ϕ) region of $(90^\circ, 90^\circ)$. In the numerical treatment (see Appendix II), reasonable solutions were found only in the region $\theta = 79 \pm 2^\circ$ and $\phi = 93 \pm 2^\circ$. A comparison of the quadrupole splitting ratios derived from experiment and calculations for this orientation is given in Table 2. The agreement between the two sets of ratios is quite satisfactory. Small changes in the values of θ or ϕ do not appreciably improve the overall agreement between experiment and calculation, although individual ratios can be brought into exact agreement. The C_6 ratio is extremely sensitive to changes in the orientation of the rotation axis since the C_6-^2H bond is oriented near the "magic angle" with respect to the rotation axis. Several sources of error preclude a more precise determination of the orientation. The principal sources of error are uncertainties in the measurement of the experimental quadrupole splittings and in the location of the hydrogen atoms in the molecule. The hydrogen atom positions were not determined explicitly in the X-ray study of cholesterol, but rather were calculated from the measured carbon atom positions assuming standard bond geometry (64). Deviations from the expected geometry would systematically bias the results. The hydrogen atoms could be located more accurately by neutron diffraction, but the accuracy available from the X-ray study is sufficient for the present

Table 2

COMPARISON OF CALCULATED AND EXPERIMENTAL QUADRUPOLE SPLITTING RATIOS[a]

Label Position	Experimental[b] Ratio	Calculated[c] Ratio
3	1	1
2 equatorial	1.46	1.50
2 axial	1.09	1.10
4 equatorial	1.59	1.58
4 axial	1.09	1.05
6	13.8	14.6
7α	1.10	1.10
7β	1.09	1.00

a) In each case, the ratio is made with respect to the C_3 deuteron splitting.

b) Based on splittings in Table 1.

c) Calculated assuming a rotation axis orientation of $\theta=79°$, $\phi=93°$.

study. Figure 37 shows a stereo projection of the A-D ring system of cholesterol, illustrating the derived orientation of the rotation axis of the molecule. It should be noted that the ^2H NMR experiment yields only the angular components of the axis orientation. In Figure 37, the axis has been drawn projecting through the oxygen atom. It is possible that the axis is located parallel to this but does not pass through this atom.

With the known orientation of the rotation axis, observed quadrupole splittings can be related to the molecular order parameter, S_{mol}, using equation 16. In the previous studies employing cholesterol-3α-d_1, it was assumed that the C-^2H bond was perpendicular to the rotation axis (i.e., $\alpha = 90^\circ$). The present study indicates that the angle between this bond and the rotation axis is approximately 79°. Using a value of 90° rather than 79° in the calculation of S_{mol} results in a systematic underestimation of about 10%. For example, using the quadrupole splitting observed here for the 3-α deuteron and assuming that the C_3-^2H bond is oriented at 90° with respect to the rotation axis leads to a calculated value for S_{mol} of 0.78. The value of S_{mol} calculated for a 79° orientation of the C_3-^2H bond is 0.87. This value correlates well with the order parameter observed for the nitroxide spin probe, 3-doxyl cholestane, in the same lipid system (Section IV.2).

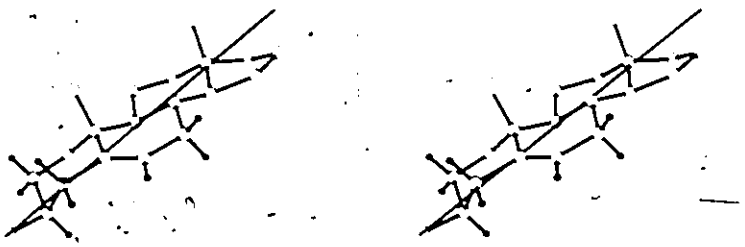

Figure 37. Stereo plot of the A-D ring system of cholesterol. The small filled circles are the deuteron label positions used in this study. The straight line which passes through the oxygen atom represents the calculated orientation of the rotation axis.

Knowledge of the orientation of the rotation axis also allows calculation of the quadrupole splittings expected for different label positions for a particular value of S_{mol}. Since any label in the fused ring system shows the same relative response to changes in S_{mol}, it would be useful to design a label with good spectroscopic characteristics.

Label orientations near 0° or 90° to the rotation axis are unfavourable since large quadrupole splittings are observed for these orientations. Such labels are difficult to detect if the amount of sample is limited as is often the case in biological studies. In the other extreme, labels oriented near the "magic angle", 54.7°, produce small quadrupole splittings. There are two problems associated with the use of such a labelled cholesterol as a probe molecule. Firstly, large component linewidths are expected for cholesterol incorporated in a membrane. For a deuterium quadrupole powder pattern, in which the component linewidth is a large fraction of the quadrupole splitting, both the linewidth and the splitting strongly affect the overall lineshape (see Section IV.6). In this case, it may be difficult to distinguish between changes in the amplitude (which affects the splitting) and the rate (which affects the linewidth) of molecular motion. Secondly, for deuterons near this orientation region, the splitting is extremely sensitive to small changes in the orientation of the rotation axis, since the function $1/2(3\cos^2\alpha-1)$ changes

rapidly for values of α near the magic angle. Thus, a small change in α results in a large change in the observed splitting and may be confused with an alteration of the molecular order parameter.

The most readily available deuterated cholesterol probe, cholesterol-3α-d_1, has its deuteron oriented at about 79° from the rotation axis. The resultant large quadrupole splittings observed in a membrane cause difficulties in detection. The cholesterol-d_5 probe used in this study has the advantage of yielding several quadrupole splittings simultaneously. The small splitting observed for the C_6 deuteron allows detection of small amounts of the compound. The difficulties arising from a small quadrupole splitting, mentioned above, may be overcome if the signals for the other deuterons (at least the equatorial C_2 and C_4 positions) can be detected. This compound is obtained by a rather straightforward and economical route. These features make it an attractive alternative to the cholesterol-3α-d_1 probe.

In order to search for other possible candidates, the orientations of all the C-^{2}H groups in the ring system were examined. A useful probe would have a deuteron oriented at an angle to the rotation axis in approximately the range of 50°-60°. The values of these angles and expected quadrupole splittings are listed in Table 3 for the individual bonds of

Table 3

BOND GEOMETRY AND PREDICTED QUADRUPOLE SPLITTINGS FOR THE FUSED RING SYSTEM OF CHOLESTEROL

Bond[a]	Angle Relative to Rotation Axis[b] degrees	Predicted Quadrupole Splitting[c] KHz
C_1 -α	76	52
C_1 -β	68	36
C_2 -α(equatorial)	68	38
C_2 -β(axial)	75	52
C_3	79	57
C_4 -α(equatorial)	68	36
C_4 -β(axial)	77	54
C_6	56	4
C_7 -α	75	52
C_7 -β	79	57
C_8	84	62
C_9	81	59
C_{11}-α	65	30
C_{11}-β	87	64
C_{12}-α	89	64
C_{12}-β	59	12
C_{14}	81	59
C_{15}-α	78	55
C_{15}-β	84	61
C_{16}-α	63	23
C_{16}-β	59	13
C_{17}	81	59
C_{13}-C_{18}	82	20
C_{10}-C_{19}	85	21

a) α and β refer to $C-^2H$ bonds projecting below and above the plane of the steroid, respectively. For the C_{18} and C_{19} methyl groups, the bonds connect the methyl groups to the fused ring system.

b) Angles are calculated for the director orientation $\theta=79^\circ$, $\phi=93^\circ$.

c) Quadrupole splittings are calculated for $S_{mol}=1$.

the rigid steroid framework. The majority of the bonds are oriented at angles greater than 65° to the rotation axis, leading to large quadrupole splittings. Position 16 would appear to be a favourable labelling site, since both C-^{2}H bonds are oriented rather close to the magic angle. In addition, relatively small splittings are expected for the C_{18} and C_{19} angular methyl groups since rapid rotation about the three-fold axis reduces the quadrupole splittings of methyl groups by a factor of three (6).

Thus far, the discussion has dealt with only the amplitude and symmetry of the anisotropic motion of cholesterol in the membrane as revealed by the quadrupole splittings of the various deuterium labels. Information on the dynamic nature of the motion of cholesterol can be obtained from the study of the relaxation behaviour of deuterated probes. The results of preliminary studies of the spin-lattice relaxation times for the deuterons of cholesterol-d_5 are given in Table 1. Previous studies of deuterium relaxation in membranes have dealt with deuterated phosphatidylcholines (46, 65, 66). Since these studies employed dipalmitoyl phosphatidylcholine, (DPPC), it is not possible to make a direct comparison with the present data for cholesterol. It is interesting to note, however, that the relaxation times measured here for cholesterol are very much shorter than those found for the acyl chain positions in DPPC (46, 65, 66). Assuming the short correlation time

regime (65), this indicates that the reorientation of cholesterol in this system is slow relative to that of DPPC. This is likely due, in part, to the high concentration of cholesterol used in the present study. Addition of cholesterol has been shown to decrease the motional rates of the related nitroxide spin probe, 3-doxyl cholestane (67). Independent of this, it would be reasonable to expect slower motion for cholesterol relative to a phospholipid at any cholesterol concentration, since the phospholipid acyl chains are able to re-orient through gauche-trans isomerisations. These segmental motions, which are unavailable to deuterons on the inflexible steroid framework, may dominate the spin-lattice relaxation of the phospholipid deuterons resulting in the longer T_1 values for phospholipid as compared to cholesterol.

The quantitative interpretation of relaxation behaviour in membranes is not straightforward due to the difficulty of modelling the motion of a molecule in an anisotropic medium. Several treatments of the theory of relaxation in membranes have been presented. The simplest models predict the following relationship (6, 46, 68):

$$\frac{1}{T_1} = \frac{3}{8}\left(\frac{e^2qQ}{\hbar}\right)^2 (1-S_z^2)\tau_C \qquad (18)$$

where S_z is the C-^{2}H bond order parameter and τ_C is the correlation time for re-orientation of the molecule. For

the data presented in Table 1, an approximately linear relationship between $1/T_1$ and $(1-S_z^2)$ is observed as required by this equation. The derived correlation time τ_c is approximately 5×10^{-10} sec which is in reasonable agreement with data for the 3-doxyl cholestane spin probe (67). Although the present data are too limited to provide an accurate test of a model for relaxation, cholesterol would serve as an excellent probe for such a study. The inflexible nature of the steroid ring system reduces the number of degrees of motional freedom for individual labels so that the details of molecular motions should be simpler to model. The possibility of examining different label positions on the same molecule allows separation of the effects of correlation time and anisotropy on the relaxation behaviour. A fuller understanding of motion in an anisotropic medium could be obtained by extending these studies, particularly by examining the T_2 and $T_{1\rho}$ relaxation times which are more sensitive to slower motions.

IV.5.3 Conclusions

The orientation of the axis of motional averaging for the cholesterol molecule intercalated in egg phosphatidylcholine bilayers was determined. The axis lies at $79^\circ \pm 2^\circ$ to the 3α-C-^{2}H bond and bisects approximately the angle between the equatorial deuterons at C_2 and C_4. Using the calculated

orientation, one can relate observed quadrupole splittings for individual label positions to the molecular order parameter for cholesterol. The cholesterol-d_5 probe used here shows several advantages for use as a monitor of the behaviour of cholesterol in biological membranes, and several other label positions on the molecule which are also attractive as spectroscopic probes were suggested. Finally, preliminary T_1 studies of cholesterol-d_5 indicate the utility of deuterated cholesterol as a tool in the study of deuterium relaxation in anisotropic media.

IV.6 Molecular Dynamics of Deuterated Cholesterol in Egg Phosphatidylcholine Membranes

IV.6.1 Introduction

The work described in the previous section was extended through a ^2H NMR study of cholesterol in egg PC bilayers. The cholesterol molecule is interesting in that it may be divided into two structural regions. The first region is the A-D fused ring system. This fused ring framework is expected to have minimal internal flexibility and thus should re-orient as a rigid body. The second region is the alkyl "tail" linked to the ring system at carbon 17. This region cannot be expected to be inflexible since rotations may occur about the C-C single bonds. Thus, the two regions may display markedly different properties in the membrane, in terms of the amplitudes and rates of reorientational motions. This

possibility was investigated through the use of deuterated cholesterol probes labelled in the ring system at positions 3 and 7 (cholesterol-3α-d_1 and cholesterol-7-d_2 respectively) and in the alkyl tail region at the 26 and 27 methyl group positions, (cholesterol-26,27-d_6).

The amplitudes of anisotropic motion were examined via the quadrupole splittings observed for each probe in egg PC bilayers. The dependence of the splittings with changes on temperature and cholesterol concentration was studied. The rates of anisotropic motion were probed via relaxation time measurements. Both T_1 (spin-lattice) and T_{2e} (quadrupole echo decay) relaxation times were measured for the cholesterol-7-d_2 and cholesterol-26,27-d_6 probes at different membrane cholesterol concentrations.

IV.6.1 Results and Discussion

A) Variation of Quadrupole Splittings With Temperature and Cholesterol Concentration

I) Fused Ring System

Figures 38 and 39 show the variation in quadrupole splittings for cholesterol-3α-d_1 (squares) and cholesterol-7,7-d_2 (triangles) for changes in temperature and cholesterol concentration, respectively. As noted in Section IV.2, increasing temperature results in a decrease in the splittings and increasing cholesterol concentration causes an increase in

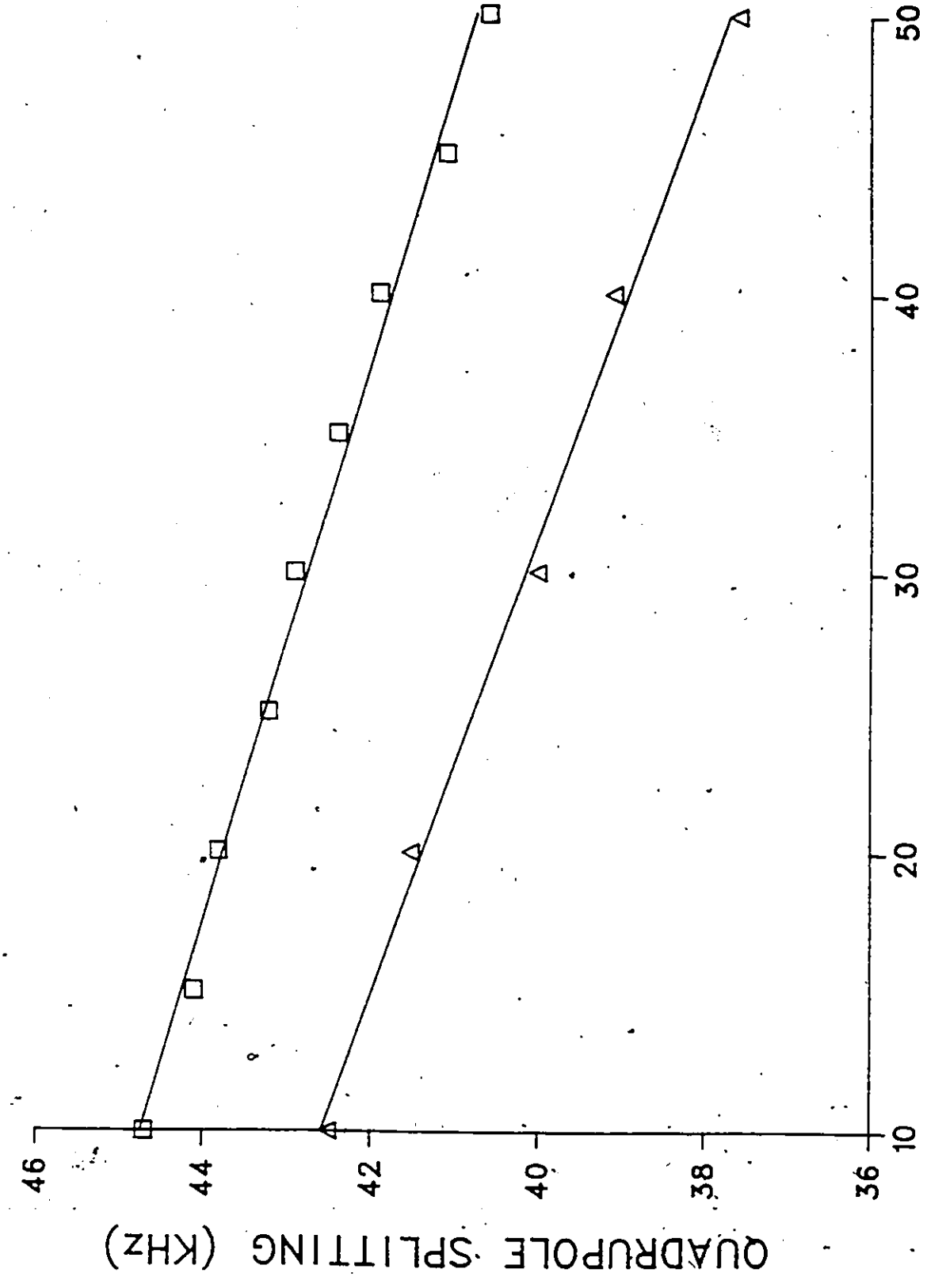

Figure 38. Temperature dependence for observed quadrupole splittings for cholesterol-3α-d_1 (squares) and cholesterol-7, 7-d_2 (triangles) in bilayers consisting of 30 mole % cholesterol in egg PC.

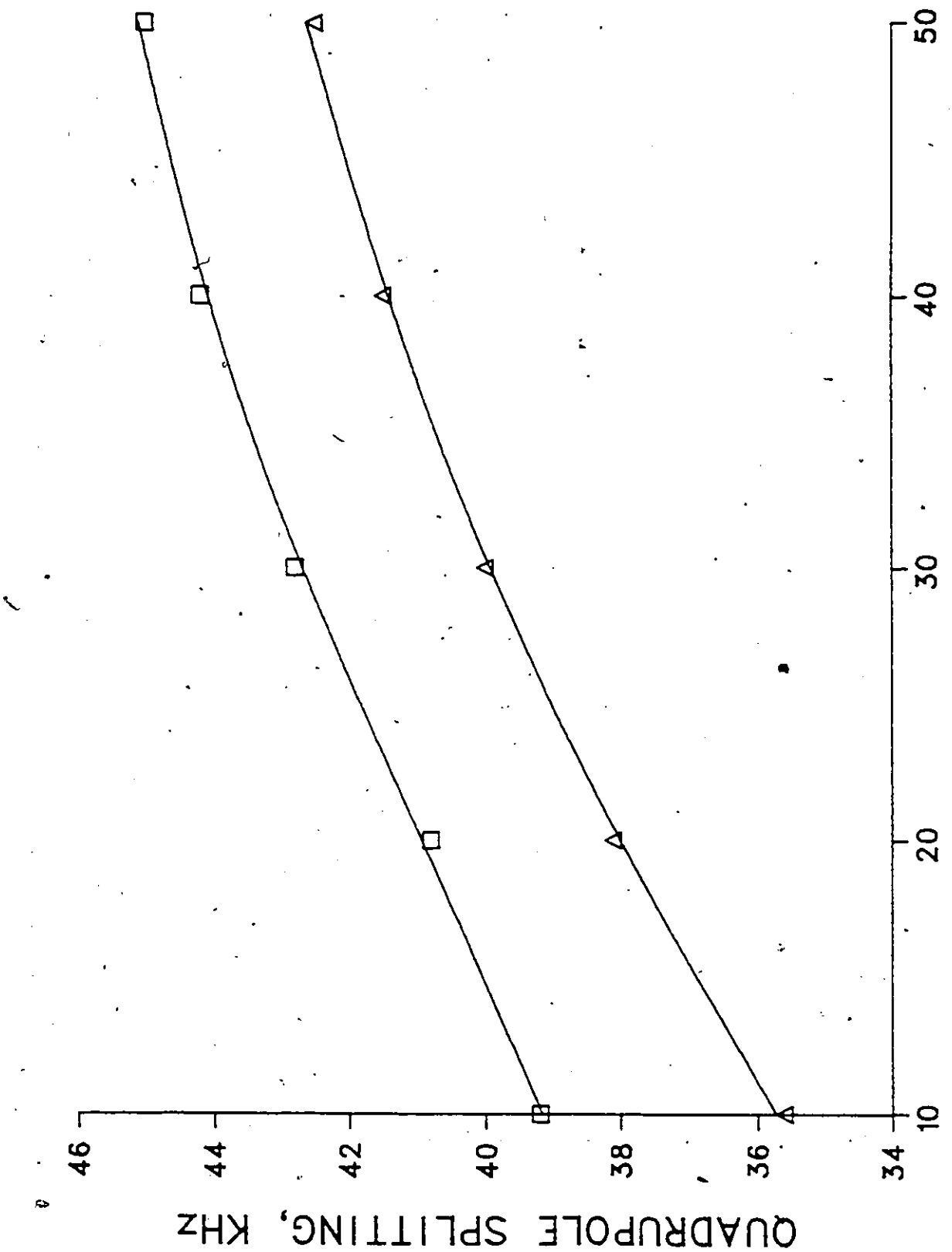

Figure 39. Variation of quadrupole splittings with cholesterol concentration for cholesterol-3α-d_1 and cholesterol-7,7-d_2 in egg PC bilayers at 30°C.

splittings for cholesterol-3α-d_1. Both probes exhibit essentially parallel responses to variation of each experimental parameter. This indicates that the orientation of the director axis remains constant over this range of sample conditions. Because of this, one can use equation 5 (Section I.2.6) for the calculation of S_{mol} for the rigid portion of the molecule. Values of S_{mol} were calculated from the observed quadrupole splitting for cholesterol-3α-d_1 using equation 5 with α set to 79° (Section IV.5). Figure 40 shows the variation of S_{mol} with temperature and cholesterol concentration. For all conditions, S_{mol} is large and approaches 1 at high concentration, indicating a high degree of ordering for the molecule in the membrane. As discussed in Section IV.1, cholesterol exerts a strong ordering effect on the phospholipid acyl chains, with the strongest effect noted for the upper region of the bilayer. The rigid framework of cholesterol acts as a physical barrier which restricts the amplitude of motion of the surrounding acyl chains. This effect is also revealed from measurements of the dimensions of the bilayer. Addition of cholesterol causes a reduction in the surface area of phospholipid monolayers (57) and an increase in the bilayer thickness (69). Both effects are consistent with an increase in the population of trans rotamer segments for the acyl chain. This "condensing" effect of cholesterol is transmitted through the membrane plane to cause an increase in order for neighbouring

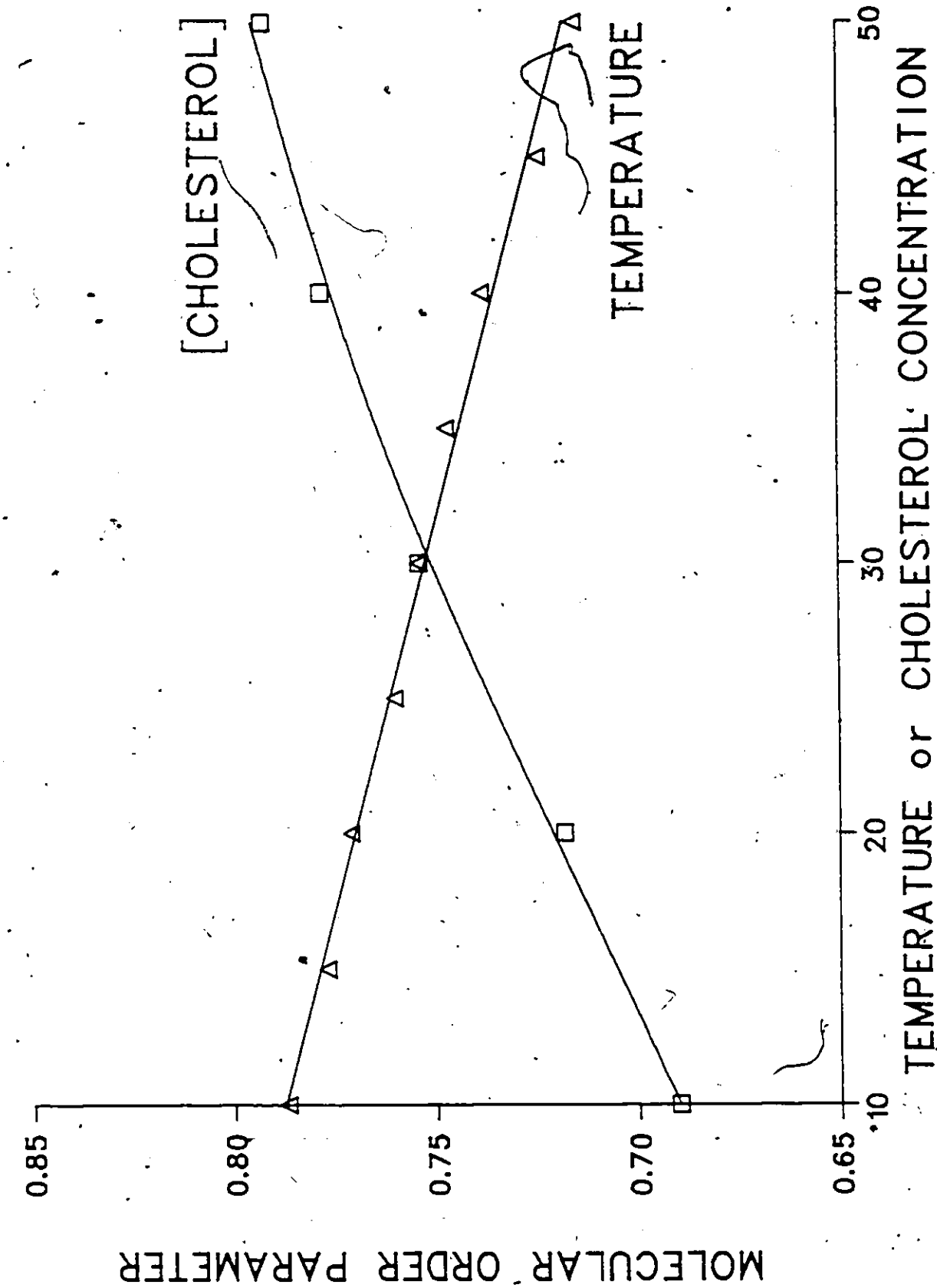

Figure 40. Variation with temperature (triangles) and cholesterol concentration (squares) of the derived molecular order parameters for cholesterol in egg PC.

cholesterol molecules. Thus, as the phospholipid matrix becomes more ordered, the motion of individual cholesterol molecules becomes more restricted resulting in the dramatic increase in the cholesterol S_{mol} noted for increasing cholesterol concentration.

II) Aliphatic Tail Region

Figure 41 shows ^2H spectra of cholesterol-26,27-d_6 in egg PC bilayers at variable cholesterol concentrations. For all cholesterol concentrations, very small (~1-2 KHz) quadrupole splittings are observed. In addition, the spectra do not show sharp edges as seen for the other cholesterol probes, indicating relatively large component linewidths for the cholesterol-d_6 probe. Before discussing the spectra in terms of probe motion in the membrane, the nature of these lineshapes will be examined.

The combination of small quadrupole splittings and large component linewidths noted here causes difficulties in resolution of different splittings and in measurement of the magnitudes of the splittings. For example, the spectrum for 10 mole % cholesterol-d_6 (Figure 41A) shows two barely resolved quadrupole patterns with apparent splittings of ~900 and 1600 Hz. Methods for improving the resolution of the spectra were investigated.

In a previous study of cholesterol-d_6 in membranes (70), distinctly different ^2H lineshapes were observed. These differences arise from the methods used in obtaining the ^2H

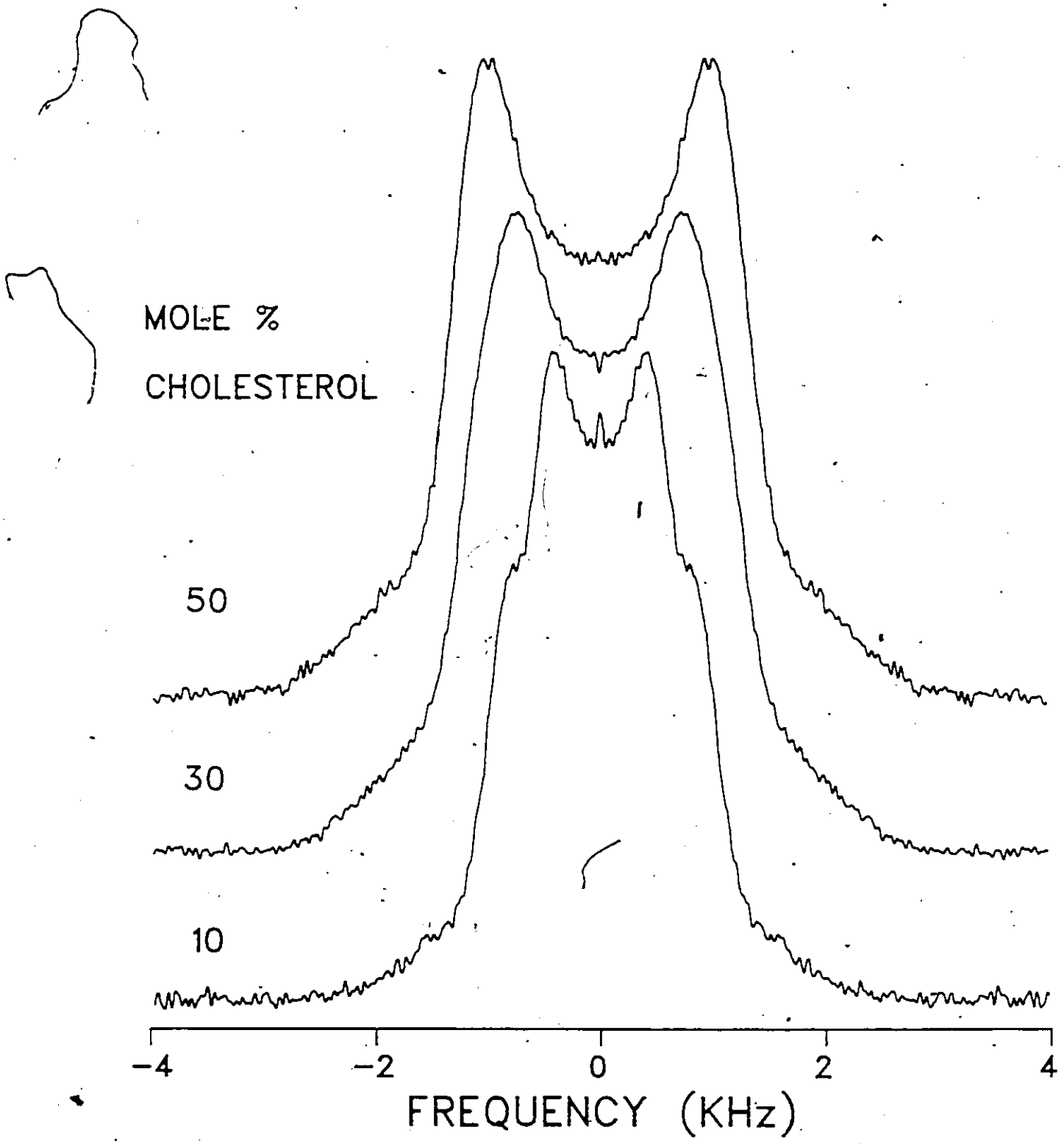

Figure 41. ^{2}H NMR spectra of cholesterol-26,27-d_6 in egg PC at the indicated concentrations at 25°C. Spectra were collected with a recycle time of 1 second, acquiring 600 transients.

NMR spectra. In the previous study, the spectra were acquired using the standard $90^{\circ}\sim\tau_D\sim$acquire pulse sequence, where τ_D is the dead time required before acquisition to avoid spectral artifacts due to the strong transmitter pulse. Fourier transformation of the free induction decay, (FID), signal after such a pulse results in a distorted ^2H NMR spectrum because the initial portion of the free induction decay, (during τ_D) is not collected. The loss of the information in the initial part of the decay causes several problems.

Firstly, the decay signal is most intense immediately following the excitation pulse. The loss of this intense signal degrades the signal to noise ratio of the transformed spectrum. Secondly, the free induction decay may contain signals which decay at different rates. Signals which decay more rapidly are lost to a greater extent than those which decay at slower rates. Thus, in a multicomponent spectrum, the intensity of the rapidly decaying components are suppressed. Finally, the failure to obtain the entire FID results in a frequency-dependent phase distortion in the transformed spectrum (26).

The spectra in the present study were collected using the quadrupole echo sequence. As with other echo sequences, this method yields an image of the entire FID. Some intensity is lost during the time required for formation of the echo due to spin relaxation, but phase distortions are removed. The

phase distortion effects noted for the standard acquisition method can be simulated using the echo signal. Thus, if the Fourier transform of the echo signal is performed starting at the peak of the echo signal, the resultant spectrum is free from phase distortions. The starting point for the transform can be shifted along the time axis of the echo signal to simulate loss of the FID during the receiver dead time, τ_D. Figure 42A shows the effect of progressively increasing this time delay. The spectra for long dead times closely resemble those obtained using a one pulse acquisition (70). As the dead time is increased, the spectra lose the lineshape expected for a quadrupole powder pattern and begin to resemble sets of doublets for each of the original quadrupole powder patterns. The enhanced resolution in these spectra suggested that this procedure of ignoring the initial points of the echo signal could be used in order to obtain the quadrupole splittings from a spectrum composed of overlapping quadrupole powder patterns. Such a method has been used for resolution enhancement in high resolution NMR (71). This possibility was investigated through spectral simulations.

As discussed in Appendix III, simulated free induction decays were generated for overlapping powder patterns. The decays were then Fourier transformed with variation of the starting point of the transform to yield a series of spectra simulating variable dead times. The procedure is outlined

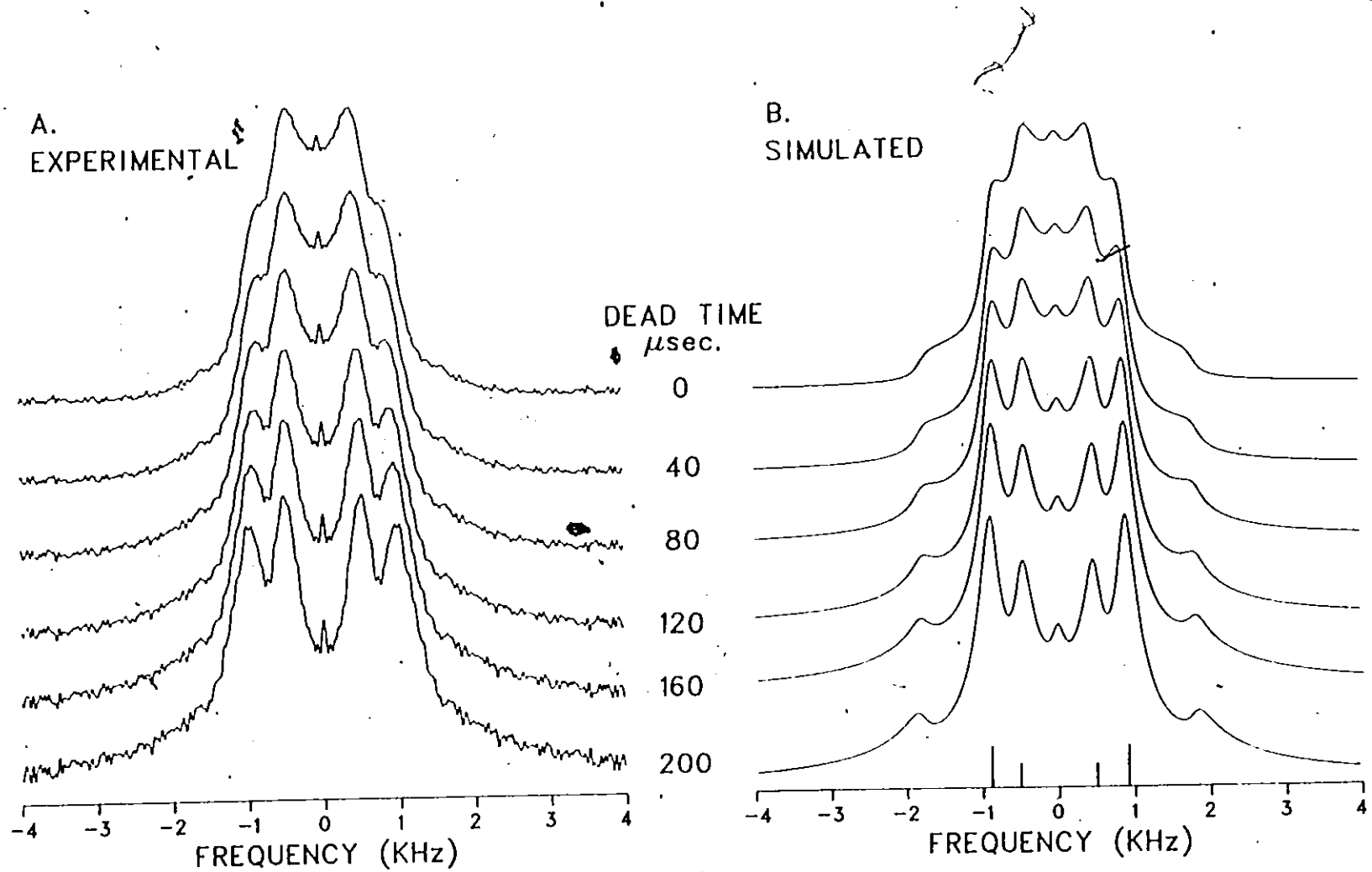

Figure 42. Effect of dead time on the Fourier transform spectra of 10 mole % cholesterol-26,27-d_6 in egg PC bilayers. A. Experimental spectra. B. Simulated spectra. The dead time used is shown for each spectrum.

schematically in Figure 43. A series of simulated spectra are shown in Figure 42B. Each spectrum consists of a summation of two powder patterns with quadrupole splittings 1 KHz and 1.8 KHz with component Lorentzian linewidths for each sub-spectrum was 100 Hz (vide infra). The simulated dead time for each is indicated on the figure. The overall agreement between the simulated and experimental spectra is reasonable with most serious discrepancy between the two sets of spectra in the relative intensities of the component patterns. The vertical lines in the simulated spectra represent the frequency separations for the values of quadrupole splittings used in the simulations. If these values are compared to the positions of the peak maxima, it can be seen that the latter provide an inaccurate estimate of the quadrupole splittings. In addition, the peak positions vary as a function of the dead time. Finally, as the dead time is increased, the signal to noise ratio for the experimental spectra degrades due to the loss of intensity in the initial portion of the free induction decay. Thus, although the phase distortion aids in the resolution of overlapping powder patterns, there are serious drawbacks in the application of this method to determine quadrupole splittings.

The effects noted above suggested that manipulation of the spectral phase could be useful in enhancing the resolution of overlapping powder patterns. Ordinarily, the absorption

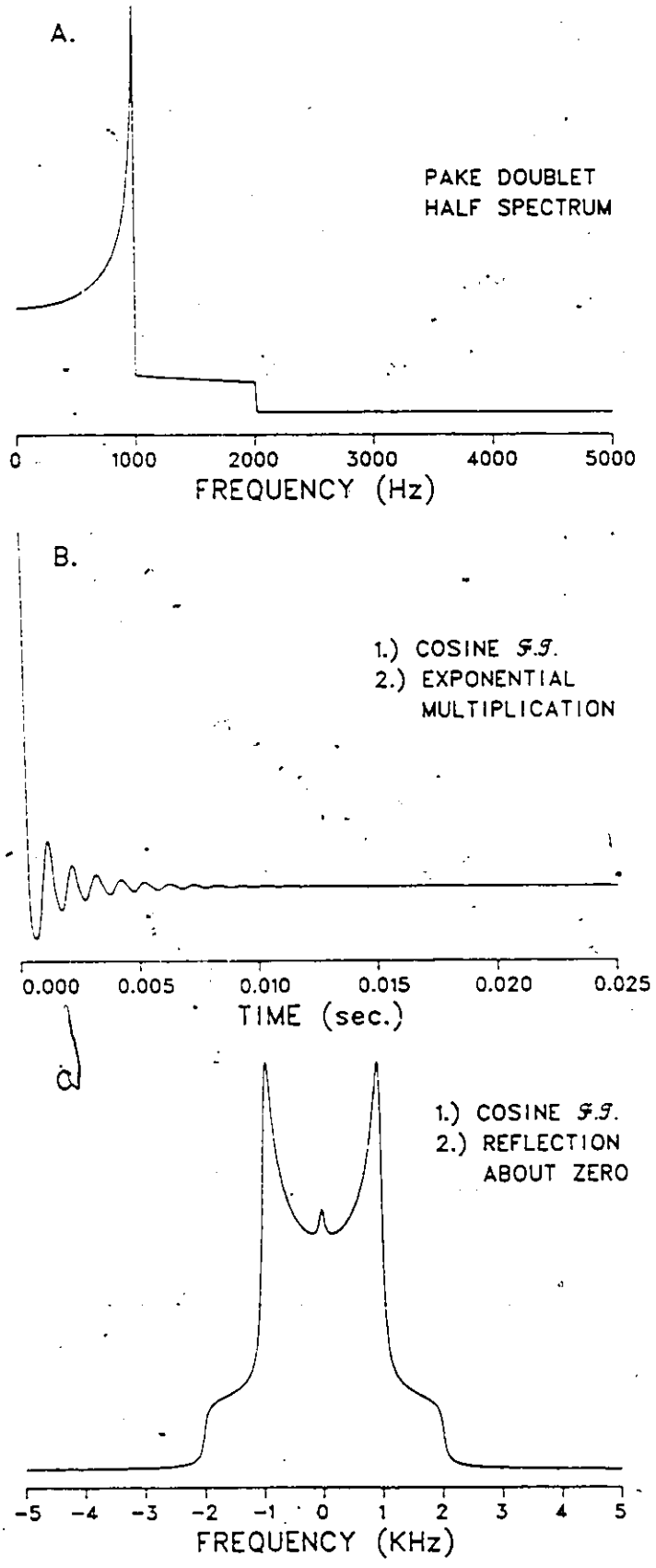

Figure 43. Outline of method used in simulating free induction decays and Fourier transform spectra as discussed in Appendix III.

mode is used for display of Fourier transform spectra. The spectra can also be displayed in dispersion mode. These two modes correspond to the cosine (absorption) and sine (dispersion) Fourier transforms of the decay signal detected at 90° to the transmitter exciting pulse (72). These two modes can be combined to generate the absolute value display, P, given by:

$$P = (u^2 + v^2)^{1/2}$$

where u and v are the absorption and dispersion components, respectively. Spectra were simulated for the three display modes using a single quadrupole powder pattern with variable amounts of Lorentzian line broadening. The results of the simulations are shown in Figure 44. The frequency axis is plotted in reduced units such that one unit is equal to the quadrupole splitting. For each mode, the component linewidth (half width at half height) varies as indicated for the absolute value spectra. The linewidths are expressed in the same reduced units so that each spectrum is general for a particular ratio of linewidth to quadrupole splitting. The absorption mode spectra agree well with previously published simulations (6). The two vertical lines indicate the frequency spacing for the true quadrupole splitting.

It can be seen that the peak maxima for the absorption mode spectra always lie at a frequency separation less than

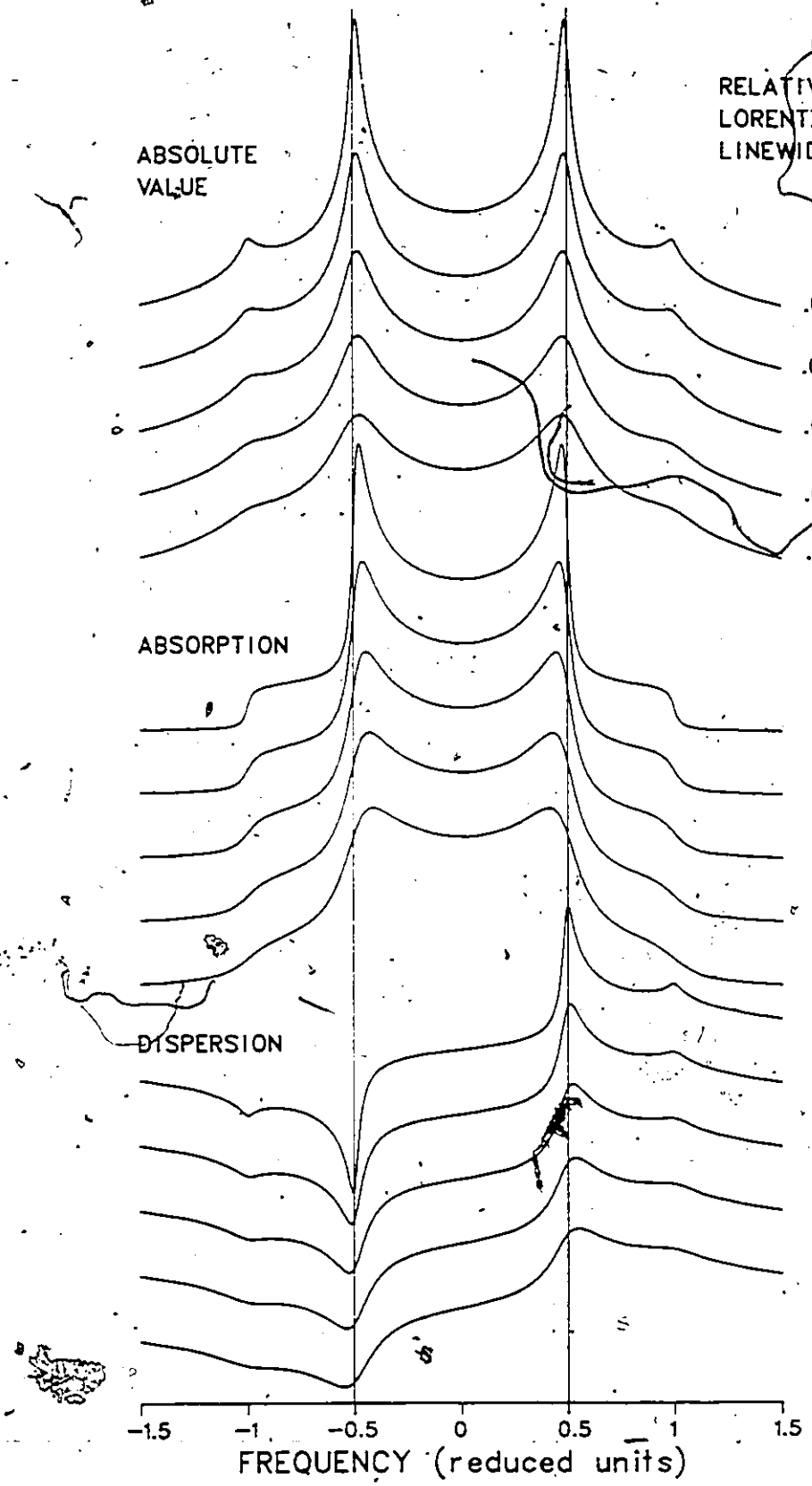

Figure 44. Simulated ^{2}H powder patterns for a single quadrupole splitting using different display modes. The Lorentzian linewidths are indicated for the absolute value spectra. Frequencies and linewidths are expressed in reduced frequency units (1 unit = quadrupole splitting).

the quadrupole splitting. Conversely, the peak to trough separation in the dispersion mode spectra is always greater than the splitting. In addition, for both modes, the difference between these spectral markers and the true quadrupole splitting increases with increasing linewidth. In the absolute value spectra, a smaller difference is noted between the peak maxima and the splitting. More importantly, this difference is less sensitive to the value of the linewidth/splitting ratio. In addition, the peaks tend to be sharper than the features of the other two modes. These properties of the absolute value spectra indicate that this phase manipulation should be useful in resolving overlapping patterns and in measuring their quadrupole splittings.

This suggestion was tested with the spectra for 10 mole % cholesterol-d_6. Figure 45 shows a comparison of experimental and simulated spectra for the three display modes discussed above. The linewidth parameters for the simulations were obtained from T_{2e} measurements (vide infra) and the quadrupole splittings were taken as the frequency separations for the peaks in the experimental absolute value spectrum. The overall agreement between experimental and simulated spectra is satisfactory. The agreement could likely be improved by freely adjusting the simulation input parameters, but the important point is that the peaks in the absolute value spectrum yield a close approximation to the actual quadrupole splittings.

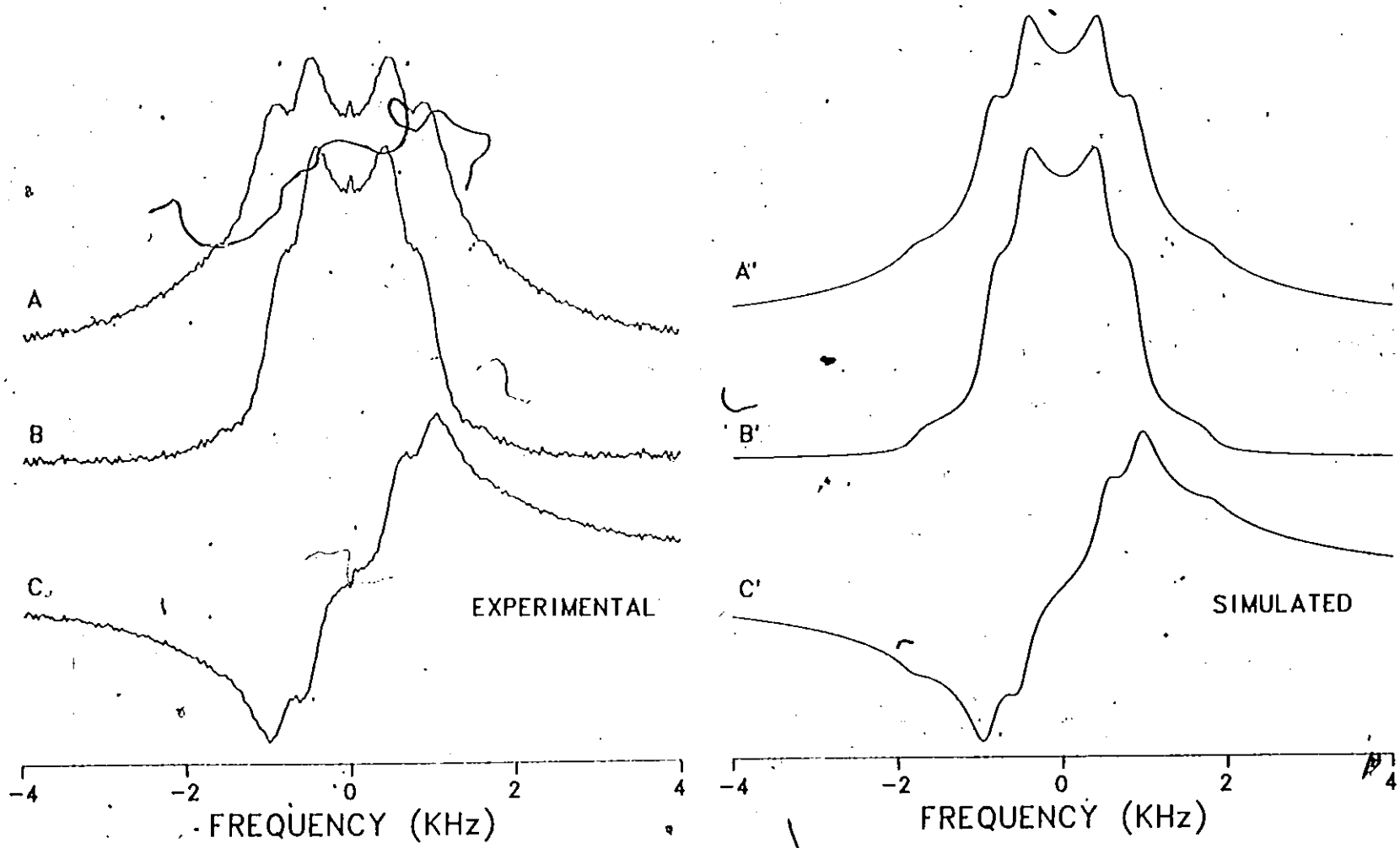

Figure 45. Experimental and simulated spectra for 10 mole % cholesterol-d_6 using different display modes.

In addition, the increased sharpness of the absolute value spectrum features relative to the other display modes allows measurement of closely spaced quadrupole splittings. Also, the signal to noise ratio of the absolute value spectrum is not degraded so that the method may be used with weak signals. For the following discussion, quadrupole splittings were extracted from the absolute value spectra.

Figure 46 shows the variation of quadrupole splittings of cholesterol-d_6 with addition of cholesterol. As seen in Figure 41, separate quadrupole splittings are observed at low cholesterol concentrations. For cholesterol concentrations greater than 30 mole %, the splittings tend to coalesce, and the points of Figure 46 represent estimates of the values with the indicated error.

Even at the highest cholesterol concentrations, the observed quadrupole splittings are very small in comparison to those for the 3 and 7 positions. As discussed above, the magnitude of the splitting is sensitive to both the geometry of the label with respect to the director and the amplitude of the fluctuations of the director. Since the alkyl tail has several degrees of motional freedom through rotations about C-C single bonds, the previously determined orientation for the director relative to the rigid ring system cannot be applied to the flexible tail segment. Without the director orientation, the effects of geometry and fluctuations cannot

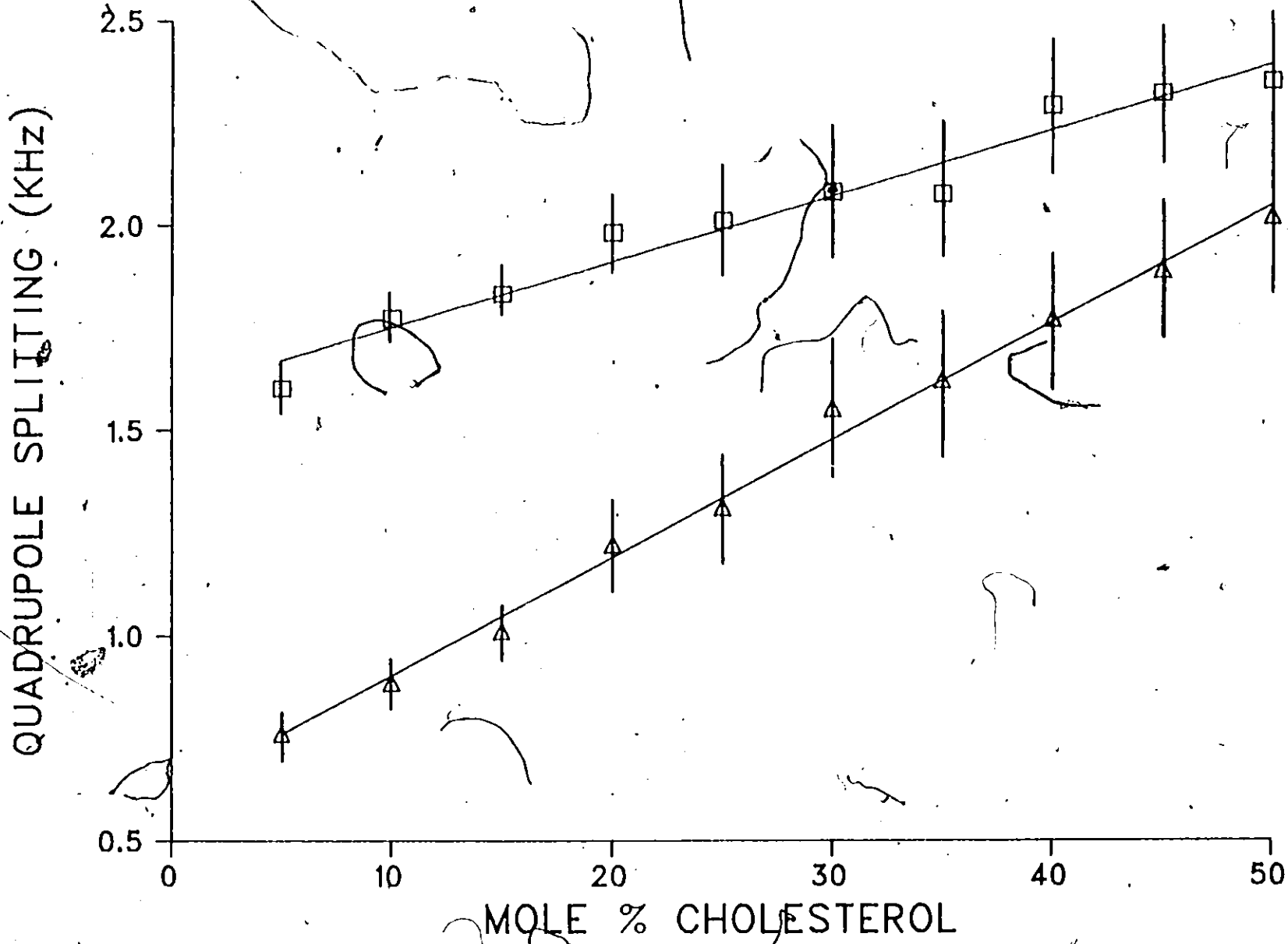

Figure 46. Variation of quadrupole splittings with cholesterol concentration for cholesterol-26,26-d_6 in egg PC bilayers. Quadrupole splittings were measured from absolute value spectra. Above 30 mole % cholesterol, the splittings are only slightly resolved.

be separated. Some insight can be gained, however, by examination of the motions available to the methyl groups.

The aliphatic tail section of cholesterol-d_6 is shown below.

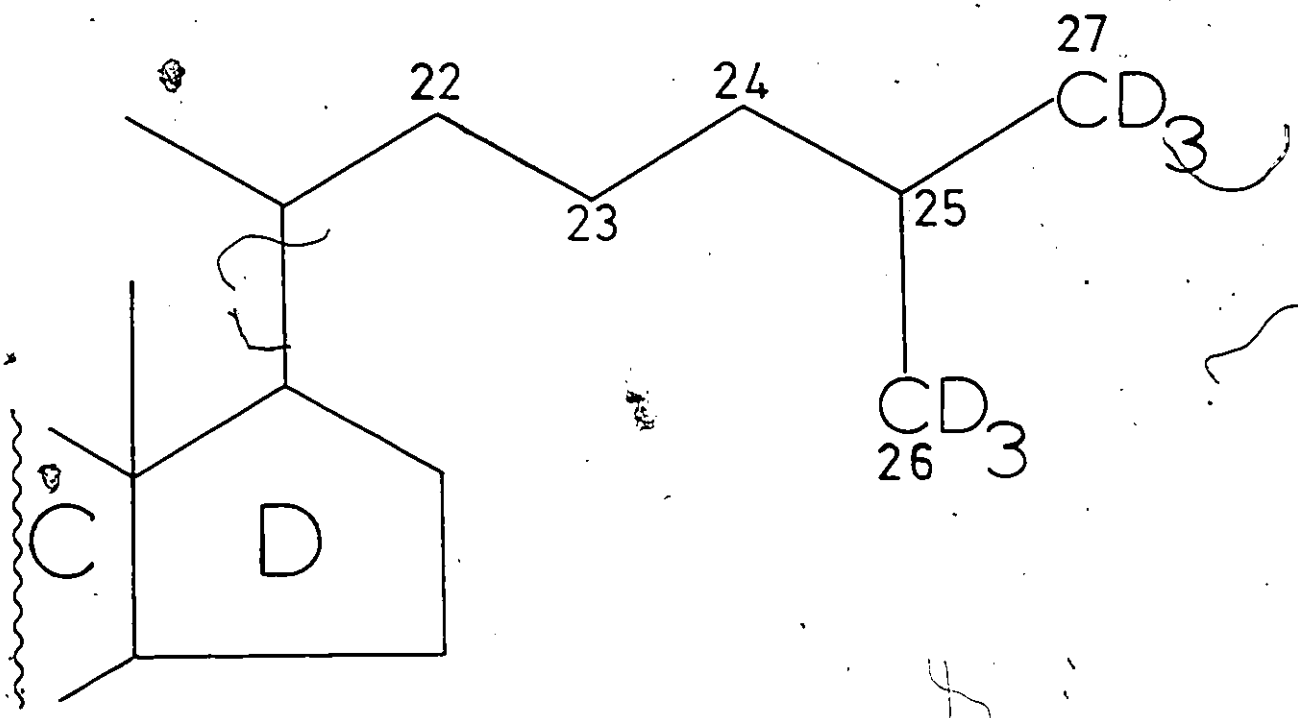

The possible motions can be considered as successive rotations about individual C-C bonds.

The first bond considered links the C-$^2H_3$ methyl group with C_{25}. The rotation of a methyl group about the three-fold symmetry axis is generally free at the temperatures studied here, even in crystalline solids. The methyl group rotation causes a three-fold reduction of the quadrupole

splittings for methyl deuterons relative to a static system (6). Thus, even in the absence of other motions, small splittings are expected for methyl groups. The next bond considered is that between C_{24} and C_{25}. In principle, the isopropyl group (C_{25}, C_{26}, C_{27}) could undergo free rotation about the C_{24}-C_{25} bond. This would result in a further three-fold reduction in the methyl group splittings. In addition, however, the motions of both the C_{26} and C_{27} methyl groups would become symmetric about the C_{24}-C_{25} bond vector. In that case, equal quadrupole splittings would be expected for the two methyl groups, in contrast to the resolved splittings observed experimentally.

It must be noted here that the observation of separate quadrupole splittings could also result from slow exchange between two sites. If the properties of the individual sites are such that the methyl groups are motionally equivalent within each site, but the degree of order is different in the two sites, two sets of splittings would also be observed. Two sets of experimental data argue against this possibility.

Firstly, good simulations of the experimental spectra were obtained using equal intensities for the overlapping powder patterns. If the difference in quadrupole splittings were due to slow exchange between two inequivalent sites, equal intensities would be observed only if the two sites were equally populated. Stronger evidence against chemical exchange as the basis of the difference in splittings is provided by the

temperature dependence of the spectra. The exchange process would presumably be thermally activated so that an increase in temperature would result in a coalescence of the overlapping patterns to yield a single, average quadrupole splitting at high temperature.

Figure 47 illustrates the temperature dependence of the quadrupole splittings for 20 mole % cholesterol-d_6. Over the range of temperature examined, no indication of coalescence is observed. It is certainly possible that the failure to observe coalescence results from a barrier to exchange which is not surmounted thermally at the temperatures studied. Taken together, however, the intensity and temperature data favour motional inequivalence of the two methyl groups over chemical exchange as the cause of the observed difference in splittings. This question could be fully resolved using a cholesterol probe stereospecifically deuterated at only one methyl group.

Thus far, the motion of the methyl groups has been decomposed into free rotation about the methyl symmetry axes and restricted motion about the C_{24}-C_{25} bond. The amplitude of motion allowed about C_{24}-C_{25} cannot be estimated although evidence has been obtained for highly restricted motion of the alkyl tail at least up to C_{23} (J. Browning, personal communication). If this limited flexibility extends down to the terminal methyl groups, the cause of the small magnitude of the quadrupole splittings must be assigned to the geometries

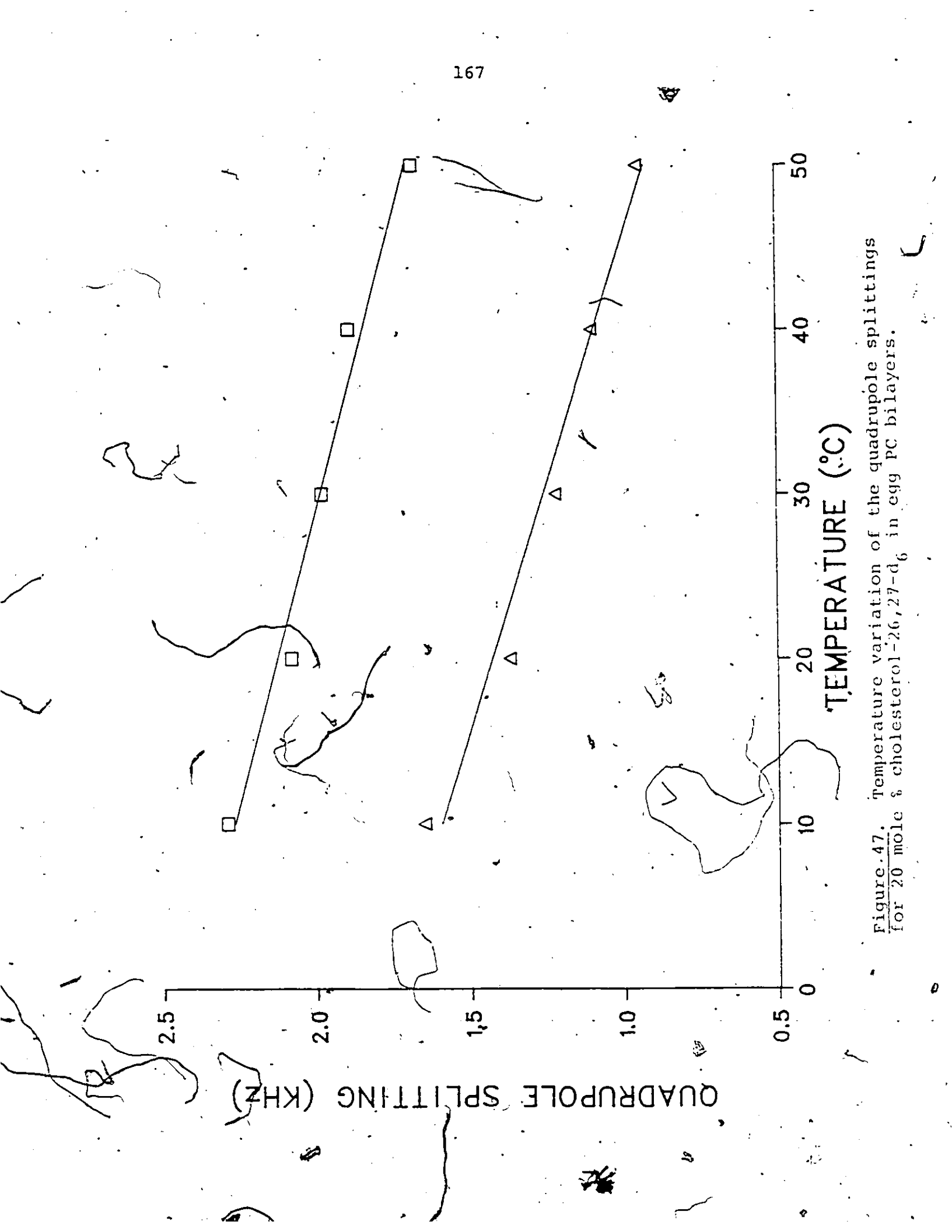

Figure.47. Temperature variation of the quadrupole splittings for 20 mole % cholesterol-26,27-d_6 in egg PC bilayers.

of the methyl groups with respect to the director. As discussed above, the quadrupole splitting is scaled by the factor $(3 \cos^2\alpha_i - 1)/2$. For the present case, α_i is the angle between the director and the C-C bond connecting C_{25} to one of the rapidly rotating methyl groups. As α_i approaches the magic angle, 54.7°, the quadrupole splitting approaches a value of zero. Thus, if both methyl groups have orientations close to this angle, the magnitudes of the observed quadrupole splittings may be dominated by this geometrical effect. For the region near the magic angle, the factor $(3 \cos^2\alpha - 1)/2$ changes rapidly with small changes in α. The large gradients in quadrupole splitting observed for variation of concentration or temperature may be partially due to small adjustments of the orientations of the methyl groups with respect to the director. Note, in particular, that the rates of change of the quadrupole splittings with increasing cholesterol concentration are greater for the alkyl tail region than for the rigid steroid ring system. This is in contrast to the behaviour of the acyl chains where the response of the tail region is much weaker than that of the upper region (Section IV.1).

The discussion above is necessarily speculative since the factors which determine quadrupole splittings cannot be separated. It has been pointed out, however, that the small quadrupole splittings observed for the tail region of cholesterol do not necessarily indicate that the motion in this region is

close to isotropic in nature. Further information on the amplitude of restricted motion in this region could be obtained with cholesterol probes, deuterium-labelled at other positions.

Motional Dynamics

Anisotropic motion can be characterized by its amplitude and symmetry and by its rate. These two sets of characteristics need not be correlated. The amplitude and symmetry of motion can be probed through the magnitudes of the motionally averaged quadrupole splittings. The rates of motion may be investigated using measurements of the nuclear relaxation times. In this study, motional rates were examined with both T_1 (spin-lattice) and T_{2e} (spin-spin) relaxation times. These two parameters are sensitive to different regions of the spectrum of motional rates (73). The T_1 relaxation time is sensitive to components of the overall motion with frequencies near the deuterium resonance frequency (46.1 MHz in the present case). The T_{2e} relaxation time senses these motions as well as motions of very low frequency. Comparison of these relaxation times yields information on the distribution of motional frequencies (the spectral density) allowed for cholesterol in the membrane. As above, these features are compared for the rigid framework and alkyl tail regions in membranes containing variable amounts of cholesterol. Representative spectra, employing 10 mole % cholesterol-d_6, are shown for the inversion-recovery T_1 experiment and for the echo decay T_{2e}

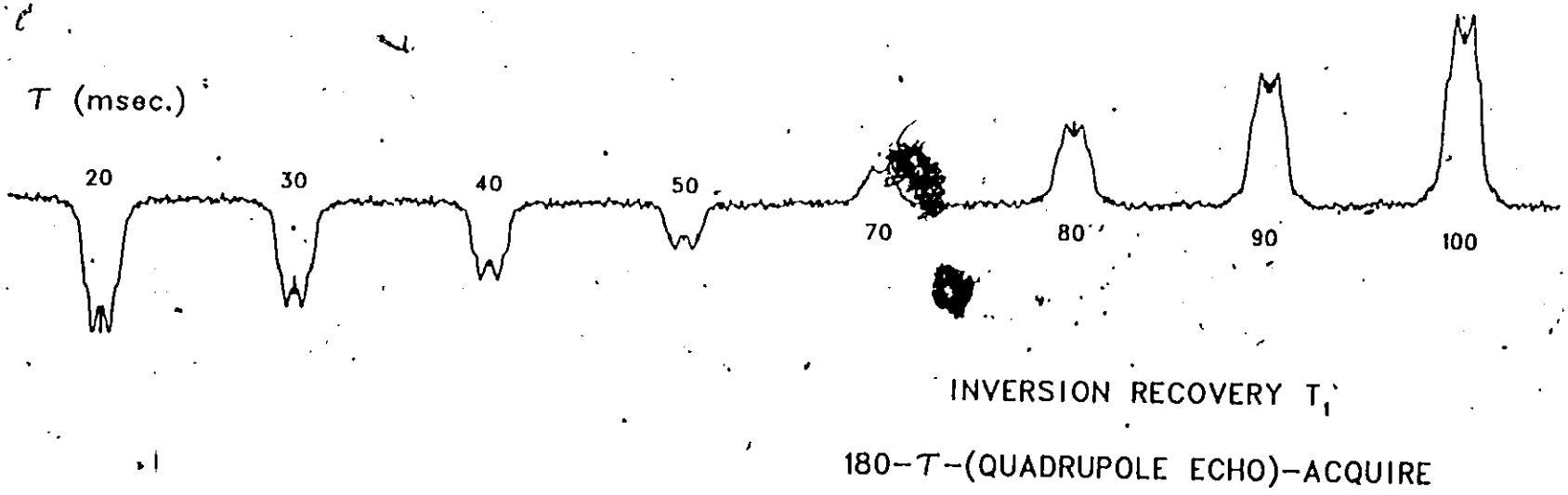

Figure 48. Experimental spectra for inversion-recovery T_1 experiment using 10 mole % cholesterol-26,27-d_6. The times indicated are between the inverting 180° pulse and the quadrupole echo sequence in milliseconds.

experiment (Figure 49). For both experiments, values of relaxation times were calculated from the slopes of semi-logarithmic plots of intensity (taken as peak heights) vs. the delay time. These plots are illustrated, using arbitrary units for intensity, for T_1 (Figures 50A, B) and T_{2e} (Figures 50C, D) with the straight lines derived from linear regression. For the 10 mole % cholesterol-d_6 sample, equal relaxation times were observed for the two splittings. The relaxation time data are presented in Table 4.

I). Fused Ring System

Within experimental error, the T_1 and T_{2e} relaxation times for the 7 position are independent of cholesterol concentration. The value of T_1 is rather similar to those measured for cholesterol-2,2,4,4,6-d_5 (Section IV.5). As discussed above, a simple model for the motion of cholesterol indicates a correlation time of approximately 10^{-10} seconds.

The observed relaxation times can be compared with those found for the acyl chains of perdeuterated dipalmitoyl PC (46). In the upper region of the bilayer, at 37°C, the values of the relaxation times were approximately 30 ms for T_1 and 0.7 ms for T_{2e}. The smaller values noted here for the 7 position of cholesterol indicate generally slower motion for the sterol relative to the acyl chains. The difference is particularly large for the T_1 relaxation time. This relaxation

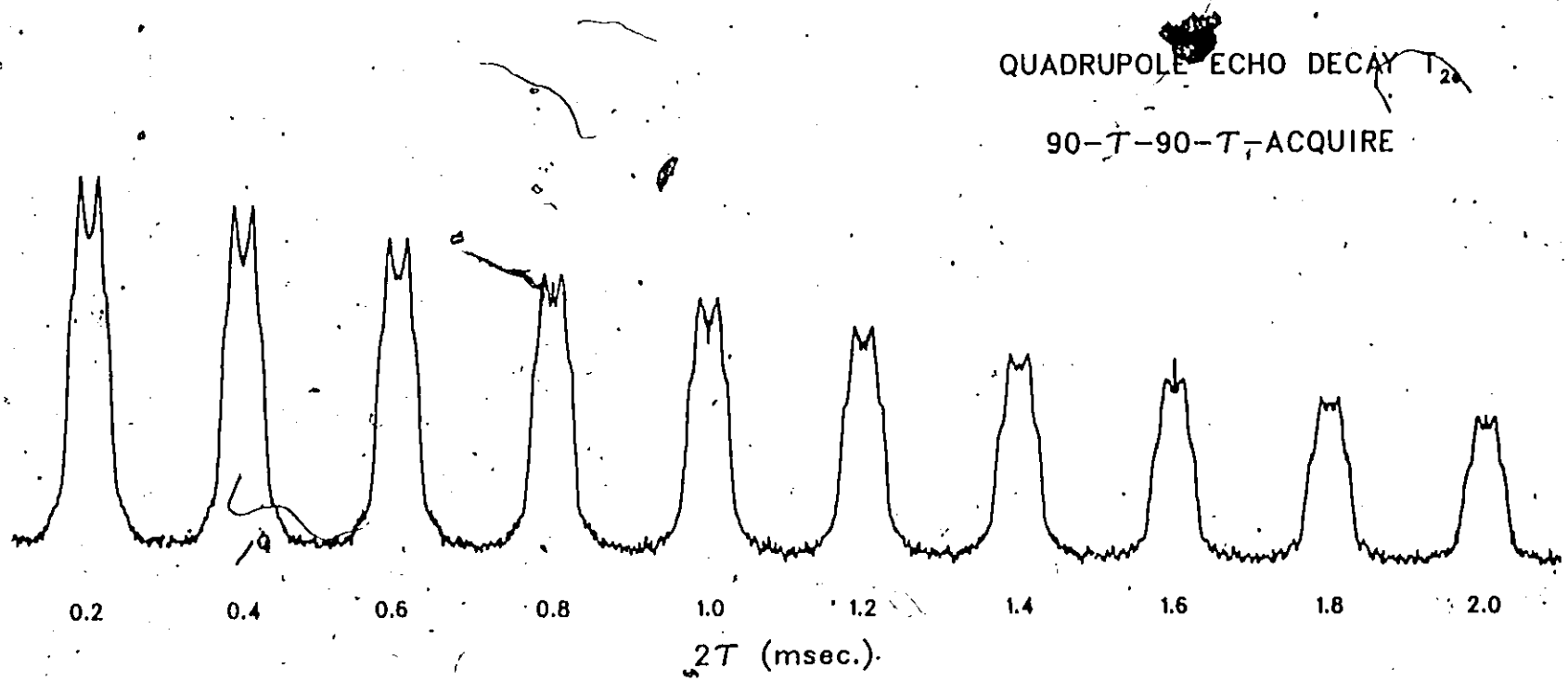

Figure 49. Experimental spectra for echo decay T_{2e} experiment using 10 mole % cholesterol-26,27-d_6. The indicated times are twice the delay times between the 90° pulses of the quadrupole echo sequence.

Figure 50. Semi-logarithmic plots of the time dependence of intensities in the T_1 and T_{2e} experiments for variable concentrations of cholesterol-7,7-d_2 and cholesterol-26, 27-d_6 in egg PC bilayers. For each plot, cholesterol concentrations are: 10 mole % (squares); 30 mole % (triangles); 50 mole % (diamonds). Intensities, in arbitrary units, were measured as peak heights in the experimental absorption spectra.

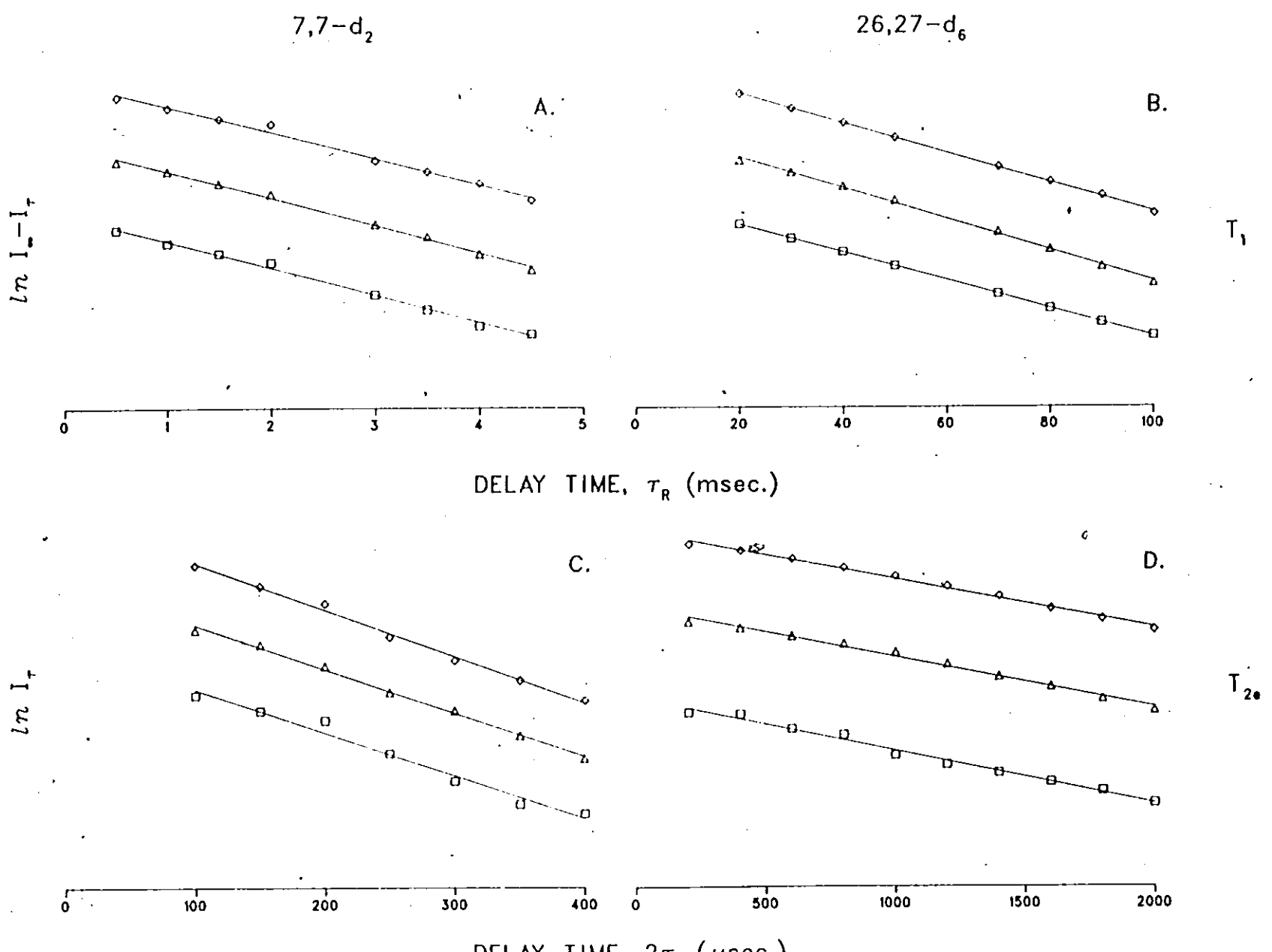
7,7-d2
26,27-d6
A.
B.
ln I∞-Iτ
T1
0
1
2
3
4
5
0
20
40
60
80
100
DELAY TIME, τR (msec.)
C.
D.
ln Iτ
T2e
0
100
200
300
400
0
500
1000
1500
2000
DELAY TIME, 2τ1 (μsec.)

Table 4

DEUTERIUM RELAXATION TIMES FOR CHOLESTEROL-7,7-d_2 AND CHOLESTEROL-26,27-d_6 IN Egg PC BILAYERS AT 27°C

Mole % Cholesterol	T_1 m sec.		T_{2e} m sec.	
	7,7-d_2	26,27-d_6	7,7-d_2	26,27-d_2
10	4.8	92	.30	1.5
30	4.7	82	.30	1.6
50	5.0	87	.28	1.6

time is most sensitive to molecular motions with frequency components near the deuterium resonance frequency. As discussed in Section IV.5, the longer relaxation times noted for the acyl chains may reflect fast trans-gauche isomerizations about the C-C bonds of the acyl chains. These motions are not available as a relaxation mechanism for fused ring system of cholesterol, resulting in an apparently slower motion for the sterol.

A smaller difference is noted between the T_{2e} values for cholesterol and the PC acyl chains. The T_{2e} relaxation time is sensitive to very low frequency motions. If the low frequency motions correspond to rigid body fluctuations of the entire molecules, similar values for T_{2e} would be expected for both cholesterol and the phospholipids. The shorter T_{2e} observed for cholesterol indicates that the distribution of motional frequencies is richer in the low frequency region.

Alkyl Tail Region

The relaxation times for the methyl groups can be compared with those of the fused ring system and the terminal methyl groups in dipalmitoyl PC (46). Firstly, longer relaxation times are noted for the 26,27 positions than for the 7 position. In particular, the T_1 values for the methyl groups are approximately twenty times larger than those of the 7 position, indicating a larger fast motion component for the methyl groups.

Fast rotation of the methyl groups, about their C_3 axes, is likely to be largely responsible for the long T_1 observed. A similar effect is noted in PC where the T_1 of the terminal methyl group is much longer than the T_1's of the neighbouring methylene segments (46). The degree to which the T_1 values for the methyl groups are affected by the C_3 axis rotation could be ascertained by examining the T_1 behaviour of deuterons at neighbouring atoms.

The T_{2e} values for the methyl groups are also longer than those for position 7. The difference in T_{2e} values for the two regions is much less than that noted for the T_1 values. The longer T_{2e} values for the methyl groups again indicates faster motion relative to the fused ring system. The smaller difference noted between T_{2e} values for the two regions reflects the fact that T_{2e} is less sensitive than T_1 to the very fast motions. Thus, methyl group rotation affects T_{2e} to a lesser extent than T_1.

All the relaxation times measured showed little variation with cholesterol concentration in marked contrast to the behaviour noted for the quadrupole splittings in the same systems. Although the amplitudes and rates of anisotropic motion are not necessarily correlated, one would intuitively expect that an increase in order would be accompanied by a decrease in motional rates. The apparent absence of a correlation between molecular order and rotational rates was

examined further by measurement of the T_1 relaxation times of cholesterol-7,7-d_2 as a function of temperature.

Figure 51 shows the variation of T_1 with temperature. A minimum in T_1 is observed at approximately 30°C. The biphasic behaviour of T_1 with temperature can be understood in terms of the dependence of T_1 on the distribution of rotational frequencies for the probe (73). The efficiency of the T_1 relaxation process increases (i.e., T_1 becomes shorter) as the density of the distribution of motional frequencies in the region of the ^2H resonance frequency increases. Apparently, this density is greatest for cholesterol at about 30°C. At higher temperatures, the distribution of frequencies becomes extended to higher frequency motions. Thus, the density at the resonance frequency decreases and the T_1 process is less efficient. At lower temperatures, the distribution is extended to lower frequencies and again, the density at the resonance frequency is decreased.

The relaxation time measurements for variable cholesterol concentration were made at 25°C. At this temperature, the relaxation times are quite insensitive to variation in motional rates as seen in Figure 51, where a 20°C change in temperature has essentially no effect on T_1. Thus, any changes in the dynamics of cholesterol caused by variation of the cholesterol concentration would be difficult to detect using relaxation

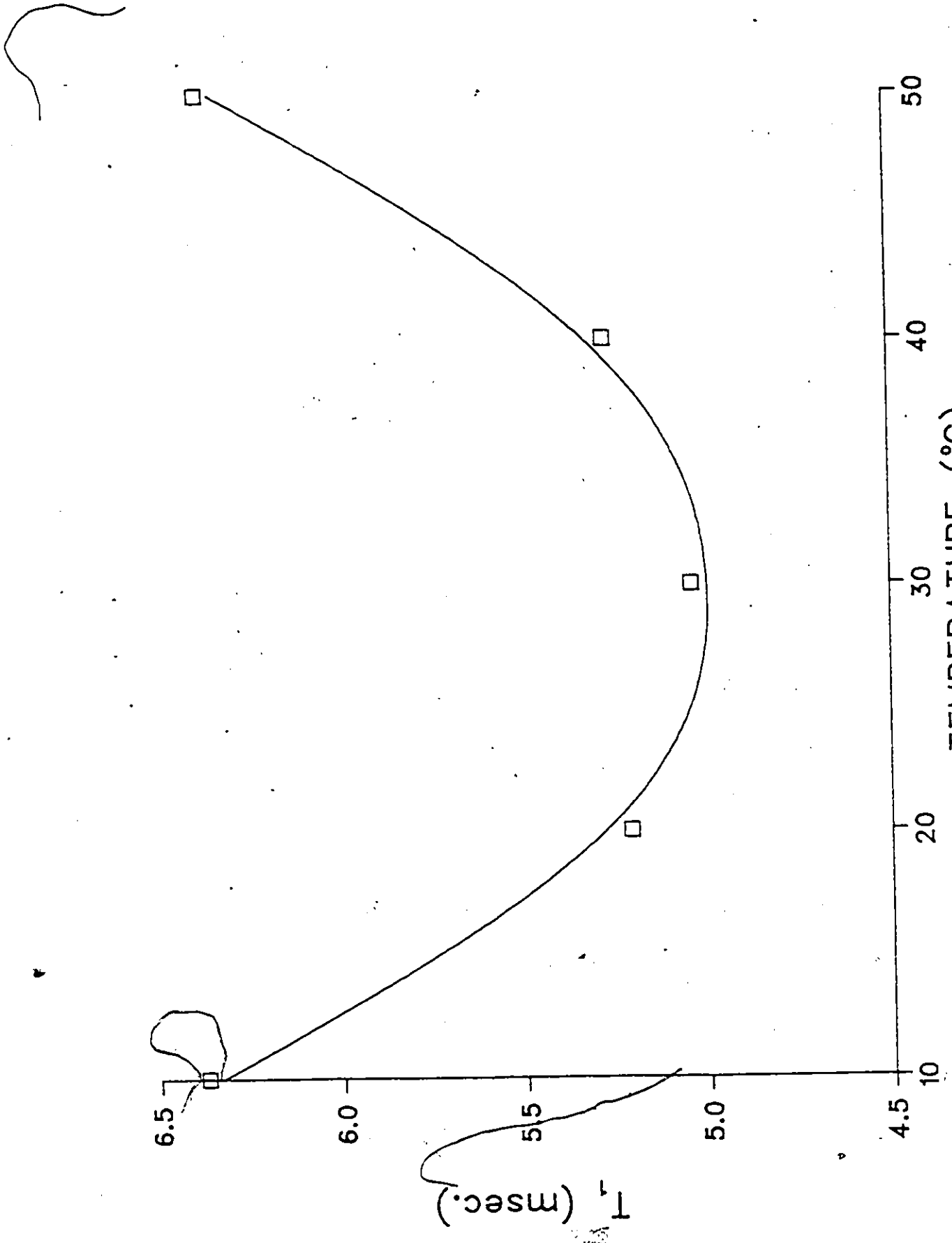

Figure 51. Temperature dependence of the T_1 relaxation time for cholesterol-7,7-d_2 (50 mole % in egg PC).

time measurements.

IV.6.3 Conclusions

^{2}H NMR can be used to investigate the motional properties of a membrane component in terms of both amplitude and rate of anisotropic motion. This method is particularly useful for a molecule such as cholesterol since deuterium labelling allows examination of specific regions of the molecule. This feature was exploited in the present study to differentiate between the properties of the rigid fused ring framework of cholesterol and its terminal alkyl tail group.

For the fused ring system, the observed quadrupole splittings may be analyzed in terms of molecular order parameters using the previously determined (Section IV.5) orientation of the director axis. A very high degree of order is found for cholesterol which is greatest at low temperature or high membrane cholesterol concentration. The relaxation data for this region indicate slower motion than is observed for the acyl chains of phosphatidylcholine. Slower motion for the sterol is reasonable due to its large bulk and the inflexible nature of the fused ring system. The observation of a T_1 minimum for the probe in the variable temperature study indicates that caution should be exercised in the interpretation of changes in T_1 for cholesterol in this temperature region. Due to the biphasic behaviour of T_1, one cannot

distinguish between an increase or decrease in motional rates based on a change of T_1. Comparisons between cholesterol and the phospholipid acyl chains can be made based on the magnitudes of T_1 relaxation times since it has been shown, (65), that the motion of the acyl chain deuterons is sufficiently rapid to apply the short correlation time formalism. Thus, the shorter T_1 values for cholesterol are indicative of slower motion for the sterol, relative to the acyl chains.

For the alkyl tail region, the observed quadrupole splittings cannot be fully interpreted since the local orientation of the director is unknown. The observation of inequivalent splittings for the terminal methyl groups does indicate a limited extent of flexibility for this region. The relaxation data for the methyl groups give evidence for generally more rapid motion than is observed for the fused ring system. Faster motion for the alkyl tail can be expected due to the availability of motional degrees of freedom through rotation about the methyl three-fold symmetry axes and the C-C single bonds of the alkyl tail system.

Finally, methods of improving the resolution of closely spaced, broad quadrupole powder patterns were investigated. It was found that the absolute value display of the spectra provides a means of determining the separate quadrupole splittings for overlapping patterns.

CHAPTER V

CONCLUDING REMARKS AND SUGGESTIONS FOR FUTURE WORK

V.1 Nitroxide Spin Probes

The reliability of the spin probes as reporters of membrane structure has been investigated through comparison of EPR spin probe and NMR data for several systems and by examination of the ^2H NMR spectra of deuterated spin probes. Because of the simultaneous influence of geometry and motional amplitude on the magnetic resonance spectra, it is not possible to determine conclusively the factors which control the spectral behaviour of the probes. Evidence has been presented, however, which indicates the importance of considering geometric features in the interpretation of spin probe data. These features are generally ignored in spin probe studies which may lead to interpretations in terms of the membrane properties which are not even qualitatively correct. Although it was not possible to provide a definitive assessment of the origin of the anomalies found for the spin probes, several suggestions have been made concerning the choice of probes which yield the most reliable data.

Future work in this area could be centred on attempting to control the influence of geometry on the spin probes. Several other types of spin probes are available, and attempts have been made to design nitroxides which mimic the natural

fatty acids more closely (74). It would be particularly interesting to study the imidazoline-derived nitroxides (75) which differ from the oxazolidine probes used here chiefly by the presence of a double bond in the five-membered ring system. Increased rigidity for the ring might serve to minimize the geometric alterations postulated here for the oxazolidines.

V.2 Deuterated Cholesterol

For the inflexible portion of cholesterol, it was possible to perform a more detailed quantitative analysis of the ^{2}H NMR spectra of deuterated probes due to the ability to separate the effects of geometry and motion on the spectra. The determination of the orientation of the motional averaging axis for the molecule allows interpretation of the ^{2}H NMR spectra for any label position on the fused ring system in terms of the overall motion of the molecule. It was not possible to analyze fully the spectra for the terminal methyl group probes due to the unknown orientation of the director for this region. The evidence presented here does suggest that the amplitude of motion for this region is somewhat limited.

The relaxation studies provided information on the dynamics of the motion of cholesterol in the membrane. These data indicated somewhat slower motion for the sterol relative to

the acyl chains of a phospholipid. In addition, comparison of the relaxation behaviour for probes with different label positions on cholesterol indicated greater motional rates for the alkyl tail region than for the fused ring system. The temperature dependence of the T_1 values for the cholesterol-7,7-d_2 probe shows that caution is required in the interpretation of changes in T_1 relaxation times in this system.

The present work with cholesterol could be extended in several ways. Firstly, the cholesterol-2,2,4,4,6-d_5 used here could serve as an excellent probe of the behaviour of cholesterol in biological or model membranes. This probe has several advantages as a reporter of the amplitude or rates of motion of cholesterol in the membrane. The relaxation studies could be extended through the use of deuterated phospholipids. Parallel studies of the relaxation behaviour of cholesterol and the phospholipids would provide information on the phospholipid-cholesterol interaction. Similar studies have been performed using ^{13}C NMR (76). Finally, it would be most interesting to apply the entire range of NMR relaxation techniques to the cholesterol-phospholipid system in order to define more fully the spectrum of motional frequencies available to the probe.

V.3 Hexagonal Phase Lipids

Several problems associated with the use of spin probes in the study of hexagonal phase lipids were pointed out. The EPR spectra of spin probes in random dispersions of these lipids are not very informative due to the relatively slow diffusion of the probes about the cylinder axes of the hexagonal phase lipids. In oriented lipid systems, there exists a strong possibility of misinterpretation of the EPR spectra due to the similarity of the spectra for the oriented hexagonal phase and a lamellar bilayer phase which is macroscopically poorly aligned.

There are several possible extensions to the work with the hexagonal phase. The difficulties with the time scale properties of the EPR spin probes may possibly be overcome using the Saturation Transfer EPR technique (ref. 10, chap. 1). This technique extends the sensitivity of the EPR spectra to a very much slower regime of molecular motions. There are also several possible applications of ^2H NMR to the study of lipid phase behaviour. The phase behaviour of multicomponent lipid systems is particularly complex (12). ^2H NMR is well suited to the study of such systems since the components may be individually examined through the use of specifically deuterium-labelled probes.

APPENDIX I

SIMULATION OF THE EPR SPECTRA OF SPIN PROBES IN THE HEXAGONAL PHASE

This section outlines the method used in calculating the simulated spectra shown in Section IV.3. Although the method used is not the most elegant, it does allow physical insight into the manner in which the spectra arise for the different geometries. A similar treatment for ^2H NMR has been described (6).

Single Cylinder

The model for the single cylinder is depicted in Figure 52. The long axis of the cylinder lies along z and the spin probe long axes are radially distributed in the x-y plane. Rotation of the cylinder in the field is simulated by rotation of the H_0 vector in the x-y plane. In order to calculate the spectrum expected for a particular cylinder orientation, the direction cosines connecting the field vector and the nitroxide axis system are required (5). For the orientation shown in Figure 52 the coordinates for the field vector and the vectors along the nitroxide axis system may be assigned by spherical geometry as:

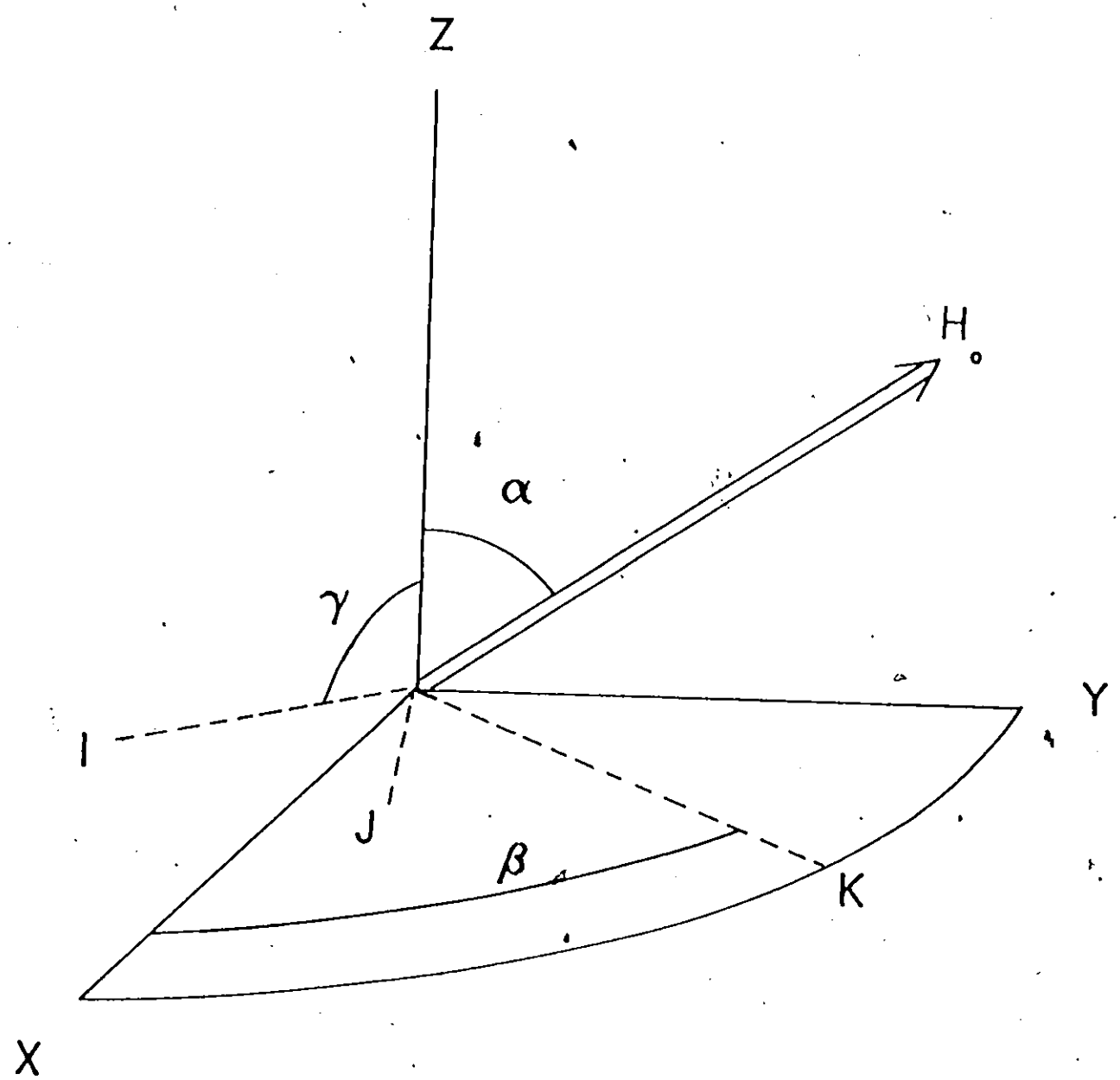

Figure 52. Axis system for single cylinder model. The cylinder long axis is along Z. I, J and K represent the nitroxide principal axis system. H_0 represents the external magnetic field.

$\vec{H}_0$ (0, sin α, cos α)

$\vec{I}$ (sinγsinβ, - sinγcosβ, cosγ)

$\vec{J}$ (cosγsinβ, - cosγcosβ, - sinγ)

$\vec{K}$ (cosβ, sinβ, 0)

The direction cosines between the field and the nitroxide vectors are obtained by taking dot products between the vectors since

$$\vec{A}\cdot\vec{B} = |A|\ |B|\ \cos\theta_{AB} \tag{A1}$$

where θ_{AB} is the angle between the two vectors. Thus for unit vectors $\vec{H}_0$ and $\vec{K}$

$$\vec{H}_0\cdot\vec{K} = \sin\alpha\sin\beta = \cos\theta_{H_0K} = \ell_{H_0K} \tag{A2}$$

The hyperfine splitting expected for the probe shown in Figure 52 with the direction cosines and the elements of the hyperfine tensor may be calculated as:

$$A = (\ell^2_{H_0I}\ A^2_{ii} + \ell^2_{H_0J}\ A^2_{jj} + \ell^2_{H_0K}\ A^2_{kk})^{1/2} \tag{A3}$$

The rather complicated expression which results from substitution of the direction cosine expressions is considerably simplified in the case of the spin probe in a fluid membrane environment. In this case, the g and hyperfine tensors are partially averaged by rapid anisotropic motion to axially symmetric forms. Associating the symmetry axis (director) with the K axis gives

$$A_{ii} \rightarrow A_{\perp}$$
$$A_{jj} \rightarrow A_{\perp}$$
$$A_{kk} \rightarrow A_{\parallel}$$

So that:

$$A = (\ell^2_{H_0K} A^2_{\parallel} + (\ell^2_{H_0I} + \ell^2_{H_0J}) A^2_{\perp})^{1/2} \qquad (A4)$$

Substitution of the expressions for the direction cosines gives:

$$A = (\sin^2\alpha\sin^2\beta\, A^2_{\parallel} + (\sin^2\alpha\cos^2\beta + \cos^2\alpha) A^2_{\perp})^{1/2} \qquad (A5)$$

Some trigonometry yields

$$A = (\sin^2\alpha\sin^2\beta\, A^2_{\parallel} + (1-\sin^2\alpha\sin^2\beta) A^2_{\perp})^{1/2} \qquad (A6)$$

or the more familiar form

$$A = (A^2_{\parallel} \cos^2\theta + A^2_{\perp} \sin^2\theta)^{1/2} \qquad (A7)$$

with $\theta = \arccos(\sin\alpha\sin\beta)$

where θ is the angle between the field and the director axis. Thus, for any particular orientation of the field and a probe in the plane only θ is required to calculate the expected spectrum.

In order to simulate the entire cylinder, β is varied and θ is calculated for each value of β and α. For each value of θ, the g value and hyperfine splittings are calculated to give the positions of a three line "stick" spectrum. Each line is then convoluted with a derivative lineshape (p. 33 in

ref. 4). This process is repeated for each value of β and the resultant spectra are co-added to simulate the spectrum for all probes in the cylinder.

Planar Distribution of Cylinders

This arrangement of cylinders is depicted in Figure 53. The long axes of the cylinders, represented by the vector $\vec{K}$, are radially distributed in the x-y plane as they would be on a flat surface. The spin probe long axes are radially distributed about $\vec{K}$. The coordinates are:

$\vec{H}_0$ $(0, \sin\phi, \cos\phi)$

$\vec{K}$ $(\cos\omega, \sin\omega, 0)$

The angle, α, between the field and the cylinder axis can be calculated:

$$\cos\alpha = \vec{H}_0 \cdot \vec{K} = \sin\phi\sin\omega \qquad \text{(A8)}$$

Thus, for a particular field orientation, the angle between the field and each cylinder can be calculated by varying the angle ω. Using the angle between the field and an individual cylinder, the spectrum for that cylinder is calculated as described above for the case of a single cylinder. This procedure is repeated for all values of ω to simulate the entire set of cylinders.

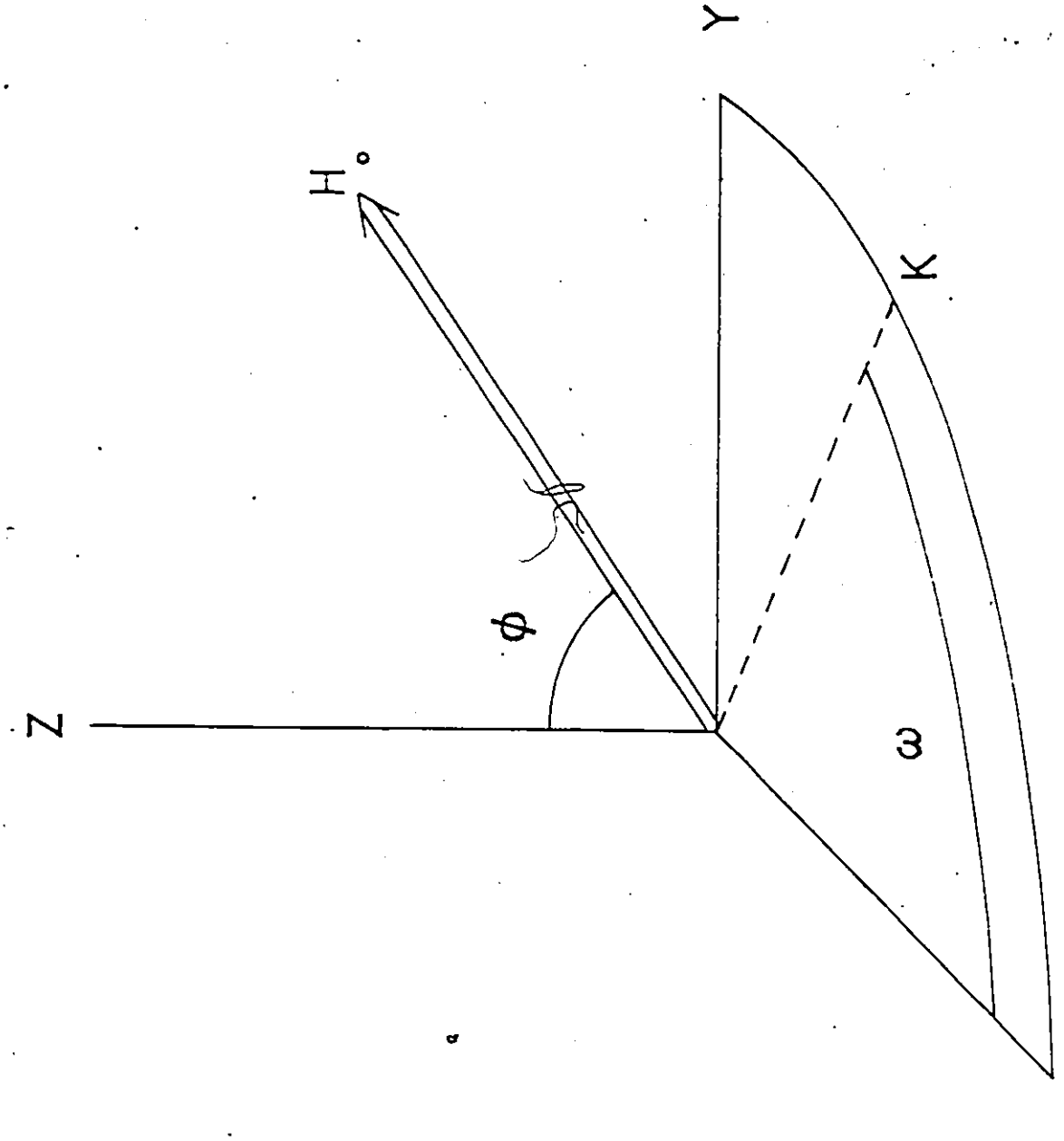

Figure 53. Axis system for planar distribution of cylinders. The x-y plane represents the flat surface of the cell. K is the long axis of one of the cylinders radially distributed in the plane.

The input parameters used in the simulations were:

	Figures 24, 25	Figure 28
$g_{\parallel}$	2.0050	2.0053
$g_{\perp}$	2.0060	2.0056
$A_{\parallel}$	6.6 G	9.56 G
$A_{\perp}$	17.9 G	16.4 G
H_0	3000 G	3300 G
S_{mol}	0.83	0.50

Lorentzian lines were assumed in all the simulations with peak to trough linewidths:

Low field	2.7 G
Central	2.5 G
High field	4.0 G

APPENDIX II

CALCULATION OF THE ORIENTATION OF THE AXIS OF ROTATION OF CHOLESTEROL

The right handed axis system described above for cholesterol is shown in Figure 54. The rotation axis is represented as a unit vector (r) with origin at (0, 0, 0). The direction cosines for this vector (l_r, m_r, n_r) are obtained from spherical geometry as

$$(\sin\theta\cos\phi,\ \sin\theta\sin\phi,\ \cos\theta)$$

The direction cosines for a particular C-^{2}H bond can be calculated, (77) from its atomic coordinates for carbon (X_c, Y_c, Z_c) and deuterium (X_d, Y_d, Z_d) by,

$$l_i = \frac{X_d - X_c}{b};\ m_i = \frac{Y_d - Y_c}{b};\ n_i = \frac{Z_d - Z_c}{b} \qquad \text{(A9)}$$

where the bond length $b = [(X_d - X_c)^2 + (Y_d - Y_c)^2 + (Z_d - Z_c)^2]^{1/2}$.

For any assumed orientation of the rotation axis, the angle between it and the i'th C-^{2}H bond, α_i, can be calculated by:

$$\cos\alpha_i = l_i l_r + m_i m_r + n_i n_r \qquad \text{(A10)}$$

$$= l_i\sin\theta\cos\phi + m_i\sin\theta\sin\phi + n_i\cos\theta$$

Using this value of α_i and equation 17 in the text, values of the quadrupole splitting ratio, R_k, can then be calculated

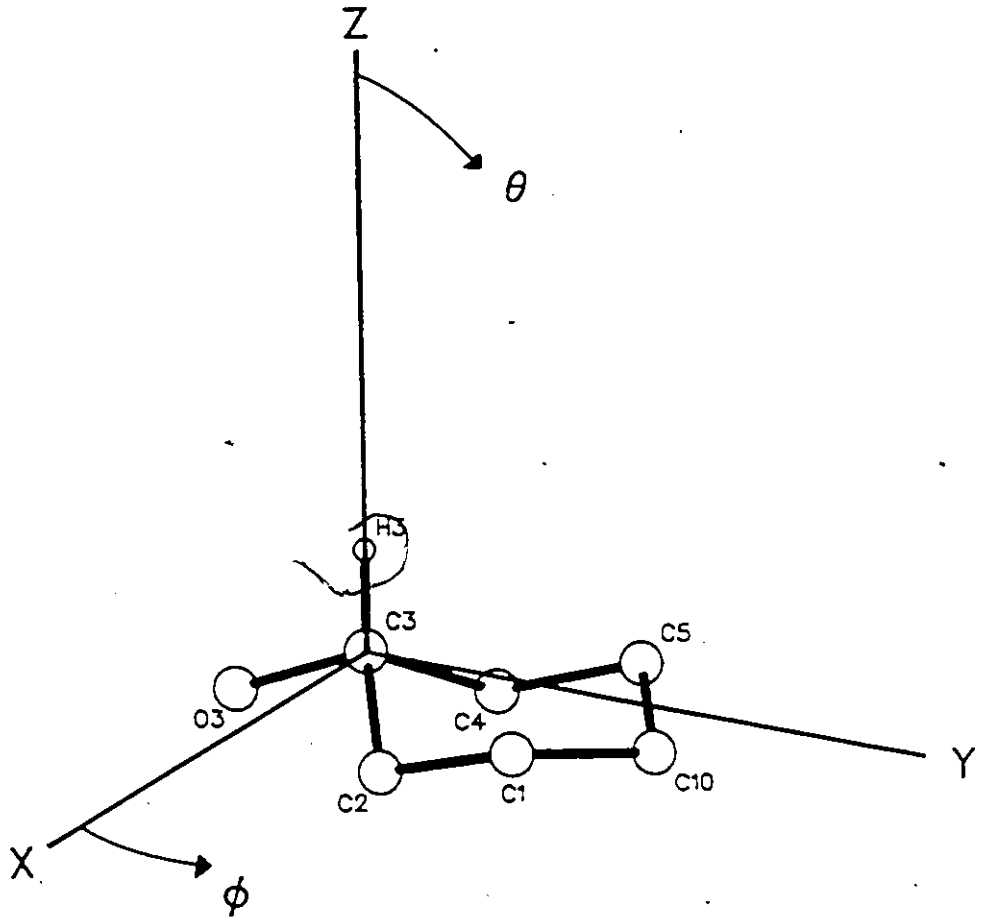

Figure 54. Axis system used for calculations. The frame has origin at C_3 and is oriented with respect to the A ring of cholesterol as shown.

for pairs of C-^{2}H bonds and a particular rotation axis orientation for comparison with the experimental ratios. The search for the correct axis orientation was carried out using the following scheme.

1) The orientation of the rotation axis was varied by selecting values of θ and ϕ. Both angles were examined at 1° intervals over the range 70° - 100°.
2) The angles, α_i, between the assumed axis orientation and the individual C-^{2}H bonds were calculated using equation A10.
3) Values of R_k were calculated for comparison with experimental values. In each case, the ratio was calculated with respect to the 3α deuteron.
4) Two criteria were applied in selecting reasonable values for θ and ϕ. Firstly, since the splittings for all positions examined were less than that of the 3α deuteron, only sets of (θ, ϕ) which gave values of R_k greater than 0.95 for all the ratios were examined further. Secondly, only orientations which gave values of R_k less than 1.8 for the C_2, C_4 equatorial deuterons (i.e., quadrupole splittings greater than ~25 KHz) were examined.
5) For orientations which met these requirements, an error estimate was calculated:

$$E = \Sigma \left[\frac{R_k^c - R_k^e}{R_k^e} \right]^2 \qquad \text{(A11)}$$

where R_k^c is the calculated ratio

R_k^e is the experimental ratio

Since the assignment of the splittings for the C_2, C_4 equatorial deuterons is not known a priori, both possible choices were used in comparing experimental and calculated ratios. For the range of (θ, ϕ) examined, best agreement between experiment and calculation was found for the region $(79 \pm 2^\circ, 93 \pm 2^\circ)$. Within the stated error range, it was not possible to make an unambiguous assignment of the resonances for the C_2, C_4 equatorial deuterons.

APPENDIX III

SIMULATION OF DELAYED START OF THE FOURIER TRANSFORM

The free induction decays and transformed spectra for a quadrupole powder pattern were simulated in the following manner.

1) The theoretical intensity distribution for a Pake doublet as a function of frequency was generated. Since this lineshape is symmetric about the zero frequency, only one-half of the powder pattern was considered. As shown previously (78), the intensity distribution, $y(\omega)$ is given by:

$$y(\omega) = (1/\sqrt{6})\{(\tfrac{1}{2} - \omega/\omega_Q)^{-1/2} + (\tfrac{1}{2} + \omega/\omega_Q)^{1/2}\}; \quad 0 \leq \omega/\omega_Q \leq .5$$

$$y(\omega) = (1/\sqrt{6})\ (\tfrac{1}{2} + \omega/\omega_Q)^{-1/2}, \qquad .5 < \omega/\omega_Q \leq 1 \quad \text{(A12)}$$

$$y(\omega) = 0, \qquad \omega/\omega_Q > 1$$

where ω is the frequency separation from zero, and ω_Q is the quadrupole splitting. An example of such an intensity distribution is shown in Figure 43A.

2) The corresponding free induction decay was generated by taking the Fourier transform of the intensity distribution. Since the full powder spectrum is an even function ($y(\omega)=y(-\omega)$), the FID can be generated using only the cosine part of the Fourier transform of the half-spectrum, $y(\omega)$, calculated above

(79). Thus, the FID was calculated by:

$$f(t) = \sum_{\omega=0}^{\omega_{max}} y(\omega) \cos 2\pi\omega t$$

Lorentzian broadening was added by multiplying the FID by a decreasing exponential of the form:

$$e^{-t/T_2}$$

where T_2 is the spin-spin relaxation time.

An example of such an FID is shown in Figure 43B. Separate free induction decays for the two overlapping patterns were generated and co-added.

3) The spectra were produced by taking the cosine Fourier transform of the FID generated above. Thus, the spectrum, $g(\omega)$, was calculated by:

$$g(\omega) = \sum_{t=0}^{t_{max}} f(t) \cos 2\pi\omega t$$

where $f(t)$ is the FID. Taking the cosine part of the Fourier transform generates one-half of the symmetric frequency spectrum. For plotting, the spectra were reflected about the zero frequency. A sample plot is shown in Figure 43C. The effect of dead time was simulated by shifting the point in the FID at which the transform was started. Thus, for no dead time, the time axis started at the first point of the FID. For dead time, τ_D, the time axis started at the point in the FID

corresponding to this time in the original FID. A series of spectra for variable values of t_b is shown in Figure 42. The small peak visible in the spectra at the central frequency is an artifact which occurs because the FID does not decay completely to zero. The small positive offset in the FID produces a peak at zero frequency in the transformed spectrum.

APPENDIX IV

LISTINGS OF FORTRAN COMPUTER PROGRAMS

```
C          SIMULATION OF EPR SPECTRA FOR SPIN
C          PROBES ORIENTED IN A SINGLE CYLINDER
C          ACCORDING TO ALGORITHM IN
C          M.G. TAYLOR AND I.C.P. SMITH
C          CHEM. PHYS. LIPIDS,28(1981)119.
C          SEE ALSO
C          LIBERTINI ET AL.
C          J. MAGN. RESON.,15(1974)460.
C
C          USES MOTIONALLY AVERAGED A,G VALUES
C          INPUT VALUES
C          APAR=A PARALLEL (GAUSS)
C          APER=A PERPENDICULAR (GAUSS)
C          GPAR=G PARALLEL
C          GPER=G PERPENDICULAR
C          NPT=NUMBER OF POINTS IN FIELD AXIS
C          HZERO=FIELD AT CENTRE OF SPECTRUM (GAUSS)
C          BI=FIELD AT START RELATIVE TO CENTRE
C          BF=FIELD AT END RELATIVE TO CENTRE
C          *** FOR 100 G SCAN, BI=-50, BF=50 ***
C          NANGL=NUMBER OF ANGLES IN SUMMATION
C          WIDC(I)=PEAK TO TROUGH LINEWIDTHS FOR
C                  LOW FIELD,CENTRAL,HIGH FIELD
C                  LINES IN GAUSS
C          ALPHD=ANGLE BETWEEN FIELD AND CYLINDER
C               LONG AXIS IN DEGREES
C
      DIMENSION SPLOT(501),FLD(501),L(3),WIDC(3),WIDV(3)
      RAD90=ARCOS(-1.)/2.
      RADEG=RAD90/90.
      SINT=0.
      DO 20 J=1,501
   20 SPLOT(I)=0.
      READ(8,1000)APAR
      READ(8,1000)APER
      READ(8,1000)GPAR
      READ(8,1000)GPER
      READ(8,1001)NPT
      READ(8,1000)HZERO
      READ(8,1000)BI
      READ(8,1000)BF
      READ(8,1001)NANGL
      DO 10 I=1,3
   10 READ(8,1000)WIDC(I)
      READ(8,1000)ALPHD
 1000 FORMAT(8F10.3)
 1001 FORMAT(I5)
      WIDFAC=SQRT(3.)/2.
      DEL=(BF-BI)/FLOAT(NPT-1)
      HS=HZERO+BI
      ALPHA=ALPHD*RADEG
C
C          SQUARES OF A AND G VALUES
C
```

```
      APAR2=APAR**2
      APER2=APER**2
      GPAR2=GPAR**2
      GPER2=GPER**2
      FACTR=HZERO*(GPAR+2.*GPER)/3.
      DIST=1.
C
C          SET UP FIELD AXIS
C
      DO 45 J=1,NPT
   45 FLD(J)=BI+DEL*FLOAT(J-1)
      SINA=SIN(ALPHA)
C
C          XINCR IS INCREMENT FOR ANGLE SUMMATION
C
      XINCR=RAD90/FLOAT(NANGL)
      DO 100 JTHET=1,NANGL
      BETA=FLOAT(JTHET-1)*XINCR
C
C          COST IS THE DIRECTION COSINE BETWEEN THE
C          FIELD AND THE SYMMETRY AXIS OF THE PROBE
C
      COST=SINA*SIN(BETA)
C
C          CALCULATE SQUARES OF THE DIRECTION
C          COSINES FOR PARALLEL AND PERPENDICULAR
C          COMPONENTS
C
      DCPAR2=COST*COST
      DCPER2=1.-DCPAR2
C
C          AP,GP ARE THE A AND G VALUES FOR
C          THE PRESENT ORIENTATION IN THE
C          SUMMATION
C
      AP=SQRT(APAR2*DCPAR2+APER2*DCPER2)
      GP=SQRT(GPAR2*DCPAR2+GPER2*DCPER2)
C
C          L(2) IS THE POSITION OF THE CENTRAL LINE
C
      L(2)=(FACTR/GP-BS)/DEL+.5
C
C          CALCULATE LOW FIELD AND HIGH FIELD
C          POSITIONS ACCORDING TO HYPERFINE SPLITTING
C
      IA=AP/DEL+.5
      L(1)=L(2)-IA
      L(3)=L(2)+IA
C
C          CHECK FOR OUT OF BOUNDS
C
      IF((L(1).LT.1).OR.(L(3).GT.NPT)) GO TO 100
C
C          INCREMENT THE SPECTRUM INTEGRAL
```

```
C
      SINT=SINT+1.
C
C          IN LOOP EXTENDING TO STATEMENT 810,
C          CONVOLUTE EACH LINE WITH DERIVATIVE
C          LORENTZIAN LINE USING M-DEPENDENT
C          LINEWIDTH
C
C          THE CONVOLUTION TAKES ADVANTAGE OF THE
C          ODDNESS OF THE DERIVATIVE LORENTZIAN
C          LINESHAPE (IE. F(W)=-F(-W) ) AND
C          SO, ONLY ONE-HALF OF THE LINE
C          IS CALCULATED
C
      DO 810 M=1,3
      J=L(M)
      WID=WIDFAC*WIDC(M)
      DO 800 KLM=1,200
      HDEL=FLOAT(KLM)*DEL
      NLOC1=J-KLM
      NLOC2=J+KLM
      IF((NLOC1.LE.0).OR.(NLOC2.GT.NPT)) GO TO 810
      WING=(2.*WID*HDEL)/(WID**2+HDEL**2)**2
      IF(WING.LT.1.0E-25) GO TO 810
      SPLOT(NLOC1)=SPLOT(NLOC1)+WING
      SPLOT(NLOC2)=SPLOT(NLOC2)-WING
  800 CONTINUE
  810 CONTINUE
  100 CONTINUE
C
C          PRINT OUT SPECTRAL INFORMATION
C
      WRITE(6,2000)APAR,APER,GPAR,GPER
 2000 FORMAT(1H1,'  MOTIONALLY AVERAGED PARAMETERS',//,'  A PARALEL= ',F-
     110.2,/,'  A PERPENDICULAR= ',F10.2,/,'  G PARALLEL= ',F10.6,/,'  G-
     2 PERPENDICULAR= ',F10.6,//)
      WRITE(6,2001) BI,BF,HZERO,NPT,NANGL
 2001 FORMAT(1X,'  SWEEP FROM ',F10.3,' TO ',F10.3,' RELATIVE TO ',F10.1-
     1,' GAUSS OVER ',I5,' POINTS USING ',I5,' ORIENTATIONS',//)
      WRITE(6,2002)
 2002 FORMAT(1X,'  CONSTANT AND VARIABLE  PARTS OF THE PEAK TO PEAK LINE-
     1WIDTHS',/)
      DO 2003 K=1,3
 2003 WRITE(6,2004)WIDC(K),WIDV(K)
 2004 FORMAT(1X,F10.3,' GAUSS + ',F10.3,' * (SIN(THETA))**4 GAUSS ',/)
      WRITE(6,2040) ALPHD
 2040 FORMAT(1X,'  ANGLE OF INCLINATION= ',F10.3)
C
C          NORMALIZE SPECTRUM TO UNIT INTEGRAL
C
      DO 86 K=1,NPT
   86 SPLOT(K)=SPLOT(K)/SINT
C
C          WRITE SPECTRUM TO PLOTTING FILE
```

```
C
      WRITE(7,2020) (SPLOT(I),FLD(I),I=1,NPT)
 2020 FORMAT(6E13.6)
      STOP
      END
```

```
C
C          SIMULATION OF EPR SPECTRA FOR LABELS
C          IN AN ENSEMBLE OF CYLINDERS ORIENTED
C          ON A FLAT SURFACE ACCORDING TO
C          ALGORITHM IN
C          M.G. TAYLOR AND I.C.P. SMITH
C          CHEM. PHYS. LIPIDS,28(1980)119.
C          SEE ALSO
C          LIBERTINI ET AL.
C          J. MAGN. RESON.,15(1974)460.
C          USES MOTIONALLY AVERAGED A,G VALUES
C          INPUT VALUES
C          APAR=A PARALLEL (GAUSS)
C          APER=A PERPENDICULAR (GAUSS)
C          GPAR=G PARALLEL
C          GPER=G PERPENDICULAR
C          NPT=NUMBER OF POINTS IN FIELD AXIS
C          HZERO=FIELD AT CENTRE OF SPECTRUM (GAUSS)
C          BI=FIELD AT START RELATIVE TO CENTRE
C          BF=FIELD AT END RELATIVE TO CENTRE
C          *** FOR 100 G SCAN, BI=-50, BF=50 ***
C          WIDC(I)=PEAK TO TROUGH LINEWIDTHS FOR
C                  LOW FIELD,CENTRAL,HIGH FIELD
C                  LINES IN GAUSS
C          PHID=ANGLE BETWEEN FIELD AND NORMAL
C                TO FLAT SURFACE IN DEGREES
C
      DIMENSION SPLOT(501),FLD(501),L(3),WIDC(3),WIDV(3)
      RAD90=ARCOS(-1.)/2.
      RADEG=RAD90/90.
      SINT=0.
      DO 20 J=1,501
   20 SPLOT(I)=0.
      READ(6,1000)APAR
      READ(6,1000)APER
      READ(6,1000)GPAR
      READ(6,1000)GPER
      READ(6,1001)NPT
      READ(6,1000)HZERO
      READ(6,1000)BI
      READ(6,1000)BF
      NANGL=2025
      DO 10 I=1,3
   10 READ(6,1000)WIDC(I)
      READ(6,1000)PHID
 1000 FORMAT(8F10.3)
 1001 FORMAT(I5)
      WIDFAC=SQRT(3.)/2.
      DEL=(BF-BI)/FLOAT(NPT-1)
      HS=HZERO+BI
      PHI=PHID*RADEG
C
C          SQUARES OF A AND G VALUES
C
```

```
      APAR2=APAR**2
      APER2=APER**2
      GPAR2=GPAR**2
      GPER2=GPER**2
      FACTR=HZERO*(GPAR+2.*GPER)/3.
      DIST=1.
C
C          SET UP FIELD AXIS
C
      DO 45 J=1,NPT
   45 FLD(J)=BI+DEL*FLOAT(J-1)
      SINP=SIN(PHI)
C
C          PERFORM SUMMATION OVER ANGLES
C          OMEGA AND BETA
C
      DO 100 IO=1,90,2
      OMEGA=FLOAT(IO)*RADEG
      ALPHA=ARCOS(SINP*SIN(OMEGA))
      SINA=SIN(ALPHA)
      DO 100 IB=1,90,2
      BETA=FLOAT(IB)*RADEG
      SINB=SIN(BETA)
C
C          CALCULATE SQUARES OF DIRECTION
C          COSINES FOR PARALLEL AND PERPENDICULAR
C          COMPONENTS FOR EACH SET OF OMEGA,BETA
C
      DCPAR2=(SINA*SINB)**2
      DCPER2=1.-DCPAR2
C
C          AP,GP ARE A AND G VALUES FOR
C          THE PRESENT ORIENTATION
C
      AP=SQRT(APAR2*DCPAR2+APER2*DCPER2)
      GP=SQRT(GPAR2*DCPAR2+GPER2*DCPER2)
C
C          L(2) IS POSITION OF CENTRAL LINE
C          IN CHANNEL NUMBERS
C
      L(2)=(FACTR/GP-HS)/DEL+.5
C
C          IA IS THE HYPERFINE SPLITTING
C          IN CHANNEL NUMBERS
C
      IA=AP/DEL+.5
C
C          CALCULATE LOW FIELD (L(1)) AND HIGH
C          FIELD (L(3)) LINE POSITIONS
C
      L(1)=L(2)-IA
      L(3)=L(2)+IA
C
C          CHECK FOR OUT OF BOUNDS
```

```
C
      IF((L(1).LT.1).OR.(L(3).GT.NPT)) GO TO 100
C
C          INCREMENT INTEGRAL
C
      SINT=SINT+1.
C
C          IN LOOP EXTENDING TO STATEMENT 810
C          CONVOLUTE EACH LINE WITH DERIVATIVE
C          LORENTZIAN LINE USING M-DEPENDENT
C          LINEWIDTH
C
C          THE CONVOLUTION TAKES ADVANTAGE OF
C          THE ODD SYMMETRY OF THE LORENTZIAN
C          DERIVATIVE LINESHAPE (IE. F(W)=-F(-W))
C          AND SO ONLY ONE-HALF OF THE LINE
C          IS CALCULATED
C
      DO 810 M=1,3
      J=L(M)
      WID=WIDFAC*WIDC(M)
      DO 800 KLM=1,100
      HDEL=FLOAT(KLM)*DEL
      NLOC1=J-KLM
      NLOC2=J+KLM
      IF((NLOC1.LE.0).OR.(NLOC2.GT.NPT)) GO TO 810
      WING=(2.*WID*HDEL)/(WID**2+HDEL**2)**2
      IF(WING.LT.1.0E-25) GO TO 810
      SPLOT(NLOC1)=SPLOT(NLOC1)+WING
      SPLOT(NLOC2)=SPLOT(NLOC2)-WING
  800 CONTINUE
  810 CONTINUE
  100 CONTINUE
C
C          PRINT OUT SPECTRAL INFORMATION
C
      WRITE(6,2000)APAR,APER,GPAR,GPER
 2000 FORMAT(1H1,'  MOTIONALLY AVERAGED PARAMETERS',//,'  A PARALEL= ',F-
     110.2,/,'  A PERPENDICULAR= ',F10.2,/,'  G PARALLEL= ',F10.6,/,'  G-
     2 PERPENDICULAR= ',F10.6,//)
      WRITE(6,2001) BI,BF,HZERO,NPT,NANGL
 2001 FORMAT(1X,'  SWEEP FROM ',F10.3,' TO ',F10.3,' RELATIVE TO ',F10.1-
     1,' GAUSS OVER ',I5,' POINTS USING ',I5,' ORIENTATIONS',//)
      WRITE(6,2002)
 2002 FORMAT(1X,'  CONSTANT AND VARIABLE  PARTS OF THE PEAK TO PEAK LINE-
     1WIDTHS',/)
      DO 2003 K=1,3
 2003 WRITE(6,2004)WIDC(K),WIDV(K)
 2004 FORMAT(1X,F10.3,' GAUSS + ',F10.3,' * (SIN(THETA))**4 GAUSS ',/)
      WRITE(6,2040)PHID
 2040 FORMAT(1X,'  ANGLE OF INCLINATION= ',F10.3)
C
C          NORMALIZE SPECTRUM TO UNIT INTEGRAL
C
```

```
      DO 86 K=1,NPT
   86 SPLOT(K)=SPLOT(K)/SINT
C
C          WRITE SPECTRUM TO PLOTTING FILE
C
      WRITE(7,2020)(SPLOT(I),FLD(I),I=1,NPT)
 2020 FORMAT(6E13.6)
      STOP
      END
```

```
C
C          PROGRAM FOR SIMULATION OF DEUTERIUM
C          NMR SPECTRA USING FOURIER TRANSFORM
C          CALCULATES INTENSITY DISTRIBUTION
C          FOR ONE-HALF OF PAKE DOUBLET.
C          COSINE FOURIER TRANSFORM OF PAKE
C          DOUBLET YIELDS THE FREE
C          INDUCTION DECAY (FID).
C          FID IS THEN MULTIPLIED BY EXPONENTIAL
C          TO SIMULATE LORENTZIAN BROADENING.
C          COSINE FT OF FID GENERATES HALF
C          SPECTRUM WHICH IS THEN FOLDED ABOUT
C          THE CENTRAL FREQUENCY.
C          STARTING POINT OF THE FT OF THE FID
C          CAN BE SHIFTED TO SIMULATE
C          SPECTROMETER DEAD TIME.
C          FOR CALCULATION METHODS, SEE
C          J. SEELIG
C          QUART. REV. BIOPHYS.,10(1977)353.
C          BLOOM ET AL.
C          CAN. J. PHYS.,58(1980)1510.
C
      DIMENSION FID(502),RFID(502),TINT(251),SPEC(251)
      DIMENSION TIME(502),OMEGA(251),FOMEGA(501),FSPEC(501)
      NPFID=502
      NPSP=NPFID/2
      NPF=NPFID-1
      TWOPI=4.*ARCOS(0.)
      ROOT6I=1./SQRT(6.)
C
C          INITIALIZE ARRAYS
C
      DO 1 I=1,NPFID
      RFID(I)=0.
    1 FID(I)=0.
      DO 2 I=1,NPSP
      OMEGA(I)=0.
      TINT(I)=0.
    2 SPEC(I)=0.
C
C          ENTER SWEEP WIDTH IN HERTZ
C
      READ(6,34) SW
C
C          ENTER THE NUMBER OF COMPONENTS
C
      READ(6,33) NS
   34 FORMAT(F10.4)
   33 FORMAT(I1)
C
C          DW IS THE DWELL TIME
C
      DW=1./(2.*SW)
C
```

```
C           HZPP IS HERTZ PER POINT
C
      HZPP=SW/FLOAT(NPSP-1)*.5
      DO 3 I=1,NPFID
C
C           CREATE THE TIME AND FRQUENCY AXES
C
    3 TIME(I)=FLOAT(I-1)*DW
      DO 4 I=1,NPSP
    4 OMEGA(I)=FLOAT(I-1)*HZPP
C
C           FOR EACH COMPONENT, ENTER
C           QUSPL=QUADRUPOLE SPLITTING IN HERTZ
C           HAFWID=LORENTZIAN LINEWIDTH,HALF WIDTH
C                  AT HALF HEIGHT IN HERTZ
C
      DO 50 NSPEC=1,NS
      READ(6,34) QUSPL
      READ(6,34) HAFWID
      T2E=1./(TWOPI*HAFWID)
C
C           INITIALIZE ARRAYS
C
      DO 5 I=1,NPFID
    5 RFID(I)=0.
      DO 6 LL=1,NPSP
    6 TINT(LL)=0.
C
C           CALCULATE INTENSITY OF PAKE
C           DOUBLET FROM FREQUENCY=0 TO
C           FREQUENCY=QUSPL
C           AND STORE IN ARRAY TINT
C
      NPSMAX=0
      DO 10 L=1,NPSP
      Y=(FLOAT(L-1)*HZPP)/QUSPL
      IF(Y.GT.1.) GO TO 11
      TINT(L)=ROOT6I/SQRT(.5+Y)
      IF(Y.LT..5) TINT(L)=TINT(L)+ROOT6I/SQRT(.5-Y)
      NPSMAX=NPSMAX+1
   10 CONTINUE
   11 CONTINUE
C
C           CALCULATE COSINE FT OF PAKE DOUBLET
C           TO GIVE RAW FID STORED IN RFID
C
      DO 100 I=1,NPFID
      DO 100 J=1,NPSMAX
  100 RFID(I)=RFID(I)+TINT(J)*COS(TWOPI*OMEGA(J)*TIME(I))
C
C           MULTIPLY RFID BY EXPONENTIAL TO
C           SIMULATE LORENTZIAN BROADENING AND
C           STORE IN ARRAY FID
C
```

```
      DO 110 I=1,NPFID
  110 FID(I)=FID(I)+RFID(I)*EXP((-FLOAT(I-1)*DW)/T2E)
   50 CONTINUE
C
C           CALCULATE AVERAGE VALUE OF LAST 10%
C           OF FID AND SUBTRACT FROM FID TO GIVE
C           ZERO BASELINE
C
      BASE=0.
      NLAST=NPFID-(NPFID/10)
      DO 60 IBASE=NLAST,NPFID
   60 BASE=BASE+FID(IBASE)
      ZERO=BASE/FLOAT(NPFID-NLAST)
      DO 70 JBASE=1,NPFID
   70 FID(JBASE)=FID(JBASE)-ZERO
   77 WRITE(6,32)
   32 FORMAT(5X,'NEGATIVE IS TO EXIT')
C
C           ENTER NUMBER OF LEFT SHIFTS
C           PERFORMED ON THE FID, EXITING
C           WITH NEGATIVE VALUE
C
      READ(6,44) IS
   44 FORMAT(I2)
      IF(LS.LT.0) GO TO 400
C
C           CALCULATE COSINE FT OF SHIFTED
C           FID TO GENERATE HALF SPECTRUM
C
      DO 200 I=1,NPSP
      DO 200 J=1,NPFID
      JP=J+IS
      FIDN=FID(JP)
      IF(JP.GT.NPFID) FIDN=ZERO
  200 SPEC(I)=SPEC(I)+FIDN*COS(TWOPI*OMEGA(I)*TIME(J))
C
C           REFLECT SPECTRUM ABOUT ZERO FREQUENCY
C
      FOMEGA(NPSP)=0.
      FSPEC(NPSP)=SPEC(1)
      DO 666 JF=2,NPSP
      J1=NPSP+JF-1
      J2=NPSP-JF+1
      FSPEC(J1)=SPEC(JF)
      FSPEC(J2)=SPEC(JF)
C
C           CONVERT HERTZ TO KILOHERTZ
C
      FOMEGA(J1)=CMEGA(JF)/1000.
  666 FOMEGA(J2)=-CMEGA(JF)/1000.
C
C           WRITE SPECTRUM TO PLOTTING FILE
C
      WRITE(7,35) (FSPEC(IW),FOMEGA(IW),IW=1,NPF)
```

```
      GO TO 77
400   CONTINUE
 35   FORMAT(6E13.6)
      STOP
      END
```

```
C
C
C          SIMULATION OF DEUTERIUM NMR SPECTRA
C          USING ALGORITHM DESCRIBED IN
C          J. SEELIG  QUART. REV. BIOPHYS.
C          10,(1977),353-418
C
C          OPTIONS
C
C          1.) POWDER PATTERN OR ISOTROPIC LINE
C          2.) ABSORPTION OR DISPERSION MODE
C          3.) LORENTZIAN LINEWIDTH CONSTANT OR
C              CONSTANT + 3 COS**2 (THETA) -1
C              ANGULAR DEPENDENCE
C          4.) VARIABLE CHEMICAL SHIFT
C          5.) SPECTRA MAY BE ADDED IN VARIABLE PROPORTIONS
C
C          REQUIRES SUBROUTINES ALOR AND DLOR FOR
C          LORENTZIAN CONVOLUTION
C
      DIMENSION SPEC(501),FLD(501),SSPEC(501),PR(50),XMOM(10)
      DIMENSION FSPEC(501),SSCOR(501),SPCOR(501)
      REAL LWDTH,LWISO,LWANIS
      RAD90=ARCOS(0.)
      PI=2.*RAD90
C
C          GET NUMBER OF COMPONENTS
C
      WRITE(6,60)
   60 FORMAT(5X,'NO. OF SPECTRA')
      READ(6,33) NSPEC
C
C          ARE THEY SUMMED? 0=NO,1=YES
C
      WRITE(6,61)
   61 FORMAT(5X,'SUM?')
      READ(6,33) NSUM
C
C          GET DISPLAY MODE, 0=ABSORPTION,1=DISPERSION
C
      WRITE(6,88)
   88 FORMAT(5X,'ABSORPTION,DISPERSION')
      READ(6,33) LSHAPE
C
C          GET SPECTRAL WIDTH IN HERTZ
C
      WRITE(6,62)
   62 FORMAT(5X,'SPECTRAL WIDTH')
      READ(6,32) SPWID
      NPTS=501
      DELF=SPWID/FLOAT(NPTS-1)
      NZERO=NPTS/2+1
      ZERO=NZERO
      NHALF=NPTS/2
```

```
   32 FORMAT(F10.4)
   33 FORMAT(I1)
      DO 1234 IFR=1,50
 1234 FR(IFR)=1.
C
C          IF MORE THAN ONE COMPONENT,GET FRACTION OF EACH
C
      IF(NSUM.EQ.0) GO TO 1
      WRITE(6,63)
   63 FORMAT(5X,'FRACTION OF SPECTRUM NO.')
      DO 53 L=1,NSPEC
      WRITE(6,64) L
   64 FORMAT(5X,I1)
      READ(6,32) FR(L)
   53 CONTINUE
C
C          INITIALIZE ARRAYS
C
    1 DO 55 I=1,NPTS
      SSCOR(I)=0.
      SSPEC(I)=0.
      FLD(I)=FLOAT(I-NZERO)*DELF
   55 CONTINUE
C
C          FOR EACH COMPONENT GET
C
C          DQ=QUADRUPOLE SPLITTING IN HERTZ
C          LWISO=ISOTROPIC LINEWIDTHIN HERTZ
C          LWANIS=ANISOTROPIC LINEWIDTH IN HERTZ
C     *****  LINEWIDTHS ARE HALF WIDTHS AT HALF HEIGHT  *****
C          SHIFT=CHEMICAL SHIFT FORM CENTRE FREQUENCY IN HERTZ
C
      WRITE(6,65)
   65 FORMAT(5X,'FOR SPECTRUM NO.')
      DO 9999 NS=1,NSPEC
      WRITE(6,66) NS
   66 FORMAT(5X,I1)
      WRITE(6,67)
   67 FORMAT(5X,'SPLITTING,ISOTROPIC LW,ANISOTROPIC LW,SHIFT')
      READ(6,32) DQ
      READ(6,32) LWISO
      READ(6,32) LWANIS
      READ(6,32) SHIFT
    9 DO 10 I=1,NPTS
      SPEC(I)=0.
      FSPEC(I)=0.
   10 CONTINUE
C
C          FIND ISOTROPIC SHIFT RELATIVE TO CENTRE OF SWEEP
C
      NZERO=NPTS/2+1
      IF(SHIFT.NE.0.) NZERO=NZERO-SHIFT/DELF+.5
C
C          IF DQ=0, IT IS ISOTROPIC LINE
```

```
C
      IF(DQ.NE.0.) GO TO 11
      XINT=1./(PI*LWISO)
      IF(LSHAPE.EQ.0) GO TO 555
C
C          IF DISPERSION MODE CALL DLOR FOR CONVOLUTION
C
       CALL DLOR(NZERO,NHALF,LWISO,DELF,FSPEC,XINT,NPTS)
      GO TO 1000
  555 FSPEC(NZERO)=FSPEC(NZERO)+XINT
C
C          IF ABSORPTION MODE, CALL ALOR FOR CONVOLUTION
C
      CALL ALOR(NZERO,NHALF,LWISO,DELF,FSPEC,XINT,NPTS)
      GO TO 1000
C
C          POWDER PATTERN SECTION
C
C          ONE TRANSITION IS CALCULATED FROM
C          -DQ/2 TO +DQ
C
C          CALCULATE FIRST AND LAST FREQUENCY POINTS
C
   11 NFIRST=(-DQ/2.)/DELF+1.5+NZERO
      NLAST=NZERO+DQ/DELF-.5
      DO 73 NPR=NFIRST,NLAST
C
C          SWEEP ACROSS THE REGION OF THE TRANSITION
C          AND CALCULATE FREQUENCY FROM CENTRE
C          IN REDUCED FREQUENCY UNITS
C
      EPS=FLOAT(NPR-NZERO)*DELF/DQ
C
C          CALCULATE TOTAL LINEWIDTH
C
      LWDTH=LWISO+ABS(EPS)*LWANIS
C
C          CALCULATE INTENSITY FROM PROBABILITY DISTRIBUTION
C
      XINT=1./(PI*LWDTH)*(1./SQRT(2.*EPS+1.))
      IF(LSHAPE.EQ.0) GO TO 666
C
C          PERFORM DISPERSION CONVOLUTION
C
      CALL DLOR(NPR,NHALF,LWDTH,DELF,SPEC,XINT,NPTS)
      GO TO 73
  666 SPEC(NPR)=XINT+SPEC(NPR)
C
C          PERFORM ABSORPTION CONVOLUTION
C
      CALL ALOR(NPR,NHALF,LWDTH,DELF,SPEC,XINT,NPTS)
   73 CONTINUE
      DO 74 IS=1,NPTS
   74 FSPEC(IS)=SPEC(IS)
```

```
C
C          REFLECT ABOUT CENTRE FREQUENCY TO GET
C          -DQ TO +DQ/2 TRANSITION
C          FLIP INVERTS PHASE IF DISPERSION
C
      FLIP=1.
      IF(LSHAPE.EQ.1) FLIP=-1.
      DO 75 IF=1,NPTS
      NREV=2*NZERO-IF
   75 FSPEC(IF)=FSPEC(IF)+SPEC(NREV)*FLIP
C
C          INTEGRATE THE SPECTRUM
C
      SINT=0.
      DO 400 IJ=1,NPTS
  400 SINT=SINT+ABS(FSPEC(IJ))
      SINT=SINT/FR(NS)
C
C          ADJUST INTENSITIES FOR FRACTIONAL WEIGHTS
C
      DO 410 IK=1,NPTS
  410 FSPEC(IK)=FSPEC(IK)/SINT
C
C          CONVERT FRQUENCIES TO KHZ
C
      DO 332 IFLD=1,NPTS
  332 FLD(IFLD)=FLD(IFLD)/1000.
  333 CONTINUE
C
C          WRITE SPECTRUM TO PLOTTING FILE
C
 1000 WRITE(7,36) (FSPEC(I),FLD(I),I=1,NPTS)
   36 FORMAT(6E13.6)
  419 IF(NSUM.EQ.0) GO TO 9999
C
C          IF SUMMATION REQUESTED, ADD INTO SUMMED SPECTRUM
C
      DO 420 IL=1,NPTS
  420 SSPEC(IL)=SSPEC(IL)+FSPEC(IL)
 9999 CONTINUE
      IF(NSUM.EQ.0) GO TO 999
C
C          WRITE SUMMED SPECTRUM TO PLOTTING FILE
C
      WRITE(7,36)(SSPEC(I),FLD(I),I=1,NPTS)
  999 STOP
      END
```

```
C
C          SUBROUTINE FOR CONVOLUTION OF LORENTZIAN
C          ABSORPTION MODE LINESHAPE.
C          TAKES ADVANTAGE OF EVEN SYMMETRY OF
C          LORENTZIAN FUNCTION AND CALCULATES
C          INTENSITY FOR ONE HALF OF SYMMETRIC
C          LINE, THEN REFLECTS ABOUT CENTRE.
C
C          REQUIRED PARAMTERS
C
C          NCEN=CHANNEL NUMBER IN SPECTRUM ABOUT
C               WHICH CONVOLUTION TAKES PLACE
C          NHALF=HALF THE NUMBER OF POINTS IN SPEC
C          LWDTH=LINEWIDTH IN HZ.  (HALF WIDTH AT
C                HALF HEIGHT)
C          DELF=FREQUENCY SEPARATION BETWEEN POINTS IN SPEC
C          SPEC=ARRAY HOLDING THE SPECTRUM
C          XINT=INTENSITY OF PROBABILITY DISTRIBUTION
C               IN THE CALLING PROGRAM
C          NPTS=NUMBER OF POINTS IN SPEC
C
      SUBROUTINE ALOR(NCEN,NHALF,LWDTH,DELF,SPEC,XINT,NPTS)
      DIMENSION SPEC(501)
      REAL LWDTH
C
C          STARTING AT CENTRAL LINE POSITION
C          CALCULATE INTENSITY OF LORENTZIAN LINE
C          FOR EACH POINT IN SPEC (=WING)
C
      DO 100 I=1,NHALF
      X=FLOAT(I)*DELF/LWDTH
      X2=X*X
      WING=XINT/(1.+X2)
C
C          N1,N2 ARE CHANNEL NUMBERS ON EACH
C          SIDE OF CENTRAL POSITION
C
      N1=NCEN+I
      N2=NCEN-I
C
C          IF STILL IN BOUNDS, ADD INTENSITY
C          TO SPECTRUM
C
      IF(N1.LE.NPTS) SPEC(N1)=SPEC(N1)+WING
      IF(N2.GE.0) SPEC(N2)=SPEC(N2)+WING
  100 CONTINUE
      RETURN
      END
```

```
C
C          SUBROUTINE FOR CONVOLUTION OF LORENTZIAN
C          DISPERSION MODE LINESHAPE.
C          TAKES ADVANTAGE OF ODD SYMMETRY OF
C          LORENTZIAN FUNCTION AND CALCULATES
C          INTENSITY FOR ONE HALF OF SYMMETRIC
C          LINE, THEN REFLECTS ABOUT CENTRE.
C
C          REQUIRED PARAMTERS
C
C          NCEN=CHANNEL NUMBER IN SPECTRUM ABOUT
C               WHICH CONVOLUTION TAKES PLACE
C          NHALF=HALF THE NUMBER OF POINTS IN SPEC
C          LWDTH=LINEWIDTH IN HZ. (HALF WIDTH AT
C                HALF HEIGHT)
C          DELF=FREQUENCY SEPARATION BETWEEN POINTS IN SPEC
C          SPEC=ARRAY HOLDING THE SPECTRUM
C          XINT=INTENSITY OF PROBABILITY DISTRIBUTION
C               IN THE CALLING PROGRAM
C          NPTS=NUMBER OF POINTS IN SPEC
C
      SUBROUTINE LLOR(NCEN,NHALF,LWDTH,DELF,SPEC,XINT,NPTS)
      DIMENSION SPEC(501)
      REAL LWDTH
C
C          STARTING AT CENTRAL LINE POSITION
C          CALCULATE INTENSITY OF LORENTZIAN LINE
C          FOR EACH POINT IN SPEC (=WING)
C
      DO 100 I=1,NHALF
      X=FLOAT(I)*DELF/LWDTH
      X2=X*X
      WING=(XINT*X)/(1.+X2)
C
C          N1,N2 ARE CHANNEL NUMBERS ON EACH
C          SIDE OF CENTRAL POSITION
C
      N1=NCEN+I
      N2=NCEN-I
C
C          IF STILL IN BOUNDS, ADD INTENSITY
C          TO SPECTRUM
C
      IF(N1.LE.NPTS) SPEC(N1)=SPEC(N1)+WING
      IF(N2.GE.0) SPEC(N2)=SPEC(N2)-WING
  100 CONTINUE
      RETURN
      END
```

REFERENCES

1. G.B. Ansell, R.M.C. Dawson and J.N. Hawthorne, eds. "Form and Function of Phospholipids", B.B.A. Library, Vol. 3, Elsevier, Amsterdam, 1973.

2. V. Luzatti and A. Tardieu, Ann. Rev. Phys. Chem., 25(1974)79.

3. E. Grell, ed. "Membrane Spectroscopy", Springer-Verlag, Berlin, 1981.

4. J.E. Wertz and J.R. Bolton, "Electron Spin Resonance, Elementary Theory and Applications", McGraw-Hill, N.Y., 1972.

5. O.H. Griffith and P.C. Jost in "Spin Labeling, Theory and Applications", (Berliner, L.J., ed.), Academic Press, N.Y., 1976, p. 453.

6. J. Seelig, Quart. Rev. Biophys., 10(1977)353.

7. J. Seelig, Biochim. Biophys. Acta, 559(1978)105.

8. L.J. Berliner, ed. "Spin Labelling, Theory and Applications", Academic Press, N.Y., 1976, chapters 10-13.

9. H.H. Mantsch, H. Saitô and I.C.P. Smith, Progress in Nuclear Magnetic Resonance Spectroscopy, 11(1977)211.

10. L.J. Berliner, ed., "Spin Labeling II, Theory and Applications", Academic Press, N.Y., 1979.

11. R.E. Jacobs and E. Oldfield, Progress in Nuclear Magnetic Resonance Spectroscopy, 14(1981)113.

12. P.R. Cullis and B. DeKruijff, Biochim. Biophys. Acta, 559(1979)399.

13. W.S. Singleton, M.S. Gray, M.L. Brown and J.L. White, J. Am. Oil Chem. Soc. 42(1965)53.

14. M.A. Wells and D.J. Hanahan, Methods in Enzymology, 14(1969)178.

15. E. Oldfield, M. Meadows, D. Rice and R. Jacobs, Biochemistry, 17(1978)2727.

16. W.L. Hubbell and H.M. McConnell, J. Amer. Chem. Soc. 93(1971)314.

17. R.L. Augustine, ed., "Oxidation, Techniques and Applications in Organic Synthesis", Vol. 1, Marcel Dekker, Inc., N.Y., p. 61.

18. A.S. Waggoner, T.J. Kingzett, S. Rothschaefer, O.H. Griffith and A.D. Keith, Chem. Phys. Lipids, 3(1969) 245.

19. E.D. Bergmann, Chem. Rev., 53(1953)309.

20. A.P. Tulloch, Lipids, 12(1977)92.

21. E.G. Rozantsev and V.A. Golubev, Izv. A.N. SSSR. Ser. Khim., 5(1966)891.

22. H.A. Staab, Angew. Chem. Internat. Edit., 7(1962)351.

23. P. Comfurius and R.F.A. Zwaal, Biochim. Biophys. Acta, 488(1977)36.

24. L.D. Gruenke and J.C. Craig, J. Labelled Compounds and Radiopharmaceuticals, 16(1979)495.

25. L.J. Fieser, Organic Syntheses, Coll. Vol. IV (1963) 195.

26. J.H. Davis, K.R. Jeffrey, M. Bloom, M.I. Valic and T.P. Miggs, Chem. Phys. Lett, 42(1976)390.

27. R.L. Hold, J.S. Waugh, M.P. Klein, and D.W. Phelps, J. Chem. Phys., 48(1966)3831.

28. M.R. Paddy, F.W. Dahlquist, J.H. Davis, and M. Bloom, Biochemistry, 20(1981)3152.

29. A.M. Vasserman, A.L. Buchachenko, E.G. Rozantsev and M.B. Neiman, J. Structural Chem., 6(1965)445.

30. B. Cannon, C.F. Polnaszek, K.W. Butler, L.E.G. Erikson and I.C.P. Smith, Arch. Biochem. Biophys., 167(1975) 505.

31. G.W. Stockton and I.C.P. Smith, Chem. Phys. Lipids, 17(1976)251.

32. B.J. Gaffney and H.M. McConnell, J. Magn. Res. 16(1974)1.

33. P. Jost, L.J. Libertini, V.C. Herbert and O.H. Griffith, J. Mol. Biol., 59(1971)77.

34. J. Seelig and W. Niederberger, Biochemistry, 13(1974) 1585.

35. J. Belle and P. Bothorel, Biochem. Biophys. Res. Commun., 58(1974)433.

36. G.B. Birrell and O.H. Griffith, Arch. Biochem. Biophys., 172(1976)455.

37. S. Schreier, C.F. Polnaszek and I.C.P. Smith, Biochem. Biophys. Acta, 515(1978)375.

38. S. Schreier-Muccillo, D. Marsh and I.C.P. Smith, Arch. Biochem. Biophys., 172(1976)1.

39. J. Seelig, J. Amer. Chem. Soc., 92(1970)3881.

40. M.A. Hemminga, Chem. Phys. Lipids, 14(1975)151.

41. S. Schreier-Muccillo, D. Marsh, H. Dugas, H. Schneider and I.C.P. Smith, Chem. Phys. Lipids, 10(1973)11.

42. H.U. Gally, A. Seelig and J. Seelig, Hoppe-Seyler's Z. Physiol. Chem., 357(1976)1447.

43. H.M. McConnell and B. Gaffney McFarland, Annals. N.Y. Acad. Sci., 195(1972)207.

44. G.W. Stockton, K.G. Johnson, K.W. Butler, A.P. Tulloch, Y. Boulanger, I.C.P. Smith, J.M. Davis and M. Bloom, Nature, 269(1977)267.

45. J. Seelig and J.L. Browning, FEBS Lett., 92(1978)41.

46. J.M. Davis, Biophys. J., 27(1979)339.

47. B. Mely, J. Charvolin and P. Keller, Chem. Phys. Lipids, 15(1975)161.

48. M.U. Gally, G. Pluschke, P. Overath and J. Seelig, Biochemistry, 19(1980)1638.

49. J. Seelig and H. Limacher, Mol. Cryst. Liq. Cryst., 25(1974)105.

50. P.R. Cullis and B. DeKruijff, Biochim. Biophys. Acta, 513(1978)31.

51. J.M. Boggs and J.C. Hsia, Can. J. Biochem., 51(1973) 1451.

52. J.M. Boggs and J.C. Hsia, Proc. Natl. Acad. Sci., U.S., 70(1972)1406.

53. S. Schreier-Muccillo, K.W. Butler and I.C.P. Smith, Arch. Biochem. Biophys., 159(1973)297.

54. H.U. Gally and J. Seelig, Biochemistry, 15(1976)5199.

55. H.C. Jarrell, R.A. Byrd and I.C.P. Smith, Biophys. J., 34(1981)451.

56. M.G. Taylor and I.C.P. Smith, Biochim. Biophys. Acta, 599(1980)140.

57. R.A. Demel, L.L.M. Van Deenen, and B.A. Pethica, Biochim. Biophys. Acta, 135(1967)11.

58. P. Michon and A. Rassat, Bull. Soc. Chim. France, 10(1971)3561 (and references cited therein).

59. J. Seelig in "Spin Labeling, Theory and Applications", (Berliner, L.J., ed.), Academic Press, N.Y., 1976, p. 373.

60. J. Seelig and N. Waespe-Šarčevič, Biochemistry, 17 (1978)3310.

61. M. Rance, K.R. Jeffrey, A.P. Tulloch, K.W. Butler, and I.C.P. Smith, Biochim. Biophys. Acta., 600(1980) 245.

62. U.P. Fringeli, Z. Naturforsch. C, 32(1977)20.

63. S.P. Sawan, T.L. James, L.D. Gruenke, and J.C. Craig, J. Magn. Reson. 35(1979)409.

64. B.M. Craven, Acta Cryst., B35(1979)1123.

65. M.F. Brown, J. Seelig, and U. Haeberlen, J. Chem. Phys., 70(1979)5045.

66. M.F. Brown, J. Magn. Reson., 35(1979)203.

67. C. Mailer, C.P.S. Taylor, S. Schreier-Muccillo, and I.C.P. Smith, Arch. Biochem. Biophys., 163(1974)671.

68. J.H. Davis, K.R. Jeffrey, and M. Bloom, J. Magn. Reson., 29(1978)191.

69. N.P. Franks, J. Mol. Biol., 100(1976)345.

70. T. Akiyama, S. Takagi, U. Sankawa, S. Inari, and H. Saitô, Biochemistry, 19(1980)1904.

71. K. Roth, J. Magn. Reson., 38(1980)65.

72. D. Shaw, "Fourier Transform N.M.R. Spectroscopy", Elsevier Scientific, Amsterdam, 1976.

73. T.C. Farrar and E.D. Becker, "Pulse and Fourier Transform NMR", Academic Press, N.Y., 1971, Chap. 4.

74. J.F.W. Keana in "Spin Labeling II, Theory and Applications", (Berliner, L.J., ed.), Academic Press, N.Y., 1979, p. 115.

75. L.B. Volodarsky, I.A. Grigor'ev, and R.Z. Sagdeev in "Biological Magnetic Resonance", Vol. 2, Plenum Press, N.Y., 1980, p. 169.

76. P.L. Yeagle, Biochim. Biophys. Acta., 640(1981)263.

77. T.A. Bak and J. Lichtenberg, "Mathematics for Scientists", W.A. Benjamin Inc., N.Y., 1966, pp. 14-28.

78. M. Bloom, J.M. Davis, and M.I. Valic, Can. J. Phys., 58(1980)1510.

79. R.N. Bracewell, "The Fourier Transform and its Applications", McGraw-Hill, N.Y., 1978, pp. 6-23.